Heterogeneity and spatial correlations in stochastic many-particle systems

From embryogenesis to evolution

Steffen Rulands

München, 2013

Heterogeneity and spatial correlations in stochastic many-particle systems

From embryogenesis to evolution

Steffen Rulands

Dissertation
an der Fakultät für Physik
Ludwig–Maximilians–Universität
München

vorgelegt von
Steffen Rulands
aus Heinsberg im Rheinland

München, den 25. Juli 2013

Erstgutachter: Prof. E. Frey
Zweitgutachter: Prof. H. Gaub

Datum der mündlichen Prüfung: 18. Juli 2013

Zusammenfassung

Leben kann nur durch einen erstaunlich hohen Grad an Organisation und Differenzierung existieren. Um diese Ordnung aufrecht zu erhalten, wird ständig Arbeit an biologischen Systemen verrichtet, die dadurch fernab vom thermischen Gleichgewicht operieren. Die daraus folgende Phänomenologie ist hochgradig komplex, sodass ein tiefgehendes Verständnis dieser Phänomene erhebliche Anforderungen an deren theoretische Beschreibung stellt.

Diese Dissertation untersucht, wie biologische Systeme Differenzierung aufrechterhalten und warum diese Spezialisierung manchmal durch evolutionäre Prozesse wieder umgangen wird. Unser Interesse gilt den fundamentalen Mechanismen, die diesen Phänomenen zugrundeliegen. Wir entwickeln paradigmatische Modelle, die einfach genug für eine mathematische und physikalische Herangehensweise sind, die aber auf der anderen Seite die wesentlichen Eigenschaften des jeweiligen Systems beinhalten.

Auf den längsten Zeitskalen unterliegt Differenzierung den Gesetzen der Evolution. Wie die Differenzierung von Ökosystemen in verschiedene Spezies aufrechterhalten werden kann, ist noch nicht volländig verstanden. Auf den ersten Blick sollte der Darwinschen Evolutionstheorie zufolge nur eine Spezies, die fitteste, überleben. Kürzlich wurde gezeigt, dass räumliche Korrelationen und nicht-hierarchischer Wettbewerb die Koexistenz von Spezies fördern können. Anhand eines paradigmatischen Modells dreier zyklisch wechselwirkender Spezies untersuchen wir die Prozesse, die zur Aufrechterhaltung von Biodiversität und letztendlich zum Aussterben von Spezies führen. Durch die Berechnung der vollen Verteilung der Extinktionszeiten zeigen wir, dass diese Prozesse weit komplexer sind als bisher angenommen. Insbesondere wird das Aussterben von Spezies durch verschiedene dynamische Zustände auf unterschiedlichen Zeitskalen bestimmt. Wir zeigen außerdem, dass die Prozesse, die zur Aufrechterhaltung von Biodiversität führen, mit den Minima eines "renormierten" Potentials verbunden sind. Diese Minima enthalten Informationen über die Skalierung der Extinktionszeiten mit der Systemgröße und damit über die Stabilität von Biodiversität. Ähnlich wie in der statistischen Physik ändert sich diese effektive freie Energie qualitativ an bestimmten Werten der Mobilität von Individuen und der Art des Wettbewerbs zwischen Spezies. Wir liefern das vollständige Phasendiagramm der Populationsdynamik und analysieren die raumzeitliche Dynamik und die Extinktionsprozesse in den verschiedenen Phasen.

Anschließend betrachten wir Biodiversität aus einer breiteren Perspektive und fragen uns, unter welchen Umständen sich Spezialisierung entwickelt und wann diese Spezialisierung durch phänotypische Heterogenität aufgehoben wird. Genetische Diversität

und phänotypische Heterogenität sind weit verbreitete Merkmale von Bakterien und Viren. Einige Bakterienarten wechseln zum Beispiel stochastisch zwischen phänotypischen Zuständen um das Extinktionsrisiko durch Antibiotika zu verringern. Motiviert durch dieses Verhalten untersuchen wir heterogene, stochastische Vielteilchensysteme. Die zugrundeliegende Idee ist, dass jedes Teilchen in einem solchen System unterschiedliche Eigenschaften hat. Zunächst interessiert uns das Wechselspiel zwischen genetischer Diversität und phänotypischer Heterogenität. Wir zeigen, dass die Persistenz genetischer Diversität und phänotypischer Heterogenität entscheidend von der Durchmischung des Systems abhängt. Ist Diffusion schwach, so ist pänotypische Spezialisierung evolutionär vorteilhaft, wohingegen sich im wohldurchmischten System phänotypische Heterogenität durchsetzt. Die Entwicklung phänotypischer Heterogenität hängt auch maßgeblich davon ab, ob der Wettbewerb direkt, wie in Räuber-Beute Beziehungen, ist oder indirekt, vermittelt durch die begrenzte Verfügbarkeit von Ressourcen.

Oftmals hat phänotypische Heterogenität auch Einfluss auf die Motilität von Bakterien, die zwischen einem motilen Zustand, bei dem sie sich durch Flagellen aktiv bewegen, und einem immotilen Zustand wechseln. Wir untersuchen deshalb den Einfluss heterogener Motilität auf fundamentale Fragestellungen der theoretischen Biologie.

Unter welchen Umständen Kooperation entstehen und bestehen kann, ist eine weithin offene Frage der Evolutionsbiologie. Eine Population von Kooperatoren sollte eigentlich anfällig für die Übernahme durch defektierende Mutanten sein. Dieses Dilemma wird oft im Rahmen der Spieltheorie untersucht, wo solche Situationen durch das *Gefangenendilemma* beschrieben werden. Wir zeigen, dass in Populationen mit heterogener Motilität Kooperation unter erstaunlich harschen Bedingungen bestehen kann. Die Dynamik ist durch drei Regimes in den Parameterwerten charakterisiert, die jeweils durch die Möglichkeit für das Überleben von Kooperation und die Selektion der optimalen Motilität innerhalb der Kooperatoren und Defektoren bestimmt sind.

Heterogene Motilität beeinflusst auch Invasionsprozesse, wie sie in nahezu allen Bereichen der Naturwissenschaften auftreten. Wir zeigen, dass sich in solchen Invasionsprozessen Sektoren homogener Motilität ausbilden und, dass verschiedene Motilitäten in unterschiedlichen Phasen der Invasion bevorzugt werden. Wir bestimmen die asymptotische Zusammensetzung der Population und zeigen, dass diese Zusammensetzung maßgeblich durch stochastische Fluktuationen verändert wird.

Im zweiten Teil dieser Doktorarbeit fragen wir uns, wie funktionale Differenzierung in der Embryonalentwicklung möglich ist. Wie entwickeln sich Zellen, die alle dieselbe genetische Information tragen, in solch unterschiedliche Arten wie Nervenzellen oder Muskelzellen? In der Fruchtfliege ist der erste Schritt zur Differenzierung von Zellen eine scharfe räumliche Grenze in der Konzentration des Proteins Hunchback. Zellen in einer Region, in der das Protein vorhanden ist, entwickeln sich später zum Kopf

der Fliege, während sich Zellen, in denen das Protein fehlt, den Rumpf der Fliege bilden. Die Stabilität dieser Grenze ist entscheidend für die weitere Entwicklung des Embryos. Wie kann durch genregulatorische Prozesse eine solche Grenze hergestellt werden, die sowohl gegenüber extrinsischen Störungen, als auch gegenüber intrinsischem Rauschen stabil ist? Wir entwickeln ein paradigmatisches Modell, das als ein "vergröbertes" genregulatorisches Netzwerk angesehen werden kann. Dieses Modell beinhaltet eine bistabile Reaktionskinetik und räumlich inhomogene Aktivierung. Anhand analytischer Berechnungen bestimmen wir Parameterwerte, die die Robustheit dieses Musterbildungsprozesses und seine Stabilität gegenüber extrinsischen Störungen und intrinsischem Rauschen optimieren. Wir zeigen, dass diese Stabilität zum einen durch eine nichtlineare Modulierung des Positionsignals verbessert werden kann, zum anderen auch durch eine schwache Kooperativität bei der Selbstaktivierung. Weiterhin finden wir einen gegensätzlichen Einfluss der Selbstaktivierung auf beide Arten der Destabilisierung: das System kann nicht gleichzeitig für beide Störquellen optimiert werden. Unsere generischen Resultate legen die Prinzipien des Aufbaus genregulatorischer Netzwerke offen und haben mögliche Auswirkungen auf Embryogenese, Ökologie und Biotechnologie.

Diese Dissertation ist in zwei Teile gegliedert. Der erste Teil behandelt die Evolution genetischer Diversität und phänotypischer Heterogenität. Im zweiten Teil untersuchen wir die Stabilität lokalisierter Domänengrenzen in der Emrbyonalentwicklung.

Abstract

Life can only exist due to an intriguingly high degree of organization and differentiation. To establish this order, biological systems rely on a constant flux of energy from their environment and they therefore operate far from thermal equilibrium. The ensuing phenomenology often is highly complex such that a deep going understanding poses significant challenges to theoretical science.

In this thesis, we investigate how biological systems maintain functional differentiation and why this specialization is sometimes disfavored by evolution. We are interested in the fundamental physical mechanisms behind these processes and develop paradigmatic models that are simple enough to be accessible by mathematical and physical reasoning, but which at the same time capture the principal characteristics of the biological system under consideration.

On the largest time scales, differentiation is subject to evolutionary forces. How species differentiation can be maintained is still an open question. Indeed, according to Darwinian evolution, only a single species - the fittest - should survive. Recent studies have shown that spatial correlations and nonhierarchical competition promote species coexistence. We study the processes that lead to the maintenance and loss of biodiversity in a paradigmatic model of three cyclically interacting species. By calculating the full distribution of extinction times we show that these processes are surprisingly rich, comprising several dynamical states on different time scales. We furthermore argue that the dynamic processes leading to the transient maintenance of biodiversity are closely linked to minima of a coarse-grained potential. These minima give information about the scaling of extinction times with the system size and thereby the stability of biodiversity. Similar as in statistical physics, this effective free energy landscape changes qualitatively at certain threshold values of the species' mobility and the relative strength of different types of competition. We provide the complete phase diagrams for the population dynamics and give a comprehensive analysis of the spatio-temporal dynamics and routes to extinction in the respective phases.

We then take a broader perspective on biodiversity and ask, under which conditions specialization arises and when it is circumvented by phenotypic heterogeneity. Genetic diversity and phenotypic heterogeneity are commonly found in bacterial populations and viruses. As an example, some bacteria stochastically switch between phenotypic states to minimize the risk of population extinction due to an attack with antibiotics. Inspired by these phenomena, we investigate heterogeneous, stochastic many-particle systems. The basic idea is that each particle is endowed with distinct

properties. We first study the interplay between genetic diversity and phenotypic heterogeneity in mobile populations. We find that the persistence of genetic diversity and phenotypic heterogeneity qualitatively depends on the degree of mixing. For small diffusion constants, specialization is favored by the evolutionary dynamics, whereas for for well-mixed systems phenotypic generalization can persist. The survival of phenotypic heterogeneity also significantly depends on whether competition is direct, as in predator-prey relations, or indirect, mediated through the limited availability of resources.

Phenotypic heterogeneity may also influence motility in many bacterial populations. In these populations, cells switch between a motile state, where swarming is enabled by propelling flagella, and a non-motile state. Motivated by these findings we study the influence of heterogeneous motility on fundamental problems in theoretical biology.

Understanding the conditions that facilitate the persistence of cooperation is one of the classic problems in evolution. The dilemma of cooperation expresses the naive point of view that cooperation should not be robust against "cheating" mutants. This dilemma is often formulated in the framework of evolutionary game theory, where such situations are described in terms of the *prisoner's dilemma*. We show that in populations exhibiting heterogeneous motility cooperation is possible under much harsher conditions as compared to homogeneous populations. We identify three parameter regimes determined by the probability of the persistence of cooperation and the selection of optimal values of the motility within the cooperating and defecting subpopulations.

Heterogeneous motility also influences invasion processes, which arise in nearly all fields of science. Examples are the range expansion of bacterial populations or the spreading of diseases. We study the expansion of heterogeneous populations and observe the formation of homogeneous sectors. Interestingly, at different stages of the invasion process different combinations of motility and reproduction are favored by the evolutionary dynamics. We determine the asymptotic composition of the population and reveal that this composition is intriguingly influenced by fluctuations.

In the second part of this thesis, we ask how functional differentiation is possible in developmental processes. How can cells, despite all sharing the same genetic information, differentiate into forms as diverse as, for example, nerve fibers or muscle cells? In the fruit fly *Drosophila melanogaster*, the first step towards cell differentiation is a sharp separation of the embryo into a region, where the protein Hunchback is present, and a region where it is absent. Cells in the former region become the fly's head, whereas cells in the latter region will form the trunk. The stable positioning of this border is paramount for the embryo's fate. How can gene regulatory processes establish a sharp border, which is stable to extrinsic perturbations as well as intrinsic noise? We develop a paradigmatic model resembling a coarse-grained gene regulatory network which comprises bistability and spatially inhomogeneous

activation. By analytical calculations, we determine parameter values which optimize the robustness of the pattern forming process, and the border's stability to extrinsic and intrinsic noise. We find that stability is enhanced upon regulating a positional signal and, surprisingly, also for a low degree of binding cooperativity. We further show a contrasting impact of self-activation on the stability of the two sources of destabilization, such that the network can not be optimized for extrinsic and intrinsic perturbations at the same time. Our general results reveal design principles of gene regulatory networks and have possible implications for embryogenesis, ecology, and biotechnology.

The outline of this thesis is as follows. In Chapter 1, we give an introduction on how functional differentiation is achieved in biological systems on vastly different scales. Part 1 is concerned with the evolution of genetic diversity and phenotypic heterogeneity. In Chapter 2, we study how biodiversity is maintained by the spatial ordering of cyclically competing species. Chapter 3 deals with the interplay between genetic diversity and phenotypic heterogeneity in several biological contexts. In Part 2, we investigate the stability of localized domain borders in developmental systems.

Contents

List of Figures

1 Introduction

Life is, one might say, an ongoing struggle for order. While the second law of thermodynamics predicts that in any closed system the degree of disorder increases with time, biological systems exhibit a great amount of organization. Indeed, functional differentiation of the organism's internal structure is a necessity for the development of life. Such functional differentiation is established through the formation of complex patterns. As an example, eukaryotic cells are complex organisms which are, in part, organized by smaller subunits, the organelles [1]. These organelles are separated from their surrounding by a lipid membrane and they perform specialized functions within the cell, cf. Fig. 1.1(a). The most important organelle certainly is the nucleus, which in most cells encapsulates all genetic information and which controls all activities of the cell. Mitochondria produce energy from the oxidation of glucose and the release of adenosine triphosphate, and the endoplasmatic reticulum is responsible for the translation and folding of proteins and the expression of lipids.

On the level of tissues, the establishment of spatial order is one of the most important tasks in embryonic development [2]. Starting from a homogeneous cluster, cells differentiate to a variety of different forms of tissue. But how can cells which share identical genetic information develop into tissue as different as, for example, nerve fibers or muscle cells? In the case of the embryogenesis of the fruit fly *Drosophila melanogaster* the signal for cell differentiation comes from the mother. She releases a substance, the morphogen Bicoid, which diffuses into the embryo tissue [3–7]. As a result of the combined effect of the maternal source, diffusion and degradation, the concentration decreases monotonically depending on the distance. The morphogen thereby provides positional information to the gene regulatory network in the cells constituting the embryo. Such a smooth concentration can, however, not mediate an unambiguous yes/no decision. To this end, the signal is modulated in a nonlinear way. Coupled to the signal substance is a protein called Hunchback, whose concentration decides which cells later develop to the fly's head and which become part of the fly's body. A sharp border arises if the concentration of the protein changes rapidly within a small, confined region in the cell cluster [8–15]. The division of the embryo into a region, where the protein Hunchback is present and a region where it is absent is one of the most striking examples of order in nonequilibrium systems. Hunchback expression in *Drosophila melanogaster* provides an example for how spatial patterns can be established by the spatio-temporal control over the cells' inner status. An alternative mechanism for establishing spatial order in cellular populations consists in changing the relative positions of different cell types [Fig. 1.1(b)].

On even larger time scales, millions of years of evolution have led to a high degree of

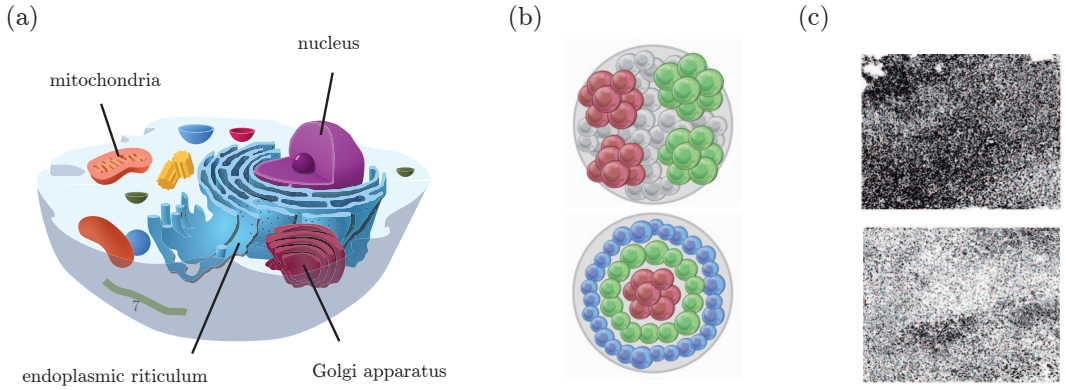

Figure 1.1: Self-organization in biological systems is a common phenomenon on various scales. (a) The illustration of a typical animal cell shows that these cells consist of highly differentiated sub units, the so-called organelles. The nucleus, for example, stores genetic information and controls the cell's behavior. The Golgi apparatus packages proteins before they are sent to their destination. Illustration has been taken from Ref. [16]. (b) On an inter cellular scale the spatial self-organization of cells is a basic prerequisite for developmental processes. Cells can arrange by two different mechanisms. First, the cells' status may change depending on their position in the embryo (top). Secondly, different cells may change their relative positions (bottom). The illustrations have been taken from Ref. [17]. (c) Self-organization on ecological scales can, for example, be found in vegetation clusters in the Kalahari. The pictures show satellite images of 4 km^2 large regions at different places in the Kalahari Transect in southern Africa. Black dots indicate trees. The upper picture is taken at a location with high precipitation and a high density of trees. The lower picture is taken at a location with less rainfall and a lower density of vegetation. In both cases, trees tend to form clusters. Interestingly, the distribution of these clusters obeys a power law, indicating that the observed patterns can be understood in terms of simple, theoretical models. The pictures have been taken from Ref. [18].

order in the genetic information carried by organisms. Not only are there mechanisms to counteract the favor of disorder induced by mutations. Also, evolution has led to high degree of differentiation and specialization of organisms. The sheer number of different species becomes strikingly clear, when one considers that a 30-g sample of soil from a Norwegian forest has been estimated to contain about 20,000 common bacterial species and about 500,000 rare ones [19]. The huge amount of biodiversity present on earth seems, however, to contradict Darwin's principle stating that only the fittest species survives. Several mechanisms have been proposed for how this seeming contradiction is circumvented in ecological systems. The most obvious explanation states that different species occupy different ecological niches and therefore do not compete for the same resources. However, this is not always the case. A striking example is given by plankton: a large number of species share the same ecological niche, in this case solar energy and minerals dissolved in water. At the first glance this

diversity is counter-intuitive and hence referred to as the *paradox of the plankton* [20]. Understanding the mechanisms that lead to the maintenance of a species diversity that is larger than the amount of available ecological niches is still a challenge in theoretical ecology.

Non-hierarchical interactions between species have been proposed as a facilitator of biodiversity in spatially extended systems [21–29]. For example, bacterial model systems comprised of three genetically distinct strains of *Escherichia coli* have been shown to exhibit stable three-strain coexistence in spatially extended homogeneous environments [26, 27]. This basic motif of cyclic dominance is metaphorically described by the rock-paper-scissors game, where rock crushes scissors, scissors cut paper, and paper wraps rock. Recent theoretical studies have explored how spatial order [28–30], and the structure of the interaction network as well as the strengths of its links [31] affect the maintenance of species diversity.

All these biological examples evolve on vastly different spatial and temporal scales. They have in common that spatial order enables functional differentiation. In the language of statistical physics, these systems produce negative entropy: they reduce the degree of uncertainty regarding their physical configuration. Indeed, according to Ludwig Boltzmann a negative flux of entropy may be thought of as a physical characterization of living systems [32]:

> *"The general struggle for existence of animate beings is not a struggle for raw materials – these, for organisms, are air, water and soil, all abundantly available – nor for energy which exists in plenty in any body in the form of heat, but a struggle for [negative] entropy, which becomes available through the transition of energy from the hot sun to the cold earth."*

Of course, it is to be understood that the second law of thermodynamics also holds for biological systems. The entropy that is lost by, for example, establishing the inner organization of a cell is transported to its environment in the form of heat. As a result, constantly work is performed on such biological systems and they are therefore out of equilibrium. The nonequilibrium nature of most biological systems is responsible for the multitude of fascinating phenomena that can be observed in living systems. However, the theoretical understanding of such systems is often difficult. While in equilibrium physics the Boltzmann distribution provides a full characterization of the steady state, it is still unknown how a corresponding quantity could look like in systems far from equilibrium.

On the other hand, biological systems are characterized by being inherently stochastic. In other words, random forces are equally important as deterministic forces. Stochasticity is a theoretical concept that is used when for a system comprising a large number of degrees of freedom the level of description is reduced to a few relevant quantities. The remaining degrees of freedom are summarized in random fluctuations around the average values of these quantities [33, 34]. As an example, a mathematical model of an ecosystem would comprise only the number of individuals of each species

and not the internal functionality of the organisms under consideration. Instead, one would consider the movement and the times of interaction between individuals as random such that the species abundances become random variables. Similarly, encounters of molecules in subcellular processes, or cell division and motion in bacterial populations, are considered being randomly distributed. The central limit theorem states that the amplitude of these fluctuations decreases with one over the square root of the number of entities in the system. Biological systems typically comprise a rather small number of constituents as compared to thermodynamic systems, hence fluctuations are strong and a description purely by average values is not always feasible.

These two characteristics, being far from equilibrium and the importance of stochastic fluctuations, are common to many biological systems on a variety of different scales. This fact suggests that all these processes may be understood in the same theoretical framework. Mathematically, such a framework is given by stochastic many-particle systems. For spatially extended systems as they arise in biology, *reaction-diffusion systems* provide one of the most important frameworks to study the dynamics of systems far from equilibrium [35]. Reaction-diffusion systems are simple examples of nonequilibrium stochastic systems of classical particles. These particles are generally labeled by their species, A, B, C, ..., which may be thought of as corresponding to different chemical reactants, biological species or more abstract entities. As the name suggests, reaction-diffusion systems comprise two types of dynamics: First, particles perform Brownian motion with associated diffusion constants D_A, D_B, D_C, ... Secondly, particles react at prescribed rates according to certain dynamical rules. These rules are often expressed in the notation of chemical reactions, e.g. $A+B \to C$, and in the most interesting cases the dynamics that follows from these reactions is nonlinear. These reactions are diffusion-limited; i.e., they are purely local and the particles have to diffuse around to find each other and react. In an experimental setup this could mean that the reactants should not be stirred. Instead one could imagine allowing the particles to diffuse in a gel or substrate. The potential applications of these ideas are vast. As the notation implies, reaction-diffusion system are naturally found in chemistry, but also in biology, geology, physics and ecology.

Simple reaction-diffusion models have been successfully employed to understand a variety of phenomena in nearly all fields of science [35, 36]. Figure 1.1(c) shows vegetation patterns in the Kalahari. These patterns are distributed according to a power law, which indicates that the ecosystem can be understood by simple interaction rules. Another example for the success of simple reaction-diffusion models are coalescence processes. Particles that perform random walks on a lattice and merge upon encounter [Fig 1.2(a)] have been used to describe phenomena as diverse as coagulation of colloids [37, 38] and genealogical trees [39–43]. On the other hand, two-species processes of the form $AB \to AA$ mimic expansion processes [Fig. 1.2(b)], for example, of advantageous genes or epidemic spreading [36, 44, 45]. Reaction-diffusion processes comprising three types of particles have become popular as prototype mod-

(a) Coalescence (b) Invasion (c) Cyclic dominance (d) Directed percolation

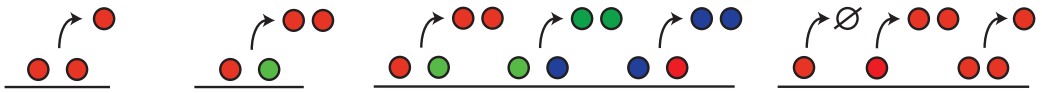

Figure 1.2: Simple reaction-diffusion systems have successfully been used to describe a variety of phenomena. (a) In coalescence processes, diffusing particles merge upon contact. Such processes have been employed to, for example, understand the coagulation of colloids or genealogical trees. (b) Invasion processes describe the spreading of advantageous genes or infectious diseases. Active particles (red) reproduce upon consumption of inactive particles (green). Cyclic dominance between three species (red, green, blue) is used as a paradigmatic model for more complex ecosystems. Each species outcompetes another species in a cyclic manner. (d) The directed percolation process comprises death, fission and coalescence of particles. It is of special importance in nonequilibrium physics as many other systems behave similarly at certain "critical" parameter values.

els for ecosystems [25, 28–30, 46–73]. In these models, three species A, B, and C interact cyclically, as in the popular children's game "Rock-Paper-Scissor": A beats B, B beats C, and C again beats A [Fig. 1.2(c)]. For predator-prey type reactions the dynamics is defined by three dynamical rules,

$$AB \to AA\,, \tag{1.1a}$$
$$BC \to BB\,, \tag{1.1b}$$
$$CA \to CC\,. \tag{1.1c}$$

Reaction-diffusion models comprising cyclic interactions have recently attracted considerable attention as they predict the loss of biodiversity above a certain threshold value in the diffusion constant [28–30, 69, 73]. The dynamics of cyclic reaction-diffusion systems is surprisingly rich, making these models also interesting from a purely theoretical point of view. Last, directed percolation models mimic fluid flow in porous media. The significance of these models lies in the fact that they serve as prototype models for many nonequilibrium systems. As in equilibrium physics, nonequilibrium systems behave surprisingly similar near certain "critical" values of the parameters. Specifically, many nonequilibrium models show the same critical behavior as models for directed percolation [36]. In fact, directed percolation is probably the most fundamental class of nonequilibrium phase transitions. As is depicted in Fig. 1.2(d), a reaction-diffusion representation of directed percolation comprises three processes,

$$A \to \emptyset\,, \tag{1.2a}$$
$$A \to AA\,, \tag{1.2b}$$
$$AA \to A\,, \tag{1.2c}$$

which can be interpreted as death, fission and coalescence of particles.

In this thesis, we are interested in how order is established and maintained in biological systems at cellular and ecological scales. We follow the great tradition of theoretical science and study biological problems in terms of simple, abstract models. While these models are not meant to give quantitative descriptions of concrete biological systems, they enable use to gain a deep understanding of the mechanisms underlying biological processes. Our general results may explain basic mechanisms of a variety of biological systems, with possible implications for morphogenesis, cell biology, ecology and biotechnology.

Biodiversity and evolution

In the first part of this thesis, we are interested in the dynamic processes that lead to the maintenance of biodiversity and which are responsible for the extinction of species. The emergence and stability of ecosystems relies on the fact that they contain a multitude of species. However, how species diversity in ecological systems can be maintained is still an open question. Mathematically, the loss of biodiversity corresponds to the system resting in *absorbing states* of the stochastic dynamics. These states can be reached, but never be left by the dynamics. Ultimately the system will always rest in such an absorbing state, which means that biodiversity is lost inevitably. How these states are reached and on what time scales is highly relevant for ecology and the understanding of nonequilibrium physics in general. If one is not too far from equilibrium, fluctuations are governed by the same laws that hold in steady state and the transient is typically an exponential decay. In absorbing states, however, no fluctuations are present. For simple reaction-diffusion systems power-law decays into absorbing states have been found [36]. We investigate the relaxation process into absorbing states in a paradigmatic ecological model comprising cyclic interactions between three species. By calculating the full distribution of first passage times into the absorbing states, we show that the transitions into the states of extinction are much more complex than previously thought. A theoretical understanding of these systems is often difficult, because they comprise a large number of degrees of freedom. We show that a few degrees of freedom suffice to characterize the essential features of such systems. This approach allows us to obtain new insights into the mechanisms responsible for the transient maintenance and the ultimate loss of biodiversity.

Genetic diversity and phenotypic heterogeneity

Order does not only play a central role in the spatial organization of ecosystems. As it can be observed in the high degree of specialization of many organisms, it is a relevant concept at the genetic level as well. However, a high degree of specialization makes organisms vulnerable to environmental changes. How can organisms specialize

to an ecological niche and at the same time be able to survive in a variety of different conditions? Many bacteria and viruses counteract their genetic specialization by switching between several phenotypic states [74–98]. As an example, phenotypic switching is a strategy commonly employed by pathogens to evade a host's immune system. Some bacteria stochastically switch between phenotypic states to minimize the risk of population extinction due to an attack with antibiotics [75, 95]. Inspired by these phenomena, we ask how genotypic and phenotypic heterogeneity co-evolve in microbial populations.

To this end, we consider reaction-diffusion systems from a new perspective. We study heterogeneous, stochastic many-particle systems. The basic idea is that each particle is endowed with distinct properties. We first consider the interplay between genetic diversity and phenotypic heterogeneity in spatially extended populations comprising cyclic interactions and more complex food webs. We find that the survival of genetic diversity and phenotypic heterogeneity qualitatively depends on the degree of mixing. For small mobilities, phenotypic specialization is favored by the evolutionary dynamics, whereas for large mobilities phenotypic generalization can persist. The survival of phenotypic heterogeneity also significantly depends on whether competition is direct, as in predator-prey relations, or indirect, mediated through the limited availability of resources.

Understanding the conditions that facilitate the persistence of cooperation is one of the classic problems in evolutionary biology. The dilemma of cooperation expresses the naive point of view that cooperation should not be robust against "cheating" mutants. Despite the temptation to defect, cooperation is frequently found in biological systems. As an example, the metabolism of *Pseudomonas aeruginosa* relies on the consumption of iron. These bacteria therefore produce an iron-scavenging siderophore which may pass the cell membrane and is therefore available to other bacteria. As siderophore production is metabolically costly the population should in principle be susceptible to the invasion by mutants who do not produce the siderophore [99]. Mathematically, the dilemma of cooperation is often formulated in the framework of evolutionary game theory, where such situations are described in terms of the *prisoner's dilemma*.

On the other hand, many bacterial species, such as *Bacillus subtilis*, are endowed with flagella which may be utilized to sense the cell's environment. Most importantly, flagella are, however, used for locomotion. For *B. subtilis* it has been found that in the mid exponential growth phase clonal populations consist of both, swarming cells that are propelled via flagella, and non-motile cells, which after division do not separate from each other, thereby forming long chains of cells [84, 94]. Cells in the motile state do not divide. This bet-hedging strategy allows the population to exploit its current location and at the same time disperse to new, possibly more favorable niches. As a result, colonies of *B. subtilis* are heterogeneous with respect to the cells' motility. The underlying mechanism behind this behavior is a bistable switch: in motile cells the alternative sigma factor σ^D is in the ON state, while for non-motile

cells σ^D is in the OFF state. The switching between these states is purely stochastic. The statistical weight of the state, and thereby the fractions of the colony in each of these states, can be biased by the regulatory proteins swrA and swrB [84, 94].

Motivated by these findings, we study the influence of heterogeneous motility on the persistence of cooperation. We show that with this kind of genetic diversity and phenotypic heterogeneity cooperation is possible under much harsher conditions. The composition of the population after many cell cycles qualitatively depends on the cost of cooperation and the average, initial motility in the population. While defectors take over the population if the cost for cooperation is high, slow cooperators dominate for intermediary costs. If, in contrast, the cost for cooperation or the average motility is low, fast cooperators tend to constitute the majority of the population for large times.

When bacteria are placed on a petri dish one finds that due to the combined effect of cell division and motility the populations expands radially. Such expansion processes have been observed in a variety of biological contexts, from the proliferation of advantageous genes to the spreading of infectious diseases. As mentioned above, these processes are often studied in terms of simple reaction-diffusion models mimicking invasion [45]. Motivated by the discovery of phenotypic heterogeneity in motility, we finally study heterogeneous versions of invasion processes. We find that the spreading process favors certain genotypes and ultimately leads to a loss of genetic diversity in the front region.

Formation of static boundaries

Another example for the importance of functional differentiation arises in the development of embryos. Starting from a homogeneous cluster, cells differentiate to a variety of different forms of tissue. But how can cells which share identical genetic information develop into tissue as different as, for example, nerve fibers or muscle cells? In his seminal work, Alan Turing investigated how spatial differentiation can be achieved out of a spatially uniform state [100]. He showed that the formation of regular structures is possible by a very simple mechanism comprising diffusion and nonlinear reactions. His findings provide a mechanism for producing a variety of regular patterns, ranging from the periodic arrangement of tentacles around the mouth of the Hydra organism to zebra stripes [35].

In the development of the fruit fly *Drosophila melanogaster*, the mother releases a substance which diffuses into the embryo tissue. As the concentration of this morphogen decreases monotonically in space it provides positional information for the gene regulatory networks in the the embryo's cells [3–7]. By nonlinearly processing the positional signal the embryo is able to establish a sharp border of the protein Hunchback which again serves as an input for downstream regulatory processes. In particular, cells, in which the protein Hunchback is present at a sufficiently high

concentration later form the embryos head, while cells, where this protein is absent, later form the embryo's trunk [8–13, 15]. The division of the embryo into a region, where the protein Hunchback is present and a region where it is absent is one of the most striking examples of order in nonequilibrium systems. The stable positioning of this domain border is pivotal to the embryo's fate. However, it is naturally subject to extrinsic perturbations due to, for example, a varying temperature, and intrinsic noise due to a finite number of particle involved in the biochemical reactions. How does the embryo cope with these two sources of destabilization?

In the second part of this thesis we investigate the problem of domain boundary formation from a theoretical perspective. We study a broad class of bistable systems subject to external gradients. These systems can be understood as coarse-grained gene regulatory networks comprising essential features of the much more complex networks found in biology. Under certain conditions, these systems allow for the localization of wave fronts, which then constitute sharp domain boundaries. We study the conditions under which wave localization is possible and find optimal parameter values for the stability of such fronts to extrinsic perturbations and intrinsic noise. In particular, we show that increasing binding cooperativity in self-activation broadens the parameter regime where wave localization becomes possible and thereby increases the robustness of the localization mechanism. Interestingly, there is a trade-off between the stability of the wave front to extrinsic and intrinsic perturbations. While weak self-activation or low birth rates enhance the stability with respect to extrinsic perturbations, defocusing due to intrinsic noise is minimized for strong self-activation. The latter also increases the spatial precision of the signal transmitted by the front to downstream processes. Moreover, we showed that processing input from external sources with a cooperative gene activation mechanism generally enhances the front's stability even far away from the source. Surprisingly, while cooperativity in external activation increases the front's stability with respect to extrinsic perturbations, the opposite holds true for self-activation.

The conflict between intrinsic and extrinsic stability affects, for example, the design of gene circuits in developmental systems. We expect these general results to be important guiding principles in the context of biological pattern forming systems, such as cell polarization or the segmentation of embryos.

Part I

Evolution of genetic diversity and phenotypic heterogeneity in mobile populations

2 Coexistence in populations of cyclically competing species

Ecosystems can only emerge and persist if they contain a multitude of species. But how diversity in ecological systems can be maintained is still an open question. Indeed, Darwin's principle "survival of the fittest" seems to contradict the rich variety of species found on earth. As an example, it has been estimated that a 30 g sample of Norwegian soil contains some 20,000 common bacterial species and about 500,000 rare ones [19]. From a naive understanding of Darwinian evolution, when species share the same resources they compete and ultimately only the fittest species survives. This argument was first formulated by G. F. Gause. In theoretical ecology, it is known as the *competitive exclusion principle* [101] and it applies to situations where different species share the same resources. Following this argument, a mechanism allowing for the coexistence of species could be that different species occupy different ecological niches. However, this is not always the case. A striking example is given by plankton, where a huge amount of species share the same ecological niche, in this case solar energy and minerals dissolved in water. At the first glance this diversity is counter-intuitive and hence referred to as the *paradox of the plankton* [20]. Understanding the mechanisms that lead to the maintenance of a species diversity that is larger than the amount of available ecological niches is still a challenge in theoretical ecology.

Cyclic interactions can be found in a variety of places in nature. Two prominent examples include competition between mating strategies of lizards and cyclic dominance in three strains of *E.coli* bacteria. First, cyclic competition has been observed in the Inner Coast Range of California, where lizard males can follow three different mating strategies [Fig. 2.1(a)]. The mating strategies differ in the way lizards defend territories for mating. The first type of males are little aggressive and guard smaller territories. These lizards invade populations of "sneaker" males, who do not defend territories. A third type is aggressive and defends large territories. Lizards of this type are inferior to the sneakers but they can invade individuals following the first mating strategy. By evaluating the frequency of the three different strategies over several years, it was found that these three types of mating behavior stably coexist, exhibiting oscillations in the relative number of lizards following each strategy [23]. Furthermore, the spatial arrangement of the three mating strategies has been investigated. It was found that lizards of the sneaker type preferably form clusters around the territories of the aggressive individuals. Probably it is easier for them to invade the large territories of the aggressive lizards as compared to the small territories of the less aggressive ones. In interesting detail is that the type of mating strategy a lizard follows is easily visible by the color of its throat. Cyclic dominance has also been investigate in a model systems of three strains of *E.coli* bacteria [Fig. 2.1(b)].

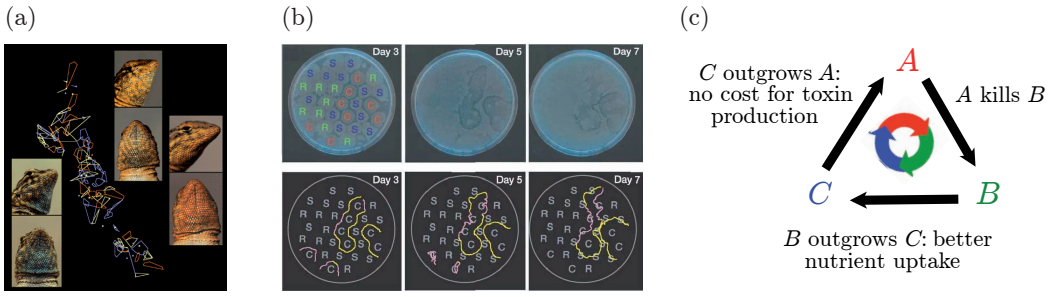

Figure 2.1: (a) Three types of mating stategies of lizards in California effectively compete each other cyclically. The mating strategies differ in the way lizards defend territories for mating. The three types of mating behavior are connected to skin polymorphisms. Blue throated males (left) are little aggressive and guard smaller territories. The blue throated lizards invade populations of "Sneaker" males, who do not defend territories and who can be identified by a yellow throat (middle). A third type with an orange throat (right) is aggressive and defends large territories. Lizards of this type are inferior to the sneakers but they can invade individuals following the first mating strategy. The picture has been reproduced from Ref. [102]. (b) Three strains of E.coli coexist on a Petri-dish by forming spatial structures. The three strains, denoted by C, S, and R, compete cyclically. The pictures have been altered and taken from [27]. (c) The rock-paper-scissors interaction scheme illustrated for cyclic competing *E.coli* strains. Type A carries a "col" plasmid letting them produce the toxin colicin. This toxin harms colicin-sensitive bacteria (type B). Bacteria of type C are colicin-resisant at the expense of a lower general fitness level.

E.coli is endowed with plasmids encoding the production and the immunity to certain toxins, the so called colicins. *E.coli* strains A producing such colicins harm a colicin-sensitive strain B of *E.coli*. The latter strain does not have the metabolic cost for immunity and therefore it outgrows a third strain C, which is resistant to the colicin. The C strain again outgrows the colicinogenic A strain, which not only has cost for producing the colicin, but also for the resistancy against it [27]. Cyclic interactions in strains of *E.coli* bacteria are illustrated in Fig. 2.1(c).

2.1 Theoretical studies of cyclically interacting systems

These experimental studies of cyclically interacting species have motivated a large body of theoretical literature exploring the role of cyclic interactions in ecological systems [25, 28–30, 46–52, 54–67, 69–71, 103–111]. Most theoretical work on cyclically interacting systems does not intend to quantitatively describe real biological systems. Rather, simple, paradigmatic models are employed to understand the basic mechanisms behind the rich variety of phenomena exhibited by these models. Nevertheless, extended versions of these prototype models are currently used to quantitatively describe experimental observations in *E. coli* populations. Most of the theoretical

work has focused on two paradigmatic examples of three-species models with cyclic interactions. In the first class of models, the direct competition between two individuals leads to the immediate replacement of the weaker species by the stronger species [25, 46–52, 54–61, 66, 105–109, 112]. This type of competition, where selection and reproduction are combined into a single process, is similar to the classical two-species Lotka-Volterra model [113, 114]. The interaction scheme of this cyclic Lotka-Volterra model may be summarized by a set of chemical reactions between the three species A, B, and C:

$$AB \to AA, \quad BC \to BB, \quad CA \to CC\,. \tag{2.1}$$

If the number N of particles is large and for a sufficiently small lattice spacing stochastic fluctuations can be neglected. The spatio-temporal dynamics is then described in terms of a set of partial differential equations for the concentrations $a(\mathbf{r},t)$, $b(\mathbf{r},t)$, and $c(\mathbf{r},t)$,

$$\partial_t a = \nu a(b-c) + D\Delta a\,, \tag{2.2a}$$
$$\partial_t b = \nu b(c-a) + D\Delta b\,, \tag{2.2b}$$
$$\partial_t c = \nu c(a-b) + D\Delta c\,, \tag{2.2c}$$

with ν being the reaction rate.

In the second class of models, originally proposed by May and Leonard [71], selection and reproduction are two separate processes. An interaction between two individuals of different type leads to the death of the weaker species and thereby to empty spaces. Reproduction then follows as a second process which recolonizes this empty space. Here, competition is mediated through the limited availability of resources. The ensuing reaction scheme reads:

$$AB \to A\emptyset, \qquad BC \to B\emptyset, \qquad CA \to C\emptyset\,, \tag{2.3a}$$
$$A\emptyset \to AA, \qquad B\emptyset \to BB, \qquad C\emptyset \to CC\,. \tag{2.3b}$$

In the continuum limit and for a large number of particles the dynamics of the spatial May-Leonard model is described by a set of reaction-diffusion equations,

$$\partial_t a = -\sigma ac + \mu a(1-\rho) + D\Delta a\,, \tag{2.4a}$$
$$\partial_t b = -\sigma ba + \mu b(1-\rho) + D\Delta b\,, \tag{2.4b}$$
$$\partial_t c = -\sigma cb + \mu c(1-\rho) + D\Delta c\,, \tag{2.4c}$$

where μ and σ are the rates for reproduction and selection, respectively. Analytical progress on these equations has been made by a mapping to the complex Ginzburg-Landau equation [28, 29].

2.1.1 Stability of cyclic population models

Both of these models exhibit absorbing states corresponding to situations where all but one species have died out. Due to the inevitable demographic fluctuations in systems with a finite number of individuals these absorbing states will be reached within a finite time. The mean first passage times into the absorbing states strongly depend on the type of model and the ecological scenario under consideration.

The stability of an ecological system can be investigated by studying the scaling of the mean first passage times into the absorbing states with the system size N. In well-mixed systems, the typical extinction time T was found to scale linearly with N for the cyclic Lotka-Volterra model [55, 58, 61, 73, 115, 116] and logarithmically for the May-Leonard model [28]. The reason for the difference is the different nature of the phase space orbits characterizing the nonlinear dynamics of these two models [110]. While the phase portrait of the cyclic Lotka-Volterra model exhibits neutrally stable orbits, the May-Leonard model is characterized by heteroclinic orbits, i.e. these orbits spiral out from an unstable reactive fixed point and finally end in a stable fixed point. For neutrally stable orbits, the stochastic dynamics performs an unbiased random walk which implies that $T \propto N$. In contrast, unstable orbits generate a drift of the trajectories in phase space towards the boundary such that the extinction process towards the absorbing states is exponentially accelerated with $T \propto \ln N$ [31, 48, 110].

Spatially extended systems have been found to exhibit a radically different behavior. There, the scaling of the mean time to extinction with the population size strongly depends on the degree of mixing. In particular, it has been shown for both models that there exists a mobility threshold below which extinction times scale exponentially in the system size. For the May-Leonard model this has been attributed to the existence of dynamic spatial patterns, which emerge as a result of the local nature of reactions and internal noise [28–30, 73]. Above a certain mobility the characteristic wave length of these patterns exceeds the system size, effectively rendering the dynamics well-mixed. In this regime, extinction occurs rapidly. In the Lotka-Volterra model, spatial patterns are unstable as a result of an Eckhaus instability [66, 73]. However, below a mobility threshold biodiversity is still maintained by strong spatial correlations. Further work has extended these findings to asymmetric reaction rates [51, 60] and more complex interaction networks [31, 54, 117, 118]. In a niche model it has been shown that interaction networks with a high connectivity and a hierarchical or cyclic interaction structure lead to increased diversity [119, 120]. For the May-Leonard and the cyclic Lotka-Volterra model it was found that spatially inhomogeneous reaction rates have only minor effects on the dynamics [56, 63]. For the classical two-species Lotka-Volterra model, analytical studies have been performed to understand the underlying mechanism leading to the stabilizing correlations [121, 122]. These studies argue that the stabilization can by understood by the desynchronization of diffusively coupled oscillators. The desynchronization is a result of the combined effect of noise, migration and the dependence of the oscillations' frequency upon

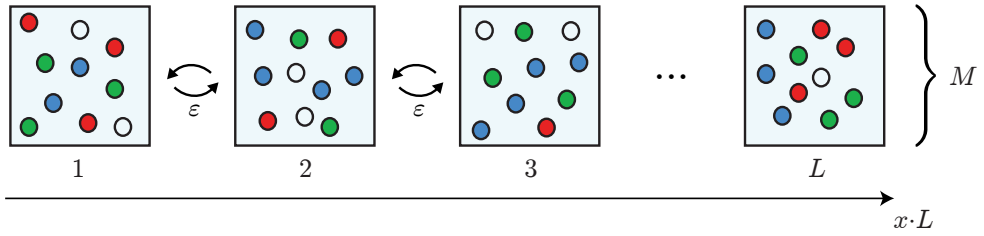

Figure 2.2: In our model we consider a coarse-grained lattice in d spatial dimensions. Reactions occur within L^d well-mixed volumes, each containing M particles. M may therefore be viewed as the carrying capacity of the ecosystem. With a rate ϵ two particles of neighboring blocks are exchanged, which macroscopically leads to diffusion with an effective diffusion constant $D = \epsilon L^{-2}/d$. The system possesses an effective size $N = M \cdot L^2$. As long as the lattice spacing L^{-1} is much smaller than the correlation length, two equivalent ways of performing the thermodynamic limit exist: $L \to \infty$ or $M \to \infty$.

their amplitude.

2.1.2 Dynamic processes leading to extinction

For the one-dimensional May-Leonard model the dynamics leading to extinction has been studied in greater detail. If the individuals diffuse only little or do not diffuse at all, coarse-graining of species' domains has been identified as the dominant dynamical process leading to extinction [56, 59, 106, 107]. With increasing diffusion constant other types of collective excitations become important [69]. The dynamics to extinction is then surprisingly rich, comprising rapid extinction, global oscillatory behavior, and traveling waves. The latter involve oscillating overall densities, *i.e.* the domain sizes for the different species change periodically. The statistical weights of these dynamical regimes change qualitatively at threshold values of the mobility and the system size. Taken together, it has turned out that the dynamics in the one-dimensional May-Leonard model is highly complex, much more than one would naively anticipate. For the two-dimensional May-Leonard and cyclic Lotka-Volterra models we recently provided a comprehensive characterization of the dynamic processes leading to extinction [73].

2.1.3 A stochastic lattice gas model

The numerical evaluation of first passage times is computationally extremely costly. As mentioned earlier, the mean times to extinction scale, in the worst case, exponentially with the system size. We therefore employ a coarse grained model, which allows us to study system size dependence for reasonably large systems, cf. Fig. 2.1.

In particular, we consider one- or two-dimensional square lattices and employ periodic boundary conditions. The spatio-temporal dynamics is not significantly altered when one considers hexagonal lattices. On the other hand, the "macroscopic" lattice structure, i.e. the boundary conditions, may affect the results. On hexagonal lattices with hexagonal boundaries and corresponding periodic boundary conditions, the details of some spatio-temporal patterns and the specific critical values change slightly. However, one observe a very similar behavior of the global dynamics and the observed attractors. Note, however, that planar waves and the pairwise appearance of spirals are not observed for absorbing boundary conditions. We also studied the dynamics on percolated lattices, which gives rise to multifractal behavior and thereby to an entirely new phenomenology. However, understanding the dynamics on unpercolated square lattices is paramount for understanding the dynamics on more complex surfaces. The linear dimension of the lattice is taken as the basic length unit such that the lattice constant $a = 1/L$ with L the number of lattice sites along each axis. At each site a fixed number M of individuals (A, B, C or empty spaces $\emptyset$) are located. M may be viewed as the carrying capacity of a lattice site, which is here considered well-mixed. In addition, individuals are also able to move on the lattice. While the reactions, Eqs. (2.3a)-(2.3b) and (2.1), are assumed to occur on the same lattice site, the individuals' mobility is implemented as an exchange process at a rate ϵ between neighboring sites, $XY \xrightarrow{\epsilon} YX$, where X and Y denote species A, B and C or empty spaces $\emptyset$. Macroscopically the nearest neighbor exchange process leads to diffusion with an effective diffusion constant $D = \epsilon L^{-2}/2$ [28–30][1].

Trajectories of the ensuing stochastic dynamics can be computed by employing a sequential updating algorithm: At each simulation step an individual is chosen at random. This individual then either reacts with another randomly chosen individual from the same site, or it is exchanged with an individual of a neighboring stack; each stochastic event occurs with probabilities corresponding to the respective reaction rates μ, σ, ν and ϵ. Typical snapshots of the stochastic simulations for the May-Leonard model in two spatial dimensions are shown in Fig. 2.3. The snapshots demonstrate the variety of spatio-temporal regimes which can be found in models comprising cyclic interactions.

2.2 Effective free energy

The differentiation of an ecosystem into stably coexisting species is a necessity for the development of life. Such functional differentiation is established through the formation of complex patterns. In particular, the maintenance of biodiversity is

1 As two particles are involved in migration, it also induces some additional nonlinear reaction terms, which we neglect here [123, 124]

originated in the formation of spatially segregated domains of species [22, 25, 28]. This form of differentiation is contingent upon an ongoing flux of entropy to work against the increase of entropy. As a result, constantly work is performed on such systems, which are therefore far from equilibrium. Non-equilibrium systems impose a challenge for the theoretical physicist: resulting from the absence of time reversal symmetry the fluctuation probability is not Boltzmann distributed, i.e. there is no Gibbs measure as in equilibrium systems.

Generally, systems with many degrees of freedom are studied by reducing the description to few degrees of freedom, which comprise the essential characteristics of the system. As an example, in statistical physics such a reduction is given by the free energy as a function of the natural variables. Similar conceptually, the dynamics of well-mixed nonlinear systems is characterized by attractors in the phase plane. Close to thermodynamic equilibrium, the Onsager theory states that relaxation towards equilibrium is described by the same laws that govern thermal fluctuations in the equilibrium steady state. However, it is still unclear how an appropriate reduced description could look like for spatially extended stochastic many-particle systems far from equilibrium.

In our articles, we show that for stochastic many particle systems with absorbing states such a reduced description is given by attractors of the nonlinear dynamics of the overall particle concentrations, the global attractors. In particular, to gain insight into the mechanisms responsible for these qualitatively different spatio-temporal patterns and how they determine the longevity of biodiversity in the population, we studied the global phase portrait of the dynamics. The dynamic processes leading to the transient maintenance of biodiversity are closely linked to attractors of the nonlinear dynamics for the overall species' concentrations

$$\Big(\overline{a}(t),\overline{b}(t),\overline{c}(t)\Big) = \int \Big(a(\mathbf{x},t),b(\mathbf{x},t),c(\mathbf{x},t)\Big)\mathrm{d}^2x\,. \tag{2.5}$$

The characteristics of these global attractors change qualitatively at certain threshold values of the mobility, and depend on the relative strength of the different types of competition between species. The attractors give information about the scaling of extinction times with the system size and thereby the stability of biodiversity. In detail, the negative logarithm of the probability $P(\overline{a},\overline{b},\overline{c})$ to find the system in a specific global state $(\overline{a},\overline{b},\overline{c})$ before reaching one of the absorbing states is projected onto the invariant manifold: We define an effective free energy as the negative logarithm of the probability $P(\overline{a},\overline{b},\overline{c})$ to find the system in a specific global state $(\overline{a},\overline{b},\overline{c})$ before reaching one of the absorbing states,

$$\mathcal{F}(\overline{a},\overline{b},\overline{c}) \equiv -\ln P(\overline{a},\overline{b},\overline{c}), \tag{2.6}$$

The quantity $\mathcal{F}$ can be considered as an effective potential in the following sense: When instead of the mean-field reaction term, which is in this case given by the reaction term of the complex Ginzburg-Landau equation, one uses $\mathcal{F}$ as a "renormalized" potential for a Ginzburg-Landau theory one obtains a reaction-diffusion

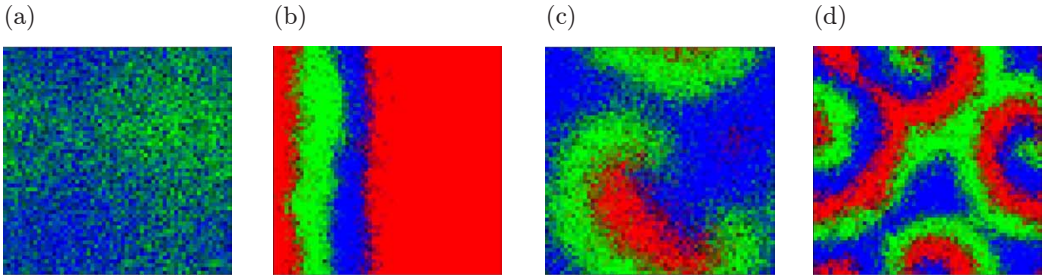

Figure 2.3: Typical spatial patterns in the May-Leonard model. Color denotes the concentration of species A, B and C, with red signifying a site dominated by species A, green a site dominated by species B, and blue being a site dominated by species C. (a) For large diffusion constants ($D = 1.5 \cdot 10^{-3}$), the we find global oscillations with periodic switching between states with mainly one species present. (b) For intermediate values of the diffusion constant ($D = 5 \cdot 10^{-4}$), we observe planar traveling waves. Here, two of the domains take a characteristic domain size dictated by the diffusion constant. The third domain then occupies the rest of the system. (c), (d) For even smaller diffusion constants ($D = 3 \cdot 10^{-4}$, and $D = 6 \cdot 10^{-5}$), pairs of rotating spirals appear. The vertices of these spirals move very slowly on a time scale much larger than the time scale corresponding to the propagation speed of their arms. The wave length of the spirals decreases when the diffusion constant is reduced. The system size for all snapshots was $L = 60$, and the carrying capacity for each site was chosen to be $M = 8$.

equation which gives a good description of the spatio-temporal dynamics. Long-lived spatio-temporal patterns correspond to regions of high probability on the manifold, and are termed *global attractors* of the spatio-temporal dynamics in the following. Equivalently, adapting terminology from statistical mechanics, these attractors may be viewed as minima of the "free energy landscape" $\mathcal{F}$. Of course, it is to be understood that these attractors are only metastable, *i.e.* while the system spends a long time in these states, ultimately demographic fluctuations will drive the system into one of the absorbing states. Intuitively, one may visualize those fluctuations as driving the escape of the dynamics from the minima in the "free energy landscape" into one of the absorbing states. We will later see that *qualitative* changes in the shape of these minima correspond to transitions in the nature of the dynamic processes leading to extinction and the mean times to extinction. These transitions should not be confused with non-equilibrium phase transitions. Rather they are to be considered as bifurcations in the nonlinear dynamics.

Figure 2.4 shows the free energy landscape of the two-dimensional May-Leonard model projected onto the invariant manifold of the rate equations, Eqs. (2.4a)-(2.4c). The global attractors correspond different dynamic processes, whose statistical weight changes with the diffusion constant D. We applied the method of global phase portraits to a generic class of cyclic populations models. We were able to gain new insight into the multitude of dynamic processes and transitions which leads to a

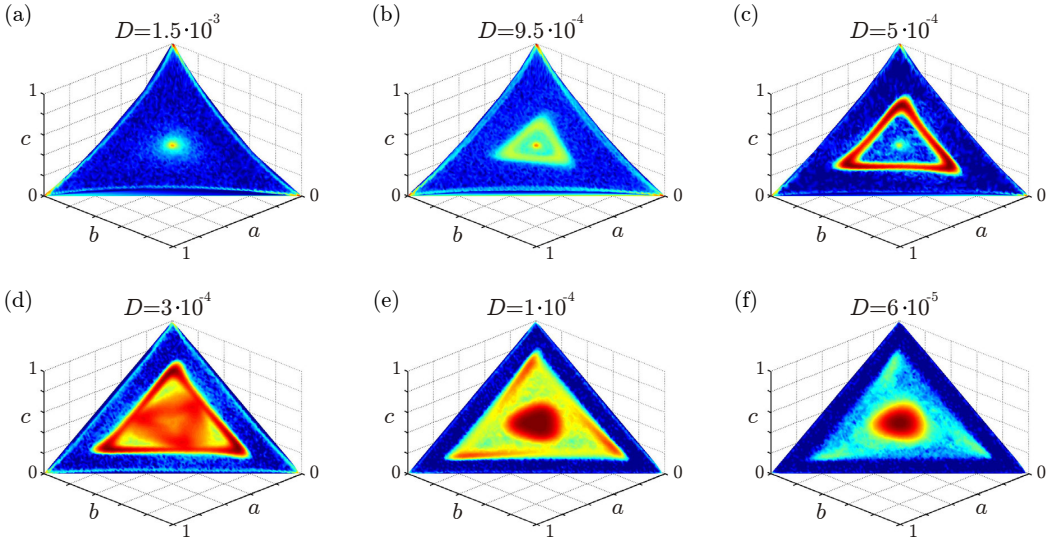

Figure 2.4: Free energy landscapes of the May-Leonard model for various values of the diffusion constant D. The dynamics of the overall densities $\overline{a}$, $\overline{b}$, $\overline{c}$ is strongly confined to the invariant manifold of the well-mixed model, Eq. (2.4). To study the mechanisms underlying the distinct spatio-temporal patterns found in the spatial, stochastic May-Leonard model we projected the probability for the overall densities onto the invariant manifold of the rate equations (2.4) for different values of the diffusion constant D. Color denotes the logarithmic probability to find the system globally in a specific state before reaching one of the absorbing states, such that red denotes a high probability, yellow a medium probability and blue a low probability. The absorbing states themselves are not part of the statistics. For large D, no stable spatial structures can form and the dynamics corresponds to the well mixed case, Eqs. (2.4). As D becomes smaller than $D \approx 9.5 \cdot 10^{-4}$ an attractor of the global dynamics emerges, effectively stabilizing the system against extinction. This attractor corresponds to planar, traveling waves with oscillating overall densities, and grows in radius with decreasing D due to a decreasing wavelength of the planar waves. For $D \leq 3 \cdot 10^{-4}$, a second attractor emerges, corresponding to rotating spirals. As a result of a decreasing wavelength of the spiral patterns the second attractor's radius decreases with the diffusion constant, while the attractor corresponding to the traveling waves diminishes. Parameters were $L = 60$ and $M = 8$. Each plot was averaged over at least 100 realizations of the stochastic spatial dynamics.

rather comprehensive understanding of one of the most surprising model classes in theoretical ecology.

2.3 Manuscripts and publications

2.3.1 Threefold way to extinction in populations of cyclically competing species

In our article "Threefold way to extinction in populations of cyclically competing species" by Steffen Rulands, Tobias Reichenbach, and Erwin Frey, *J. Stat. Mech.* L01003 (2011) we study the transitions to the absorbing states in a paradigmatic model of cyclically competing species. While extinction has previously been thought of as a coarsening process we show that these transitions unexpectedly are much richer. We identify three distinct dynamical regimes, governing the dynamics to extinction. Performing extensive stochastic simulations we present the full distribution of first passage times into these absorbing states. Interestingly, this distribution has a complex functional form, exhibiting two maxima, an intermediary asymptotic power law and an exponential tail. The scaling of these tails with the system size reveals a crossover behavior in the processes governing the asymptotic dynamics. Based on phenomenological arguments we provide calculations yielding the characteristics of the distribution of first passage times and its scaling with the system size.

2.3.2 Global attractors and extinction dynamics of cyclically competing species

The complex transition into the absorbing states made it clear that new methods are needed to systematically study the dynamics of cyclic population models in two spatial dimensions. In the paper "Global attractors and extinction dynamics of cyclically competing species", *Phys. Rev. E* **87**, 052710 (2013), by Steffen Rulands, Alejandro Zielinski, and Erwin Frey we introduce a "coarse grained" level of description which allows us to scrutinize the spatio-temporal dynamics of a generic class of cyclic population models. We thereby obtain a comprehensive understanding of the rich dynamic processes and transitions in these models. In particular, we study the population dynamics of three cyclically interacting species in two spatial dimensions. The interaction scheme comprises both, direct competition between species as in the cyclic Lotka-Volterra model, and separated selection and reproduction processes as in the May-Leonard model. We show that the dynamic processes leading to the transient maintenance of biodiversity are closely linked to attractors of the nonlinear dynamics for the overall species' concentrations. The characteristics of these global attractors change qualitatively at certain threshold values of the mobility, and depend on the relative strength of the different types of competition between species. They give information about the scaling of extinction times with the system size and thereby the stability of biodiversity. Specifically, we define an effective free energy as

the negative logarithm of the probability to find the system in a specific global state before reaching one of the absorbing states. The global attractors then correspond to minima of this effective energy landscape and determine the most probable values for the species' global concentrations. As in equilibrium thermodynamics, qualitative changes in the effective free energy landscape indicate and characterize the underlying non-equilibrium phase transitions. We provide the complete phase diagrams for the population dynamics, and give a comprehensive analysis of the spatio-temporal dynamics and routes to extinction in the respective phases.

2.3.3 Conclusion and outlook

Our results show that the behavior of spatial population models comprising cyclic interactions between species is much richer than previously thought. In one spatial dimension we found that the dynamics into the absorbing states is governed by different dynamic processes, each scaling differently with the system size. We computed the complete distribution of extinction times and identified distinct scaling regimes of the asymptotic dynamics.

These surprising results motivated further work on two-dimensional cyclic population models. The scaling of extinction times with the system size changes abruptly at certain threshold values of the mobility and the relative strength of the two types of competition. We show that the dynamic processes leading to the transient maintenance of biodiversity are linked to attractors of an effective free energy of the overall concentrations. The characteristics of these attractors change upon certain threshold values, thereby giving insight into the mechanisms underlying these transitions. By means of extensive numerical simulations we provide the complete phase diagrams, which are rationalized by scaling arguments based on properties of the complex Ginzburg-Landau equation.

We believe that the method of global phase portraits and the ensuing effective free energy landscapes might also give a deeper insight into the dynamics of other spatial ecological models and reaction-diffusion systems in other fields of biology. In particular, further studies may apply this method to understand epidemic models, asymmetric four species models or more complex food webs.

Journal of Statistical Mechanics: Theory and Experiment
An IOP and SISSA journal

LETTER

Threefold way to extinction in populations of cyclically competing species

S Rulands[1], T Reichenbach[2] and E Frey[1]

[1] Arnold Sommerfeld Center for Theoretical Physics (ASC) and Center for NanoScience (CeNS), LMU München, Theresienstraße 37, 80333 München, Germany
[2] Howard Hughes Medical Institute and Laboratory of Sensory Neuroscience, The Rockefeller University, 1230 York Avenue, New York, NY 10065-6399, USA
E-mail: steffen.rulands@physik.lmu.de, tobias.reichenbach@mail.rockefeller.edu and frey@lmu.de

Received 19 October 2010
Accepted 28 December 2010
Published 27 January 2011

Online at stacks.iop.org/JSTAT/2011/L01003
doi:10.1088/1742-5468/2011/01/L01003

Abstract. Species extinction occurs regularly and unavoidably in ecological systems. The time scales for extinction can vary broadly and provide information on the ecosystem's stability. We study the spatio-temporal extinction dynamics of a paradigmatic population model where three species exhibit cyclic competition. The cyclic dynamics reflects the non-equilibrium nature of the species interactions. While previous work focuses on the coarsening process as a mechanism that drives the system to extinction, we found that unexpectedly the dynamics in going to extinction is much richer. We observed dynamics of three different types. In addition to coarsening, in the evolutionarily relevant limit of large times, oscillating traveling waves and heteroclinic orbits play a dominant role. The weights of the different processes depend on the degree of mixing and the system size. By means of analytical arguments and extensive numerical simulations we provide the full characteristics of scenarios leading to extinction in one of the most surprising models of ecology.

Keywords: coarsening processes (theory), phase transitions into absorbing states (theory), population dynamics (theory), stochastic processes

ArXiv ePrint: 1005.5704

1742-5468/11/L01003+10$33.00

Contents

1. Introduction

Stochastic many-particle systems provide a testing ground for non-equilibrium dynamics. In nature, systems frequently evolve away from equilibrium and then relax to an equilibrium steady state. Understanding the relaxation process is a central topic in non-equilibrium physics. Near-equilibrium fluctuations are governed by the same laws as hold in the steady state and the transient is typically an exponential decay. Many systems, however, comprise absorbing states, which can be reached but never be left by the dynamics. In this case no fluctuations are present in the steady states. Such systems arise in a broad variety of problems, e.g. physics, chemistry and epidemics [1]. Much effort has been spent on the investigation of simple, diffusion-limited chemical reactions where the decay to equilibrium can obey power laws [2].

Understanding transitions into absorbing states is not only fundamental for non-equilibrium physics, but is also highly relevant for ecology. Here, absorbing states correspond to the extinction of species. Another characteristic feature of ecological systems is cyclic interactions. The work of Lotka and Volterra describes, as a classic example, the dynamics of fish populations in the Adriatic as persistent oscillations due to predator–prey interactions. Other examples include coral reef invertebrates [3], rodents in the High Arctic tundra in Greenland [4], cyclic competition between different mating strategies of lizards [5] and chemical warfare of *Escherichia coli* bacteria under laboratory conditions [6].

Recent work has investigated cyclic competition in one-dimensional systems with no or only weak diffusion of the reacting agents [7]–[10]. Coarse graining of temporally growing and annihilating domains has been identified as the mechanism that eventually leads to species extinction. However, an individual's mobility may be significant and alter this picture qualitatively.

In this article, we investigate the spatio-temporal dynamics of extinction in a paradigmatic model of three species in cyclic competition. Individuals are positioned on a one-dimensional lattice and are equipped with fast mobility that leads to effective diffusion. The system possesses absorbing states in the form of the extinction of two of the three species and, because of fluctuations, the dynamics eventually comes to

J. Stat. Mech. (2011) L01003

rest there. However, the time scales until extinction occurs provide information on the stability of species diversity [11]. We identify three distinct types of dynamics that lead to extinction. These types of dynamics arise from the possible influences that intrinsic fluctuations can have on the coarsening process and on the traveling waves that the cyclic dynamics induces. The different dynamics lead to characteristic dependences of the extinction-time probability on the elapsed time t and the system size N. We provide semi-phenomenological arguments that quantify the functional form and the scaling behavior of the extinction-time probability. These arguments yield information on the emergence and characteristics of the different types of dynamics.

2. The model

Consider a stochastic, spatial variant of the May–Leonard model which serves as a prototype for cyclic, rock–paper–scissors-like species interactions. Three species A, B, C compete with each other in a cyclic manner, at rate σ, and reproduce at rate μ upon the availability of empty space $\emptyset$:

$$\begin{aligned} AB &\xrightarrow{\sigma} A\emptyset, \qquad BC \xrightarrow{\sigma} B\emptyset, \qquad CA \xrightarrow{\sigma} C\emptyset, \\ A\emptyset &\xrightarrow{\mu} AA, \qquad B\emptyset \xrightarrow{\mu} BB, \qquad C\emptyset \xrightarrow{\mu} CC. \end{aligned} \tag{1}$$

For increasingly large populations, intrinsic fluctuations eventually become negligible. If in addition spatial structure is absent, i.e., if every individual can interact with every other in the population at equal probability, the population dynamics is aptly described by deterministic rate equations for the densities $\vec{s} = (a, b, c)$ of the species A, B and C:

$$\partial_t s_i = s_i[\mu(1-\rho) - \sigma s_{i+2}], \qquad \text{for } i \in \{1, 2, 3\}. \tag{2}$$

Here the indices are understood as modulo 3 and $\rho = a + b + c$ denotes the total density. May and Leonard showed that these equations possess four absorbing fixed points, corresponding to the survival of one of the species and to an empty system [12]. Furthermore a reactive fixed point $s^* = (\mu/(\sigma + 3\mu))(1, 1, 1)$ exists that represents the coexistence of all three species. Linear stability analysis shows that s^* is unstable. The absorbing steady states that correspond to extinction, $(1, 0, 0)$, $(0, 1, 0)$ and $(0, 0, 1)$, are heteroclinic points. The Lyapunov function $\mathcal{L} = abc/\rho^3$ demonstrates that the trajectories of the deterministic equation (2), when initially close to the reactive fixed point, spiral outward on an invariant manifold. On this manifold the trajectories then approach the boundary of the phase space and form heteroclinic cycles, converging to the boundary and the absorbing states without ever reaching them.

However, intrinsic noise from finite-system sizes [13, 14] and spatial correlations alter the above behavior [15]–[18]. While fluctuations ultimately drive the system into one of the absorbing fixed points [19], the formation of spatial patterns can substantially delay extinction and promote species coexistence [16, 20, 21]. The resulting spatio-temporal dynamics of extinction is nontrivial and highly interesting.

3. Numerical results

We consider a one-dimensional lattice of L sites with periodic boundary conditions. Each lattice site hosts a fixed number M of individuals A, B, C and empty spaces $\emptyset$, such that the

J. Stat. Mech. (2011) L01003

concentrations in the rate equation (2) are given by the number of particles of a specified type divided by M. M may hence be viewed as the carrying capacity of a lattice site. The reactions (1) occur between individuals on the same lattice site. Individuals may change place with another individual or an empty space on a neighboring lattice site at rate ϵ. In order to keep the length scale, i.e. the characteristic length scale for diffusion, fixed when changing the lattice spacing L^{-1} we have to rescale ϵ appropriately. In the continuum limit the exchange processes therefore lead to an effective diffusion of individuals at a diffusion constant $D \equiv \epsilon L^{-2}$ and thus to coupling between the lattice sites. In our simulations we implemented a continuous-time Markov process with sequential updating. At each simulation step an individual is randomly chosen. It then either reacts with a randomly chosen individual of the same site or changes place with a randomly chosen individual of the two neighboring stacks, at probabilities corresponding to the rates σ, μ and ϵ.

The population model introduced above possesses a net system size of $N \equiv ML$ which plays the role of an overall carrying capacity. For large enough M and L the intrinsic fluctuations have a strength proportional to the inverse square root of N [22]. Different equivalent ways therefore exist for taking the thermodynamic limit, e.g., increasing the number M of individuals per lattice site while keeping the lattice size L fixed or increasing the lattice size L keeping M fixed. Because for large L a huge amount of exchange processes take place between the reactions, requiring long computation time, we took the thermodynamic limit as $M \to \infty$ and kept $L = 100$ fixed. The insensitivity of the results to the choice of the limit is supported by recent studies [10]. L was chosen sufficiently large, such that L^{-1} was much smaller than the correlation length.

We here consider the case of equal reproduction and selection rates $\mu = \sigma = 1$. Similar behavior can be expected for $\mu \neq \sigma$, when D is rescaled appropriately [20], and species dependent interaction rates [10, 23]. We chose a random initial configuration in which the density of the species approximately equals those of the internal fixed point s^* of the rate equation (2).

Our simulations reveal three distinct classes of dynamics (figure 1). First, at short time scales stochastic effects lead to the emergence of domains due to coarsening. In this scenario, after a short coarsening process, domains emerge whose order does not correspond to the rules of cyclic dominance, leading to oppositely moving fronts and hence immediate annihilation. Extinction occurs rapidly in this scenario. The coarsening dynamics to extinction has been extensively studied [7]–[9]. However, our simulations reveal a much richer dynamics going to extinction. Two more processes dominate the dynamics for large times. Second, we observe situations where the population is almost entirely taken over by a species at the cost of a second species, which dies out. A few individuals of the other surviving species are present in the system and, being the dominant one, slowly fixate. This scenario is intimately related to the heteroclinic orbits of the rate equation (2). The global dynamics moves along the boundary of the invariant manifold of (2). Spatial patterns are of minor importance. Third, the system can enter a state of propagating waves of cyclically aligned, uniform domains. These states are only metastable: fluctuating front positions result in domain annihilation and eventual extinction. For small D this effect was also noted in [10] and corresponds to the spiral waves found in the two-dimensional model [20]. Rare events at the leading edge of the fronts cause the tunneling of domains and oscillating overall species densities.

doi:10.1088/1742-5468/2011/01/L01003

J. Stat. Mech. (2011) L01003

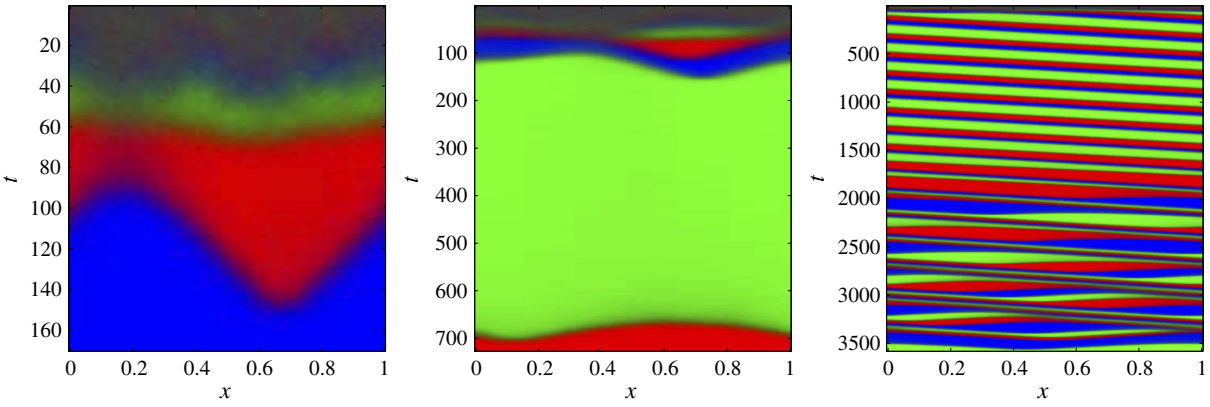

Figure 1. Spatio-temporal dynamics of three exemplary runs that correspond to the three classes of dynamics ($M = 100$, $L = 600$): rapid annihilation (left), heteroclinic orbits (center), and propagating waves (right). In the latter case an initially stable wave formation changes periodically at later times, leading to oscillating total densities. Color encodes the concentrations of the three species (A, red; B, green; C, blue).

Figure 2(a) provides a concrete picture of the different dynamical processes. The system's state probability is projected onto the invariant manifold of the rate equation (2). The color signifies the logarithmic probability of finding a given net density of species on the manifold before reaching an absorbing fixed point. We recognize that the system spends considerable time in the vicinity of the boundary, especially near the corners of the simplex, corresponding to the heteroclinic orbits occurring in the second scenario. The stochastic limit cycle around the unstable fixed point reflects the oscillating traveling waves from the third scenario (see also, e.g., [24]). In the center, single trajectories of non-oscillating waves are visible.

The influence of mobility is visualized in figure 2(b). The Lyapunov function $\mathcal{L} = abc/\rho^3$ characterizes the system's behavior: it is zero at the boundaries and increases monotonically to the unstable fixed point s^*. $\mathcal{L}$ therefore provides a measure for the distance of the system's state from the boundaries. The logarithmic probability of finding the system at a certain value of $\mathcal{L}$, depending on the diffusivity D, is given in figure 2(b). A drastic change in the system's behavior occurs at a critical mobility $D_c \approx 8 \times 10^{-4}$. Above D_c we observe only heteroclinic orbits, characterized by a high probability of finding the system at small values of $\mathcal{L}$. For very small D the system exhibits traveling waves, performing random walks in concentration space. Below D_c both types of dynamics are present. The high probabilities for small values of $\mathcal{L}$ indicate heteroclinic orbits, while the ridge at larger values is caused by oscillating traveling waves.

Quantification of the three different dynamical scenarios is feasible through the extinction-time probability, $P(t)$, meaning the probability density for two species going extinct at a certain time t. Mathematically this gives the probability distribution function for times of first passage to one of the absorbing fixed points. In our simulations we varied M from 1 to 2800 and set $D = 3 \times 10^{-4}$, i.e. in the region where all types of dynamics arise simultaneously. Figure 3(a) shows the extinction-time probability distribution for various system sizes. The sharp peak at small times results from the annihilation of

J. Stat. Mech. (2011) L01003

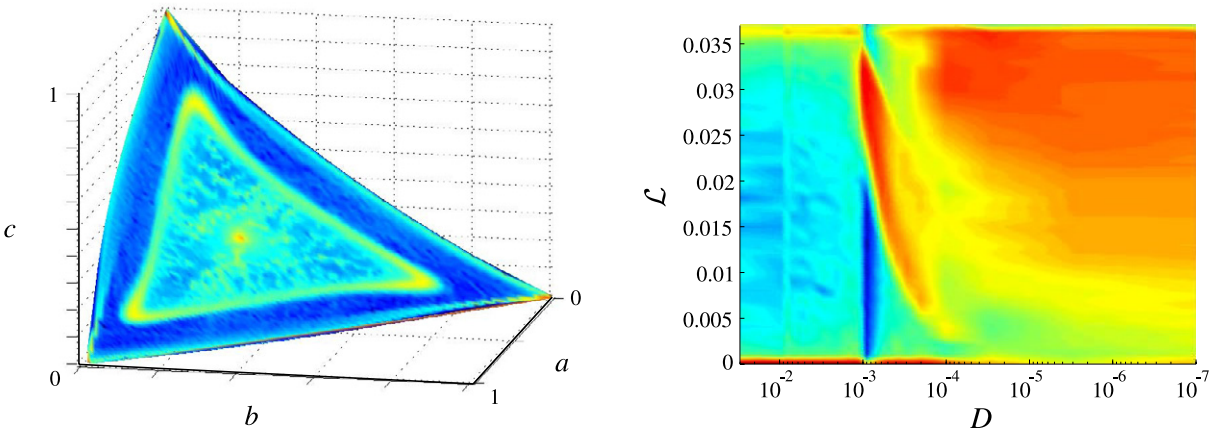

Figure 2. (a) Probability of net densities a, b, c for $M = 600$, $L = 100$, projected onto the invariant manifold of the rate equation (2). Color encodes the logarithm of the probability of finding the system in a specific state, where red denotes the highest, yellow an intermediate, and blue a low probability. Note that the absorbing points themselves have not been included in the statistics. The graph allows us to identify the reactive fixed point, an attractor for metastable oscillating waves, and the heteroclinic orbits. (b) The Lyapunov function $\mathcal{L}$ provides a measure for the distance of the system's state from the boundary of the simplex. The plot shows the logarithmic probability of net densities for different values of the diffusion constant D. Above a critical value of D we find heteroclinic orbits. For very small D we find traveling waves. Below D_c there is a region where both heteroclinic orbits and traveling waves are present ($M = 300$, $L = 100$).

oppositely propagating waves as a result of the coarsening process, i.e. the first scenario. The functional form of the extinction-time probability distribution for intermediate and large times is determined by the heteroclinic orbits and propagating waves, the second and third types of dynamics. We find an exponentially decaying tail that is, for large N, preceded by a $-3/2$ intermediate asymptotic power-law interval. The length of this intermediate interval scales linearly with N. The plateau or second maximum originates in the short term dynamics of the latter two scenarios.

4. Semi-phenomenological arguments

The characteristics of the critical behavior shown in figure 2(b) can be understood through a spatial variant of the rate equation (2). Following [25], the system's dynamics on the invariant manifold can, through a nonlinear transformation to variables z_A and z_B, be recast in terms of the complex Ginzburg–Landau equation

$$\partial_t z = D\nabla^2 + (c_1 - \mathrm{i}\omega_0)z - c_2(1 + \mathrm{i}c_3)|z|^2 z, \tag{3}$$

with $c_1 \equiv \mu\sigma/2(3\mu + \sigma)$, $c_2 \equiv \sigma(3\mu + \sigma)(48\mu + 11\sigma)/56\mu(3\mu + 2\sigma)$, and $c_3 \equiv \sqrt{3}(18\mu + 5\sigma)/(48\mu + 11\sigma)$ [26]. The theory of front propagation into unstable states predicts that (3) always admits traveling waves as stable solutions [27]. Following a

J. Stat. Mech. (2011) L01003

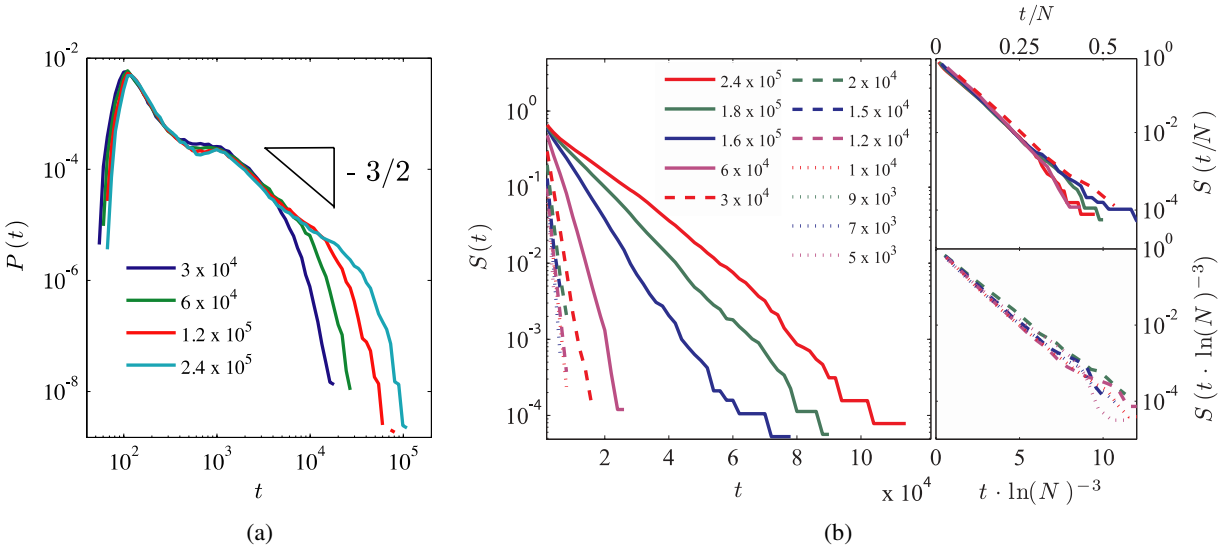

Figure 3. (a) Double-logarithmic plot of the extinction-time distribution $P(t)$ for several system sizes. A sharp peak at small times is followed by a second maximum or plateau and by an intermediate $t^{-3/2}$ power law. The length of the power-law region scales with N. The tail of the distribution decays exponentially. (b) Semi-logarithmic plots of the survival probability $S(t) = 1 - \int_0^t P(t')\,\mathrm{d}t'$ for different N. $S(t)$ exhibits the same long time exponential decay as $P(t)$. With the rescaling t/N for large systems (top right, $N = 30\,000$–$280\,000$) and $t\ln(N)^{-3}$ for small systems (bottom right, $N = 5000$–$20\,000$) the exponential tails collapse onto universal curves, in agreement with our analytical predictions.

classic treatment of the problem of front-speed selection we obtain their wavelength as $\lambda = -(2\pi c_3\sqrt{D}/\sqrt{c_1}(1-\sqrt{1+c_3^2}))$. At the critical diffusivity D_c the wavelength λ exceeds the system size such that the fronts become unstable. From the condition $\lambda = 1$ and accounting for the rescaling factor mentioned in [26] we obtain $D_c \approx 7.6\times10^{-4}$, which is in very good agreement with our numerical results.

The behavior of the extinction-time probability distribution can be understood through semi-phenomenological models. In the following we show how such models yield the shape of the extinction-time probability distribution and its dependence on N. In particular, we give an explanation for the scaling behavior of the power-law interval and the long time exponential decay. We show that, depending on the system size, either heteroclinic orbits or traveling waves dominate the long time dynamics.

The dynamics of the heteroclinic orbits can be quantified as follows. Consider a small density $a_0 \in \mathcal{O}(N^{-1})$ of individuals of species A in a large pool of species B ($b \in \mathcal{O}(1)$). Due to the reproduction of B, empty space is as sparse as A individuals are: $1-a-b \in \mathcal{O}(N^{-1})$. Simulations inform us that spatial patterns are not relevant in this scenario. We therefore consider a well-mixed system of size N. Three reactions lead to the takeover of the population through the dominating species A:

$$AB \xrightarrow{\sigma} A\emptyset \qquad \text{at rate } N\sigma ab \in \mathcal{O}(1),$$
$$B\emptyset \xrightarrow{\mu} BB \qquad \text{at rate } N\mu b(1-a-b) \in \mathcal{O}(1),$$
$$A\emptyset \xrightarrow{\mu} AA \qquad \text{at rate } N\mu a(1-a-b) \in \mathcal{O}(N^{-1}).$$

Here the rates are meant as transitions per unit time. The fast processes are in equilibrium and can be adiabatically eliminated for large N, yielding $a = (\mu/\sigma)(1-a-b)$. Species A occurs at the same density as empty sites times μ/σ. A series of reproduction events remains, each with an exponentially distributed waiting time. In the language of stochastic processes this is a pure birth process, studied as arising in preferential attachment problems. The extinction-time probability distribution $P_{\rm h}(t;a_0)$ is thus given by a convolution over exponential functions. By applying the Laplace transform one can show that it can be expressed in closed form as

$$P_{\rm h}(t;a_0) = \sum_{i=0}^{N(1-a_0)} \lambda_i {\rm e}^{-\lambda_i t} \prod_{i,j=0,i\neq j}^{N(1-a_0)} \frac{\lambda_j}{\lambda_j - \lambda_i}, \tag{4}$$

with rates $\lambda_i = N\sigma(a_0 + i/N)^2$ [28]. One finally has to marginalize over the probability $p(a_0)$ of starting with an initial density a_0 of species A to obtain the extinction-time probability distribution $P_{\rm h}(t)$ as results from the heteroclinic orbit dynamics:

$$P_{\rm h}(t) = \sum_{k=1}^{N} P_{\rm h}\left(t; a_0 = \frac{k}{N}\right) p\left(a_0 = \frac{k}{N}\right). \tag{5}$$

For any reasonable $p(a_0)$ the asymptotic behavior is dominated by the term for the lowest initial concentration $a_0 = 1/N$ and the lowest reproduction rate λ_0: $P_{\rm h}(t) \sim \exp(-\sigma t/N)$ for $t \longrightarrow \infty$. We thus find an N^{-1}-dependence of the exponential tail on the system size. For intermediate times we have to take the full convolution and marginalization sums of equation (5) into account. Numerical evaluation does indeed yield a $-3/2$ power-law interval for uniformly distributed a_0. The time of crossover between the power law and the exponential decay scales with N. We therefore find that the second type of dynamics, heteroclinic orbits, lead to the intermediate power-law regime in the extinction-time probability distribution. The exponential tail of this distribution can result either from heteroclinic orbits or from propagating waves as shown below.

The third type of spatio-temporal dynamics, propagating waves, is metastable. They disappear only through the rare annihilation of neighboring fronts. By symmetry, the waves move with the same average velocity. For small D the domain interfaces are sharp and therefore interact only on distances that are much smaller than the average domain size. The extinction dynamics in this scenario can therefore be described within an interface picture, where, in a comoving frame, the wavefronts behave as random walkers on a one-dimensional lattice with diffusion coefficient $D_{\rm f}$. For larger D long-range interactions between the interfaces become important, leading to a tunneling of domains. However, within the interface picture this merely corresponds to a relabeling of interfaces and therefore does not influence the extinction dynamics. Numerical simulations validate the assumption of normal diffusion. For a single series of subsequent A, B, C domains the survival probability $S_w(t)$, meaning the probability that all three domains still coexist at time t, follows as the survival probability of a single random walker between absorbing boundaries at distance l. The probability distribution $c_w(t,x;x_0,l)$ for the random walker being at position x and time t when starting at x_0 obeys a diffusion equation subject to absorbing boundary conditions. The solution is well known:

$$c_w(t,x;x_0,l) = \sum_{n=1}^{\infty} A_n \sin\left(\frac{n\pi x}{l}\right) {\rm e}^{-(n\pi/l)^2 D_{\rm f} t}, \tag{6}$$

J. Stat. Mech. (2011) L01003

with the coefficients $A_n = (2/L)\sin(n\pi x_0/l)$ being determined by the initial condition $c_w(x,t;x_0,l) = \delta(x-x_0)$; see e.g. [29]. Averaging over space, the initial positions x_0 and identically distributed interval lengths l yield the survival probability $S_w(t)$ from the traveling-wave dynamics:

$$S_w(t) = \frac{8}{\pi^2}\sum_{m=0}^{\infty}\frac{1}{(2m+1)^2}\int_0^1 \mathrm{e}^{-(2m+1)^2\pi^2 D_\mathrm{f} t/l^2}\,\mathrm{d}l. \tag{7}$$

In the asymptotic limit the expression evaluates to $S_w(t) \sim \mathrm{e}^{-4D_\mathrm{f}\pi^2 t}$, for $t \longrightarrow \infty$. The extinction-time probability distribution follows as $P_w(t) = -\mathrm{d}S_w(t)/\mathrm{d}t$. What is the diffusion constant D_f of the domain front? Brunet *et al* proposed [30] that the diffusion constant for a broad class of stochastic propagating waves depends on N as $D_\mathrm{f} \sim \ln(N)^{-3}$. Therewith the exponential decay of the extinction-time probability distribution's tail, as resulting from the traveling-wave dynamics, is proportional to $\ln(N)^{-3}$. This result is validated by our numerical simulations; see figure 3(b), bottom right. Heteroclinic orbits and traveling waves both contribute to the asymptotic limit of the net extinction-time probability distribution $P(t)$: $P(t) \sim P_\mathrm{h}(t) + P_w(t)$, for $t \longrightarrow \infty$. Both contributions yield exponential decays at large times, but with different scalings in N. For small systems the $\ln(N)^{-3}$ term in $P_w(t)$, resulting from the traveling-wave dynamics, dominates. In contrast, the $1/N$-decay in $P_\mathrm{h}(t)$ resulting from heteroclinic orbits yields the major contribution when N is large. In agreement with these analytical results, our numerical finding is indeed that the exponential decay scales as $\ln(N)^{-3}$ for small N and as $1/N$ for large N (figure 3(b)). Numerically we identified the crossover between the two regimes to occur at $N \approx 20\,000$.

5. Conclusion

We investigated the spatio-temporal extinction dynamics in a three-species stochastic population model with cyclic interactions. While previous work has mainly focused on the coarse graining process that drives the system to extinction we identified two more types of dynamics that are rare but, due to their lifetime, most important from an evolutionary perspective. The three classes of dynamics, namely rapid annihilation of domains, heteroclinic orbits, and traveling waves, are correlated with features of the phase portrait and leave their fingerprints in the extinction-time probability distribution. The weight of these processes depends on the degree of mixing as well as on the system size. On the basis of the different dynamical scenarios, we provided semi-phenomenological calculations that yield the functional form of this probability distribution and its dependence on the system size. We believe that our results are of general relevance as we expect a similar phenomenology in other systems described by the complex Ginzburg–Landau equation.

Acknowledgments

This research was supported by the German Excellence Initiative via the program 'Nanosystems Initiative Munich' and the German Research Foundation via contract FR 850/9-1. TR acknowledges support from the Alexander von Humboldt Foundation through a fellowship.

J. Stat. Mech. (2011) L01003

References

[1] Hinrichsen H, 2000 *Adv. Phys.* **49** 815
[2] Täuber U C, Howard M and Vollmayr-Lee B P, 2005 *J. Phys. A: Math. Gen.* **38** R79
[3] Jackson J B C and Buss L, 1975 *Proc. Nat. Acad. Sci.* **72** 5160
[4] Gilg O, Hanski I and Sittler B, 2001 *Science* **302** 866
[5] Sinervo B and Lively C M, 1996 *Nature* **380** 240
[6] Kerr B, Riley M A, Feldman M W and Bohannan B J M, 2002 *Nature* **418** 171
[7] Tainaka K, 1988 *J. Phys. Soc. Japan* **57** 2588
[8] Frachebourg L, Krapivsky P L and Ben-Naim E, 1996 *Phys. Rev. Lett.* **77** 2125
[9] Frachebourg L, Krapivsky P L and Ben-Naim E, 1996 *Phys. Rev.* E **54** 6186
[10] He Q, Mobilia M and Täuber U, 2010 *Phys. Rev.* E **82** 051909
[11] Cremer J, Reichenbach T and Frey E, 2009 *New J. Phys.* **11** 093029
[12] May R and Leonard W, 1975 *SIAM J. Appl. Math.* **29** 243
[13] Claussen J C and Traulsen A, 2008 *Phys. Rev. Lett.* **100** 058104
[14] Boland R P, Galla T and McKane A J, 2009 *Phys. Rev.* E **79** 051131
[15] Durrett R and Levin S, 1998 *Theor. Pop. Biol.* **53** 30
[16] Szabó G and Fath G, 2007 *Phys. Rep.* **446** 97
[17] Abta R, Schiffer M and Shnerb N M, 2007 *Phys. Rev. Lett.* **98** 098104
[18] Peltomäki M and Alava M, 2008 *Phys. Rev.* E **78** 031906
[19] Parker M and Kamenev A, 2009 *Phys. Rev.* E **80** 021129
[20] Reichenbach T, Mobilia M and Frey E, 2007 *Nature* **448** 1046
[21] Efimov A, Shabunin A and Provata A, 2008 *Phys. Rev.* E **78** 056201
[22] Gardiner C, 2004 *Handbook of Stochastic Methods* (Berlin: Springer)
[23] Venkat S and Pleimling M, 2010 *Phys. Rev.* E **81** 021917
[24] Bladon A J, Galla T and McKane A J, 2010 *Phys. Rev.* E **81** 066122
[25] Reichenbach T, Mobilia M and Frey E, 2008 *J. Theor. Biol.* **254** 368
[26] Reichenbach T, Mobilia M and Frey E, 2007 *Phys. Rev. Lett.* **99** 238105
[27] van Saarlos W, 2003 *Phys. Rep.* **386** 29
[28] Kannan D, 1979 *Introduction to Stochastic Processes* (Amsterdam: Elsevier, New York: North-Holland)
[29] Redner S, 2001 *A Guide to First Passage Processes* (Cambridge: Cambridge University Press)
[30] Brunet E, Derrida B, Mueller A H and Munier S, 2006 *Phys. Rev.* E **73** 056126

J. Stat. Mech. (2011) L01003

Global attractors and extinction dynamics of cyclically competing species

Steffen Rulands, Alejandro Zielinski, and Erwin Frey
Arnold Sommerfeld Center for Theoretical Physics and Center for NanoScience, Physics Department, Ludwig-Maximilians-Universität München, Theresienstraße 33, D-80333 München, Germany
(Received 14 January 2013; published 17 May 2013)

Transitions to absorbing states are of fundamental importance in nonequilibrium physics as well as ecology. In ecology, absorbing states correspond to the extinction of species. We here study the spatial population dynamics of three cyclically interacting species. The interaction scheme comprises both direct competition between species as in the cyclic Lotka-Volterra model, and separated selection and reproduction processes as in the May-Leonard model. We show that the dynamic processes leading to the transient maintenance of biodiversity are closely linked to attractors of the nonlinear dynamics for the overall species' concentrations. The characteristics of these global attractors change qualitatively at certain threshold values of the mobility and depend on the relative strength of the different types of competition between species. They give information about the scaling of extinction times with the system size and thereby the stability of biodiversity. We define an effective free energy as the negative logarithm of the probability to find the system in a specific global state before reaching one of the absorbing states. The global attractors then correspond to minima of this effective energy landscape and determine the most probable values for the species' global concentrations. As in equilibrium thermodynamics, qualitative changes in the effective free energy landscape indicate and characterize the underlying nonequilibrium phase transitions. We provide the complete phase diagrams for the population dynamics and give a comprehensive analysis of the spatio-temporal dynamics and routes to extinction in the respective phases.

DOI: 10.1103/PhysRevE.87.052710 PACS number(s): 87.23.Cc, 05.40.−a, 02.50.Ey

Absorbing states play an important role in ecology, where they correspond to the extinction of species [1]. While any stochastic system will eventually end up in one of its absorbing states, in nature, one finds a surprisingly long-term maintenance of biodiversity in ecosystems containing a broad variety of coexisting species. A structured environment in combination with cyclic competition between species was proposed to be a main facilitator of biodiversity [2,3]. Classical ecological examples for cyclic interactions comprise coral reef invertebrates [4], rodents in the high arctic tundra in Greenland [5], and cyclic competition between different mating strategies of lizards [6]. However, long reproduction times and large spatial scales involved make it difficult to quantitatively analyze these ecological systems. To circumvent these problems, recent experimental studies have turned to microbial model systems comprising three genetically distinct strains of *Escherichia coli* which cyclically dominate each other like in the children's game rock-paper-scissors [7,8].

These experimental studies of microbial model systems have motivated a large body of theoretical literature exploring the role of cyclic interactions in ecological systems [1,3,9–43]. Most of this work has focused on two paradigmatic examples of three-species models with cyclic interactions. In a first class of models, direct competition between two individuals leads to the immediate replacement of the weaker species by the stronger one [3,11–18,20–32]. This type of competition, where selection and reproduction are combined into a single process, is similar as in the classical two-species Lotka-Volterra model [44–46]. The interaction scheme of this cyclic Lotka-Volterra model may be summarized by a set of chemical reactions between the three species A, B, and C:

$$AB \to AA, \quad BC \to BB, \quad CA \to CC. \tag{1}$$

In the second class of models, originally proposed by May and Leonard [19], selection and reproduction are two separate processes. An interaction between two individuals with different traits (strategies) leads to the death of the weaker species and thereby to empty spaces. Reproduction then follows as a second process which recolonizes this empty space. The ensuing reaction scheme reads:

$$AB \to A\emptyset, \quad BC \to B\emptyset, \quad CA \to C\emptyset, \tag{2a}$$
$$A\emptyset \to AA, \quad B\emptyset \to BB, \quad C\emptyset \to CC. \tag{2b}$$

Both of these models exhibit absorbing states where all but one species have died out. Due to the inevitable demographic fluctuations in systems with a finite number of individuals these absorbing states will with certainty be reached if one just waits long enough. How long one has to wait strongly depends on the type of model and the ecological scenario under consideration.

In well-mixed systems, the typical extinction time T was found to scale linearly with the population size N for the cyclic Lotka-Volterra model [11,12,17,47,48] and logarithmically for the May-Leonard model [34]. The reason for the difference is the different nature of the phase space orbits characterizing the nonlinear dynamics of these two models [1]. While the phase portrait of the cyclic Lotka-Volterra model exhibits neutrally stable orbits, the May-Leonard model is characterized by heteroclinic orbits emerging from orbits which spiral out from an unstable reactive fixed point. For neutrally stable orbits, the stochastic dynamics performs an unbiased random walk, which implies that $T \propto N$. In contrast, unstable orbits generate a drift of the trajectories in phase space towards the boundary such that the extinction process towards the absorbing states is exponentially accelerated with $T \propto \ln N$ [1,16,49].

In spatially extended systems, the scaling of T with population size strongly depends on the degree of mixing. In particular, it has been shown for both models that there exists a mobility threshold below which extinction times scale

exponentially in the system size. For the May-Leonard model this has been attributed to the existence of spiral waves, which emerge as a result of the local nature of reactions and internal noise [33,34,36]. Above a certain mobility the characteristic wave length of the spirals exceeds the system size, effectively rendering the dynamics well-mixed. In this regime, extinctions occurs rapidly. In the cyclic Lotka-Volterra model, spatial patterns are unstable as a result of an Eckhaus instability [26]. However, below a mobility threshold biodiversity is still maintained by strong spatial correlations. Further work has extended these findings to asymmetric reaction rates [14,29] and more complex interaction networks [32,49–51]. In a niche model it has been shown that interaction networks with a high connectivity and a hierarchical or cyclic interaction structure lead to increased diversity [52,53]. For the May-Leonard and the cyclic Lotka-Volterra model it was found that spatially inhomogeneous reaction rates have only minor effects on the dynamics [27,39]. For the classical two-species Lotka-Volterra model, analytical studies have been performed to understand the underlying mechanism leading to the stabilizing correlations [54,55]. These studies argue that the stabilization can by understood by the desynchronization of diffusively coupled oscillators. The desynchronization is a result of the combined effect of noise, migration, and the dependence of the oscillations' frequency upon their amplitude.

For the one-dimensional May-Leonard model the dynamics leading to extinction has been studied in greater detail. If the individuals diffuse only little or do not diffuse at all, coarse graining of species' domains has been identified as the dominant dynamical process leading to extinction [20,23,24,27]. With increasing diffusion constant other types of collective excitations become important [38]. The dynamics to extinction is then surprisingly rich, comprising rapid extinction, global oscillatory behavior, and traveling waves. The latter involve oscillating overall densities, i.e., the domain sizes for the different species change periodically. The statistical weights of these dynamical regimes change qualitatively at threshold values of the mobility and the system size. Taken together, it has turned out that the dynamics in the one-dimensional May-Leonard model is highly complex, much more than one would naively anticipate.

In this paper we extend these studies to two-dimensional models with cyclic competition between species. Specifically, we study a generic model comprising both direct competition between species as in the cyclic Lotka-Volterra model, and separated selection and reproduction processes as in the May-Leonard model. Our goal is to identify and characterize the dynamic processes which are responsible for the transient maintenance of biodiversity and which finally lead to the extinction of all but one species. In particular, we are interested in how factors like species mobility and the relative strength of the different competition types govern the complex spatio-temporal dynamics of the system. Employing extensive numerical simulations, we show that the dominant dynamic processes responsible for the transient maintenance of biodiversity correspond to attractors of the global dynamics, i.e., the overall density of species in the system. The characteristic features of these attractors give information about the scaling of extinction times with the system size and thereby the stability of biodiversity. Importantly, the attractors change qualitatively at certain threshold values of the mobility and the relative strength of the different competition types. The phase transitions at these threshold values correspond to abrupt changes of the scaling of the extinction time T with the population size N. These global attractors can be envisioned as minima in an effective free energy landscape. As their counterparts from equilibrium thermodynamics, they give valuable information about the physics underlying the observed transitions and thereby give insight into the mechanisms leading to the stability of ecosystems. Our numerical studies are complemented by scaling arguments based on properties of the complex Ginzburg-Landau equation [26,33,34,36,56].

I. A GENERIC MODEL OF CYCLICALLY INTERACTING SPECIES

We consider a spatially extended population consisting of three distinct species A, B, and C that compete with each other cyclically in two different ways: either by immediately replacing the competitor by an individual of its own kind, or by killing the inferior species and creating an empty site $\emptyset$. In addition, individuals may also reproduce if empty spaces are available. These processes are summarized by the following reaction scheme:

$$A B \xrightarrow{\sigma} A\emptyset, \quad A\emptyset \xrightarrow{\mu} AA, \quad A B \xrightarrow{\nu} AA, \tag{3a}$$

$$B C \xrightarrow{\sigma} B\emptyset, \quad B\emptyset \xrightarrow{\mu} BB, \quad B C \xrightarrow{\nu} BB, \tag{3b}$$

$$C A \xrightarrow{\sigma} C\emptyset, \quad C\emptyset \xrightarrow{\mu} CC, \quad C A \xrightarrow{\nu} CC. \tag{3c}$$

The reaction rules (3) describe two competing types of selection processes: On the one hand, with rates σ and μ, selection and reproduction are separate processes. Selection produces empty sites which are in turn required for reproduction. An empty space is not necessarily occupied by the individual who produced it. We refer to these processes as May-Leonard processes. On the other hand, Lotka-Volterra processes, with a rate ν, couple selection and reproduction: success in competition directly translates into reproduction. In the following, when we use the term Lotka-Volterra process, this will always imply that the reactions are cyclic. There are two limiting cases which correspond to well-established models: for $\nu \to 0$ and for $\mu = \sigma = 0$ we recover the May-Leonard model [19] and a three species model with cyclic interactions of Lotka-Volterra type [9,44,45], respectively.

A. Stochastic lattice gas model

We consider a two-dimensional square lattice and employ periodic boundary conditions [57]. The linear dimension of the lattice is taken as the basic length unit such that the lattice constant $a = 1/L$ with L the number of lattice sites along each axis. At each site a fixed number M of individuals (A, B, C or empty spaces $\emptyset$) are located. M may be viewed as the carrying capacity of a lattice site. In addition, individuals are also able to move on the lattice. While the reactions, Eqs. (3a)–(3c), are assumed to occur on the same lattice site, the individuals' mobility is implemented as an exchange process at a rate ϵ between neighboring sites, $XY \xrightarrow{\epsilon} YX$, where X and Y denote species A, B, and C or empty spaces $\emptyset$. Macroscopically the nearest-neighbor exchange process leads to diffusion with

an effective diffusion constant $D = \epsilon L^{-2}/2$ [33,34,36]. As two particles are involved in migration, it also induces some additional nonlinear reaction terms, which we neglect here [58,59].

We performed extensive simulations of the ensuing stochastic particle dynamics employing a sequential updating algorithm: At each simulation step an individual is chosen at random. It then either reacts with another also randomly chosen individual from the same site, or is exchanged with an individual of a neighboring stack; each stochastic event occurs with probabilities corresponding to the respective reaction rates μ, σ, ν, and ϵ. Typical snapshots of the stochastic simulations for the May-Leonard model are shown in Fig. 1.

The effective size of the system is $N = M \cdot L^2$. If M and L are large enough, the strength of fluctuations is proportional to $1/\sqrt{N}$ [60]. The simulation results therefore do not depend on the specific choice of M and L, as long as both are not too small and the net system size is kept constant. In particular, the lattice spacing $a = L^{-1}$ must be much smaller than the correlation length ξ.

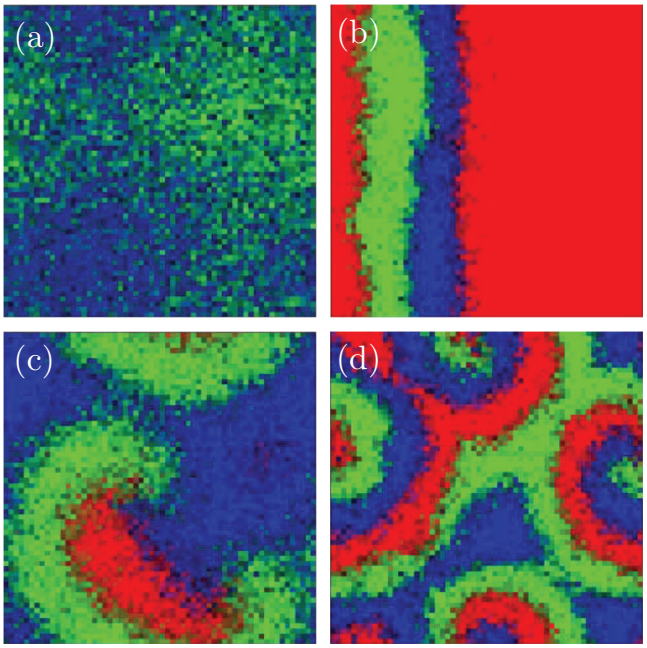

FIG. 1. (Color online) Typical spatial patterns in the May-Leonard model. Color (gray scale) denotes the concentration of species A, B, and C, with red (medium gray) signifying a site dominated by species A, green (light gray) a site dominated by species B, and blue (dark gray) being a site dominated by species C. (a) For large diffusion constants ($D = 1.5 \times 10^{-3}$), the dynamics shows global oscillations with periodic switching between states with mainly one species present. (b) For intermediate values of the diffusion constant ($D = 5 \times 10^{-4}$), we observe planar traveling waves. Here two of the domains take a characteristic domain size dictated by the diffusion constant. The third domain then occupies the rest of the system. (c), (d) For even smaller diffusion constants ($D = 3 \times 10^{-4}$ and $D = 6 \times 10^{-5}$), pairs of rotating spirals appear. The vertices of these spirals move very slowly on a time scale much larger than the time scale corresponding to the propagation speed of their arms. The wave length of the spirals decreases when the diffusion constant is reduced. The system size for all snapshots was $L = 60$, and the carrying capacity for each site was chosen to be $M = 8$.

Different reaction rates for the species should not limit the validity of our results, as long as the differences between the species are not too large. It has recently been shown that small asymmetries in the reaction rates do not alter the dynamics [35]. A general discussion of species-dependent reactions rates is given in Refs. [27,29]. In the following we will also set $\mu = \sigma$. While the relation between the selection and reproduction rates in the May-Leonard model affects certain properties of the dynamics (such as the wavelength and velocity of spiral waves), qualitatively the results remain the same [36]. This view is supported by some sample runs that we carried out for different values of μ/σ. It is, however, important to note that our results are not valid for extreme choices of the rate, corresponding, for example, to two species predator prey models [46,61,62]. In all simulations the initial condition was chosen to be a randomly populated lattice with average concentrations corresponding to the reactive fixed point of the well-mixed model.

We fixed the time scale by setting $\mu = \sigma = 1$ for the May-Leonard and $\nu = 1$ for the Lotka-Volterra limit. The diffusion constant D then gives the mean square displacement of an average particle between two reactions. As an example, with the system size as the unit length a value of $D = 10^{-3}$ implies that a particle covers an area of one thousandth of the system size between two succeeding reactions. We study a regime where the correlation length is much larger then the lattice spacing. As a result, the lattice spacing is irrelevant as a length scale. The only relevant quantity is the ratio of the characteristic length of spatial patterns given by D and the system size.

B. Well-mixed limit and invariant manifolds

For large populations, intrinsic fluctuations are negligible in our stochastic lattice gas model. If in addition every individual can interact with every other individual with equal probability, i.e., for a well-mixed system, the dynamics is aptly described by deterministic rate equations for the densities a, b, and c of the species A, B, and C, respectively:

$$\partial_t a = -\sigma ac + \mu a(1-\rho) + \nu a(b-c), \tag{4a}$$

$$\partial_t b = -\sigma ba + \mu b(1-\rho) + \nu b(c-a), \tag{4b}$$

$$\partial_t c = -\sigma cb + \mu c(1-\rho) + \nu c(a-b). \tag{4c}$$

Here $\rho = a + b + c$ is the total density of species and $0 \leqslant a,b,c,\rho \leqslant 1$. Equation (4) exhibits three absorbing fixed points: (1,0,0), (0,1,0), and (0,0,1). They correspond to the extinction of two of the three species. Another fixed point at (0,0,0) corresponds to the extinction of all three species. However, this fixed point cannot be reached by the stochastic dynamics from the initial conditions we study here. In addition, there is a reactive fixed point

$$(a^*,b^*,c^*) = \frac{\mu}{3\mu+\sigma}(1,1,1) \tag{5}$$

at which all three species coexist. The dynamics in the vicinity of the reactive fixed point can be studied by linearizing Eq. (4) around (a^*,b^*,c^*) and by determining the eigenvalues of the corresponding Jacobian. We find that the dynamics close

to the reactive fixed point is characterized by an attractive eigendirection with a negative eigenvalue $\kappa_0 = -\mu$ and two further eigendirections with eigenvalues

$$\kappa_\pm = \frac{1}{2}\frac{\mu}{3\mu+\sigma}[(1 \pm \mathrm{i}\sqrt{3})\sigma \pm \mathrm{i}\,2\sqrt{3}\nu]. \tag{6}$$

Therefore, the eigenvectors corresponding to $\kappa_\pm$ span, to linear order, an invariant manifold onto which the dynamics relaxes exponentially fast. To obtain an approximation for the invariant manifold, valid to second order in the concentrations, we follow the steps given in Ref. [36]. We first transform to a new reference frame whose origin is the unstable fixed point, $(x_A,x_B,x_C) = (a-a^*,b-b^*,c-c^*)$. Further, we choose the eigendirections of the fixed point as basis vectors for our new reference frame. To this end, we employ a rotation of the coordinate system:

$$\mathbf{y} = \frac{1}{3}\begin{pmatrix} \sqrt{3} & 0 & -\sqrt{3} \\ -1 & 2 & -1 \\ 1 & 1 & 1 \end{pmatrix}\mathbf{x}. \tag{7}$$

The stable eigendirection corresponding to κ_0 is then given by the y_C direction, while y_A and y_B span the invariant manifold to linear order. We parametrize the invariant manifold by $y_C = G(y_A,y_B)$. Using the ansatz $G(y_A,y_B) \sim y_A^2 + y_B^2$ and determining the proportionality constant such that

$$\partial_t G(y_A(t),y_B(t)) = \partial_{y_A} G \cdot \partial_t y_A + \partial_{y_B} G \cdot \partial_t y_B \stackrel{!}{=} \partial_t y_C|_{y_C=G},$$

we find that $G(y_A,y_B)$ is, to second order, given by

$$G(y_A,y_B) = \frac{\sigma}{4\mu}\frac{3\mu+\sigma}{3\mu+2\sigma}\left(y_A^2+y_B^2\right). \tag{8}$$

This equation is valid only for $\mu \neq 0$. In the limit of a cyclic Lotka-Volterra model, $\mu = 0 = \sigma$, we find $G_{\mu=0,\sigma=0}(y_A,y_B) = 0$, and the invariant manifold is given by the unit simplex defined by $a+b+c=1$. This result can also be directly inferred from the Lotka-Volterra reactions, which preserve the total density and thereby lead to dynamics on an invariant manifold given by $a(t)+b(t)+c(t)=1$.

The rate equations in the new reference frame read

$$\begin{aligned}\partial_t y_A &= \frac{\sqrt{3}}{4}(2\nu+\sigma)\left(y_A^2-y_B^2\right) \\ &\quad + \frac{\sqrt{3}}{2}(2\nu+\sigma)y_B\left(\frac{\mu}{3\mu+\sigma}+y_C\right) \\ &\quad + \frac{y_A\{\mu\sigma-(3\mu+\sigma)[\sigma y_B+(6\mu+\sigma)y_C]\}}{2(3\mu+\sigma)} \\ &\quad + \frac{\sqrt{3}(2\nu+\sigma)y_B[\mu+(3\mu+\sigma)y_C]}{2(3\mu+\sigma)}, \end{aligned} \tag{9a}$$

$$\begin{aligned}\partial_t y_B &= -\frac{1}{4}\sigma^2\left(y_A^2-y_B^2\right) \\ &\quad - \frac{\sqrt{3}(2\nu+\sigma)}{2}y_A\left(\frac{\mu}{3\mu+\sigma}+y_B+y_C\right) \\ &\quad + \frac{y_B}{2(3\mu+\sigma)}[\mu\sigma-(3\mu+\sigma)(6\mu+\sigma)y_C], \end{aligned} \tag{9b}$$

$$\partial_t y_C = -\mu y_C - (3\mu+\sigma)y_C^2 + \frac{\sigma}{4}\left(y_A^2+y_B^2\right). \tag{9c}$$

What is the simplest differential equation that captures the essential features of the rate equations (4)? Such a differential equation is called normal form, and is obtained by a nonlinear transformation which eliminates the quadratic terms. Following the steps in Ref. [36], one makes a quadratic ansatz for the transformation and determines the coefficients canceling the quadratic terms. We find that the transformation is given by

$$z_A = y_A + \alpha_1\left(\sqrt{3}y_A^2 + \alpha_2 y_A y_B - \sqrt{3}y_B^2\right), \tag{10a}$$

$$z_B = y_B + \alpha_1\left(\frac{\alpha_2}{2}y_A^2 - 2\sqrt{3}y_A y_B - \frac{\alpha_2}{2}y_B^2\right), \tag{10b}$$

with prefactors

$$\alpha_1 = \frac{3\mu+\sigma}{28\mu}\frac{7(2\nu+\sigma)\sigma}{27\nu^2+27\nu\sigma+7\sigma^2}, \tag{11a}$$

$$\alpha_2 = 10 + \frac{18\nu}{\sigma} - \frac{2\nu}{2\nu+\sigma}. \tag{11b}$$

Upon introducing a complex variable $z = z_A + \mathrm{i}z_B$ and neglecting terms of order $O(z^4)$, the dynamics can finally be written in the form

$$\partial_t z = (c_1 - \mathrm{i}\omega)z - c_2(1-\mathrm{i}c_3)|z|^2 z\,, \tag{12}$$

where

$$\omega = \frac{\sqrt{3}}{2}\frac{\mu(2\nu+\sigma)}{3\mu+\sigma}, \tag{13a}$$

$$c_1 = \frac{1}{2}\frac{\mu\sigma}{3\mu+\sigma}, \tag{13b}$$

$$\begin{aligned} c_2 &= \frac{\sigma(3\mu+\sigma)}{56\mu(3\mu+2\sigma)} \\ &\quad \times \frac{\sigma^2(48\mu+11\sigma)+3\nu(60\mu+13\sigma)(\nu+\sigma)}{\sigma^2+\frac{27}{7}\nu(\nu+\sigma)}, \end{aligned} \tag{13c}$$

$$\begin{aligned} c_3 &= \frac{1}{c_2}\frac{(3\mu+\sigma)\sqrt{3}(2\nu+\sigma)}{56\mu(3\mu+2\sigma)} \\ &\quad \times \frac{\sigma^2(18\mu+5\sigma)+9\nu(6\mu+\sigma)(\nu+\sigma)}{\sigma^2+\frac{27}{7}\nu(\nu+\sigma)}. \end{aligned} \tag{13d}$$

While the limiting case of a May-Leonard model is found by simply setting $\nu = 0$, the cyclic Lotka-Volterra model is recovered by first taking the limit $\sigma \to 0$ and then $\mu \to 0$. Other ways for performing this limit are possible. However, taking the limit in σ first, ensures that we obtain the established cyclic Lotka-Volterra model, which does not comprise empty sites: $a+b+c=1$ [63].

C. Spatially extended continuum model

In a continuum formulation, the nearest neighbor exchange process macroscopically leads to diffusion with a diffusion constant $D = \epsilon L^{-2}/2$. The ensuing diffusion-reaction equations are simply obtained from the rate equations (4) by supplementing them with diffusion terms $D\nabla^2 a$, $D\nabla^2 b$, and $D\nabla^2 c$, respectively [26,33,34,36]. Then, upon applying the above transformations to the diffusion terms one obtains

$$\partial_t z = D[\nabla^2 z - \mathrm{i}(\nabla z^*)^2] + \text{reaction terms}, \tag{14}$$

where we have neglected gradient terms of order $O[(\nabla z)^3]$. We expect that the dynamics is dominated by the long wavelength

modes, and therefore only keep the leading order gradient term, leading to normal diffusion in the complex concentration z. This finally leads to the complex Ginzburg-Landau equation,

$$\partial_t z = D\nabla^2 z + (c_1 - \mathrm{i}\omega)z - c_2(1 - \mathrm{i}c_3)|z|^2 z, \qquad (15)$$

a paradigmatic equation in nonlinear dynamics [56].

II. THE MAY-LEONARD LIMIT

The May-Leonard model, obtained in the limit $\nu \to 0$, is characterized by the following reduced set of reaction rules:

$$AB \xrightarrow{\sigma} A\emptyset, \quad BC \xrightarrow{\sigma} B\emptyset, \quad CA \xrightarrow{\sigma} C\emptyset, \qquad (16a)$$

$$A\emptyset \xrightarrow{\mu} AA, \quad B\emptyset \xrightarrow{\mu} BB, \quad C\emptyset \xrightarrow{\mu} CC. \qquad (16b)$$

For large systems in the well-mixed limit, the dynamics is described by the May-Leonard equations [19],

$$\partial_t a = -\sigma ac + \mu a(1 - \rho), \qquad (17a)$$

$$\partial_t b = -\sigma ba + \mu b(1 - \rho), \qquad (17b)$$

$$\partial_t c = -\sigma cb + \mu c(1 - \rho). \qquad (17c)$$

The nonlinear dynamics of these equations is characterized by the same types of fixed points and invariant manifold as the general model (4). The reactive fixed point (a^*,b^*,c^*) is globally unstable, as manifested by the existence of the Lyapunov function $\mathcal{L} = abc/\rho^3$. When starting in the vicinity of the unstable fixed point, the trajectories spiral outward on the invariant manifold and form heteroclinic cycles, approaching the boundary of the phase space and the absorbing states without ever reaching them [19]. However, intrinsic noise due to the stochastic nature of the interactions, and spatial structure drastically alter the observed behavior. While in well-mixed systems stochastic fluctuations drive the system into one of the absorbing states within a short time proportional to the logarithm of the system size [11,12,14,15,17,18,64], spatial structures may effectively delay extinction by orders of magnitude [3,34].

Similar to the previously studied one-dimensional case [38], the two-dimensional, stochastic May-Leonard model exhibits distinct dynamical regimes as a function of the diffusion constant D (Fig. 1). From our simulations we find the following phenomenology: For large values of D, we observe that the system (after some initial transient) is first almost entirely taken over by one species, but with a few individuals of a second species surviving, which dominates over the more abundant species. This second species will then slowly take over the system and thereby lead to a dynamical behavior that is reminiscent of the heteroclinic orbits of the deterministic, well-mixed system, where the global dynamics approaches the boundary of the invariant manifold. In this regime, spatial patterns are of minor importance and the dynamics can be understood in terms of a quadratic coagulation process as outlined in Ref. [38]. With decreasing diffusion constant we observe planar waves of cyclically aligned uniform domains as well as rotating spiral waves [Figs. 1(b)–1(d)]. In planar waves the overall concentrations may be constant, corresponding to stable domain borders, or change periodically, as a result of "tunneling" events in the leading edges of the fronts. The leading edges of the fronts may reach into second next domains, i.e., there is a finite probability for particles to penetrate domains of prey via "tunneling" events [38]. As a consequence domain sizes oscillate periodically between characteristic length scales, thereby leading to oscillating overall densities. The dynamics of rotating spirals has been extensively studied in Refs. [34,35]. Both planar waves and rotating spirals are only metastable, as stochastic fluctuations eventually lead to the annihilation of neighboring fronts and the dynamics will ultimately end in one of the three absorbing states which correspond to the extinction of two of the three species. The dynamics into the absorbing states has been found to be highly nontrivial, as the dynamical regimes described above lead to transitions into the absorbing states on different time scales. Furthermore, their statistical weight heavily depends on the diffusion coefficient D [30,33,34,38,41].

A. Global attractors and "free energy landscape" of the spatio-temporal dynamics

To gain insight into the mechanisms responsible for these qualitatively different spatio-temporal patterns and how they determine the longevity of biodiversity in the population, we studied the global phase portrait of the dynamics. Figure 2 shows histograms for the overall concentrations

$$(\overline{a}(t),\overline{b}(t),\overline{c}(t)) = \int [a(\mathbf{x},t),b(\mathbf{x},t),c(\mathbf{x},t)]\, d^2x \qquad (18)$$

of the three species on the invariant manifold of the rate equations, Eqs. (17a)–(17c). In detail, the negative logarithm of the probability $P(\overline{a},\overline{b},\overline{c})$ to find the system in a specific global state $(\overline{a},\overline{b},\overline{c})$ before reaching one of the absorbing states is projected onto the invariant manifold:

$$\mathcal{F}(\overline{a},\overline{b},\overline{c}) \equiv -\ln P(\overline{a},\overline{b},\overline{c}). \qquad (19)$$

The quantity $\mathcal{F}$ hence gives the logarithmic density of global trajectories in phase space, and it can be considered as an effective potential in the following sense: When instead of the mean-field reaction term, as given by the right-hand side of Eq. (15), one uses $\mathcal{F}$ as a "renormalized" potential for a Ginzburg-Landau theory, one obtains a reaction-diffusion equation, which gives a good description of the spatio-temporal dynamics. Long-lived spatio-temporal patterns correspond to regions of high probability on the manifold and are termed *global attractors* of the spatio-temporal dynamics in the following. Equivalently, adapting terminology from statistical mechanics, these attractors may be viewed as minima of the "free energy landscape" $\mathcal{F}$. Of course, it is to be understood that these attractors are only metastable, i.e., while the system spends a long time in these states, ultimately demographic fluctuations will drive the system into one of the absorbing states. Intuitively, one may visualize those fluctuations as driving the escape of the dynamics from the minima in the "free energy landscape" into one of the absorbing states. We will later see that *qualitative* changes in the shape of these minima correspond to transitions in the nature of the dynamic processes leading to extinction and the mean times to extinction. These transitions should not be confused with nonequilibrium phase transitions. Rather they are to be considered as bifurcations in the nonlinear dynamics.

Figure 2 shows that the shape of these global attractors strongly depends on the magnitude of the diffusion constant

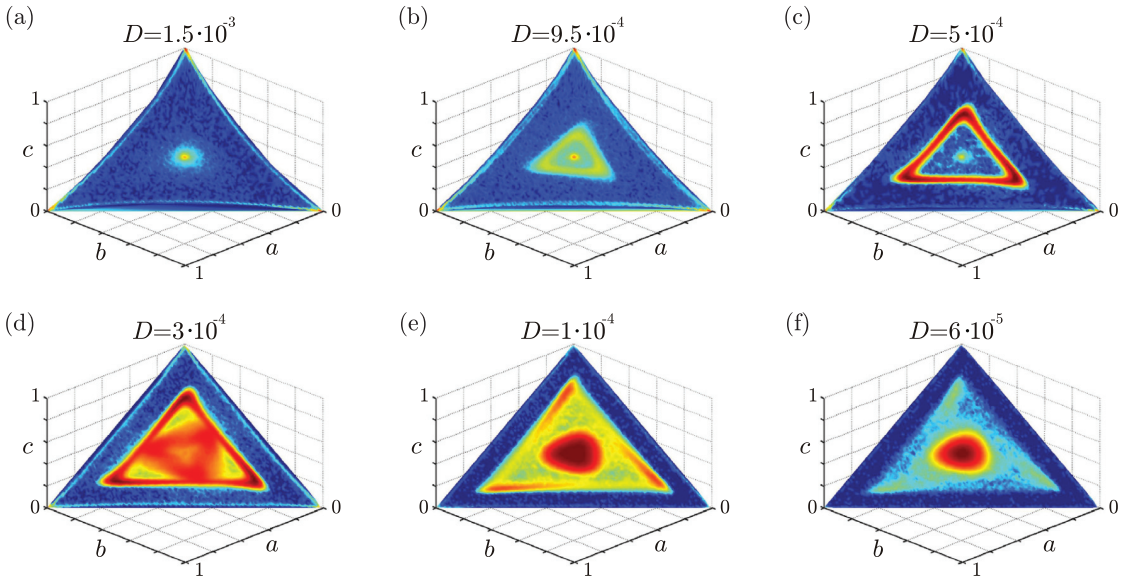

FIG. 2. (Color online) Free energy landscapes of the May-Leonard model for various values of the diffusion constant D. The dynamics of the overall densities $\overline{a}, \overline{b}, \overline{c}$ is strongly confined to the invariant manifold of the well-mixed model, Eq. (17). To study the mechanisms underlying the distinct spatio-temporal patterns found in the spatial, stochastic May-Leonard model we projected the probability for the overall densities onto the invariant manifold of the rate equations (17) for different values of the diffusion constant D. Color (gray scale) denotes the logarithmic probability to find the system globally in a specific state before reaching one of the absorbing states, such that red (medium gray) denotes a high probability, yellow (light gray) a medium probability, and blue (dark gray) a low probability. The absorbing states themselves are not part of the statistics. For large D, no stable spatial structures can form and the dynamics corresponds to the well-mixed case, Eqs. (17). As D becomes smaller than $D \approx 9.5 \times 10^{-4}$ an attractor of the global dynamics emerges, effectively stabilizing the system against extinction. This attractor corresponds to planar, traveling waves with oscillating overall densities, and grows in radius with decreasing D due to a decreasing wavelength of the planar waves. For $D \leqslant 3 \times 10^{-4}$, a second attractor emerges, corresponding to rotating spirals. As a result of a decreasing wavelength of the spiral patterns the second attractor's radius decreases with the diffusion constant, while the attractor corresponding to the traveling waves diminishes. Parameters were $L = 60$ and $M = 8$. Each plot was averaged over at least 100 realizations of the stochastic spatial dynamics.

D. For $D > 10^{-3}$, there are no attractors other than the regions in the immediate vicinity of the three absorbing states. All trajectories describing the global dynamics quickly leave the unstable fixed point (a^*,b^*,c^*) and approach the boundaries of the invariant manifold. Therefore, the probability is highest in the center (because the dynamics starts there) and at the boundaries. In this regime, the system can be considered as well-mixed. The heteroclinic orbits in the global phase portrait then correspond to spatially uniform oscillations between states where one of the three species dominates; cf. Fig. 1(a). With decreasing diffusion constant D the nature of the global attractor changes qualitatively. Starting at the center of the manifold, the free energy develops a distinct local minimum which then evolves into a triangular shaped closed region; see Figs. 2(a)–2(c). In other words, the phase portrait of the global population dynamics changes from an unstable fixed point with heteroclinic orbits to a pronounced *limit cylce*. Inspecting the spatio-temporal patterns as obtained from our stochastic simulations, we find that this limit cycle of the global dynamics corresponds to planar traveling waves; see also Fig. 1(b). The triangular shape is the result of oscillating overall densities. In the following we will refer to this particular limit cycle as the *wave attractor*. Further lowering the diffusion constant, a second global attractor emerges as a smaller triangle inside the triangle corresponding to the planar waves; cf. Figs. 2(d)–2(f). The inner triangular attractor corresponds to rotating spirals and will henceforth be denotes as the *spiral attractor*. We find that in this regime of diffusion constants the two attractors coexist, meaning that we observe both planar waves and rotating spirals. Both processes may even be found within the same realization. With even further decreasing the diffusion constant, the weight of the triangular-shaped attractor corresponding to planar waves decreases, and the attractor eventually disappears completely. As a consequence, the attractor of spiral waves gains weight, such that the dynamics at low mobilities is dominated by spiral waves. Taken together, we find that the phase portrait of the global dynamics changes qualitatively upon decreasing the diffusion constant, and that those qualitative changes have a one-to-one correspondence with distinct spatio-temporal patterns in the population dynamics. As a consequence, the free energy landscape on the invariant manifold can be taken as a fingerprint of the spatio-temporal dynamics. We will use it in the following to identify transitions between different patterns and analyze the ensuing changes in the dependence of the extinction times on system size.

B. Pattern selection and extinction times

The attractors in Fig. 2 show a triangular symmetry. A reduced representation for the global dynamics on the invariant manifold can therefore be obtained in terms of a properly

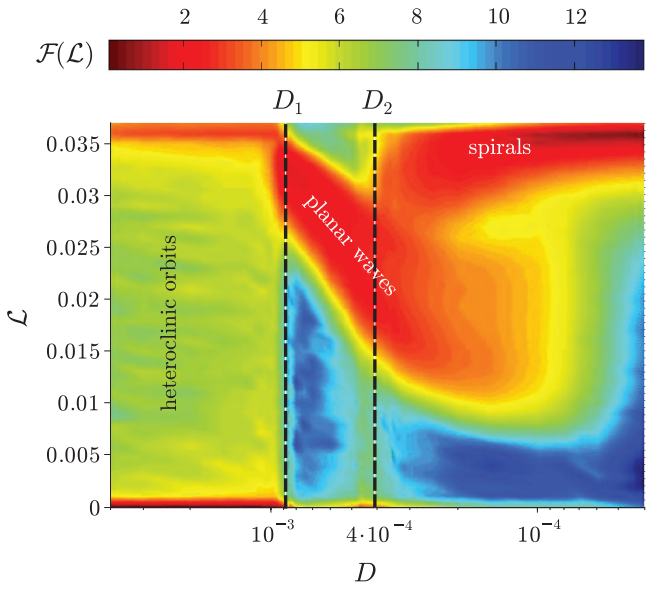

FIG. 3. (Color online) Free energy landscape of the global dynamics of the two-dimensional May-Leonard system. The value of the Lyapunov function $\mathcal{L}$ is a measure of how close a specific state is to the boundary of the invariant manifold ($\mathcal{L} = 0$). Color (gray scale) denotes the logarithmic probability to find the system at a specific value of $\mathcal{L}$, i.e., the free energy formally defined in Eq. (19). Red (medium gray) signifies small values of the free energy (minima of the potential) and thereby an attractor of the global dynamics. Yellow (light gray) denotes intermediate values, and blue large values of the free energy. The free energy landscape changes qualitatively at two threshold values for the diffusion constant D. For large values of D the effective free energy has minima in the center ($\mathcal{L} = 0.037$), where the dynamics starts, and at the boundaries of the invariant manifold ($\mathcal{L} = 0$). At a first threshold $D_1 \approx 9 \times 10^{-4}$ an attractor emerges, which moves away from the reactive fixed point ($\mathcal{L} = 0.037$) with decreasing values of D. Below a second threshold, $D \approx 4.5 \times 10^{-4}$, a second attractor emerges near the reactive fixed point, coexisting with the first one. For even smaller mobilities the dynamics is solely determined by the attractor near the reactive fixed point. Comparing with our simulations we find that these attractors correspond to global oscillations (heteroclinic orbits), planar waves, and rotating spirals, respectively. The stochastic simulations were performed on a square lattice of linear size $L = 60$ and with a carrying capacity $M = 8$ for each site. For each values of D, the histogram was averaged over at least 100 realizations.

defined radial variable. A convenient choice is the Lyapunov function

$$\mathcal{L} \equiv \frac{\overline{a}\,\overline{b}\,\overline{c}}{(\overline{a}+\overline{b}+\overline{c})^3} \tag{20}$$

evaluated with the global concentrations $\overline{a}$, $\overline{b}$, $\overline{c}$. It measures the distance of a global state to the boundaries of the invariant manifold and is approximately constant along the attractor for the planar waves. Figure 3 shows the effective free energy $\mathcal{F}(\overline{a},\overline{b},\overline{c})$ as a function of the Lyapunov function and the diffusion constant. One easily identifies two threshold values of the diffusion constant where there are qualitative changes in the free energy landscape. We recover a threshold value $D_1 \approx 9 \times 10^{-4}$ marking a transition from a well-mixed dynamics to a dynamics with spatio-temporal patterns [33,34]. However, the range of patterns is much richer than previously noted. Actually, the first threshold D_1 marks a transition from spatially uniform oscillations between states dominated by a single species to planar waves where the three species cyclically chase each other. Note that the global oscillations still form part of the dynamics, albeit with a lower probability. Upon lowering the diffusion constant below a second threshold value, $D_2 \approx 4.5 \times 10^{-4}$, the histogram of system trajectories becomes bimodal with a second metastable attractor emerging which is located close to the center of the invariant manifold. It can hence be identified with the inner, triangular attractor on the invariant manifold. As discussed before, this second attractor corresponds to rotating spiral waves. The coexistence of two attractors in this regime of mobilities means that both, planar waves and rotating spirals, are observed. Depending on the choice of initial conditions, the dynamics may at first end up in either one of the two attractors. Due to stochastic fluctuations it may, however, from time to time switch between the two attractors akin to thermal fluctuations causing rare transitions between different potential minima. With further decreasing D we observe that the metastable attractor corresponding to planar waves dissolves, and only the attractor corresponding to rotating spirals remains.

To further scrutinize the effect of these spatio-temporal patterns and the ensuing metastable global attractors on the system's dynamics, we analyzed the mean first passage time into the absorbing states as a function of D; see Fig. 4. We find that the mean time to extinction increases abruptly at

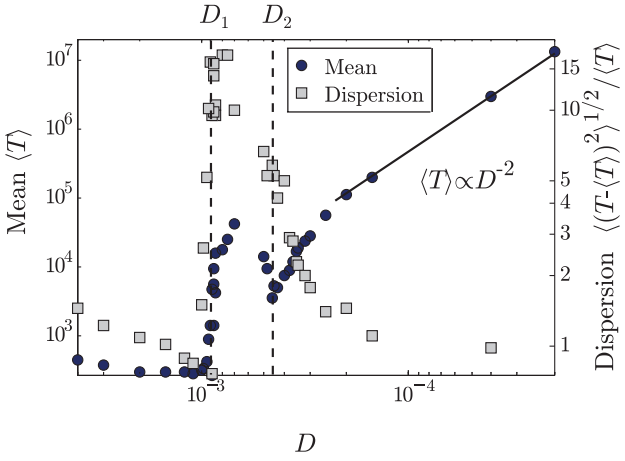

FIG. 4. (Color online) Mean lifetimes (dark dots) and coefficient of variation (gray squares) of the two-dimensional May-Leonard system as a function of the diffusion constant D. The mean lifetime increases abruptly at a first threshold value D_1 (indicated by a dashed line) where planar waves form. After passing through a maximum the lifetime decreases again. This is due to planar waves which become unstable with decreasing correlation length. At the second threshold D_2 (dashed line) rotating spirals become possible. With further decreasing diffusion constant the mean lifetime is asymptotically described by a power law D^{-2}. The coefficient of variation is a dimensionless measure for the dispersion of the probability distribution of T. The dispersion near the upper threshold D_1 becomes large, i.e., we observe dynamical regimes on a variety of different time scales.

D_1, where the global attractor of planar waves emerges. After passing a peak value the mean lifetime then decreases again, as the wavelength of the planar waves becomes smaller. Then, as a result, these waves become more prone to fluctuations, and the rate of domain annihilation increases. Finally, below D_2 the lifetime increases again, which we attribute to the emergence of stable spiral waves. For small values of D the mean lifetime follows a power law $\langle T\rangle \propto D^{-2}$. This dependence can be understood by a simple scaling argument: Since spirals annihilate pairwise as they meet, the mean lifetime should scale quadratically with their number, $\langle T\rangle \propto (n_{\text{spirals}})^2$. The number of spirals in the system scales with their wavelength as $n_{\text{spirals}} \propto \lambda^{-2}$. With $\lambda \propto \sqrt{D}$ we then infer that the mean lifetime scales as $\langle T\rangle \propto D^{-2}$, which is in good agreement with our numerical results.

Figure 4 also shows the coefficient of variation, defined as the standard deviation divided by the mean:

$$c_v \equiv \sqrt{\langle (T - \langle T\rangle)^2\rangle}/\langle T\rangle. \tag{21}$$

It gives a dimensionless measure for the dispersion of the probability distribution of T. We find that the dispersion increases drastically right at the threshold D_1. In this regime the standard deviation is much larger than the mean. From the spatio-temporal dynamics observed in our simulations we infer that this is due to the fact that there are several distinct dynamic processes driving the system towards an absorbing state and that these processes occur on greatly different time scales. There are rapid extinction processes, where, after a short transient, domains in a planar wave are aligned in a noncyclic order and thus immediately annihilate. We also find a process, where the global dynamics performs heteroclinic orbits. Last, one observes metastable planar waves; cf. Fig. 1. Note that although the planar waves process is metastable, it does not necessarily mean that it dominates the long time properties of the system. In Ref. [38] it has been shown for the one dimensional model that the probability of extinction scales differently with system size for these two processes. In particular, one observes a crossover, such that for small systems planar waves determine the long time tails, while for very large systems global heteroclinic orbits are responsible for the longest living states. The relative weight of these processes depends on the diffusion coefficient D. As we have already learned from the above analyses, below the lower threshold value, D_2, there are also spiral waves emerging. With decreasing D, spirals become the dominant patterns while all the other dynamic processes become less and less probable. As a result, the mean time to extinction is dominated by an escape out of the spiral attractor. The dispersion therefore decreases again.

The probability distributions of first passage times of the above dynamical processes leading into the absorbing states show significantly different scaling behavior with the system size; cf. Ref. [38]. From an evolutionary perspective, the tails of these distributions are most relevant because they correspond to rare, but extremely long-living communities maintaining biodiversity. The reason for their relevance is that the probability to observe a short-living (transient) ecosystem in nature is much lower than the probability to observe an ecosystem which persists for a long time. In Ref. [38] two of the authors showed that the tail of the distributions of first passage times of heteroclinic orbits scale like $\exp(T/N)$, while for traveling waves the tail scales like $\exp[T/(\ln N)^3]$. As a consequence, there is a crossover in the tail of the overall distribution of first passage times. Interestingly, while for small systems the long time dynamics is dominated by traveling waves, for large systems it is dominated by heteroclinic orbits. Although the computation of the distribution of first passage times is not feasible in two dimensions, we expect that similar arguments will hold here, as well.

As shown in Refs. [33,34], there is a transition from a spatially uniform dynamics reminiscent of a well-mixed system to a dynamics dominated by spatio-temporal patterns when the wavelength of the pattern exceeds the system size. Following the classical theory of front propagation into unstable states [65], the wavelength of the traveling and spiral waves can be determined using the complex Ginzburg-Landau equation (15) [33,36]:

$$\lambda = -\frac{2\pi c_3}{\sqrt{c_1}\left(1 - \sqrt{1 + c_3^2}\right)}\sqrt{D}. \tag{22}$$

Due to the difference in geometry between planar and spiral waves this implies two distinct thresholds, D_1 and D_2. For planar waves on a square lattice we simply have the condition that the wavelength equals the system size, $\lambda(D_1) = 1$. In Refs. [33,34] it was found that the calculated wavelength deviates by a constant factor of 1.6 from the numerical value of the wavelength. This rescaling factor accounts for the renormalization of the reaction term due to spatio-temporal correlations, as captured by the global attractors. Using this rescaling factor we find a threshold value $D_1 \approx 7.6 \times 10^{-4}$, in good agreement with the numerically found value, $D_1 \approx 9 \times 10^{-4}$; cf. Fig. 3. The very same threshold is also found in the one-dimensional model [38]. There planar waves are the only possible spatial pattern and the threshold stems from their wavelength outgrowing the system size. Remarkably, the numerical values for D_1 coincide in both, one and two spatial dimensions, as the complex Ginzburg-Landau equation predicts equal wavelengths for both cases; see further below. Since spirals always arise as pairs of antirotating spirals, stable pairs are possible, as long as the minimum distance $d_{\min}$ between two vertices of the spirals is smaller than half of the system size. In other words, the threshold D_2 is given by $d_{\min}(D_2) = 1/2$. To obey geometric constrains dictated by the periodic boundary conditions and the spirals' wavelength, the minimum distance of two antirotating spirals is $d_{\min} = 2/3\lambda(D)$; cf. also Fig. 1(d). This implies a threshold value of $\lambda = 3/4$, which is close to $\lambda \approx 0.8$ obtained numerically in Ref. [34]. Hence, from $2/3\lambda(D_2) = 1/2$ we obtain $D_2 \approx 4.3 \times 10^{-4}$, in good agreement with the numerical results shown in Fig. 3.

In the following we provide a scaling argument giving the scaling of the size of the wave attractor with the mobility D. In the intermediate regime between the two threshold values of D the wavelength of the planar wave patterns is of the same order as the system size. Hence, in this regime the finite spatial extension of the system is important. In our case, periodic boundary conditions allow stationary domain profiles only for certain values of the wave length, $\lambda = 1/n$, $n = 1,2,\ldots$ [66].

If the wavelength does not match any of these values, we observe oscillations in the overall concentrations, corresponding to the triangular attractor in Fig. 2. In the intermediate regime, $D_1 > D > D_2$, where λ is slightly smaller than 1, two domains take the characteristic domain size dictated by D, and the third domain occupies the rest of the system. We now employ these intuitive observations to obtain the scaling of the wave attractor. Our numerical simulations reveal that the radius of the wave attractor increases with D according to a power law with an exponent of approximately 0.9, meaning that the corresponding values of the Lyapunov function increases with this exponent. If the system size is not a multiple of $\lambda \sim D^{1/2}$ one of the three domains will be of different wavelength. Assuming the concentration of empty sites is independent of D we set without loss of generality $\overline{a} = \overline{b} \sim D^{-1/2}$ and $\overline{c} \sim 1 - 2D^{-1/2}$. Upon inserting these concentrations into the Lyapunov function, we obtain $\mathcal{L} \sim D - 2D^{3/2}$, which is to leading order in agreement with our results [67].

Summarizing, we find that the spatio-temporal dynamics changes qualitatively at certain threshold values of the diffusion constant. These changes are finite size effects in the sense that they arise as a result of the comparison of certain length scales. We use the term "transition" for this behavior in the sense that macroscopic properties of the system change qualitatively and abruptly at these threshold values. This is particularly evident in the mean first passage times to extinction. In the language of nonlinear dynamics the system undergoes bifurcations as a function of the mobility.

III. THE CYCLIC LOTKA-VOLTERRA LIMIT

In the limit $\sigma \to 0$, $\mu \to 0$ only reactions remain, where the replication of predators does not require the availability of empty spaces. The resulting model is then of the Lotka-Volterra type [44,45], and characterized by a reduced set of chemical reactions:

$$AB \xrightarrow{\nu} AA, \quad BC \xrightarrow{\nu} BB, \quad CA \xrightarrow{\nu} CC\,. \tag{23}$$

This model is often referred to as the three-species Lotka-Volterra model. Although at a first glance there are no dramatic differences to the May-Leonard reactions, Eq. (16), the ensuing nonlinear dynamics is vastly different. The deterministic rate equations read

$$\partial_t a = \nu a(b-c), \quad \partial_t b = \nu b(c-a), \quad \partial_t c = \nu c(a-b). \tag{24}$$

Without loss of generality, we also fix the normalization of total concentrations: $a + b + c = 1$. The nonlinear dynamics of the well-mixed cyclic Lotka-Volterra model again exhibits the same absorbing fixed points as the general model (3). The reactive fixed point is now given by

$$(a^*, b^*, c^*) = \left(\frac{1}{3}, \frac{1}{3}, \frac{1}{3}\right). \tag{25}$$

It is, however, neutrally stable as the real parts of the eigenvalues, Eq. (6), are zero. In fact, $\dot{\mathcal{L}} = 0$ for any a, b, and c, such that starting from any point on the phase plane, the trajectories form neutrally stable cycles.

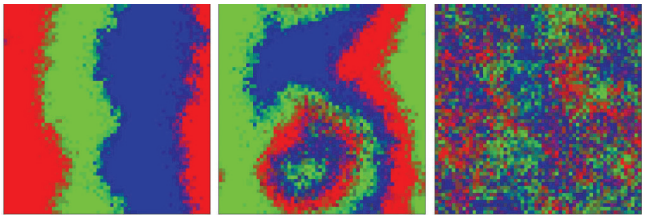

FIG. 5. (Color online) Illustration of the instability of wave fronts in the cyclic Lotka-Volterra system. The initial condition at $t = 0$ was chosen as three domains of equal size in cyclic order. The pictures show snapshots at times $t = 135$, 180, and 300. Color (gray scale) denotes species concentrations as described in Fig. 1. Parameters were $D = 10^{-4}$, $M = 8$, and $L = 80$.

Similar to the May-Leonard model, species' mobility drastically alters the system's collective dynamics [26]. However, the ensuing spatio-temporal dynamics of the cyclic Lotka-Volterra and the May-Leonard model differ qualitatively. This behavior can be understood upon considering the dynamics of domain boundaries separating different species. In the May-Leonard model the separation of selection and reproduction processes is counteracting the roughening of these domain boundaries due to stochastic fluctuations: If a species from one domain enters the other species' domain, it first creates empty sites. Since these empty sites are occupied with a higher probability by offsprings of individuals from the invaded species rather than by invaders, the invasion process is unlikely to be successful. This stabilizes spatially separated domains in the May-Leonard model. In contrast, in the cyclic Lotka-Volterra model an invader directly replaces the invaded species such that it has a higher probability of success. As illustrated in Fig. 5, this leads to a roughening instability of planar wave fronts. However, this does not imply the total loss of any spatial correlations. To the contrary, there are still strong correlations and they play a fundamental, yet subtle, role in the spatio-temporal dynamics and the processes leading to the extinction of all but one species.

In our simulations we observe different dynamic processes depending on the mobility. For large diffusion constants, where the system can be considered well-mixed, we recover the homogeneous oscillations as predicted by the rate equations (24). We still find homogeneous oscillations if the mobility is decreased. However, as we will see below, these system-wide oscillations are of entirely different nature as the neutrally stable orbits found in the well-mixed system. For even lower mobility we finally find a seemingly random appearance and dissolution of spatial clusters. These clusters are convectively unstable spiral waves, which, due to a roughening transition associated with an Eckhaus instability, appear, move and annihilate.

A. Extinction times and extinction probabilities

As discussed previously [26,33,34], a convenient measure to characterize the stability of the system is the probability P_{ext} that the system has reached an absorbing state within a time proportional to the system size N. The simulations for our model reproduce the results found in Ref. [26]. For large D our result coincides with the analytically obtained value

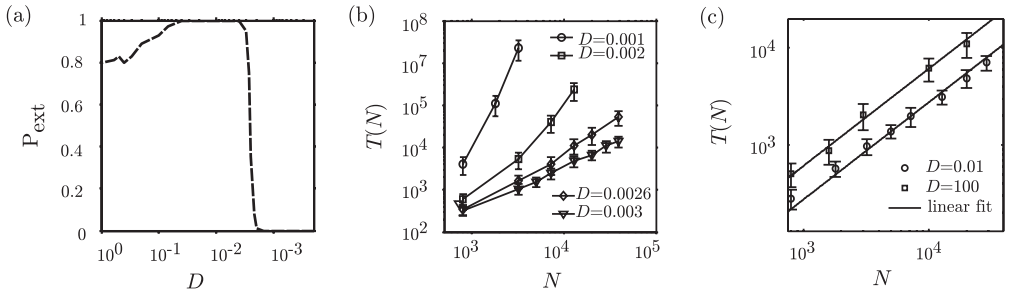

FIG. 6. (a) Probability that the system with Lotka-Volterra reactions reaches an absorbing state before $t = N$. We observe a sharp transition from survival to extinction at $D \approx 3 \times 10^{-3}$. In the well-mixed limit the extinction probability converges to a finite value of 0.8 ($M = 8$, $L = 60$). (b) and (c) The scaling of the mean first passage time into any of the absorbing states with the system size N. Two phases can be identified. For $D < 3 \times 10^{-3}$ the scaling becomes exponential, hinting at an escape process from a metastable state. In the well-mixed case ($D = 100$) the scaling is linear, in agreement with the escape out of a neutrally stable state. In the intermediary regime our results are in agreement with both a logarithmic and a linear scaling.

found for the nonspatial system [17]; see Fig. 6(a). For low mobilities the extinction probability is close to zero. Hence, the system is in a metastable state with extinction times scaling exponentially in the system size, cf. Fig. 6(b). At a threshold value $D_c \approx 3 \times 10^{-3}$, there is a sharp transition to $P_{\text{ext}} \approx 1$ indicating that extinction times scale logarithmically in the system size N. Indeed, Fig. 6(c) indicates that the scaling of mean first passage times is sublinear. For even larger values of the diffusion constant, the extinction probability decreases again until it reaches a value of 0.8 in the well-mixed limit. Here, extinction times scale linearly, as demonstrated by Fig. 6(c). Hence, the global dynamics is characterized by the escape out of a neutrally stable state. We conclude that spatial correlations increase the system's stability for small D and destabilize it above a threshold value D_c.

B. Global attractors and free energy landscapes

As for the May-Leonard model we now employ a study of the global phase portraits to gain a deeper understanding of the ambiguous impact of spatial structures on the longevity of biodiversity. The existence of metastable states below a certain mobility threshold, suggested by the scaling of extinction times with system size, is supported by histograms of the global dynamics. Figure 7 shows the free energy landscape projected onto the invariant manifold of Eqs. (24). For very small values of D we find an attracting region in the center of the simplex. This attractor corresponds to convectively unstable spirals. As mentioned before, smooth domain borders are subject to roughening and therefore become unstable in the Lotka-Volterra model. However, while spatial patterns can not be maintained, strong correlations exist and effectively render the global dynamics metastable. With increasing values of D we observe that the trajectories describing the overall dynamics of the system are attracted towards a *limit cycle*, which grows in radius and eventually reaches the boundary of the invariant manifold. This limit cycle corresponds to *system-wide oscillations*. As these oscillations are linked to a metastable attractor, they are much more long-lived compared to the neutrally stable oscillations found in the well-mixed case, i.e., their mean lifetime scales exponentially with the system size. At some threshold value of the diffusion constant the attractor coincides with the boundary of the simplex. Then, the absorbing states are embedded within the limit cycle. As a consequence, the global dynamics is effectively attracted towards the boundaries of the phase plane once it reaches the limit cycle's basin of attraction, and therefore rapidly reaches one of the absorbing fixed points. The global dynamics is therefore effectively heteroclinic and approaches the absorbing states exponentially fast. Hence, in this regime spatial structure destabilize the system, which explains the sub linear scaling of extinction times as shown in Figs. 6(a) and 6(c). For large D, the attractor lies outside of the simplex, such that the global

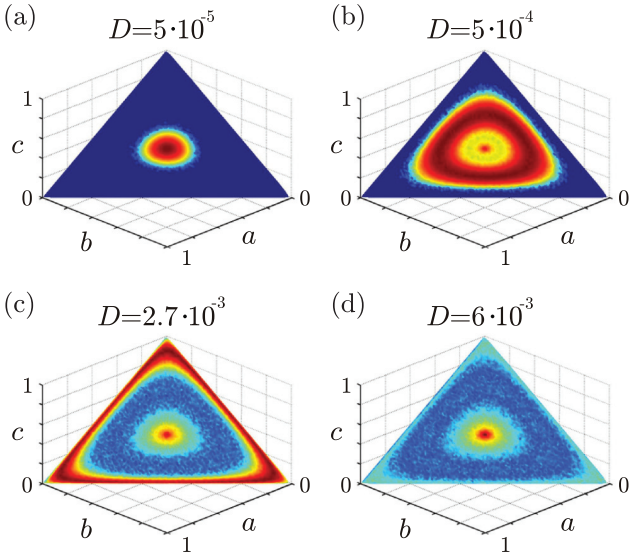

FIG. 7. (Color online) Probability to find the system globally in a specific state before reaching one of the absorbing states. Red (medium gray) denotes a high probability, yellow (light gray) a medium probability, and blue (dark gray) a low probability. One observes the emergence of an attracting limit cycle of the global dynamics. The attractor grows in radius with increasing D and eventually reaches the boundaries of the invariant manifold. For even larger values of the diffusion constant the attractor lies outside of the invariant manifold and the global dynamics is essentially neutral. The histograms were sampled over 100 trajectories until $T = N$. Parameters were $M = 8$ and $L = 60$.

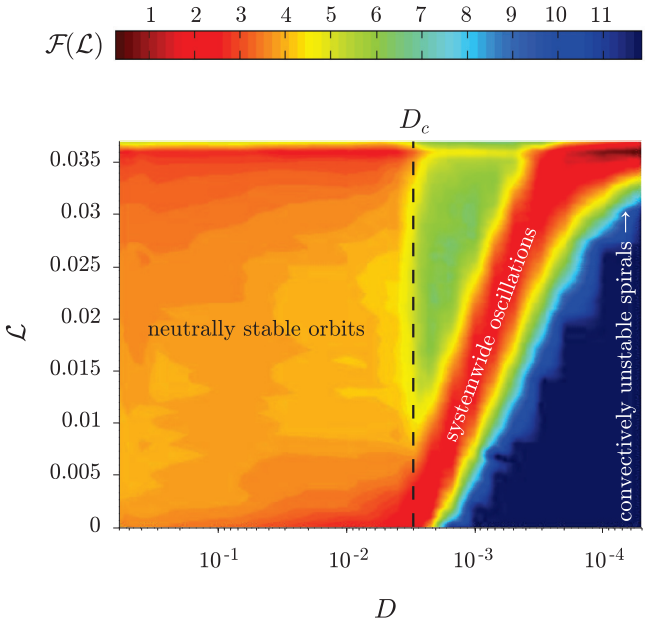

FIG. 8. (Color online) The global phase portrait of the Lotka-Volterra system. For each diffusion constant D we plot (in color code or gray scale) the probability to find the system before $t = N$ at a specific value of the Lyapunov function $\mathcal{L} = \bar{a}\bar{b}\bar{c}$. Red (medium gray) denotes a high probability, yellow (light gray) a medium probability, and blue (dark gray) a low probability. Three dynamical regimes corresponding to neutrally stable orbits, system-wide oscillations, and convectively unstable spirals can be identified and linked to their corresponding attractors of the global dynamics. Note that the attractor vanishes at $D \approx 3 \times 10^{-3}$ corresponding to the abrupt increase of extinction probabilities in Fig. 6. The simulations were done with $M = 8$ and $L = 60$, and, for numerical reasons, stopped at $T = N$. For each of roughly 20 data points in D we averaged over approximately 100 trajectories.

dynamics on the simplex is essentially governed by neutrally stable orbits.

Figure 8 illustrates the different dynamical regimes by means of the effective free energy $\mathcal{F}$ for the cyclic Lotka-Volterra model. We identify three distinct regime, which are characterized by the shape of the effective free energy. For the well-mixed system, $D > D_c \approx 3 \times 10^{-3}$, the potential is flat and the global dynamics is neutrally stable as predicted by the rate equations (24). At D_c an attractor emerges, which at this point coincides with the boundaries of the simplex ($\mathcal{L} = 0$). With decreasing values of D the attractor is located at increasingly large values of the Lyapunov function until at $D \approx 4 \times 10^{-4}$ it coincides with the reactive fixed point of the rate equations (24). Comparing with our simulations we therefore identify three regimes: neutrally stable orbits, metastable system-wide oscillations, and convectively unstable spirals. In conclusion, the behavior of the attractors of the global dynamics provides an intuitive explanation for the observed transitions in the extinction probabilities.

IV. THE INTERMEDIATE REGIME

While the previous sections considered important limiting cases of the reactions (3), we now study the general case with $\sigma, \mu, \nu \neq 0$. We will use the following parametrization, which allows one to tune the relative weight of Lotka-Volterra-type reactions and May-Leonard-type reactions:

$$\nu(s) \equiv s, \quad \mu(s) \equiv 1, \quad \sigma(s) \equiv 1 - s. \tag{26}$$

Here the parameter s is the fraction of Lotka-Volterra type reactions and is varied between 0 and 1. This choice of parametrization has two important properties: First, it conserves the limits discussed in the previous sections and makes them comparable. In the Lotka-Volterra limit and in the May-Leonard limit per time step each individual performs, on average, one active selection process or passive process, respectively. This holds for any value of s. Second, our simulations show that the correlation length of species concentrations stays approximately constant when changing s (data not shown here). This is because in our parametrization we fix the relevant time scale, and thereby by dimensional analysis, for a given mobility, the correlation length.

Figure 9 shows that with increasing values of s spiral patterns become convectively unstable, i.e., the vertices start to move and annihilate. The destabilizing effect of Lotka-Volterra reactions on spiral patterns can also be visualized by considering the absolute value of the coordinates defined in Eq. (7), $|\mathbf{y}(a,b,c)|$. It gives a measure of how far the system is locally away from the reactive fixed point. Low values of $|\mathbf{y}|$ correspond to a locus where each species is present at approximately equal concentrations, and therefore indicate the position of spiral vertices. In Figs. 9(d)–9(f) black dots correspond to positions, where this absolute value is smaller than 0.13 [68]. We thus infer that the spirals become unstable with increasing s. Indeed, the complex Ginzburg-Landau equation (15) predicts an Eckhaus instability, implying that the

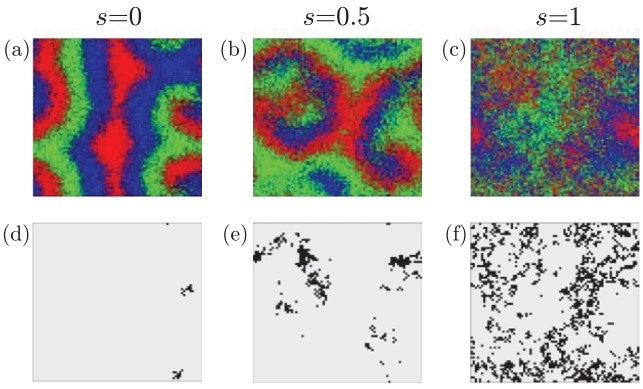

FIG. 9. (Color online) (a)–(c) Snapshots of the spatial distribution of species for different values of the fraction of Lotka-Volterra reactions s indicated in the graph. Color denotes (gray scale) the concentration of the species A, B, and C, as described in Fig. 1. With increasing s spirals become convectively unstable, i.e., they move, annihilate, and then appear again. (d)–(f) To illustrate the destabilization of spiral waves we computed for each lattice site the distance from the reactive fixed point $|\mathbf{y}(a,b,c)|$. Dark points show sites where $|\mathbf{y}(a,b,c)|$ is below a certain threshold, thereby indicating the position of spiral vertices. Parameters were $D = 10^{-4}$ (corresponding to the regime, where spirals and waves are possible in the May-Leonard model), $M = 8$, and $L = 80$.

spirals vertices become convectively unstable [26], i.e., they move, annihilate, and appear again constantly above a certain value of s. To determine this value we follow the steps given in Ref. [56], where the stability of planar wave solutions was studied. The waves are stable, as long as the generalized Eckhaus criterion,

$$1 - 2\frac{\left(1 + c_3^2\right)Q^2}{1 - Q^2} > 0, \tag{27}$$

holds, where Q is the selected wave vector:

$$Q = \frac{2\pi}{\lambda}\sqrt{\frac{D}{c_1(s)}} = \frac{\sqrt{1 + c_3(s)^2} - 1}{c_3(s)}. \tag{28}$$

Inserting $c_3(s)$ and solving for s we find a critical value of $s_E \approx 0.32$. The breakdown of stable spatial structures as the result of a roughening transition is indeed confirmed by our numerical simulations. In contrast to the transitions in D, the Eckhaus instability is independent of the size of spatial patterns, and it can therefore be considered a transition in the strict thermodynamic sense. It has significant, yet ambiguous, implications for the stability of biodiversity, as will be discussed in the following.

A. Extinction times

Figure 10 shows the mean first passage time to one of the absorbing states as a function of D and s. The color code as indicated in the figure is chosen such that red corresponds to large and blue to short extinction times. Dark red indicates the longest time simulated, $t = 10^7$. The limits $s = 0$ and $s = 1$ correspond to the May-Leonard and Lotka-Volterra models, respectively. Varying s, however, does not simply interpolate between these two limits, but leads to a rather rich and complex dynamics. In particular, there is a local maximum in the mean extinction time for finite values of s below s_E. We infer from our simulations that this maximum is linked to the emergence of planar traveling waves. In contrast to the May-Leonard model ($s = 0$), planar waves seem to be increasingly important in this regime: They dominate the dynamics for a rather broad range in the diffusion coefficient. Moreover, they seem to be much more stable as compared to the May-Leonard case, which can be seen by comparing Figs. 4 and 10. While the exact reason for this remains unclear, the stabilization of planar waves seems to be related to a change in the wavelength and thereby a reduction in the oscillations of the global concentrations. This can be inferred from the global phase portraits, as discussed below. For small D, we again find metastable rotating spirals. For the well-mixed system we find short first passage times. The concentrations there perform homogeneous oscillation, which we identified with heteroclinic orbits of the global trajectories for the May-Leonard case $s = 0$. These orbits cover a broad parameter regime. In particular, they also arise for values of s, where most of the reactions are of Lotka-Volterra type. The reason for this can be inferred from the stability of the reactive fixed point of the rate equations (4). The corresponding eigenvalues (6) retain a nonvanishing positive real part. The trajectories of the global dynamics are therefore driven to the vicinities of

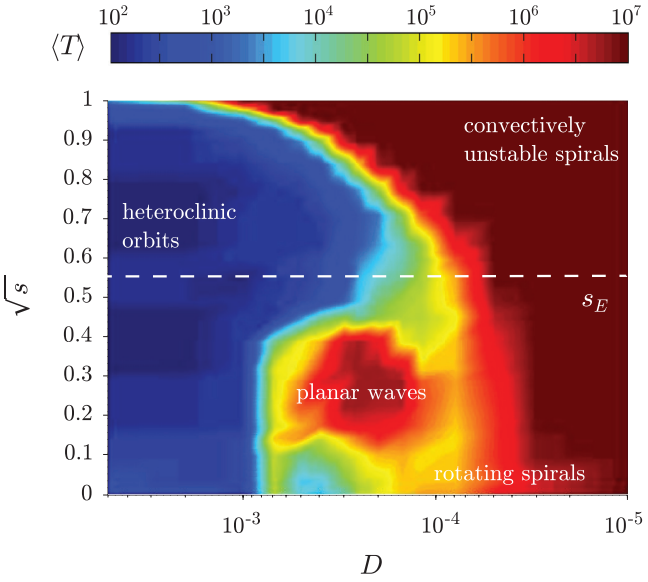

FIG. 10. (Color online) Average first passage time into any of the absorbing states as a function of the diffusion constant D and the fraction of Lotka-Volterra reactions s. Red (medium gray) denotes a large lifetime, yellow (light gray) a medium lifetime, and blue (dark gray) a small lifetime. For $s = 0$ we obtain the mean lifetimes shown in Fig. 4. The dynamics is essentially governed by heteroclinic orbits, traveling waves, and rotating spirals. With increasing s the planar waves become more and more stable and dominate the dynamics for a full order of magnitude in D. The prominence of traveling waves leads to a local maximum in the mean lifetimes. For even higher s the system undergoes an Eckhaus instability (the analytical value is denoted by a dashed line), where planar waves become unstable. The dynamics is roughly comparable to the heteroclinic orbits in the May-Leonard model. Neutral orbits are driven to the boundary of the invariant manifold by a limited fraction of May-Leonard reactions. For $s = 1$ we again recover the dynamics of the Lotka-Volterra model studied in Sec. III. For each of the approximately 400 data points averages were taken over about 100 trajectories. Due to numerical constrains simulations were stopped at $T = 10^7$. Parameters were $M = 8$ and $L = 60$.

the absorbing points exponentially fast. As a result, even for $s \approx 0.9$ the global dynamics is determined by a tiny fraction of May-Leonard reactions.

The roughening transition is complicated by threshold values in D, corresponding to the onset of planar waves and spirals, and the dissolution of the former. These threshold values take the same values as in the limiting case of only May-Leonard reactions. As the value of s exceeds the roughening transition (Eckhaus instability) we observe a sharp transition between long extinction times for small values of D and short extinction times for large values of D. In the latter regime, spirals and planar waves become convectively unstable as predicted by the complex Ginzburg-Landau equation (15). For spiral waves this is illustrated by Fig. 9. Nevertheless, strong correlations exist, and mean times to extinction are large in this regime. From our simulations we infer that the dominant dynamic process in this regime can be identified as the convectively unstable spirals also found in the Lotka-Volterra

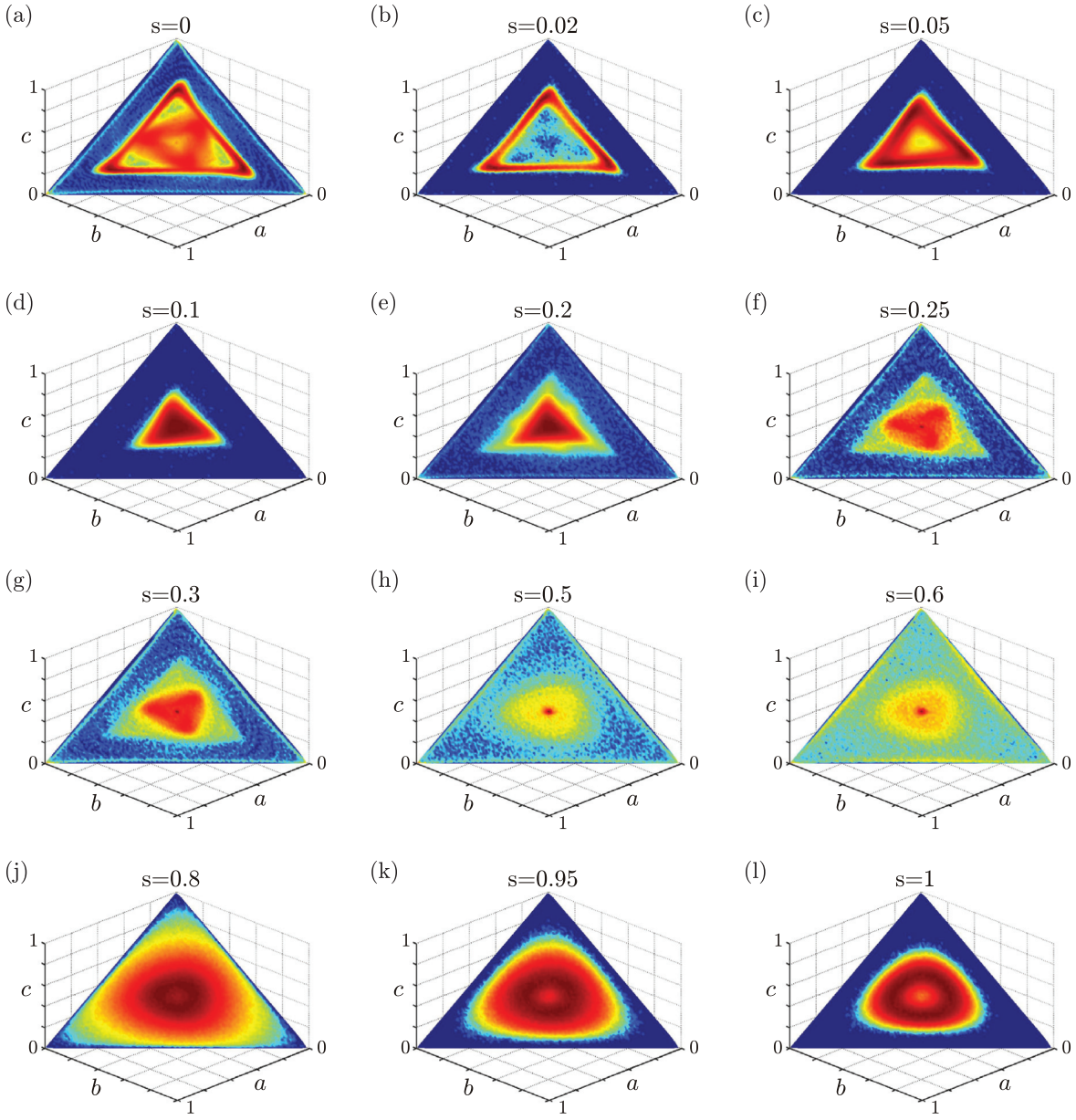

FIG. 11. (Color online) Probability to find the system in a specific state before reaching one of the absorbing fixed points for fixed $D = 3 \times 10^{-4}$. The histogram is projected onto the invariant manifold of the rate equations (4). We varied the fraction of Lotka-Voltera reactions from $s = 0$ (top left) to $s = 1$ (bottom right). Starting at the classic May-Leonard model ($s = 0$), where attractors for planar waves and rotating spirals can be identified, the attractor for the spirals disappears with growing s. The remaining attractor contracts to the reactive fixed point and also, when the system undergoes an Eckhaus instability, dissolves. For an even larger fraction of Lotka-Volterra reactions the global dynamics is driven outward by a limited fraction of May-Leonard reactions and is comparable to the heteroclinic orbits found in the May-Leonard model. When a majority of the reactions are of Lotka-Volterra type, i.e., for s not much smaller than 1, we again observe the emergence of an attracting limit cycle corresponding to system-wide oscillations. Parameters where $M = 8$ and $L = 60$.

limit. Note, however, that due to a truncation of simulation times not all details may be resolved in this regime.

B. Effective free energy and Lotka-Volterra limit

To study how the Lotka-Volterra limit is reached, we computed the effective free energy $\mathcal{F}$ as a function of $\mathcal{L}$. We focus on the case $D = 3 \times 10^{-4}$, which entails the regime of stable planar waves,; cf. Fig. 10. In the May-Leonard model this corresponds to the regime shortly below the lower critical point in the diffusion constant, where the wave attractor and the spiral attractor coexist. Figure 11 demonstrates that the observed changes in extinction times are related to the emergence, disappearance, and changes in the characteristics of attractors of the global dynamics. The limit of the May-Leonard model ($s = 0$) was already discussed in Sec. II. Attractors for rotating spirals and planar waves are visible. When the fraction of Lotka-Volterra reactions is

slightly increased the spiral attractor disappears while the wave attractor remains; see Fig. 11(b). The latter shrinks in size, hinting at an increasing wave length [Figs. 11(c)–11(e)]. The attractor then contracts towards the reactive fixed point [Figs. 11(d)–11(f)]. In Fig. 10 this regime corresponds to the local maximum in extinction times. At the point, where the system undergoes an Eckhaus instability, the attractor dissolves [Figs. 11(g) and 11(h)]. The dynamics is then dominated by global oscillations which are driven outward by a limited number of May-Leonard reactions [Figs. 11(h) and 11(i)]. This regime is therefore closely related to the heteroclinic orbits found in the May-Leonard model. For an even larger fraction of Lotka-Volterra reactions a new attracting limit cycle emerges, corresponding to the system-wide oscillations found in Sec. III [Figs. 11(j)–11(l)].

The results are summarized in a free energy landscape as a function of s; cf. Fig. 12. For $s = 0$ we find the attractors of the planar and spiral waves of the May-Leonard model; cf. Fig. 3. When the fraction s of Lotka-Volterra reactions is

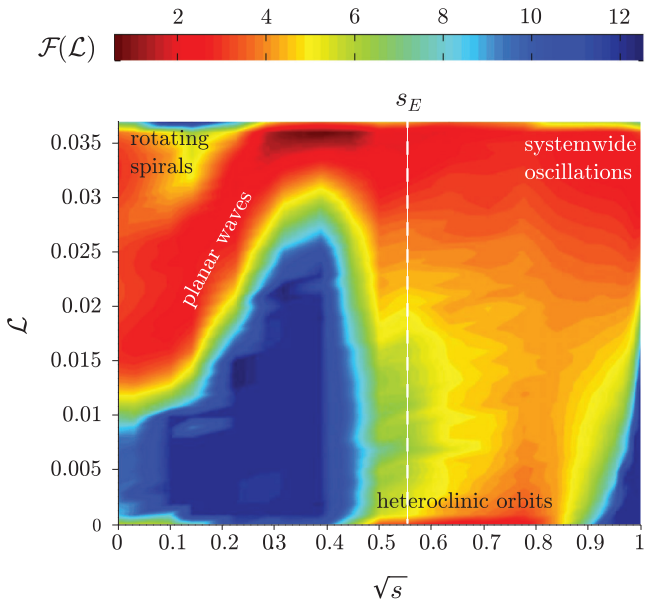

FIG. 12. (Color online) To study the most intriguing line of Fig. 10, $D = 3 \times 10^{-4}$, in more detail we computed the effective free energy $\mathcal{F}$ at specific values of the Lyapunov function $\mathcal{L}$ for different values of s. Red (dark gray) denotes minima of the potential and thereby attractors of the global dynamics. Yellow (light gray) signifies intermediate values, and blue (dark gray) large values of the effective free energy. We identify several regimes depending on the relative strength s of the different types of competition. For $s = 0$ we recover the coexisting wave and spiral attractors of the May-Leonard model. With increasing values of s only the wave attractor remains and approaches the reactive fixed point of the global dynamics ($\mathcal{L} = 0.037$). At the Eckhaus instability (dashed line) the wave attractor dissolves. Instead, an attractor corresponding to global heteroclinic orbits emerges. Only when almost all reactions are of Lotka-Volterra type does an attractor close to the reactive fixed point emerge. The latter corresponds to the limit cycle found in the cyclic Lotka-Volterra model; see Sec. III. Comparing with our simulations we find that these attractors are linked to rotating spirals, planar waves, global, heteroclinic orbits, and system-wide oscillations. Simulation parameters were $M = 8$ and $L = 60$.

increased the attractor of planar waves shrinks to the center of the manifold. As a result, there are no oscillations in the overall densities, which is in contrast to the May-Leonard model, where these oscillations stem from waves having a wavelength close but unequal to the system size. As a result of the lack of oscillations, planar waves become increasingly stable in this regime. At the Eckhaus instability, s_E, spatial patterns become unstable. The dynamics can then be best described as heteroclinic orbits. The system globally performs orbits, which are driven to the boundary of the manifold by the reactions of May-Leonard type. Hence, even a tiny fraction of May-Leonard reactions determines the global dynamics in this regime. This is not surprising, as the conservation law associated with the cyclic Lotka-Volterra model holds precisely only in the case $s = 1$. For values of s close to 1 reactions involving empty sites become unimportant. We then find the attractor corresponding to system-wide oscillations, cf. Fig. 8. Summarizing, in the model with direct and indirect competition we find a surprisingly rich variety of dynamic processes affecting the longevity of biodiversity in a much more complex manner than one would naively expect from an Eckhaus instability. In particular, we observed a local maximum in mean lifetimes if direct competition is weak but nonvanishing.

V. CONCLUSION

We studied the population dynamics of three-species models where species interact with each other cyclically through both direct and indirect competition. In the limiting cases of only direct or indirect competition our model reduces to the cyclic Lotka-Volterra or May-Leonard model, respectively. For a well-mixed system, the nonlinear dynamics of these models differs significantly. While in both cases the trajectories lie on two-dimensional invariant manifolds comprising the absorbing states of extinction, their phase portraits differ qualitatively. The dynamics of the cyclic Lotka-Volterra model is characterized by neutrally stable orbits. In contrast, the dynamics of the May-Leonard model features an unstable fixed point in the center of the invariant manifold and heteroclinic orbits which approach the boundaries of the invariant manifold and hence the absorbing states exponentially fast. In the spatial versions of these models, these attractors of the well-mixed system still act locally on each lattice site. However, if one views the spatially extended system as a set of interconnected local patches, the coupling between these patches due to diffusion may lead to qualitative changes in the type and stability of these attractors.

Indeed, numerical simulations show that in spatially extended systems there is a rich diversity of spatio-temporal patterns depending on the systems' parameters. The goal of this work was to identify and characterize the dynamic processes responsible for the transient maintenance of biodiversity and ultimately leading to extinction in the spatial models. To this end, we investigated the phase portrait of the overall concentrations for the species comprising the system and analyzed the ensuing global attractors of the dynamics and how they are connected with the different types of spatio-temporal dynamics. Moreover, based on a statistical analysis of the system trajectories on the global phase portrait, we defined

an effective free energy which gave us valuable information about the scaling of extinction times with the system size. In particular, the minima of the free energy correspond to metastable dynamical processes.

In the limit corresponding to the spatial May-Leonard model, the minima in the effective free energy landscape of the global phase portrait are linked to three distinct spatio-temporal patterns: (i) spatially homogeneous oscillatory behavior, (ii) planar traveling waves, and (iii) rotating spirals. Importantly, the characteristics of the global attractors change qualitatively at certain threshold values of the mobility. This means that the length scales associated with the spatial patterns changes, which affects their stability and thereby the probability to find the system in such a state. In particular, below an upper threshold value of the mobility a triangular attractor corresponding to traveling waves emerges. This attractor can be regarded as a limit cycle of the global dynamics. It grows in size for decreasing mobility, reflecting a decreasing wavelength. At a lower threshold value of the mobility a second limit cycle of the global concentrations is found, which is located inside the attractor of the traveling waves. There, rotating spirals emerge. In this regime we observe the coexistence of two dynamic processes, planar waves and rotating spirals. Which of the two dynamic regimes is actually realized is determined by stochasticity and the initial conditions. For even lower mobility, the attractor of the traveling waves dissolves, as the correlation length is too small compared to the system size to maintain planar domain borders. In this regime only the attractor of rotating spirals remains, which dominates the dynamics predominantly.

As opposed to this behavior, in the limit of reactions of Lotka-Volterra type only, the system does not exhibit stable spatial patterns. However, there are strong spatial correlations, and they manifest themselves in an attractor of the global dynamics. This attractor has the form of a rounded triangle around the reactive fixed point and corresponds to a limit cycle of the global concentrations. The radius of the limit cycle grows with increasing mobility: when the attractor, with increasing mobility, reaches the boundaries of the invariant manifold the dynamics passes from metastability (exponential scaling of extinction times with the system size) to rapid extinction (sublinear scaling of extinction times with the system size). For even larger mobilities, the radius of the global limit cycle outgrows the boundaries of the simplex. The mean time to extinction then scales linearly with the system size. Hence, in contrast to the May-Leonard model a single attractor here is responsible for three distinct scaling regimes.

Finally, we found a remarkably complex behavior when varying the relative strengths of direct (Lotka-Volterra) and indirect (May-Leonard) competition. If direct competition is weak compared to indirect competition, planar traveling waves are an increasingly important constituent of the extinction dynamics as compared to the May-Leonard case. These planar waves are very stable, leading to a local maximum of extinction times in the phase diagram. Simultaneously, we observe that in contrast to the May-Leonard model rotating spirals do not form for intermediary mobilities. This is reflected in the dissolution of the corresponding attractor. At a specific fraction of Lotka-Volterra reactions the system undergoes an Eckhaus instability: traveling waves and rotating spirals become unstable. The Eckhaus instability manifests itself in the vanishing of the attractors of planar waves and rotating spirals. Beyond the Eckhaus instability, a new attractor emerges, corresponding to global oscillatory behavior for high mobility and convectively unstable spirals for low mobilities. Summarizing, we find that the spatio-temporal dynamics of cyclic populations models with both direct and indirect competition is surprisingly rich and differs qualitatively from the cyclic Lotka-Volterra and May-Leonard models. We identified several threshold values of the mobility and the relative strength of the two types of competition.

In conclusion, the scaling of extinction times with the system size changes abruptly at certain threshold values of the mobility and the relative strength of the two types of competition. We showed that the dynamic processes leading to the transient maintenance of biodiversity are linked to attractors of an effective free energy of the overall concentrations. The characteristics of these attractors change upon certain threshold values, thereby giving insight into the mechanisms underlying these phase transitions. By means of extensive numerical simulations we provide the complete phase diagrams, which are rationalized by scaling arguments based on properties of the complex Ginzburg-Landau equation.

We believe that the method of global phase portraits and the ensuing effective free energy landscapes (renormalized reaction terms) might also give a deeper insight into the dynamics of spatial ecological models and reaction-diffusion systems in other fields of biology. In particular, further studies may apply this method to understand epidemic models, asymmetric four species models or more complex food webs.

ACKNOWLEDGMENTS

This research was supported by the German Excellence Initiative via the program "Nanosystems Initiative Munich" and the German Research Foundation via contract FR 850/9-1. We thank David Jahn, Johannes Knebel, Markus Weber, and Tobias Reichenbach for fruitful discussions.

[1] E. Frey, Physica A **389**, 4265 (2010).
[2] R. Durrett and S. Levin, J. Theor. Biol. **185**, 165 (1997).
[3] R. Durrett and S. Levin, Theor. Pop. Biol. **53**, 30 (1998).
[4] J. B. C. Jackson and L. Buss, Proc. Natl. Acad. Sci. USA **72**, 5160 (1975).
[5] O. Gilg, I. Hanski, and B. Sittler, Science **302**, 866 (2001).
[6] B. Sinervo and C. M. Lively, Nature (London) **380**, 240 (1996).
[7] B. Kerr, M. A. Riley, M. W. Feldman, and M. B. J. Bohannan, Nature (London) **418**, 171 (2002).
[8] B. Kerr, in *Bacteriocins*, edited by M. A. Riley and M. A. Chavan (Springer, New York, 2007), Chap. 6, pp. 111–134.
[9] Y. Itoh, Proc. Jpn. Acad. **47**, 854 (1971).

[10] M. Frean and E. R. Abraham, Proc. R. Soc. **268**, 1323 (2001).
[11] T. Reichenbach, M. Mobilia, and E. Frey, Phys. Rev. E **74**, 051907 (2006).
[12] J. C. Claussen and A. Traulsen, Phys. Rev. Lett. **100**, 058104 (2008).
[13] J. Cremer, Diploma thesis, Ludwigs-Maximilians Universität, 2008.
[14] M. Berr, T. Reichenbach, M. Schottenloher, and E. Frey, Phys. Rev. Lett. **102**, 048102 (2009).
[15] B. Andrae, J. Cremer, T. Reichenbach, and E. Frey, Phys. Rev. Lett. **104**, 218102 (2010).
[16] M. Mobilia, J. Theor. Biol. **264**, 1 (2010).
[17] A. Dobrinevski and E. Frey, Phys. Rev. E **85**, 051903 (2012).
[18] A. Traulsen, J. C. Claussen, and C. Hauert, Phys. Rev. E **85**, 041901 (2012).
[19] R. M. May and W. J. Leonard, SIAM J. Appl. Math. **29**, 243 (1975).
[20] K. I. Tainaka, J. Phys. Soc. Jpn. **57**, 2588 (1988).
[21] K. I. Tainaka, Phys. Rev. Lett. **63**, 2688 (1989).
[22] K. I. Tainaka, Phys. Rev. E **50**, 3401 (1994).
[23] L. Frachebourg, P. L. Krapivsky, and E. Ben-Naim, Phys. Rev. E **54**, 6186 (1996).
[24] L. Frachebourg, P. L. Krapivsky, and E. Ben-Naim, Phys. Rev. Lett. **77**, 2125 (1996).
[25] T. L. Czárán, R. F. Hoekstra, and L. Pagie, Proc. Nat. Acad. Sci. USA **99**, 786 (2002).
[26] T. Reichenbach and E. Frey, Phys. Rev. Lett. **101**, 058102 (2008).
[27] Q. He, M. Mobilia, and U. C. Täuber, Phys. Rev. E **82**, 051909 (2010).
[28] A. A. Winkler, T. Reichenbach, and E. Frey, Phys. Rev. E **81**, 060901 (2010).
[29] S. Venkat and M. Pleimling, Phys. Rev. E **81**, 021917 (2010).
[30] X. Ni, W.-X. Wang, Y.-C. Lai, and C. Grebogi, Phys. Rev. E **82**, 066211 (2010).
[31] Q. He, U. C. Täuber, and R. K. P. Zia, Eur. Phys. J. B **85**, 141 (2012).
[32] A. Roman, D. Konrad, and M. Pleimling, J. Stat. Mech. (2012) P07014.
[33] T. Reichenbach, M. Mobilia, and E. Frey, Phys. Rev. Lett. **99**, 238105 (2007).
[34] T. Reichenbach, M. Mobilia, and E. Frey, Nature (London) **448**, 1046 (2007).
[35] M. Peltomaki and M. Alava, Phys. Rev. E **78**, 031906 (2008).
[36] T. Reichenbach, M. Mobilia, and E. Frey, J. Theor. Biol **254**, 368 (2008).
[37] Ana Paula O. Müller and J. A. C. Gallas, Phys. Rev. E **82**, 052901 (2010).
[38] S. Rulands, T. Reichenbach, and E. Frey, J. Stat. Mech. (2011) L01003.
[39] Q. He, M. Mobilia, and U. C. Täuber, Eur. Phys. J. B **82**, 97 (2011).
[40] L.-L. Jiang, T. Zhou, M. Perc, and B.-H. Wang, Phys. Rev. E **84**, 021912 (2011).
[41] D. Lamouroux, S. Eule, T. Geisel, and J. Nagler, Phys. Rev. E **86**, 021911 (2012).
[42] P. P. Avelino, D. Bazeia, L. Losano, J. Menezes, and B. F. Oliveira, Phys. Rev. E **86**, 036112 (2012).
[43] B. Szczesny, M. Mobilia, and A. M. Rucklidge, Europhys. Lett. **102**, 28012 (2013).
[44] A. J. Lotka, J. Am. Chem. Soc. **42**, 1595 (1920).
[45] V. Volterra, Mem. Accad. Lincei **2**, 31 (1926).
[46] U. Dobramysl and U. C. Täuber, Phys. Rev. Lett. **101**, 258102 (2008).
[47] R. P. Boland, T. Galla, and A. J. McKane, Phys. Rev. E **79**, 051131 (2009).
[48] M. Parker and A. Kamenev, Phys. Rev. E **80**, 021129 (2009).
[49] J. Knebel, T. Krüger, M. F. Weber, and E. Frey, Phys. Rev. Lett. **110**, 168106 (2013).
[50] P. Szabó, T. Czárán, and G. Szabó, J. Theor. Biol. **248**, 736 (2007).
[51] G. Szabó, A. Szolnoki, and I. Borsos, Phys. Rev. E **77**, 041919 (2008).
[52] N. Mitarai, J. Mathiesen, and K. Sneppen, Phys. Rev. E **86**, 011929 (2012).
[53] J. Mathiesen, N. Mitarai, K. Sneppen, and A. Trusina, Phys. Rev. Lett. **107**, 188101 (2011).
[54] R. Abta, M. Schiffer, and N. M. Shnerb, Phys. Rev. Lett. **98**, 098104 (2007).
[55] R. Abta and N. M. Shnerb, Phys. Rev. E **75**, 051914 (2007).
[56] I. Aranson and L. Kramer, Rev. Mod. Phys. **74**, 99 (2002).
[57] We also performed simulations on hexagonal lattices and found identical results. To investigate the influence of the "macroscopic" lattice structure we performed simulations on hexagonal lattices with hexagonal boundaries and corresponding periodic boundary conditions. While the details of some spatio-temporal patterns and the specific critical values changed slightly, we observed a very similar behavior of the global dynamics and the observed attractors. Note, however, that planar waves and the pairwise appearance of spirals are not observed for absorbing boundary conditions.
[58] C. A. Lugo and A. J. McKane, Phys. Rev. E **78**, 051911 (2008).
[59] T. Butler and N. Goldenfeld, Phys. Rev. E **80**, 030902 (2009).
[60] C. Gardiner, *Stochastic Methods: A Handbook for the Natural and Social Sciences.*, 4th ed. (Springer, New York, 2009).
[61] U. C. Täuber, J. Phys. A: Math. and Theor. **45**, 405002 (2012).
[62] U. Dobramysl and U. C. Täuber, Phys. Rev. Lett. **110**, 048105 (2013).
[63] Explicitly, consider taking the limit in the total equilibrium concentration $a^* + b^* + c^* = 1/(1 + \sigma/3\mu)$. This dictates that in order to obtain a system without empty sites $\sigma/\mu \to 0$, i.e., the production rate of empty sites per concentration must vanish faster than the consumption rate.
[64] J. Cremer, T. Reichenbach, and E. Frey, New J. Phys. **11**, 93029 (2009).
[65] W. van Saarlos, Phys. Rep. **386**, 29 (2003).
[66] Note that for $n > 1$ such patterns are only observed for specific initial conditions.
[67] The reason for the slight deviation of the numerical data from the linear scaling might be that the wave attractor is slightly asymmetric. The value of the Lyapunov function is therefore not an optimal indicator for its radius.
[68] The threshold value was chosen to optimize the accentuation of the spiral vertices.

3 Phenotypic heterogeneity and genetic diversity in mobile populations

Genotypic diversity and phenotypic heterogeneity are both commonly found in microbial and viral populations [74, 76, 77, 81, 83, 90, 95]. They are frequently used strategies to rapidly adapt to new environment, or to evade a host's immune system [87, 88]. However, in a homogeneous environment without niches, genotypic diversity is difficult to maintain. In the first part of this thesis we showed that cyclic dominance between genotypes is one factor promoting biodiversity in spatially extended systems [23–29, 69, 73]. For example, bacterial model systems comprised of three genetically distinct strains of *Escherichia coli* have been shown to exhibit stable three-strain coexistence in spatially extended homogeneous environments [26]. Recent theoretical studies have explored how demographic noise [28, 29, 50, 55, 61, 69, 125], mobility of individuals [28–30, 69, 73], and the structure of the interaction network as well as the strengths of its links [31] affect the maintenance of genotypic diversity. All of these studies assume that genotypes are linked to a single phenotype. But what happens if an individual microbe is able to change it's strategy, or in other words shows phenotypic heterogeneity? Some bacteria use a bet-hedging strategy by stochastically switching between different phenotypic states to minimize the risk of population extinction due to an attack with antibiotics [75, 81]. Does such phenotypic heterogeneity favor or disfavor genetic diversity and how does the population dynamics depend on the mobility of individuals and the type of interaction between them?

There are many ways in which phenotypic heterogeneity may affect the evolutionary dynamics. Phenotypic heterogeneity may influence the growth rates of bacteria, but also their motility. It may alter the the frequencies of different kinds of behaviors and the way they interact in general. In this chapter, we will investigate how all these types of heterogeneity affect the evolutionary dynamics in mobile populations. To this end, we study simple, paradigmatic models whose homogeneous versions have been successfully employed to understand a variety of biological phenomena. We show that heterogeneity sheds a new light on these models. We find a variety of intriguing phenomena which are not only relevant biologically, but are also interesting from the perspective of theoretical nonequilibrium physics. In the following, we will first give a short overview over some examples of where phenotypic heterogeneity arises in biology. We will then introduce paradigmatic models which allow us to investigate the influence heterogeneity on a variety of biological systems.

3.1 Biological foundations of phenotypic heterogeneity

Phenotypic heterogeneity has several origins. First, it can be a direct result of genetic alterations, the most prominent form of which are mutations. However, mutations are undirected and they are effective on the phenotypic level only on very large time scales. In many scenarios it is advantageous if phenotypes can be changed rapidly. Indeed, the rapid phenotypic changes is a strategy often used by pathogens to evade a host's immune system. Genetic alterations can be a result of the reversible rearrangement of specific DNA fragments. Such mechanisms allow phenotypic changes on a shorter time scale and they are used, for example, in *Escheria coli*, Influenza and Salmonella [87, 88]. As an example, phenotypic heterogeneity can be induced by a change in the number of repeats of short DNA sequence units. If the location of these repeats is in such a way that either transcription or translation is affected changes in the number of repeats can influence the phenotypic state [88]. Other mechanisms for the rearrangement of DNA fragments include the inversion of DNA fragments, intramolecular recombination or recombination on pre-mRNA level.

A second source for phenotypic heterogeneity is the heterogeneous expression of genes. Sometimes changes in the genome, such as DNA methylation and histone modification, do not involve modifications in the DNA sequence itself, but nevertheless influence the expression of genes. On the other hand, as the number of particles involved in gene expression is relatively low, these processes are inherently stochastic [126, 127]. In multistable genetic circuits, switching between phenotypic states may therefore be entirely driven by extrinsic and intrinsic noise [84].

In the following, we introduce several examples of phenotypic heterogeneity in bacterial populations.

Persister cells

As an example, several bacteria employ phenotypic heterogeneity as a bet hedging strategy to survive antibiotic attacks. Some cells in a clonal population enter a dormant "persister" state in which these cells stop growing and thereby escape death caused by certain antibiotics [75, 81]. The dormant state is not caused by mutant microbes and it is non-inheritable. Rather, dormant cells arise spontaneously and at very low abundances. In *E. coli* populations, for example, they constitute a fraction of 10^{-6} to 10^{-5} of the overall colony [97]. It is believed that the development of dormancy is the result of stochastic switching in a bistable genetic circuit. For *E. coli* bacteria, the molecular mechanism has been understood in greater detail [97]. There, the persistence factor hipA has been identified to induce dormancy. The low frequency of persister cells is a result of the repressor hipB, which binds to hipA and thereby inactivates it [92].

Competence switching

Phenotypic switching is also responsible for the development of competence for DNA transformation. DNA transformation denotes the ability of bacteria to uptake, incorporate and express exogeneous DNA strands from the environment. To be able to transform DNA bacteria must be in a specific physiological state called 'competence'. Being in the state of competence is energetically costly for bacteria, but it becomes important in situations that likely induce DNA damage. As an example, in *Bacillus subtilis* DNA transformation is increased by UV light [128]. In *B. subtilis*, competence development is regulated through a nonlinear positive feedback of a transcriptional master regulator. The ensuing nonlinear dynamics is bistable and bacteria may stochastically switch between the two states of competence [86]. Interestingly, the switching probability can be tuned by controlling noise in the transcription of the master regulator, the timing of its expression, or by a rewiring of the corresponding regulatory network [86, 91, 93].

White-opaque (mating type) switching in *Candida albicans*

Candida albicans is a yeast which naturally resides in various locations in the body of many healthy people [90, 96]. In people with a weak immune system, such as HIV patients, the pathogen can infect nearly all body locations. This variability is paramount for *C. albicans'* pathogenity and it is partly attributed to phenotypic switching. Most prominently, upon environmental cues the pathogen switches from the budding yeast form to filamentous growth forms. Interestingly, mutants which are locked in any of these growth forms loose virulence to a certain degree.

In addition to this so called yeast-hyphal dimorphism, *C. albicans* can also switch between two different morphologies: the normal, round cell shape (termed white) and an elongated cell shape with an altered surface structure (termed opaque). White-opaque switching helps the pathogen to adapt to new host niches. While cells in the white state have a high virulence when infected intravenously, opaque cells are better able to infect the skin. Withe-opaque switching can occur spontaneously at a low rate, such that in a white or opaque colony a percentage of 0.1% is in the opposite phenotypic state. Furthermore the switching can be induced by anaerobic environmental conditions [90]. As the the phenotypic state is inherited the molecular basis of the switching is believed to be an epigenetic mechanism.

Being in one of the phenotypic states 'white' or 'opaque' is also closely related to mating. Opaque cells are the mating competent form of *C. albicans* with an approximately 10^6 times higher frequency of mating as compared to white cells. The white-opaque switch, and thereby the mating types denoted by a and α, are strictly regulated by genes present at the Mating-Type Like (MTL) locus. As a result, only $MTLa$ or $MTL\alpha$ strains can switch from the white to the opaque form,

while heterogeneous $MTLa|\alpha$ strains are exclusively present in the white state [96]. On a molecular level, white-opaque switching is induced if the transcription factor WOR1 exceeds a certain threshold value in its concentration.

The core switching system of *Candida glabrata*

Candida glabrata is a widespread pathogenic yeast which can be carried by a variety of body locations. Like *Candida albicans*, it performs high-frequency phenotypic switching, allowing the pathogen to rapidly adapt to a a variety of environmental conditions. Of course, rapid adaptation makes medical treatment difficult. Specifically, it was found that *C. glabrata* switches with high frequency between four phenotypic states, which are named according to their color on $CuSO_4$ containing agar: White, Light Brown, Dark Brown, and very Dark Brown [74, 79]. From a specific phenotypic state not all other states are equally accessible. Indeed the switching rates between these phenotypic states vary over several time scales [74]. Figure 3.1(a) shows the resulting transition graph. For example, the switching rate from the White state to the Light Brown state is roughly 100 times higher than the rate to switch from the White state to the very Dark Brown state.

Heterogeneous motility in populations of *Bacillus subtilis*

As many other bacterial species *Bacillus subtilis* is endowed with flagella which may be utilized to sense the cell's environment. Most importantly, flagella are, however, used for locomotion. It has been found that in mid exponential growth phase clonal populations consist of both, swarming cells that are propelled via flagella, and non-motile cells, which after division do not separate from each other, thereby forming long chains of cells. This bet hedging strategy allows the population to exploit its current location and at the same time disperse to new, possibly more favorable niches. As a result, colonies of *B. subtilis* are heterogeneous with respect to the cells' motility. The underlying mechanism behind this behavior is a bistable switch: in motile cells the alternative sigma factor σ^D is in the ON state, while for non-motile cells σ^D is in the OFF state. The switching between these states is purely stochastic. The statistical weight of the each state, and thereby the fractions of the colony exhibiting each state, can be biased by the regulatory proteins *swrA* and *swrB* [84, 94]. Specifically, it has been found that the fraction of motile cells in the wild type strain 3610 differs significantly from laboratory strains [94]. Similarly, in populations of *Salmonella* motility is regulated through the production of the protein flagellin, which is expressed by a bistable gene regulatory network [89].

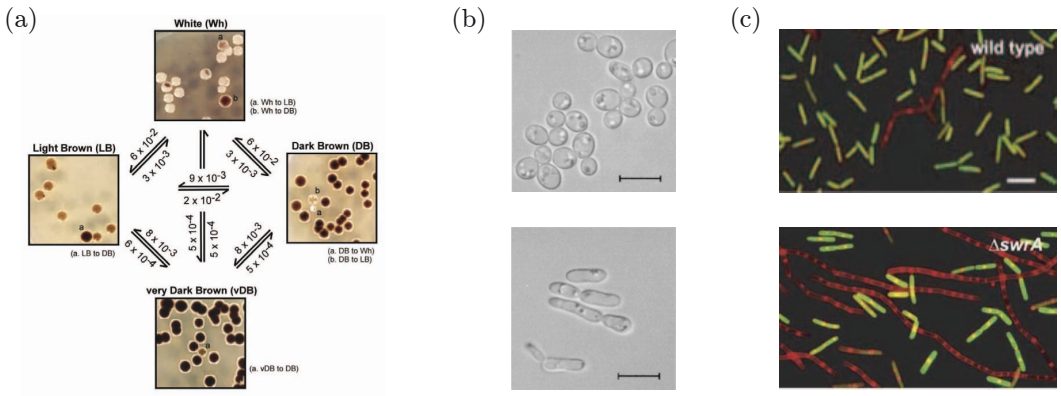

Figure 3.1: (a) The core switching system of *Candida glabrata* allows transitions between four distinct phenotypic states: White, Light Brown, Dark Brown and very Dark Brown. The arrows denote possible directions of switching and are labeled with the corresponding frequencies. The illustration was taken from Ref. [74]. (b) Switching between different morphologies in in *Candida albicans*. Cells can be in a round [white, (top)] or elongated [opaque, (bottom)] shape. The pictures were taken from Ref. [96]. (c) Populations of *Bacillus subtilis* consist of swarming cells (green) and non-motile cells (red). Non-motile cells do not separate after division and therefore form chains. In the wild type (top) a high fraction of the population is in the motile state, whereas in *swrA* mutants (bottom) the motile state occurs at a lower rate. Hence, the bistable switch responsible for phenotypic heterogeneity is biased by the regulatory protein *swrA*. The pictures have been taken from Ref. [94]

3.2 Paradigmatic models for heterogeneous populations

Mathematically, bacterial colonies are often studied in the framework of stochastic many-particle systems. Motivated by the biological examples introduced above we now are interested in stochastic many-particle systems, where each particle can be in a distinct phenotypic state. To this end, we consider populations, which exhibit phenotypic heterogeneity. At the same time, we also assume the population to be genetically diverse. In other words, the probability to be in a specific phenotypic state depends on a particle's genotype. Our approach to heterogeneous populations makes use of simple mathematical models. These models are simple enough to gain a theoretical understanding of the ensuing phenomenology, but on the other hand allow us to obtain a deep insight into the mechanisms acting in real biological systems. However, the language of mathematics does on first sight not seem to be adequate to describe systems lacking any symmetry in the properties of its constituents. Indeed, the mathematical description of heterogeneous many particles systems is difficult and, in most cases, impossible. In the following, we give an idea of how these models, despite the vast number of degrees of freedom and the apparent lack of symmetry in

the interactions, can be formulated mathematically. Already in 1916 Smoluchowski began investigating the dynamics of a system where heterogeneity arises as a result of the dynamics [37, 38]. In the following, we present several classes of mathematical models for heterogeneous populations. Starting with Smoluchowski's seminal work on coagulation, we will develop models for genetically diverse and phenotypically heterogeneous populations. We introduce analytic approaches for understanding the often highly complex dynamics in these models. However, the spatio-temporal dynamics can in most cases only be assessed via stochastic simulations.

3.2.1 Smoluchowski's coagulation equation

Smoluchowski studied the coagulation processes of colloids. There, heterogeneity in the particles' radii and mobilities was a result of the system's dynamics. He investigated a situation, where initially the system consists of identical, spherical monomers performing Brownian motion. If two particles approach closer than a certain distance they may stick together and form a polymer with a mass corresponding to the combined masses of the monomers. This new polymer is now considered identical to any other particle, but, as a result of its larger mass, it moves more slowly. It may again coagulate with other particles, monomers and polymers, thereby forming larger and larger compounds. This process continues until a single polymer remains. Smoluchowski's idea was to change into the reference frame of one of the particles, which thereby could be considered as a "trap" for the other particles.

In a mathematical formulation of this process we are interested in the number of particles of mass k at time t, denoted by $n(k,t)$. The time evolution of $n(k,t)$ was first studied by Smoluchowski [37, 38] and it is today usually written in the form

$$\dot{n}(k,t) = \frac{1}{2}\sum_{j=1}^{k-1} K(j,k-j)n(j,t)n(k-j,t) - n(k,t)\sum_{j=1}^{\infty} K(j,k)n(j,t). \tag{3.1}$$

$K(k,j)$ gives the rate at which particles of mass k coagulate with particles of mass j and it is known as the *coalescence kernel*. In Smoluchowski's seminal paper K was proportional to the mean diffusion constant times the mean radii of the reaction particles, $K(k,j) = 1/2(D_k + D_j)(R_k + R_j)$. The mathematical difficulty of Eq. (3.1) stems from the fact that it is an infinitely dimensional nonlinear differential equation and, in particular, it involves an infinite series on its right hand side. As a result, the theory of ordinary differential equations does not apply to Eq. (3.1).

In continuous form, Smoluchowski's coagulation equation can be expressed as an inetrgo-differential equation,

$$\dot{n}(x,t) = \frac{1}{2}\int_0^x K(y,x-y)n(y,t)n(x-y,t)\mathrm{d}y - n(x,t)\int_0^\infty K(x,y)n(y,t)\,. \tag{3.2}$$

Analytic solutions for integro-differential equations of this form only exist for three very simple types of kernels, namely $K = 1$, $K = x + y$, and $K = xy$ [16]. In general, the analytical solution of heterogeneous many particle systems, in particular those involving spatial degrees of freedom, is hardly feasible. Here, Monte Carlo simulations can give further insight into the dynamics and they often give indication of how these systems can be described in terms of a reduced mathematical theory.

3.2.2 Genetic diversity and phenotypic heterogeneity in mobile populations

We are now interested in how phenotypic heterogeneity and genetic diversity influence the spatio-temporal dynamics of cyclically interacting species. To this end, we consider a spatially extended population of N individuals exhibiting phenotypic heterogeneity. Each individual can stochastically switch between M phenotypic states $(s_1, \ldots, s_M)$. The probability to be in any of these states is determined by one of G different genotypes $\alpha \in \{1, \ldots, G\}$, which are here represented by probability distributions $\vec{p}_\alpha = \left(p_\alpha^1, \ldots, p_\alpha^M\right)$. When individuals engage they interact based on their stochastically chosen phenotypic state. The nature of this interaction is determined by an interaction network, which encodes the outcome of pairwise competition among phenotypes. Mathematically, such an interaction network can be described in terms of a matrix $\underline{\underline{A}}$, where $a_{ss'} = 1$ if the phenotype s dominates the phenotype s' and $a_{ss'} = 0$ otherwise. This specific choice for $\underline{\underline{A}}$ fixes the time scale. As an example, consider three cyclically interacting phenotypes ($M = 3$), such that s_1 dominates s_2, s_2 dominates s_3 and s_3 in turn dominates s_1. The interaction matrix $\underline{\underline{A}}$ is then given by

$$\underline{\underline{A}} = \begin{pmatrix} 0 & 1 & 0 \\ 0 & 0 & 1 \\ 1 & 0 & 0 \end{pmatrix}.$$

The probability for an individual with genotype α to dominate an individual β after many interactions is given by $w_{\alpha\beta} \equiv \vec{p}_\alpha^{\mathrm{T}} \underline{\underline{A}} \vec{p}_\beta$, which effectively leads to a net transition rate between genotypes $W_{\alpha\beta} \equiv w_{\alpha\beta} - w_{\beta\alpha}$. In a spatial setting, $W_{\alpha\beta}$ therefore can be understood as the invasion speed per concentration between domains of genotypes α and β.

There are two prominent ways of defining competition between phenotypes on a microscopic level. Firstly, phenotypes may compete directly. When two individuals of genotypes α and β react, the dominating individual replaces the other one with a rate $\omega_{\alpha\beta}$, in chemical notation $\alpha + \beta \xrightarrow{w_{\alpha\beta}} \alpha + \beta$. The genotype $\vec{p}_\alpha$ is inherited to the newly produced individual. This replacement scheme mimics predator-prey relations and is related to the established class of Lotka-Volterra models [113, 114]. Secondly, in indirect competition the vanished individual β is replaced by an empty site, $\alpha + \beta \xrightarrow{w_{\alpha\beta}} \alpha + \emptyset$. In the context of ecology these empty sites account for the limited availability of resources. Independently, empty sites are then used for

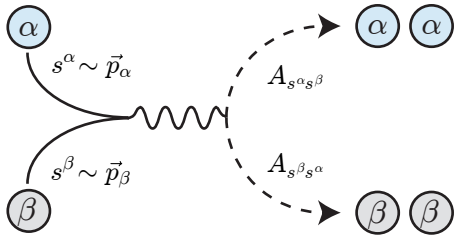

Figure 3.2: Illustration of our model for phenotypic switching in genetically diverse populations. When particles with genotypes α and β engage, their phenotypic states s^α and s^β are chosen randomly according to the probability distributions $\vec{p}_\alpha$ and $\vec{p}_\beta$. The reaction channel is then determined by the interaction matrix $\underline{\underline{A}}$: in the LV model the individual with genotype β is replaced by an offspring with genotype α with probability $A_{s^\alpha s^\beta}$, and vice versa.

reproduction at a rate μ, $\alpha + \emptyset \xrightarrow{\mu} \alpha + \alpha$. This way of replacement is often referred to as May-Leonard type [28, 71]. Thus, at any time t the state $\mathcal{C}$ of the system is given by the genotypes α_i and the position $\mathbf{r}_i(t)$ of each individual, $\mathcal{C}(t) = (\{\alpha_i, \mathbf{r_i}(t)\})_{i=1,\ldots,N}$.

The dynamics of this model can be studied by stochastic simulations. In these simulations, particles are located on a two-dimensional square lattice of linear size $L = \sqrt{N}$ with periodic boundary conditions and sequential updating. Initially, the genotypes are chosen randomly according to a uniform distribution of genotypes on the unit simlex Δ^2. Interactions occur between individuals on neighboring sites. Mobility was implemented as a nearest neighbor exchange process at a rate ϵ, $XY \to YX$, where X and Y denote individuals or empty spaces $\emptyset$. Macroscopically the nearest neighbor exchange process leads to diffusion with an effective diffusion constant $D = \epsilon N^{-1}/2$ [28][1].

Mean field equations for reactions of Lotka-Volterra type

Analytical progress can be made by considering a well-mixed system in the mean field limit. We require that the total number of particles, N, is much larger than the number G of distinct genotypes at $t = 0$, $N \gg G$. We then may define concentrations x_α, $\alpha = 1, \ldots, G$ such that Nx_α gives the number of individuals with a certain genotype $\vec{p}_\alpha$. How are these concentrations affected by the reactions between individuals? The probability for a genotype α to outcompete a genotype β is given by $w_{\alpha\beta} = \vec{p}_\alpha \underline{\underline{A}} \vec{p}_\beta$, where $\underline{\underline{A}}$ is the interaction matrix. This implies a net transition rate per unit time

1 As compared to a single particle Brownian motion the nearest neighbor exchange process induces additional nonlinear reaction terms, which are commonly neglected.

and concentration between two genotypes, $W_{\alpha\beta} = w_{\alpha\beta} - w_{\beta\alpha} = \vec{p}_\alpha^{\,\mathrm{T}}(\underline{\underline{A}} - \underline{\underline{A}}^{\mathrm{T}})\vec{p}_\beta$. Competition with a genotype β therefore changes the concentration of genotype α by $W_{\alpha\beta}x_\alpha x_\beta$. Including competition with any genotype we arrive at G coupled rate equations,

$$\dot{x}_\alpha = x_\alpha \sum_{\beta=1}^{G} W_{\alpha\beta}x_\beta,\ \alpha = 1, \ldots, G\,. \tag{3.3}$$

As, by definition, $\underline{\underline{U}} \equiv \underline{\underline{A}} - \underline{\underline{A}}^{\mathrm{T}}$ and thereby $\underline{\underline{W}}$ are skew-symmetric matrices, Eq. (3.3) conserves the sum over all species concentrations, $\sum_{\alpha=1}^{G} x_\alpha = 1$. We can therefore interpret Eq. (3.3) as the replicator equation of a conservative Lotka-Volterra system of G competing species. As a result of the conservation of concentrations, $\triangle^G$ is invariant under the dynamics of Eqs. (3.3).

To study the nonlinear dynamics of Eqs. (3.3) we are now interested in further quantities which are conserved by the dynamics[2]. In analogy to non heterogeneous Lotka-Volterra models [31] we assume that these conserved quantities are of the form

$$\kappa = \prod_{\alpha=1}^{G} x_\alpha^{c_\alpha}, \qquad \mathbf{c} \in \mathbb{R}^G\,. \tag{3.4}$$

We take the derivative with respect to t to obtain the time evolution of κ,

$$\dot{\kappa} = \sum_{\alpha=1}^{G} c_\alpha \frac{\kappa}{x_\alpha}\dot{x_\alpha} = \kappa \sum_{\alpha=1}^{G}\sum_{\beta=1}^{G} c_\alpha x_\beta W_{\alpha\beta} = -\kappa \sum_{\beta=1}^{N} x_\beta \left(\underline{\underline{W}}\mathbf{c}\right)_\beta\,. \tag{3.5}$$

Therefore, if κ is a conserved quantity $\mathbf{c}$ must be positive and in the kernel of $\underline{\underline{W}}$: $\underline{\underline{W}}\mathbf{c} = 0$. For now, we assume that the kernel of $\underline{\underline{W}}$ has positive elements. An argument for this is given further below. The dimension of the kernel of $\underline{\underline{W}}$ hence gives the number of conserved quantities. Employing the rank-nullity theorem, we obtain

$$\mathrm{rank}(\underline{\underline{W}}) + \dim[\ker(\underline{\underline{W}})] = G\,. \tag{3.6}$$

Let $\underline{\underline{\Lambda}}$ be the matrix containing all genotypes, $\underline{\underline{\Lambda}} = (\vec{p}_1, \ldots, \vec{p}_G) \in \mathbb{R}^{M\times G}$ with M being the number of distinct phenotypic states. With this definition we can write $\underline{\underline{W}} = \underline{\underline{\Lambda}}^{\mathrm{T}}\underline{\underline{U}}\underline{\underline{\Lambda}}$. In the following, we assume that the number of genotypes is greater or equal the number of phenotypic states, $G \geq M$. $\underline{\underline{\Lambda}}$ has M linearly independent columns, in the language of linear algebra $\mathrm{rank}(\underline{\underline{\Lambda}}) = M$. We infer

$$\mathrm{rank}(\underline{\underline{W}}) \leq \min\{\mathrm{rank}(\underline{\underline{U}}), \mathrm{rank}(\underline{\underline{\Lambda}})\} = \mathrm{rank}(\underline{\underline{U}})\,, \tag{3.7}$$

2 We here sketch a proof that goes back to a collaborative work with David Jahn and Johannes Knebel.

and, by substituting Eq. (3.6),

$$\dim[\ker(\underline{\underline{W}})] \geq G - \operatorname{rank}(\underline{\underline{U}})\,. \tag{3.8}$$

Hence, the number of conserved quantities is greater than the number of distinct genotypes minus the rank of $\underline{\underline{U}}$. In other words, the number of the degrees of freedom $G - \dim[\ker(\underline{\underline{W}})]$ is bounded above by the structure of the interaction network determined by $\underline{\underline{U}}$. We conjecture that adding a new genotype to the population also yields an additional conserved quantity.

Conserved quantities are particularly relevant, if the kernel is positive, i.e. $c_\alpha > 0$. For $G \to \infty$, the mean reaction rate is zero, $\sum_\beta W_{\alpha\beta} \to 0$, and $1/G(1,\ldots,1)^{\mathrm{T}}$ is a fixed point of the dynamics, and thereby a positive element of the kernel of $\underline{\underline{W}}$. From this we infer that there exist further kernel elements in the surrounding of this fixed point [3].

As an example, consider three cyclically competing phenotypes. The dimension of the image of $\underline{\underline{U}}$ is two, $\operatorname{rank}(\underline{\underline{U}}) = 2$. We obtain $\dim[\ker(\underline{\underline{W}})] \geq G - 2$, which tells us that the system comprises at least $G - 2$ conserved quantities. Equivalently, the number of degrees of freedom is less or equal 2. Together with particle number conservation this proofs the existence of $G - 1$ conserved quantities. As $\underline{\underline{W}}$ is skew-symmetric, the eigenvalues of the Jacobian of Eq. (3.3) are imaginary [31, 129]. Hence, the conserved quantities correspond to neutrally stable periodic orbits. The numerical evaluation of Eq. (3.3) shows that the amplitude of oscillations in the component α scales linearly with the standard deviation of the corresponding net transition rates, $\sqrt{\operatorname{Var}(W_{\alpha\beta})}$. The standard deviation again increases with the degree of specialization of the genotype $\vec{p}_\alpha$. We conclude that the mean first passage times to extinction are smallest for specialists and largest for generalists. We therefore expect that in the stochastic system the population is asymptotically dominated by bet hedgers, which is confirmed by stochastic simulations.

Mean field equations for reactions of May-Leonard type

In models of May-Leonard type competition is mediated through the limited availabiligy of resources. A definition of the homogeneous model and a summary of the large body of theoretic work on the three cyclically competing species was given in the aforegoing chapter. In the thermodynamic limit and for well-mixed systems the dynamics of the heterogeneous May-Leonard model is aptly described by G coupled

3 In this form, the argument was first formulated by Johannes Knebel.

differential equations for the concentrations of the genotypes α,

$$\dot{x}_\alpha = x_\alpha \left[\mu \left(1 - \sum_{\beta=1}^{G} x_\beta \right) - \vec{p}_\alpha^{\mathrm{T}} \underline{\underline{A}}^{\mathrm{T}} \sum_{\beta=1}^{G} x_\beta \vec{p}_\beta \right], \quad \alpha \in 1, \ldots, G\,. \tag{3.9}$$

To study the nonlinear dynamics we multiply Eq. (3.9) with $\vec{p}_\alpha$ and then sum over α,

$$\sum_\alpha \vec{p}_\alpha \dot{x}_\alpha = \mu \sum_\alpha \vec{p}_\alpha x_\alpha \left(1 - \sum_\beta x_\beta \right) - \sum_\alpha x_\alpha \vec{p}_\alpha \cdot \vec{p}_\alpha^{\mathrm{T}} \underline{\underline{A}} \sum_\beta \vec{p}_\beta x_\beta\,. \tag{3.10}$$

We define the "moments" of $\vec{p}_\alpha$ by $\sigma_k \equiv \sum_\alpha (\vec{p}_\alpha)^k x_\alpha$. $\sigma_0 \equiv \sum_\alpha x_\alpha$ then is the total concentration of individuals. The first moment gives the mean genotype, $\vec{\sigma}_1 \equiv \sum_\alpha \vec{p}_\alpha x_\alpha$. The second moment, $\sigma_2 \equiv \sum_\alpha x_\alpha \vec{p}_\alpha \cdot \vec{p}_\alpha$, can be interpreted as the genetic variety in the population. Using these definition we obtain the time evolution of the average state of the system,

$$\dot{\vec{\sigma}}_1 = \mu \vec{\sigma}_1 (1 - \sigma_0) - \left(\sum_\alpha x_\alpha \vec{p}_\alpha \cdot \vec{p}_\alpha^{\mathrm{T}} \right) \underline{\underline{A}} \vec{\sigma}_1 \tag{3.11}$$

$$= \mu \vec{\sigma}_1 (1 - \sigma_0) - \sigma_2 \underline{\underline{A}} \vec{\sigma}_1\,. \tag{3.12}$$

We now expand $\vec{p}_\alpha \cdot \vec{p}_\alpha$ to first order around the bet hedging genotype, given by an equal probability to be in any of the G phenotypic states, $(1/G, 1/G, \ldots, 1/G)$. We obtain

$$\sum_\alpha x_\alpha \vec{p}_\alpha \cdot \vec{p}_\alpha \approx \frac{2}{G} \sum_\alpha \sum_j x_\alpha p_\alpha^j - \frac{1}{G}\,. \tag{3.13}$$

With this we can express the time evolution of the average genotype as

$$\dot{\vec{\sigma}}_1 = \mu \vec{\sigma}_1 (1 - \sigma_0) - \left(\frac{2}{3} \vec{\sigma}_1 \cdot \mathbb{I} - \frac{1}{3} \right) \underline{\underline{A}}^{\mathrm{T}} \vec{\sigma}_1\,. \tag{3.14}$$

Interesingly, for three cyclically competing species, this equation is structurally similar to the classic May-Leonard equation (G=3) [71]. However, while the dynamics of the May-Leonard equation comprises a nonlinear invariant manifold, the time evolution of the mean genotype takes place on the unit simplex Δ^2. From the formal similarity of the nonlinear terms on the right hand side we infer, that the fixed point $(1/3, 1/3, 1/3)$ is unstable to perturbations and the dynamics is driven towards the boundaries of the simplex performing heteroclinic orbits. This is indeed in agreement with Monte Carlo simulations of the stochastic system. What can we conclude for the dynamics of the concentrations x_α? We consider intitial conditions corresponding to $\sigma_1(t = 0) = (1/3, 1/3, 1/3)$. As the dynamics of σ_1 is characterized by heteroclinic orbits out of this fixed point and the genotypes $\vec{p}_\alpha$ do not depend on time we find that small differences in the concentrations are amplified by the nonlinear dynamics. Therefore, also the dynamics of Eqs. (3.9) is unstable.

3.2.3 Heterogeneous motility

As mentioned before, heterogeneous motility is a common feature of bacterial populations. We are therefore interested in models, which comprise heterogeneity in individuals' motilities. Consider the case of an infinite system size. We also require that each genotype, here given by its diffusion constant D, is present in a macroscopic number of individuals. We may then again define concentrations $\mathbf{u}_D = (u_D^1, u_D^2, \ldots, u_D^S)$ giving the fraction of individuals of S different species and with diffusion constant D. We assume that the diffusion constant densely fill an interval I on $\mathbb{R}$. In this case we can give a general form of partial integro-differential equations describing the time evolution of diffusively heterogeneous systems,

$$\partial_t \mathbf{u}_D(\mathbf{r},t) = \underline{\underline{D}}\Delta \mathbf{u}_D(\mathbf{r},t) + \int_I \underline{\underline{K}}(D,D')\mathbf{f}(\mathbf{u}_D,\mathbf{u}_{D'})\mathrm{d}D' \,, \tag{3.15}$$

where $\underline{\underline{D}}$ is a diagonal matrix with entries D. $\underline{\underline{K}}(D,D')$ is a diagonal interaction matrix whose diagonal elements give the reaction rate per concentration between individuals with diffusion constants D and D' for each species i. Last, $\mathbf{f}$ is a (nonlinear) function defining the dynamics. We now introduce two paradigmatic models comprising heterogeneous mobility. The homogeneous versions of each of these models has been used to study fundamental questions in theoretical biology. But how does phenotypic heterogeneity affect the answers to these questions?

Range expansion of heterogeneous populations

Waves propagating into an unstable state are an ubiquitous phenomenon in nature. They describe, for example, the spreading of advantageous genes [44] or infectous diseases [130]. Recently, they have attracted considerable attention as a model for the range expansion of bacterial populations [131–133]. How does phenotypic heterogeneity in bacteria's motility affect the expansion process?

To study the expansion of heterogeneous populations, we consider individuals A on a d-dimensional lattice who exhibit phenotypic heterogeneity in their rates to migrate and reproduce. The population is also genetically diverse in the sense that the probabilities to be in the motile or non motile state depend on the individual. An individual i may reproduce with a rate μ_i upon consumption of resources B, in chemical notation $A_iB \xrightarrow{\mu_i} A_iA_i$. Upon reproduction, an individual's genotype is inherited to its offspring. In addition, individuals perform random walks with a rate ϵ_i. Motivated by the behavior of *B. subtilis* we assume that migration and reproduction are complementary skills, i.e. individuals with a high motility reproduce less often. In particular, the characteristic time for individuals to react or migrate is set equal for all individuals, $1/(\epsilon_i + \mu_i) = 1$. This choice fixes the time scale. We here consider a stochastic lattice gas model in one and two dimensions. Each site can be occupied by an arbitrary number of individuals. While reproduction

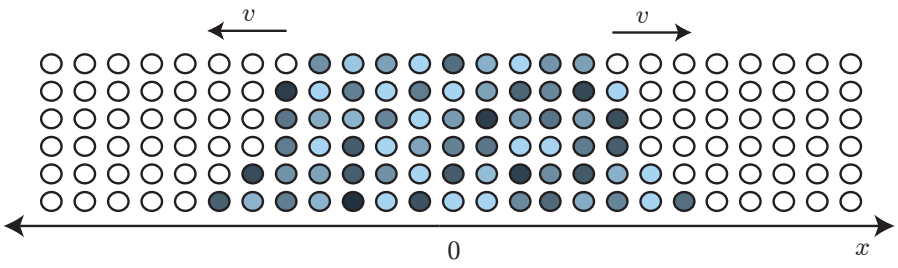

Figure 3.3: Illustration of the model for heterogeneous range expansion. Each lattice site is occupied by mobile individuals A (blue circles) and immobile resources B (white circles). Individuals perform random walks on the lattice with an individual based rate ϵ_i. They may reproduce with a rate $1-\epsilon_i$ upon consumption of resources on the same site. The new individual inherits the rates for reproduction and hopping. Our model comprises an unstable state corresponding to an unpopulated lattice, and a stable state corresponding to a lattice fully occupied by individuals A. If the unstable state is perturbed the perturbation grows exponentially and one observes the propagation of a front into the unstable state.

happens locally, i.e. the descendant is placed on the same lattice site, migration is implemented as a hopping process on neighboring sites. The total number of particles A and B is conserved by the reaction. With Ω being the average number of particles per site in the mean field theory, we may define concentrations $a(\mathbf{r},t)$ and $b(\mathbf{r},t)$ by $N_A(\mathbf{r},t) \equiv a(\mathbf{r},t)\Omega$ and $N_B(\mathbf{r},t) \equiv b(\mathbf{r},t)\Omega$. Here, $\mathbf{r} \in \mathbb{Z}^d$ denotes the position on the lattice and N_A and N_B are the local number of particles of types A and B. The spatio-temporal dynamics is then described by partial integro-differential equations of the form (3.15), with diag $\underline{\underline{D}} \equiv [\epsilon/(2d), 0]$, diag $K(\epsilon,\epsilon') \equiv [(1-\epsilon)\delta(\epsilon-\epsilon'), 1-\epsilon]$, and $\mathbf{f}(\mathbf{u}_\epsilon, \mathbf{u}_{\epsilon'}) \equiv (u^1_\epsilon u^2_{\epsilon'}, -u^1_\epsilon u^2_{\epsilon'})$. We here parametrized the genotypes with the individual based rate for the random walk, $\epsilon = 2dD$, to parametrize the genotypes. We obtain

$$\partial_t a_\epsilon(\mathbf{r},t) = \frac{\epsilon}{2d}\Delta a_\epsilon(\mathbf{r},t) + (1-\epsilon)a_\epsilon(\mathbf{r},t)b(\mathbf{r},t) \tag{3.16a}$$

$$\partial_t b(\mathbf{r},t) = -b(\mathbf{r},t)\int_0^1 (1-\epsilon)a_\epsilon(\mathbf{r},t)\,\mathrm{d}\epsilon\,. \tag{3.16b}$$

These equations comprise an unstable homogeneous solution corresponding to an empty lattice, $\int_0^1 a_\epsilon(\mathbf{x},t), \mathrm{d}\epsilon = 0$, $b(\mathbf{x},t) = 1$, whereas the state $a_\epsilon(\mathbf{x},t) = 0$ and $b(\mathbf{x},t) = 1$ is a stable solution. This can be seen by considering the dynamics of the total concentration of particles of type A,

$$\partial_t \int_0^1 a_\epsilon\,\mathrm{d}\epsilon = \int_0^1 (1-\epsilon)a_\epsilon\,\mathrm{d}\epsilon(1-\int_0^1 a_\epsilon\,\mathrm{d}\epsilon)\,. \tag{3.17}$$

Hence, small perturbations to the unstable state will grow and eventually lead the propagation of the stable phase into the unstable phase. Fronts propagating into unstable state have been subject to extensive studies [45, 134]. However, the dynamics

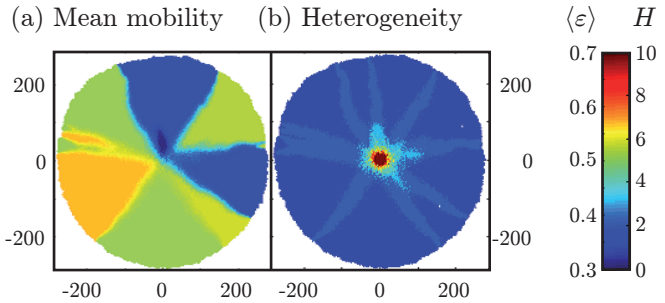

Figure 3.4: (a) Typical configuration of a stochastic simulation for a circularly expanding population ($t = 490$). Color denotes the local average mobility $\langle\epsilon\rangle$, such that blue signifies a low mobility, yellow a medium mobility and red a high mobility. We observe the formation of homogeneous sectors. (b) The same situation, but plotted is the local genetic heterogeneity, such that blue sites are homogeneous and red sites are heterogeneous. We find that genetic diversity is rapidly lost during the expansion process. The population remains diverse at the origin and at sector boundaries. In this figure, space is measured in units of the lattice spacing. Simulations were run on a hexagonal lattice with $L^2 = 500^2$, $\Omega = 100$, and $t = 490$.

is much more complex for heterogeneous fronts. We studied the range expansion of heterogeneous populations by means of stochastic simulations and finite difference simulations of Eq. (3.16). Figure 3.4 shows that homogeneous sectors form of individuals with the same genotype. During the expansion process genetic diversity in the front region is lost. Interestingly, the expansion process can be divided into different stages, where different evolutionary forces select distinct genotypes. Specifically, for small times a low motility is favored, while for large times individuals with a balance between reproduction and migration dominate the population. Asymptotically, the evolutionary dynamics selects certain genotypes which dominate the population with a high probability. These genotypes correspond to individuals who migrate and reproduce at an equal rate. Interestingly, the asymptotic behavior is altered by fluctuations both due to random nature of reactions and diffusion.

Heterogenous motility in the prisoner's dilemma

Understanding the conditions that facilitate the persistence of cooperation is one of the classic problems in evolutionary biology. The dilemma of cooperation expresses the naive point of view that cooperation should not be robust against "cheating" mutants. However, cooperation is frequently found in biological systems. As an example, the metabolism of *Pseudomonas aeruginosa* relies on the consumption of iron. These bacteria therefore produce an iron-scavenging siderophore which may pass the cell membrane and is therefore available to other bacteria. As siderophore production is metabolically costly the population should in principle be susceptible to the invasion by mutants who do not produce the siderophore [99]. Mathematically, the dilemma

	C	D
C	$b-c$	$-c$
D	b	0

Table 3.1: The payoff matrix defines how much two individuals gain or loose as a result of an interaction. In the prisoner's dilemma, if both players are distinct, the defector collects a benefit b, while the cooperator has a cost c with $0 < c < b$ for providing a public good. A cooperator engaging a cooperator results in a payoff $b - c$ for both, while defectors do not profit from a mutual interaction.

of cooperation is often formulated in the framework of evolutionary game theory, where such situations are described in terms of the so-called *prisoner's dilemma* [135]. Spatial structures have been identified as a key promoter of cooperation [136–138], while even a low mobility has been shown to jeopardize cooperation in spatially extended populations [139].

How does heterogeneity in the individuals' motility influence the chances for the persistence of cooperation? We study a heterogeneous version of the proisoner's dilemma. The stochastic dynamics is described by a Moran process: Each individual is either a cooperator (C) or defector (D). Individuals can interact ('play') with other individuals on the same lattice site at a rate r. The profit they gain from such an interaction is encoded in a so-called payoff matrix describing how much each reactant benefits from the reaction. If both players are distinct, the defector collects a benefit b, while the cooperator has, in addition, a cost $0 < c < b$ for providing a public good. A cooperator engaging a cooperator yields a payoff $b-c$ for both, while two defectors collect payoff 0. The payoff matrix is summarized in Table 3.1. How well does an individual perform compared to others? The average payoff an individual collected is called accumulated fitness,

$$f_i = f_0 + \frac{1}{n}\sum_{l=1}^{n} p_j^{(l)}, \tag{3.18}$$

where p_i^l is the payoff that was collected in the l^{th} interaction. Success in interactions translates into a high reproduction rate, which is proportional to f_i. Upon reproduction, individuals replace a randomly chosen individual on the same lattice site. Each individual is therefore characterized by a 'genotype' $\mathbf{g} \in \{C, D\} \times \{\epsilon_1, \epsilon_2, ...\}$ consisting of the type and the individual mobility. Upon reproduction, the newly produced individuals inherit these traits of their ancestor. Last, individuals perform random walks with an individual rate ϵ_i. We assume that initially motility is assigned randomly to each individual according to a uniform distribution on $[0, 2\epsilon_0]$. ϵ_0 is the initial average mobility in the population.

For infinitely small lattice spacing the spatial variables can be regarded continuous. Macroscopically, the hopping processes then effectively lead to diffusion with a diffusion constant $\epsilon\big/(2L^2)$, with L being the linear dimension of the lattice. If, in

addition, the number of individuals is large, we can consider the local concentrations $c_\epsilon(\mathbf{r},t)$ and $d_\epsilon(\mathbf{r},t)$ of cooperators and defectors with a given mobility ϵ. Neglecting fluctuations the dynamics is then aptly described by partial integro-differential equations,

$$\partial_t c_\epsilon = \frac{N}{2\epsilon_0}\int_0^{2\epsilon_0} K_c(\epsilon,\epsilon')\, c_\epsilon d_{\epsilon'} + \frac{\epsilon}{2L^2}\nabla^2 c_\epsilon\,, \tag{3.19a}$$

$$\partial_t d_\epsilon = \frac{N}{2\epsilon_0}\int_0^{2\epsilon_0} K_d(\epsilon,\epsilon')\, d_\epsilon c_{\epsilon'} + \frac{\epsilon}{2L^2}\nabla^2 d_\epsilon\,. \tag{3.19b}$$

The interaction kernels $K_c(\epsilon,\epsilon')$ and $K_d(\epsilon,\epsilon')$ can be expressed by approximating an individuals fitness by the average fitness $\overline{f}$ of all individuals with the same genotype. We obtain $K_c(\epsilon,\epsilon') = \overline{f}^c_\epsilon - \overline{f}^d_{\epsilon'}$ and $K_d(\epsilon,\epsilon') = \overline{f}^d_\epsilon - \overline{f}^c_{\epsilon'}$ with $\overline{f}^c_\epsilon(\mathbf{r},t) = f_0 + bc_\epsilon(\mathbf{r},t) - c$ and $\overline{f}^d_\epsilon(\mathbf{r},t) = f_0 + bc_\epsilon(\mathbf{r},t)$. Equations (3.19) possess infinitely many stable spatially, uniform states corresponding to a system fully occupied by individuals of any genotype. In our stochastic model these states are absorbing states, i.e. they are reached with probability one after a finite time. The probability distribution of which of these states is reached asymptotically and the corresponding time scale depend qualitatively on the average mobility ϵ_0 in the initial condition and the cost for cooperation c.

3.3 Manuscripts and publications

3.3.1 Speciation and bet hedging in heterogeneous populations

In the manuscript "Speciation and bet hedging in heterogeneous populations" by David Jahn, Steffen Rulands, and Erwin Frey we studied the interplay between genetic diversity and phenotypic heterogeneity in mobile populations. We showed that the evolutionary dynamics is reflected in the rate of decrease in genetic diversity. Remarkably, we found that individuals' mobility and the type of competition qualitatively affect the the survival of phenotypic heterogeneity. For direct competition we identified threshold values in the mobility determining the characteristics of evolutionarily successful genotypes: if the system is well-mixed we observe the survival of bet-hedgers, while for little or no diffusion specialists take over the population. In a third regime biased bet-hedgers turned out to be the most successful individuals. In contrast, for direct competition, specialists asymptotically constitute the population. We observed the same transitions in a more complex foodweb comprising four species. We therefore expect that our findings are generic in the sense that they only rely on basic properties of the underlying nonlinear dynamics.

3.3.2 Heterogeneous motility facilitates the persistence of cooperation

In the manuscript "Heterogeneous motility facilitates the persistence of cooperation" by Steffen Rulands, Jörg Martin and Erwin Frey we investigated under which conditions cooperation is possible in heterogeneous populations. By studying a version of the spatial prisoner's dilemma, where individuals are endowed with distinct motility we showed that heterogeneity may significantly promote the persistence of cooperation. In particular, we identified three regimes which qualitatively differ in the dynamics and in the genetic composition of the population at large times. In analogy to previous work on the homogeneous model we found that if the cost for cooperation is high defectors dominate the population at large times. As opposed to this, for very low costs, fast cooperators take over the population. Importantly, for intermediate values of the cost for cooperation, slow cooperators may persist and even constitute the majority of the population at large times.

3.3.3 Range expansion of heterogeneous populations

Invasion fronts arise in nearly all fields of science. They describe phenomena as diverse as combustion fronts, epidemic spreading or range expansion in bacterial populations. In the manuscript "Range expansion of heterogeneous populations" by Matthias Reiter, Steffen Rulands, and Erwin Frey we studied the range expansion of a population that exhibits heterogeneous motility and reproduction rates. We showed that the expansion process decreases genetic diversity in the front region. This selection is driven by fitness differences of different genotypes. We identify distinct temporal regimes characterized by different evolutionary forces acting on the foremost individuals. Interestingly, stochastic fluctuations play an intriguing role in the selection of the genotype that ultimately dominates the population. While a finite particle number tends to favor individuals who reproduce with higher probability, noise due to diffusion favors individuals with a higher mobility.

3.3.4 Conclusion and outlook

Genotypic and phenotypic heterogeneity are commonly found in bacterial populations and viruses. As an example, viruses switch between phenotypic states to evade a host's immune system. Some bacteria stochastically switch between phenotypic states to minimize the risk of population extinction due to an attack with antibiotics. Inspired by these phenomena we investigated heterogeneous, stochastic many-particle systems. The basic idea was that each particle should be endowed with distinct properties. This field of research becomes increasingly fascinating, yielding a multitude of interesting phenomena.

We studied the interplay between genetic diversity and phenotypic heterogeneity in spatially extended populations comprising cyclic interactions and more complex food

webs. In our model, individual can be in different phenotypic states. The probability to be in any of these state is given by an individual's genotype. We found that the survival of genetic diversity and phenotypic heterogeneity qualitatively depends on the degree of mixing. For small mobilities, phenotypic specialization is favored by the evolutionary dynamics, whereas for large mobilities phenotypic generalization can persist. The survival of phenotypic heterogeneity also significantly depends on whether the competition is direct, as in predator-prey relations, or indirect, mediated through the limited availability of resources. Our results are not restricted to the models we studied. Rather, we expect that they show a generic behavior which only depends of on basic properties of the attractors of the underlying nonlinear dynamics.

Another fundamental problem in biology is the evolution of cooperation. Experimental studies show that many bacterial populations exhibit phenotypic heterogeneity with respect to individuals' mobilities. As an example, *Pseudomonas aeruginosa* produces an iron scavenging enzyme that is also available for neighboring cells. How can cooperation persist in situations, where cheating individuals should have a reproductive advantage? This dilemma of cooperation is often formulated in the framework of evolutionary game theory, where such situations are described in terms of the prisoner's dilemma. We investigated how cooperation can evolve in heterogeneous populations. To this end we studied the heterogeneous version of the prisoner's dilemma, where each player was endowed with a distinct mobility. We showed that under these circumstances cooperation is significantly enhanced in the spatial prisoner's dilemma. The asymptotic composition of the population qualitatively depends on the average initial mobility and the cost for cooperation. In particular, we identified three regimes which differ by the probability for the survival of cooperation and the average mobility of cooperators and defectors at large times. Importantly, cooperation is significantly enhanced for a broad range of parameters. Our findings contribute to a better understanding of the evolution of cooperation in biological systems.

Finally, we studied heterogeneous versions of invasion processes, which arise, for example, in the range expansion of bacterial colonies or the spreading of diseases. Motivated by phenotypic heterogeneity found in populations of *Bacillus subtilis* we studied the range expansion of a population, where each individual can be in a motile or reproductive state with distinct probabilities. We observed a radial spreading process and the formation of homogeneous sectors in the expanding populations. The spreading process favors certain genotypes at different stages and ultimately leads to a loss of genetic diversity. The asymptotic behavior of the front is significantly influenced by stochastic fluctuations.

Heterogeneous, stochastic many-particle systems proved to be a fascinating field of research. An interesting extension of the models we studied here would be to introduce temporal correlations in the switching between phenotypic states. Further work might also extend our findings to other models of theoretical biology. For example, the snowdrift game with heterogeneous mobilities might by worth looking at. In addition,

studying other forms of phenotypic heterogeneity could yield an entirely different phenomenology. How could one, for example, study the phenotypic heterogeneity in the competence for DNA transformation in the framework of stochastic many-particle systems? In addition, one could study heterogeneity in the way individuals interact with each other. Such a model could comprise, for example, direct competition and indirect competition, such as in the Lotka-Volterra and May-Leonard model, respectively.

Speciation and bet hedging in heterogeneous populations

David Jahn,* Steffen Rulands,* and Erwin Frey†
Arnold-Sommerfeld-Center for Theoretical Physics and Center for NanoScience , Department of Physics, Ludwig-Maximilians-Universität München, Theresienstrasse 37, D-80333 Munich, Germany

We study the interplay between genetic diversity and phenotypic heterogeneity in mobile populations. In particular, we consider three and four species models with direct or indirect competition. We show that individuals' mobility and the type of competition qualitatively influence the loss of genetic diversity and the persistence of phenotypic heterogeneity. For direct competition, as in Lotka-Volterra models, we identify three distinct regimes determining the characteristics of evolutionarily successful genotypes.

PACS numbers: 87.23.Cc, 05.40.-a, 02.50.Ey

Genotypic and phenotypic heterogeneity are both commonly found in microbial and viral populations [1–7]. However, in a constant environment without niches, genotypic heterogeneity is difficult to maintain. Cyclic dominance between genotypes has been identified as one factor promoting biodiversity in spatially extended systems [8–14]. For example, bacterial model systems comprised of three genetically distinct strains of *Escherichia coli* have been shown to exhibit stable three-strain coexistence in spatially extended homogeneous environments [11]. In this system, a strain releasing a toxin kills a sensitive strain but not a resistant strain. The sensitive strain grows faster than the resistant strain which in turn grows faster than the toxin-producing strain. This basic motif of cyclic dominance is metaphorically described by the rock-paper-scissors game, where rock crushes scissors, scissors cut paper, and paper wraps rock. Recent experimental studies have explored how demographic noise [13–19], mobility of individuals [13, 14, 20], and the structure of the interaction network as well as the strengths of its links [21] affect the maintenance of genotypic diversity. All of these studies assume that genotypes are linked to a single phenotype. But what happens if an individual microbe is able to change it's strategy, or in other words shows phenotypic heterogeneity? Some bacteria use a bet-hedging strategy by stochastically switching between different phenotypic states to minimize the risk of population extinction due to an attack with antibiotics [2, 22]. Does such phenotypic heterogeneity favor or disfavor population heterogeneity and how does the population dynamics depend on the mobility of individuals and the type of interaction between them?

Here we address these questions by studying the dynamics of spatially extended populations which initially contains N individuals of G different genotypes. Each of these genotypes $\alpha \in \{1, \dots, G\}$ is defined by its degree of phenotypic heterogeneity, *i.e.* a set of probabilities $\vec{p}_\alpha = \left(p_\alpha^1, \dots, p_\alpha^M\right)$ with p_α^m signifying the probability that genotype α is in a particular phenotypic state $s_m \in \{s_1, \dots, s_M\}$. Biologically, phenotypic heterogeneity is often the result of stochastic fluctuations of critical cellular components within metabolic pathways or regulatory circuits of microbes, and the values of the probabilities reflect differences in the rates or architectures of these pathways and circuits. For specificity, we will mainly focus on systems with $M = 3$ states and defer a discussion of a larger number of states to the Supplementary Material. Then, the phenotypes s_m may, for example, refer to one of the three phenotypic traits of *E. coli* discussed above [11]. We will consider two distinct ecological scenarios with cyclic dominance. In the first class of models, termed Lotka-Volterra (LV) model [23, 24], selection and reproduction is combined into a single event where the competition between two individuals leads to the immediate replacement of the weaker by the stronger individual: $I + J \to I + I$. In the second class of models, originally proposed by May and Leonard (ML) [25], selection and reproduction are two separate processes. An interaction between two individuals with different phenotypes leads to the death of the weaker phenotype and thereby to empty spaces: $I + J \to I + \emptyset$. Reproduction then follows as a second process which recolonizes this empty space with a birth rate μ: $I + \emptyset \to I + I$. In an ecological context these empty sites account for the limited availability of resources. In each of these models, the genotype α_i of individual I is inherited to the newly produced individual.

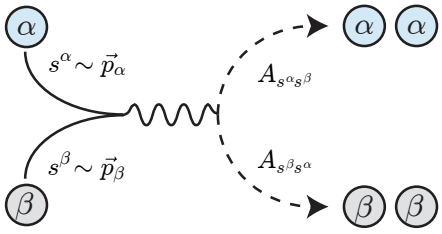

FIG. 1. (Color online) Illustration of the model. When individuals with genotypes α and β engage, their phenotypic states s^α and s^β are chosen randomly according to the probability distributions $\vec{p}_\alpha$ and $\vec{p}_\beta$. The reaction channel is then determined by the interaction matrix $\mathbf{A}$: in the LV model the individual with genotype β is replaced by an offspring with genotype α with probability $A_{s^\alpha s^\beta}$, and vice versa.

We show that individuals' mobility and the type of competition qualitatively influence the loss of genetic diversity and the persistence of phenotypic heterogeneity. For direct competition, as in the class of Lotka-Volterra models, we observe three regimes in the mobility. While permanent local environments promote specialization, fast changing local environments enhance phenotypic generalization.

At a given time t, the state $\mathcal{C}$ of the population is characterized by a set of genotypes $\vec{p}_{\alpha_i}$ (short: α_i) and lattice positions $\mathbf{r}_i(t)$ for each individual $i \in \{1,\ldots,N\}$: $\mathcal{C}(t) = \{\alpha_i, \mathbf{r}_i(t)\}_{i=1,\ldots,N}$. We assume that each lattice site on a two-dimensional square lattice with L^2 sites is occupied by at most one individual. The linear dimension L of the lattice is taken as the basic length unit such that the lattice constant $a = 1/L$ [26]. Every time two neighboring individuals engage in an interaction they each randomly choose a phenotype according to their respective probability vectors. The outcome of the pairwise competitions among phenotypes is described in terms of an interaction matrix $\mathbf{A}$ where its entries $A_{ss'}$ denotes the rate at which phenotype s outcompetes phenotype s'. For simplicity, we choose a symmetric model where all finite rates are the same, and equal to 1 to fix the time scale [27]. Mobility of individuals is implemented as a nearest neighbor exchange process at a rate ϵ, $I + J \to J + I$, where I and J denote individuals or also empty spaces $\emptyset$. Macroscopically this nearest neighbor exchange process leads to diffusion with an effective diffusion constant $D = \epsilon a^2/2$ [13]. The diffusion constant D then gives the mean square displacement of an average particle between two reactions. As an example, with the system size as the unit length a value of $D = 10^{-3}$ implies that a particle covers an area of one thousandth of the system size between two succeeding reactions.

We performed stochastic simulations of both lattice gas model employing periodic boundary conditions and a sequential updating algorithm, where at each time step a random pair of neighboring individuals is chosen. All simulations were started from an initial condition where G genotypes were chosen randomly according to a uniform distribution on the unit simplex Δ^2, and then distributed randomly over the lattice. As time progresses the competition between these genotypes reduces genetic heterogeneity in the population. This is illustrated in Figs. 2 (a) and (c) which show the number of different genotypes, $H(t)$, averaged over many realizations $\mathcal{C}$ of the population dynamics. Concomitant with the loss of genetic diversity spatio-temporal patterns and correlations develop. How genetic diversity is lost as well as the nature of these patterns and correlations depend strongly on the type of model and the value of the diffusion constant. While for large diffusion constants both models quickly reach a state where only one genotype is left in the population, there are quite long-lived metastable states containing three distinct genotypes [Fig. 2 (a) and (c)]. For the ML model this transient biodiversity is maintained by spiral waves as previously found for the ML model with three cyclically competing homogeneous species [13] [Fig. 2(b)]. In contrast, for the LV model a high degree of genetic diversity remains [Fig. 2(d)].

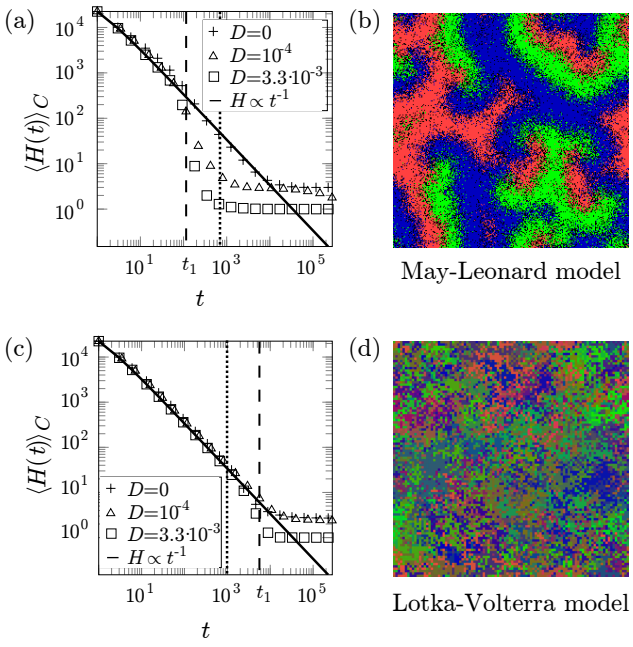

FIG. 2. (Color online) The average decay of genotypic heterogeneity $\langle H(t)\rangle_{\mathcal{C}}$ gives information about the evolutionary processes going on in different temporal regimes. (a) In the ML model we find an initial decay according to a power law t^{-1}, in accordance with neutral evolution. After a characteristic time $t_1 \approx 10^2$ (dashed line) we find that an evolutionary drift accelerates the loss of heterogeneity. For large times, the number of surviving genotypes takes values of 1 or 3 depending on the diffusion constant. (b) A typical configuration of the ML model for large times [$t = 660$, dotted line in (a)] and a low value of the diffusion constant ($D = 10^{-4}$). Different colors (gray scales) signify the probability to be in any of three phenotypic states: red (light gray), green (medium gray) or blue (dark gray) denotes a high probability to be in the phenotypic states s_1, s_2 or s_3, respectively. We observe spiral waves of individuals with a high probability to be in one of the phenotypic states ($L = 250$). (c) Surprisingly, in the LV model the neutral regimes lasts much longer than expected. After a characteristic time, $t_1 \approx 10^3$ (dashed line), the heterogeneity takes stationary values of 1 or 3, depending on the diffusion constant. (d) In a typical configuration of the LV model we find for large times [$t = 10^3$, dotted line in (c)] a multitude of different genotypes ($L = 100$).

Quite model independent we observe that initially genotypic heterogeneity decreases like a power law, $\langle H(t)\rangle_{\mathcal{C}} \propto t^{-1}$. Because genotypic heterogeneity is high selection occurs irrespectively of the genotype, and the decrease of H is described by a neutral coalescence process, $A+A \to A$; the rate is given by the probability that the two competing individuals are in a different pheno-

typic state, $k = 2/3$. Fluctuations can be neglected and the dynamics of this process is aptly described in terms of mean field reaction kinetics, $\dot{H} = -kH^2$, which is solved by $H(t) = N/(kt+1)$ and agrees well with our numerical results [solid lines in Fig. 2].

For intermediate times, $t_1 < t < t_2$, we find a rapid decrease in genetic heterogeneity, which is most prominent for the ML model. Here, the genealogical dynamics is driven by evolutionary forces, *i.e.* success in reproduction depends on an individual's genotype. To understand this, note that in the model involving empty sites, small differences in the concentrations are amplified by the evolutionary dynamics. In other words, for large values D the ML model is characterized by the escape out of an unstable state, resulting in the acceleration of the decrease of heterogeneity. The characteristic time t_1 is therefore given by the time in which fluctuations drive the system globally out of an unstable fixed point. This view is supported by the logarithmic scaling of t_1 with the system size, $t_1 \propto \ln N$, cf. Supplemental Material.

We also find that in the ML model the rate of decrease of the heterogeneity changes with the diffusion constant D: the smaller D the slower the extinction of genetic diversity. Hence, spatial structures not only stabilize systems of cyclically interacting species [13, 19, 20, 28, 32], but also promote genotypic heterogeneity therein. The reason for this remarkable behavior is that spatial structures consist of genetically identical individuals. Reactions between different genotypes therefore only happen at the boundaries of domains and thereby globally at a lower rate.

The amplification of perturbations in the reactive fixed point is not present in the model of LV type. In the Supplemental Material we show that the LV model comprises N conserved quantities corresponding to neutrally stable orbits. Here, the approach of the absorbing states is purely driven by fluctuations and therefore occurs on a larger time scale and is less pronounced. This is supported by the scaling of t_1 with the system size, namely $t_1 \propto N$, see Supplemental Material.

For times larger than a second characteristic time t_2, genetic heterogeneity reaches a stationary level. We find two qualitatively different regimes. For low diffusion constants, we observe a metastable state comprised of three distinct genotypes. As discussed below, they are analogous to metastable states found previously in models lacking phenotypic heterogenetity [13, 20, 28, 32]. In contrast, for high diffusion constants, the dynamics end in absorbing states corresponding to the extinction of all but one genotype, which we will call the asymptotic genotype $\vec{\pi}$.

What kind of asymptotic genotypes will dominate and how does this depend on the kind of competition between individuals? To answer this question we consider many realizations $\mathcal{C}$ of the population dynamics and determine the probability density $\mathcal{P}_\infty(\vec{\pi})$ of asymptotic genotypes on the unit simplex $\vec{\pi} \in \Delta^2$ [Figs. 3(a,b)]; maxima of $\mathcal{P}_\infty$ identify those genotypes which are evolutionarily most successful [29].

Interestingly, we find that the type of evolutionary successful genotypes qualitatively depend on the mobility. We identify three distinct regimes: If diffusion is weak, we observe a high probability in the corners of the unit simplex [Fig. 3(a), top left], *i.e.* it is evolutionarily most advantageous to *specialize* to one of the three phenotypes. In contrast, for large diffusion constants, the most successful individuals are *bet-hedgers*, *i.e.* have a genotype with (nearly) equal probabilities for each of the three phenotypes [Fig. 3(a), bottom right]. For intermediate values of D, the most successful individuals adopt a bet-hedging strategy that is biased towards any of the three phenotypes. The boundaries between these three qualitatively different regimes, D_1 and D_2, can be clearly identified from Fig. 3(b) which shows the marginal distribution in any of the three components of $\vec{\pi}$ [30]

For large diffusion constants, $D > D_2$, the characteristic length scale of spatial patterns is larger than the system size [13, 28], and therefore the dynamics are effectively that of a well-mixed system. In such an environment the interaction between individuals with two different genotypes can be described by a mean-field approximation: the probability that an individual of genotype α outcompetes one of genotype β is given by $w_{\alpha\beta} = \vec{p}_\alpha^{\,\mathrm{T}} \mathbf{A} \vec{p}_\beta = p_\alpha^1 p_\beta^2 + p_\alpha^2 p_\beta^3 + p_\alpha^3 p_\beta^1$. This implies a net transition rate between genotypes $W_{\alpha\beta} = w_{\alpha\beta} - w_{\beta\alpha}$, such that the fraction x_α of individuals with genotype α obeys the rate equation

$$\partial_t x_\alpha(t) = x_\alpha(t) \sum_{\beta=1}^{G} W_{\alpha\beta}\, x_\beta(t)\,. \tag{1}$$

Since $\mathbf{W}$ is a skew-symmetric matrix, this corresponds to the replicator equation of a G-species conservative LV model whose dynamics has recently been classified [21]. Obviously, a bet-hedging strategy with $\vec{p}_\mathrm{b} = (\frac{1}{3}, \frac{1}{3}, \frac{1}{3})$ is a fixed-point of this rate equation; since $W_{b\beta} = 0$ it can not be outcompeted by any other genotype β. Moreover, the particular form of $\mathbf{W}$ implies that all orbits $\mathbf{x}(t) \in \Delta^{G-1}$ are neutrally stable periodic orbits. For finite system sizes, the mean first passage time into the absorbing states is therefore longest for bet-hedgers which, as a result, constitute the majority of the population for large times [16, 31].

For small diffusion constants, $D < D_1$, we observe that the dynamics reaches a metastable state comprised of three distinct genotypes which are specialized to one of the three phenotypic states, respectively [Fig. 3(b)]. Actually the origin of this regime is due to a separation in time scales between the exchange rate ϵ and the reaction rates, $\epsilon \ll 1$. This is clearly indicated by the scaling of the threshold value with system size, $\epsilon_1 \sim D_1 \cdot N \sim 1$ [Fig. 3 (c)]. As a consequence, a domain boundary be-

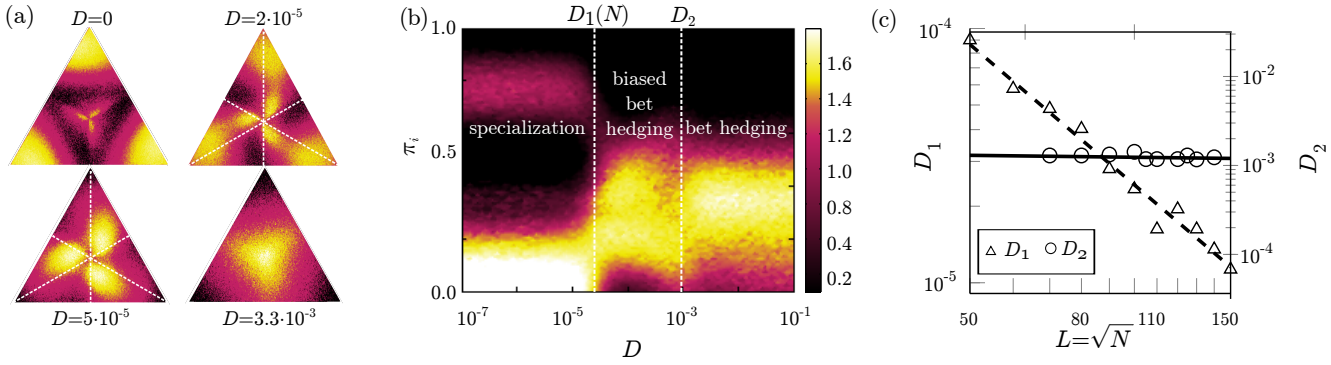

FIG. 3. (Color online) (a) To study the dependence of the asymptotic states on the individuals' mobility, we computed the probability density $\mathcal{P}_\infty$ of the asymptotic genotypes for four different values of the diffusion coefficient D. Color (gray scale) denotes the value of $\mathcal{P}_\infty$, such that white signifies a high value and black a low value. The maxima of $\mathcal{P}_\infty$ identify successful genotypes. For very low diffusion constants specialization to one of the phenotypic states is most successful (top left). In contrast, for high diffusion constants, $\mathcal{P}_\infty$ is highest in the center of the simplex, i.e. the longest living individuals are generalists who choose each phenotype with equal probability (bottom right). For intermediate values of D we find a maximum corresponding to a biased bet hedging strategy (top right and bottom left). Dashed lines denote perpendicular bisectors. (b) Phase portrait of the marginal distribution in any of the components of $\vec{\pi}$. We identify two threshold values D separating different outcomes of the evolutionary dynamics. Below a first threshold value $D_1 \approx 1.5 \cdot 10^{-5}$ mostly non-heterogeneous genotypes survive. In between D_1 and a second threshold $D_2 \approx 1.25 \cdot 10^{-3}$ a bimodal distribution is found, corresponding to biased bet-hedgers. For $D > D_2$ bet-hedgers dominate the population for large times. Averages were computed over 10^6 trajectories ($L = 80$). (c) The scaling of the threshold values with the system size gives information about the origin of the phase transitions. $D_1 \propto N^{-1}$ indicates that the underlying mechanism is of local nature, while $D_2 \propto$ const. suggests that this transition has its origin in changes in certain length scales.

tween two different genotypes changes mainly due to competitive takeover and not mutual exchange of lattice sites. This leads to rather smooth domain boundaries which move at a speed proportional to the net transition rate $W_{\alpha\beta}$. The invasion speed of domains of specialists into any domain is maximal. Likewise, by the skew-symmetry of $\mathbf{W}$, also the invasion speed any domain into domains of specialists is maximal. On first sight the invasion speed should therefore not be a distinguishing mark of successful genotypes. However, fast invasion allows the corresponding individuals privileged access to limited prey. Following a "first come first served" principle specialized genotypes therefore outcompete their bet hedging counterparts. For large times, the dynamics hence comprises cyclic competition between three specialized genotypes.

In the parameter regime $D_1 < D < D_2$, we again find a prolonged metastable state where clusters of similar genotypes emerge. As opposed to the specialists observed for $D < D_1$, these genotypes now favor one phenotype but still keep a non-vanishing probability to be in the other states [Fig. 3(a), bottom left]. Since now diffusion mediated by site exchange occurs at the same time scale as competitive interactions the domain boundaries are fuzzy, and, as a result of an increasing mean path length associated with D, domains are frequently intruded by particles with a distinct genotype. As a result, the surviving genotypes are characterized by a trade-off between invasion speed given by $\mathbf{W}$ and robustness against hostile invasion given by a broad distribution of phenotypic states.

The degree of bet hedging is not only determined by the radial dimension on the simplex. We observe that the probability is highest in three of the six triangles defined by the perpendicular bisectors of the simplex, cf. Fig. 3(a), bottom left. Interestingly, these genotypes obey a hierarchy in the components of the probability distributions $\vec{p}_\alpha$: They have a relatively high probability to be in one phenotypic state, the genotype's bias. The ensuing phenotype with the highest rate of being dominated takes the second largest value. Last, the component which is dominated by the genotype's bias has the lowest probability. Mathematically speaking, the components obey $p^1_\alpha > p^3_\alpha > p^2_\alpha$, or cyclically. This hierarchy of phenotypic states ensures that domains are less susceptible to invasion by the most aggressive genotypes.

The genotypes in these triangles (bet hedging triangles) are characterized by outcompeting a large number of genotypes at a lower average rate. As opposed to this, genotypes in the remaining triangles outcompete fewer genotypes, but with a higher average rate. To understand this, we assume that a domain of genotype α is randomly invaded by genotypes β, which are uniformly drawn from the simplex Δ^2. The intersection of the kernel of the linear form $\vec{p}_\alpha(\mathbf{A} - \mathbf{A}^{\mathrm{T}})$ with the simplex Δ^2 defines genotypes, which are mutually non interacting: $W_{\alpha\beta} = 0$. Note that the bet hedging genotype $\vec{b}$ is in this kernel for any genotype α. By linearity the result-

ing line divides the simplex into two regions: Δ_α^+, where $W_{\alpha\beta}$ is positive and Δ_α^- where $W_{\alpha\beta}$ is negative. If α is in one of the bet hedging triangles the number Z^+ of genotypes in Δ_α^+ is greater than the number Z^- of genotypes in Δ_α^- . In particular, one easily finds that $1 < Z^+/Z^- < 5/4$. For genotypes α' from the remaining triangles we find $4/5 < Z_{\alpha'}^+/Z_{\alpha'}^- < 1$. As the mean consumption rate $\sum_{\beta\in\Delta_\alpha^+} W_{\alpha\beta}$ only depends on the degree of specialization, genotypes α in the bet hedging triangles have a lower average invasion rate as compared to genotypes α' in the remaining triangles:

$$(Z_\alpha^+)^{-1} \sum_{\beta\in\Delta_\alpha^+} W_{\alpha\beta} < (Z_{\alpha'}^+)^{-1} \sum_{\beta\in\Delta_{\alpha'}^+} W_{\alpha'\beta} \qquad (2)$$

We conclude that the surviving genotypes achieve robustness against random invaders by outcompeting a larger set of genotypes in cost of a lower average invasion rate.

For indirect competition, we find a remarkably different behavior. There, for any value of D, the population is asymptotically dominated by specialists, see Supplementary Material. Phenotypic heterogeneity does not provide an evolutionary advantage in this setting. In particular, below a threshold value in D, we observe a metastable state of the three specialists. As opposed to this, for large values of D, only a single specialist survives. The reason for the different number of surviving genotypes is that coexistence of cyclically competing species strongly depends on the degree of mixing [13, 19, 20, 32]. To understand the success of specialists under indirect competition, note that interactions between genetically identical individuals potentially are of disadvantage, as they involve the creation of empty sites. These empty sites can independently be used for reproduction by individuals with different genotypes. The reaction rate $w_{ii} = 1-\vec{p}_i^2$ of genetically identical genotypes is zero, if $\vec{p}_i$ has probability one in any of its components. Specialists are therefore generally better off in indirect competition. This effect is even stronger, for low mobilities. There, the formation of stable spatial structures is inhibited by reactions between identical genotypes.

In conclusion, we studied the interplay of genetic and phenotypic diversity in spatial populations. We showed that the evolutionary dynamics is reflected in the rate of decrease in genetic diversity. Remarkably, we found that individuals' mobility and the type of competition qualitatively affect the the survival of phenotypic heterogeneity. For direct competition we identified threshold values in the mobility determining the characteristics of evolutionary successful genotypes: if the system is well-mixed we observe the survival of bet-hedgers, while for little or no diffusion specialists take over the population. In a third regime biased bet-hedgers turned out to be the most successful individuals. In contrast, for direct competition, specialists asymptotically constitute the population. We observed the same transitions in a more complex food-web comprising four species. We therefore believe that our findings are generic in the sense that they only rely on basic properties of the underlying nonlinear dynamics.

The impact of mobility and the type of competition on the survival of phenotypic heterogeneity is not restricted to the models discussed here. We believe that qualitatively similar results hold for any model as long as the basic properties of the nonlinear dynamics are conserved. In the Supplementary Material we show that our results also hold true for a more complex food web comprising four species.

This research was supported by the German Excellence Initiative via the program 'Nanosystems Initiative Munich' and the German Research Foundation via contract FR 850/9-1. We thank Alejandro Zielinski, Johannes Knebel and Markus Weber for fruitful discussions.

* David Jahn and Steffen Rulands contributed equally to this work
† frey@lmu.de

[1] W. K. Smits, O. P. Kuipers, and J.-W. Veening, Nature reviews. Microbiology **4**, 259 (2006).
[2] O. Gefen and N. Q. Balaban, FEMS Microbiol. Rev. **33**, 704 (2009).
[3] P. B. Rainey, H. J. E. Beaumont, G. C. Ferguson, J. Gallie, C. Kost, E. Libby, and X.-X. Zhang, Microb. Cell Fact. **10 Suppl 1**, S14 (2011).
[4] P. J. Brockert, S. A. Lachke, T. Srikantha, C. Pujol, R. Galask, and D. R. Soll, Infect Immun. **71**, 7109 (2003).
[5] A. M. Porman, K. Alby, M. P. Hirakawa, and R. J. Bennett, Proc. Nat. Acad. Sci. USA **108**, 21158 (2011).
[6] B. Ramírez-Zavala, O. Reuss, Y.-N. Park, K. Ohlsen, and J. Morschhäuser, PLoS Pathog. **4**, e1000089 (2008).
[7] D. R. Soll, Clin. Microbiol. Rev. **5**, 183 (1992).
[8] B. Sinervo and C. M. Lively, Nature **380**, 240 (1996).
[9] R. Durrett and S. Levin, J. Theor. Biol. **185**, 165 (1997).
[10] R. Durrett and S. Levin, Theor. Pop. Biol. **53**, 30 (1998).
[11] B. Kerr, M. A. Riley, M. W. Feldman, and B. J. Bohannan, Nature **418**, 171 (2002).
[12] B. Kerr, in *Bacteriocins*, edited by M. A. Riley and M. A. Chavan (Springer, New York, 2007) pp. 111–134.
[13] T. Reichenbach, M. Mobilia, and E. Frey, Nature **448**, 1046 (2007).
[14] T. Reichenbach, M. Mobilia, and E. Frey, Phys. Rev. Lett. **99**, 238105 (2007).
[15] J. C. C. A. Traulsen and C. Hauert, Phys. Rev. Lett. **95**, 238701 (2005).
[16] T. Reichenbach, M. Mobilia, and E. Frey, Phys. Rev. E **74**, 051907 (2006).
[17] J. C. Claussen and A. Traulsen, Phys. Rev. Lett. **100**, 058104 (2008).
[18] A. Traulsen, J. C. Claussen, and C. Hauert, Phys. Rev. E **85**, 041901 (2012).
[19] S. Rulands, T. Reichenbach, and E. Frey, J. Stat. Mech. **2011**, L01003 (2011).
[20] T. Reichenbach, M. Mobilia, and E. Frey, J. Theor. Biol **254**, 368 (2008).
[21] J. Knebel, T. Krüger, M. F. Weber, and E. Frey, Phys.

Rev. Lett. **110**, 0168106 (2013), arXiv:1303.7116.
[22] N. Q. Balaban, J. Merrin, R. Chait, L. Kowalik, and S. Leibler, Science (New York, N.Y.) **305**, 1622 (2004).
[23] A. J. Lotka, J. Am. Chem. Soc. **42**, 1595 (1920).
[24] V. Volterra, Mem. Accad. Lincei **2**, 31 (1926).
[25] R. M. May and W. J. Leonard, SIAM J. Appl. Math. **29**, 243 (1975).
[26] For our simulations we chose L large enough such that the correlation length of iidentical genotypes is much larger than a.
[27] This could be generalized to asymmetric competition between phenotypes by taking phenotype dependent competition rates.
[28] T. Reichenbach and E. Frey, Phys. Rev. Lett. **101**, 058102 (2008).
[29] Our simulations show that the three surviving genotypes in the metastable regime contribute with equal probability to the asymptotic states. For the reason of numerical efficiency we therefore computed $P_\infty(\vec{p})$ at times corresponding to the metastable regime.
[30] For symmetry reasons all three of these marginal distributions are identical.
[31] M. Parker and A. Kamenev, arXiv **q-bio.PE** (2009).
[32] S. Rulands, A. Zielinski, and E. Frey, Phys. Rev. E **87**, 052710 (2013), arXiv:1305.0119.

Supplementary Material

In the Supplementary Material we provide calculations and numerical results the arguments presented in the main text.

CONSERVED QUANTITIES IN HETEROGENEOUS LOTKA-VOLTERRA SYSTEMS

Consider a well-mixed population of Lotka-Volterra type. For a mean field description we require that the total number of particles, N, is much larger than the number G of distinct genotypes at $t = 0$, $N \gg G$. We then may define concentrations x_α, $\alpha = 1, \ldots, G$ such that Nx_α gives the number of individuals with a certain genotypes p_α. How are these concentrations affected by the reactions between individuals? The probability for a genotype α to outcompete a genotype β is given by $w_{\alpha\beta} = \vec{p}_\alpha \mathbf{A} \vec{p}_\beta$, where $\mathbf{A}$ is the interaction matrix. This implies a net transition rate per unit time and concentration between two genotypes, $W_{\alpha\beta} = w_{\alpha\beta} - w_{\beta\alpha} = \vec{p}_\alpha^{\mathrm{T}} (\mathbf{A} - \mathbf{A}^{\mathrm{T}}) \tilde{\mathbf{p}}_\beta$. Competition with a genotype β therefore changes the concentration of genotype α by $W_{\alpha\beta} x_\alpha x_\beta$. Including competition with any genotype we arrive at G coupled rate equations,

$$\dot{x}_\alpha = x_\alpha \sum_{\beta=1}^{G} W_{\alpha\beta} x_\beta, \ \alpha = 1, \ldots, G \,. \tag{1}$$

As, by definition, $\mathbf{U} \equiv \mathbf{A} - \mathbf{A}^{\mathrm{T}}$ and thereby $\mathbf{W}$ are skew-symmetric matrices, Eq. (1) conserves the sum over all species concentrations, $\sum_{\alpha=1}^{G} x_\alpha = 1$. We can therefore interpret Eq. (1) as the replicator equation of a conservative Lotka-Volterra system of G competing species. As a result of the conservation of concentrations, $\triangle^G$ is invariant under the dynamics of Eqs. (1).

To study the nonlinear dynamics of Eqs. (1) we are now interested in further quantities which are conserved by the dynamics. In analogy to non heterogeneous Lotka-Volterra models we assume that these conserved quantities are of the form

$$\kappa = \prod_{\alpha=1}^{G} x_\alpha^{c_\alpha} , \qquad \vec{c} \in \mathbb{R}^G \,. \tag{2}$$

We take the derivative with respect to t to obtain the time evolution of κ,

$$\dot{\kappa} = \sum_{\alpha=1}^{G} c_\alpha \frac{\kappa}{x_\alpha} \dot{x_\alpha} = \kappa \sum_{\alpha=1}^{G} \sum_{\beta=1}^{G} c_\alpha x_\beta W_{\alpha\beta} = -\kappa \sum_{\beta=1}^{N} x_\beta \left(\mathbf{W}\vec{c}\right)_\beta \,. \tag{3}$$

Therefore, if κ is a conserved quantity $\vec{c}$ must be in the kernel of $\mathbf{W}$: $\mathbf{W}\vec{c} = 0$. The dimension of the kernel of $\mathbf{W}$ hence gives the number of conserved quantities. Employing the rank-nullity theorem, we obtain

$$\mathrm{rank}(\mathbf{W}) + \dim[\ker(\mathbf{W})] = G \,. \tag{4}$$

Let $\mathbf{\Lambda}$ be the matrix containing all genotypes, $\mathbf{\Lambda} = (\vec{p}_1, \ldots, \vec{p}_G) \in \mathbb{R}^{M \times G}$ with M being the number of distinct phenotypic states. With this definition we can write $\mathbf{W} = \mathbf{\Lambda}^{\mathrm{T}} \mathbf{U} \mathbf{\Lambda}$. In the following, we assume that the number of genotypes is greater or equal the number of phenotypic states, $G \geq M$. $\mathbf{\Lambda}$ has M linearly independent columns, in the language of linear algebra $\mathrm{rank}(\mathbf{\Lambda}) = M$. We infer

$$\mathrm{rank}(\mathbf{W}) \leq \min\{\mathrm{rank}(\mathbf{U}), \mathrm{rank}(\mathbf{\Lambda})\} = \mathrm{rank}(\mathbf{U}) \,, \tag{5}$$

and by substituting Eq. (4)

$$\dim[\ker(\mathbf{W})] \geq G - \mathrm{rank}(\mathbf{U}) \,. \tag{6}$$

Hence, the number of conserved quantities is greater than the number of distinct genotypes minus the rank of $\mathbf{U}$. In other words, the number of the degrees of freedom $G - \dim[\ker(\tilde{\mathbf{W}})]$ is bounded above by the structure of the interaction network determined by $\mathbf{U}$. We infer that adding a new genotype to the population also yields an additional

conserved quantity. Hence, for well-mixed systems the number of degrees of freedom of the heterogeneous model and its homogeneous version are equal.

Conserved quantities are particularly relevant, if the kernel is positive, i.e. $c_\alpha > 0$.

As an example, consider three cyclically competing species. The dimension of the image of $\mathbf{U}$ is two, rank$\mathbf{U} = 2$. We obtain $\dim[\ker(\mathbf{W})] \geq G - 2$, which tells us that the system comprises at least $G - 2$ conserved quantities. Equivalently, the number of degrees of freedom is less or equal 2. Together with particle number conservation this proofs the existence of $G-1$ conserved quantities. As $\mathbf{W}$ is skew-symmetric, the eigenvalues of the Jacobian of Eq. (1) are imaginary [1, 2]. Hence, the conserved quantities correspond to neutrally stable periodic orbits.

The numerical evaluation of Eq. (1) shows that the amplitude of oscillations in the component α scales linearly with the standard deviation of the corresponding net transition rates, $\sqrt{\mathrm{Var}(W_{\alpha\beta})}$. The standard deviation increases with the degree of specialization of the genotype $\vec{p}_\alpha$. The reason for this is discussed further below.

A GEOMETRIC INTERPRETATION OF THE NET TRANSITION RATES

In this section we give a geometric interpretation of the transition rates $W_{\alpha\beta}$, which in spatially structured systems determine the propagation speed of domain borders. In particular, the sign of $W_{\alpha\beta}$ gives the direction of invasion and thereby the net outcome of competition.

The matrix of net transition rates $\mathbf{W}$ is defined as $W_{\alpha\beta} = \vec{p}_\alpha^{\mathrm{T}}(\mathbf{A} - \mathbf{A}^{\mathrm{T}})\vec{p}_\beta$. We hence consider the bilinear form $U(\vec{p}_\alpha, \vec{p_\beta})$ given by the matrix $\mathbf{U} = A - A^{\mathrm{T}}$. U therefore gives the net transition rate as a function of the genotypes $\vec{p}_\alpha$ and $\vec{p}_\beta$. Due to the linearity of U, and as Δ^2 is flat we know that the iso lines of equal values of U are straight lines. One also easily finds that $U(\vec{p}_\alpha, \vec{p_\alpha}) = 0$ and $U((1/3, 1/3, 1/3), \vec{p}_\beta) = 0$ for any genotype $\vec{p}_\beta$. We infer that the iso lines of equal transition rates are parallel to the straight line through the vector $\vec{p}_\alpha$ itself and the center of the simplex Δ^2, $(1/3, 1/3, 1/3)$. We denote this particular line corresponding to vanishing net transition rate by I_α^0 and its parallel lines corresponding values $U = s$ by I_α^s. Figure 1 shows I_α^0 for the three specialist genotypes.

Consider a genotype $\vec{p}_\alpha$ and any iso line I_α^s. As U is linear in its arguments we infer that vectors $\vec{p}_\beta$ left of I_α^s have higher net transition rates then vectors right of I_α^s. Here, we defined the direction as going from $\vec{p}_\alpha$ through $(1/3, 1/3, 1/3)$. The biological interpretation is that genotypes left of I_α^s perform better in competition against $\vec{p}_\alpha$ than genotypes left of this line.

From this geometric interpretation we can follow, that the best response to any genotype $\vec{p}_\alpha \in \triangle^2$ is a genotype on the boundary of $\triangle^2$. The maxima and minima of U are always those points in $\triangle^2$ that have the largest distance from the line I_α^0. If this line is not parallel to one of the borders, the best response against the genotype $\vec{p}_\alpha$ is one of the three specialist genotypes. In conclusion, the best and worst responses to nearly all genotypes are specialists.

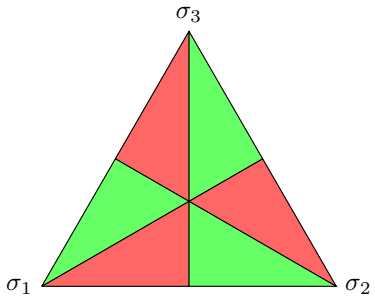

FIG. 1. Geometric interpretation for the net transition rates $W_{\alpha\beta}$. Genotypes correspond the vectors on the two dimensional simplex $\triangle^2$. Genotypes $\vec{p}_\alpha$ in green regions have a positive net transition rate $U(\vec{p}_\alpha, \vec{e}_i)$ for two specialist genotypes $\vec{e}_i$, whereas genotypes in the red regions have negative net transition rates when competing with two specialist genotypes.

We now show how the geometric interpretation for the net transition rates helps understanding the observed transitions in the asymptotic genotypes. The green regions in Fig. 1 are particularly significant. Genotypes in these regions outcompete two specialist genotypes, while genotypes in the red region outcompete only one specialist genotype.

The invasion speed of a boundary between genotypes is proportional to $U(\vec{p}_i, \vec{p}_j)$. A fast invasion speed is the distinguishing mark of succesful genotypes in the regime $D < D_1$ which explains the survival of specialists for whom $U(\vec{p}_\alpha, \cdot)$ is maximal. In the regime in between the fractal like structures of the clusters threatens individuals

which specialized only one pronounced phenotype. Individuals, which are on the one hand specialized to one of the phenotypic states but on the other hand are able to switch their phenotypic state have the advantage that they are able to win on average in more heterogeneous neighborhoods.

FINITE SIZE SCALING OF THE CHARACTERISTIC TIME t_1

The rate of decrease of the number of distinct genotypes in the population gives information about the underlying evolutionary dynamics. We here study the scaling of the characteristic time t_1, which marks the crossover from neutral evolution to selection driven evolution, with the system size.

For the model comprising direct competition (Lotka-Volterra type) we find that the mean value of t_1 scales linearly with the system size, $\langle t_1 \rangle \propto N$. This result suggests that for $t < t_1$ the dynamics is characterized by the escape out of a neutrally stable fixed point. Indeed, for large D, the rate equations (1) comprise neutrally stable, periodic oscillations. This result also pertains to smaller values of D as for small times spatial structures can be neglected. For the model with reactions of May-Leonard type we find that the mean value of t_1 scales logarithmicaly with the system size, $\langle t_1 \rangle \propto \ln(N)$. We infer that the underlying dynamics is characterized by the fluctuation driven escape out of an unstable fixed point. In both models, the absolute value of the heterogeneity scales linearly with N. Employing the scaling behavior we may write the heterogeneity $H(t, N)$ as

$$H_{\mathrm{LV}}(t, N) = N t^{-1} h_{\mathrm{LV}} \left(\frac{t}{N} \right), \tag{7}$$

and

$$H_{\mathrm{ML}}(t, N) = N t^{-1} h_{\mathrm{ML}} \left(\frac{t}{\ln N} \right), \tag{8}$$

where h_{LV} and h_{ML} are universal scaling functions of the heterogeneous Lotka-Volterra and the May-Leonard model, respectively. Figure 2 shows the universal scaling functions and, as the curves overlap lie on top of each other, confirm the measured scaling behavior.

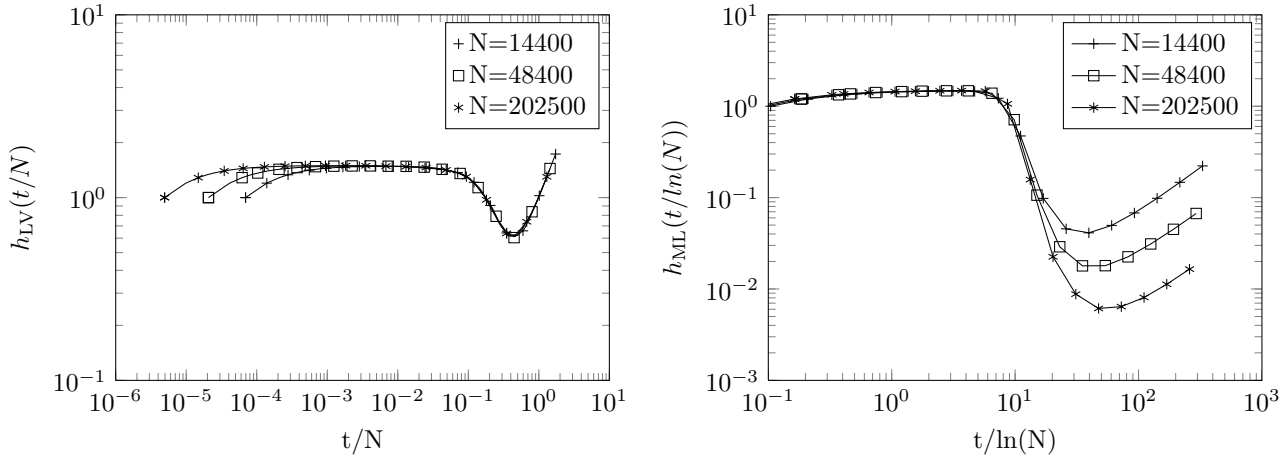

FIG. 2. The universal scaling functions h for the Lotka-Volterra (left) and the May-Leonard model (right). The collapse of the curves for different values of N confirms the scaling of the characteristic time t_1. For the direct competition, as in the Lotka-Volterra model we find $\langle t_1 \rangle \propto N$ (left), whereas for indirect competition, as in the May-Leonard model, the scaling is logarithmic, $\langle t_1 \rangle \propto \ln(N)$. The simulations were performed for well-mixed systems.

[1] R. M. May, *Stability and Complexity in Model Ecosystems* (Princeton University Press, Princeton, 2001).
[2] J. Knebel, T. Krüger, M. F. Weber, and E. Frey, Phys. Rev. Lett. **110**, 0168106 (2013), arXiv:1303.7116.

Heterogeneous motility facilitates the persistence of cooperation

Steffen Rulands, Jörg Martin, and Erwin Frey*
Arnold Sommerfeld Center for Theoretical Physics and Center for NanoScience, Department of Physics, Ludwig-Maximilians-Universität München, Theresienstr. 37, D-80333 München, Germany
(Dated: July 25, 2013)

The presence of cooperation in nature is a fundamental, still unsolved problem in modern biology. We here study the evolution of cooperation in populations exhibiting heterogeneous motility. We show that under these circumstances cooperation can persist under surprisingly harsh conditions. We identify three distinct parameter regimes which are characterized by the possibility for the persistence of cooperation and the average motility dominating at large times.

PACS numbers: 87.23.Kg, 05.40.-a, 64.60.ah, 02.50.Le

Understanding the conditions that facilitate the persistence of cooperation is one of the classic problems in evolutionary biology. The dilemma of cooperation expresses the naive point of view that cooperation should not be robust against "cheating" mutants. However, cooperation is frequently found in biological systems. As an example, the metabolism of *Pseudomonas aeruginosa* relies on the consumption of iron. These bacteria therefore produce an iron-scavenging siderophore which may pass the cell membrane and is therefore available to other bacteria. As siderophore production is metabolically costly the population should in principle be susceptible to the invasion by mutants who do not produce the siderophore [1]. Mathematically, the dilemma of cooperation is often formulated in the framework of evolutionary game theory, where such situations are described in terms of the *prisoner's dilemma* [2–7]. Among other mechanisms such as direct and indirect reciprocity, spatial structures have been identified as a key promoter of cooperation [8–11]. However, even a low mobility has been shown to jeopardize cooperation in spatially extended populations [12].

Recent advances in microbiology have made it possible to investigate the phenotypic status of a population on the level of individual bacteria. It has been found that even clonal populations may be heterogeneous in their phenotypic properties [13]. As an example, many bacterial species are endowed with flagella which may be utilized to sense the cell's environment. Most importantly, flagella are, however, used for locomotion. For *Bacillus subtilis* it has been found that in mid exponential growth phase clonal populations consist of both, swarming cells that are propelled via flagella, and non-motile cells, which after division do not separate from each other, thereby forming long chains of cells [14]. Cells in the motile state do not divide. This bet hedging strategy allows the population to exploit its current location and at the same time disperse to new, possibly more favorable niches. As a result, colonies of *B. subtilis* are heterogeneous with respect to the cells' motilities. The underlying mechanism behind this behavior is a bistable switch: in motile cells the alternative sigma factor σ^D is in the ON state, while for non-motile cells σ^D is in the OFF state. The switching between these states is purely stochastic. The statistical weight of the state, and thereby the fractions of the colony in each of these states, can be biased by the regulatory proteins swrA and swrB [13, 14].

Motivated by these findings we study the influence of heterogeneous motility on the persistence of cooperation. We show that phenotypic heterogeneity significantly enhances the conditions for the persistence of cooperation. Moreover, we identify parameter regimes being characterized by the the possibility of the survival of cooperators or defectors and the average motility in the subpopulations at large times.

Specifically, we study the spatial prisoner's dilemma game where, in contrast to previous work, each individual is endowed with a distinct motility. The stochastic dynamics is described by a Moran process. Consider N individuals on a two-dimensional lattice with $L \times L$ sites. Each site can be occupied by an arbitrary number of individuals, which are either cooperators (C) or defectors (D). Individuals can interact ('play') with other individuals on the same lattice site at a rate r. The profit they gain from such an interaction is encoded in a so-called payoff matrix whose elements give the payoff two individuals earn upon an interaction. If both players are distinct, the defector collects a benefit b, while the cooperator has a cost $0 < c < b$ for providing a public good. A cooperator engaging a cooperator yields a payoff $b - c$ for both, while two defectors collect payoff 0. How well does an individual perform compared to others? The average payoff an individual collects is called accumulated fitness,

$$f_i = f_0 + \frac{1}{n}\sum_{l=1}^{n} p_j^{(l)}, \tag{1}$$

where p_i^l is the payoff that was collected in the l^{th} interaction. Success in interactions translates into a high reproduction rate, which is proportional to f_i. Upon reproduction, individuals replace a randomly chosen individual on the same lattice site. Last, individuals perform random walks with an individual based rate μ_i. For infinitely large lattices the spatial variables can be

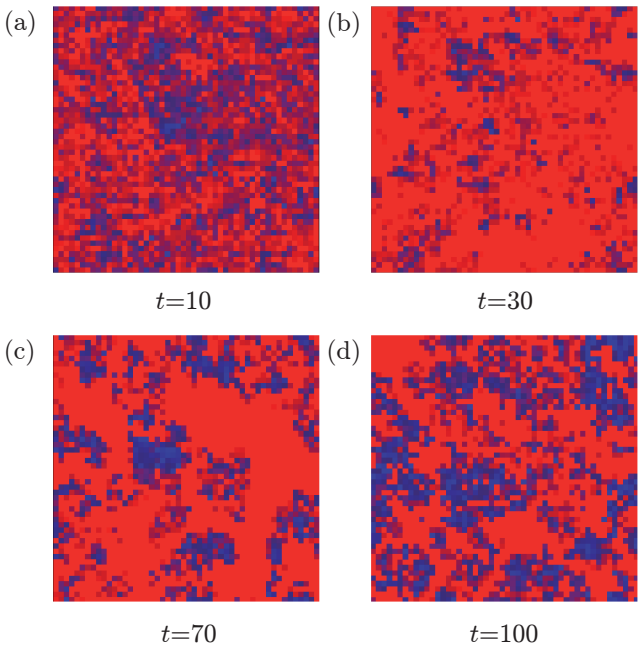

Figure 1. (Color online) Snapshots of a representative run of the stochastic simulation. Color (gray scale) denotes the concentration of cooperators and defectors on each lattice site, such that blue (dark gray) and red (medium gray) denote the predominance of cooperators and defectors, respectively. Initially, cooperators and defectors are randomly distributed. After a short time, defectors seem to take over the system. However, cooperators are able to form clusters and establish the majority of the population for large times. Parameters were $c = 0.16$, $\mu_0 = 1.25$.

regarded continuous. Macroscopically, the hopping processes then effectively lead to diffusion with a diffusion constant $\mu/(2L^2)$. In summary, each individual is characterized by a 'genotype' $\{C, D\} \times \{\mu_1, \mu_2, ...\}$ consisting of its type and the individual based mobility. Upon reproduction, the newly produced individuals inherit these genotypes from their ancestor.

If the number of individuals is large, we may define local concentration densities $c_\mu(\vec{x}, t)$ and $d_\mu(\vec{x}, t)$ of cooperators and defectors with a given mobility μ. Neglecting fluctuations the dynamics is described by partial integro-differential equations of the form,

$$\partial_t c_\mu = \frac{N}{2\mu_0} \int_0^{2\mu_0} K_c(\mu, \mu')\, c_\mu d_{\mu'} + \frac{\mu}{2L^2} \nabla^2 c_\mu \,, \qquad (2a)$$

$$\partial_t d_\mu = \frac{N}{2\mu_0} \int_0^{2\mu_0} K_d(\mu, \mu')\, d_\mu c_{\mu'} + \frac{\mu}{2L^2} \nabla^2 d_\mu \,. \qquad (2b)$$

The interaction kernels $K_c(\mu, \mu')$ and $K_d(\mu, \mu')$ can be expressed by approximating an individual's fitness by the average fitness $\overline{f}$ of all individuals with the same genotype.We obtain $K_c(\mu, \mu') = \overline{f}^c_\mu - \overline{f}^d_{\mu'}$ and $K_d(\mu, \mu') = \overline{f}^d_\mu - \overline{f}^c_{\mu'}$ with $\overline{f}^c_\mu(x, t) = f_0 + bc_\mu - c$ and $\overline{f}^d_\mu(x, t) = f_0 + bc_\mu$. Equations (2) posses infinitely many stable, spatially uniform states corresponding to a system fully occupied by individuals of any genotype. In our stochastic model these states are absorbing states, i.e. they are reached with probability 1 after a finite time. As we will show below, the probability distribution of which of these states is reached asymptotically and the corresponding time scale depend qualitatively on the average mobility μ_0 in the initial condition and the cost for cooperation c.

We performed extensive stochastic simulations employing Gillespie's algorithm with parallel updating. Individuals are located on a two-dimensional square lattice of linear size L with periodic boundary conditions. Each lattice site can host an arbitrary number of individuals. Initially, motility is assigned randomly to each individual according to a uniform distribution on $[0, 2\mu_0]$, where μ_0 is the mean mobility at $t = 0$. For all our simulations we set $b = 1$, $r = 5$, $L = 50$, and $N = 2 \cdot 10^5$. Figure 1 shows typical configurations at four different times. We find that after a short transient clusters of cooperators form. The overall concentration of defectors increases at intermediary times but then decreases again for large times. For this particular realization, the population is asymptotically dominated by cooperators.

To which extend is cooperation possible in heterogeneous populations? The cost c^* up to which cooperation persists is a measure for how robust cooperation is under harsh conditions. To determine the critical cost c^* we numerically computed stochastic trajectories and calculated the overall concentrations of cooperators and defectors at a large time $t = 10^3$. The critical cost was then determined as the minimal value of c for which the population at large times is composed of more than one half of defectors. In Fig. 2(a) the solid line shows c^* depending on the mean, initial mobility μ_0. All combinations of c and μ_0 lying below this line allow for the persistence of cooperation. For low motility the lattice disintegrates into uncoupled, well-mixed patches. In this limit, our model corresponds to earlier studied models for the spatial prisoner's dilemma [12] and we obtain a constant value of c^*. The shaded area denotes parameter values, where cooperation can persist in the prisoner's dilemma with homogeneous motility [12]. Importantly, we find that the critical cost is significantly increased if μ_0 is on the same scale or a larger scale as the reaction rates. In particular, while for homogeneous systems the critical cost decreases with the mobility [12], we find for heterogeneous systems that the critical cost only weakly depends on the mean mobility for large values of μ_0. The critical cost of the homogeneous model also affects the dynamics in the heterogeneous model. The lines for the critical costs in the homogeneous and in the heterogeneous model divide the parameter space into three regions, denoted by I, II, and III. These regions qualitatively differ in the attractors of the global concentrations (i.e. the possibility for the persistence of cooperation), and the

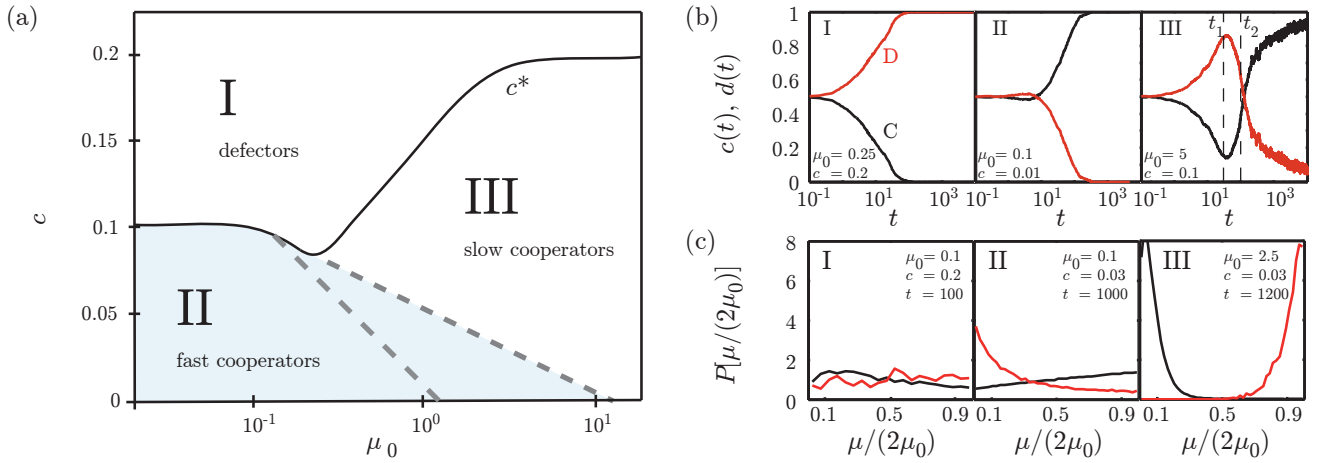

Figure 2. (Color online) (a) The behavior of the heterogeneous, spatial prisoner's dilemma qualitatively changes with the mean initial mobility μ_0 and the cost for cooperation c. The solid line is the critical cost c^* below which cooperation can persist. The shaded area denotes parameter values, for which the homogeneous, spatial prisoner's dilemma allows for the survival of cooperation. We find that cooperation is significantly enhanced if μ_0 is not too small. We identify three parameter regimes determined by the probability for the persistence of cooperation and the selection of optimal values of the motility within the cooperating and defecting subpopulations. While the solid line marks an absorbing state phase transition, the dashed lines denote a crossover behavior. (b) The overall concentrations evolve differently in each of the three regimes. In Regime I, we observe the rapid domination of defectors (red, grey), while in Regime II cooperators (black) rapidly take over the population. In Regime III, defectors dominate the population at small times. At a characteristic time t_1 the fraction of cooperators increases again and the overall concentrations approach algebraically the value 1. (c) To investigate in how far the three regimes influence the selection of genotypes in the subpopulations we computed histograms of the mobilities at times shortly before an absorbing state is reached. In Regime I, the extinction of cooperators happens on a shorter time scale than the evolution of the internal structure of the subpopulations. In Regime II slow defectors and fast cooperators survive, while in Regime III slow cooperators and fast defectors take over the respective subpopulations.

distribution of genotypes that asymptotically dominate the two subpopulations.

In Regime I, the cost for cooperation is high. Ultimately, defectors take over the population. A typical trajectory of the global concentrations is shown in Fig. 2(b), left. During the evolutionary dynamics, selection does not only happen between cooperators and defectors, but also on the genotypes present in each subpopulation. We find that in Regime I slow cooperators are selected, while the selection of defectors happens on much larger time scales as the first passage time into the absorbing state [Fig. 2(c), left]. Regime II corresponds to the persistence of cooperators in the homogeneous model. We find that also in the heterogeneous case cooperators dominate the population at large times [Fig. 2 (b), middle]. Interestingly, in this region fast cooperators and slow defectors dominate the subpopulations at large times [Fig. 2(c), middle]. The reason for this behavior is that slow defectors may form clusters and thereby have a lower chance of being replaced by cooperators - who generally have a higher fitness in this regime. Cooperators, on the other hand, can only take over the entire population by invading these clusters and outperforming the defectors. Regime III denotes parameter values, where cooperation is possible in the heterogeneous model, but not in the homogeneous model. We here find an initial decrease in the total concentration of cooperators. However, after a characteristic time t_1, the subpopulation of cooperators grows again and asymptotically dominates the overall population [cf. Fig. 1 and Fig. 2(b), right]. Asymptotically, the cooperators have a high probability to be slow, while defectors tend to be fast [Fig. 2(c), right]. The dynamics on the critical line $c^*(\mu_0)$ is characterized by the long term coexistence of cooperators and defectors. In particular, we find oscillations in the total concentrations $\overline{c}(t)$ and $\overline{d}(t)$, with exponentially decreasing frequency. While the critical line c^* marks a continuous phase transition [12], the boundary between Regime I and II (dashed lines) is a crossover.

Regime III is of special interest, as it defines parameter values, where the persistence of cooperation is facilitated by heterogeneous motility. In the following, we scrutinize the spatio-temporal dynamics leading to the persistence of cooperators in Region III. Figures 1 and 2(c), right, demonstrate that, as in the homogeneous prisoner's dilemma, defectors at small times outgrow cooperators. Interestingly, after a characteristic time t_1, the overall concentration of cooperators then increases again. Figure 3(a) shows that this behavior involves the decrease of the average motility $\langle\mu\rangle$ of cooperators. Slow cooperators

may form tight clusters, which allow them to play with a higher probability against other cooperators rather than defectors. Their average payoff therefore increases, which leads to an increase in the average fitness of the overall cooperator population as is shown in Fig. 3(b). As a result, cooperators have an increased average growth rate and constitute an increasingly large fraction of the overall population. Finally, after the time t_2, as a reaction to the formation of clusters of cooperators, a selection pressure on defectors begins to act. Fast defectors, may invade these clusters and they benefit from interactions with cooperators. As a result, the average motility of defectors increases and so does their average fitness. However, overall cooperators benefit more from heterogeneous motility than defectors. For fast moving individuals the possible gain in fitness is limited. No further increase in fitness can be achieved when the length scale associated with the diffusion coefficient becomes much larger than the correlation length of cooperators.

Our model comprises a genetically diverse population. Genealogical processes, i.e. the dynamics of lineages in the population, therefore become important. At each time t we define $h(t)$ to be the number of distinct genotypes that can be found in the population divided by the population size N. In other words, at the time t the population is descended from $Nh(t)$ of common ancestors. $h(t)$ therefore is a measure of the degree of diversity in the population. In the following, we are interested in the genetic diversity $h_{c,t}$ within each the two subpopulations consisting of cooperators and defectors, such that, for example, $Nc(t)h_c(t)$ is the number of common ancestors of cooperators. As there is no mechanism for creating new genotypes, genetic diversity decreases monotonically. The rate of decrease, however, gives information about the characteristics of the underlying evolutionary dynamics. Specifically, a decrease according to a power law $h_{c,d}(t) \propto t^{-1}$ indicates neutral evolution, as the process is aptly described by a neutral coalescence process, $AA \to A$. Since spatial structures can be neglected it is sufficient to consider the high density regime where the density of particles A decreases according to a power law t^{-1} [15]. As opposed to this, a faster decrease of diversity is observed for processes, where particles coalesce at different rates. In the language of biology, this would mean the evolution is driven selective advantage. Figure 3 (c) shows $h_{c,d}(t)$ for two values of the cost c. If the cost is high, we observe that for $t_1 < t < t_2$ evolution is neutral for defectors, while cooperators are subject to evolutionary pressure. At large times, $t > t_2$, cooperators have formed tight clusters, such that the loss of genetic diversity of cooperators decelerates, whereas selection plays an increasingly important role for defectors. If the cost is low, evolution is neutral for cooperators, while defectors are subject to selection.

Interestingly, we observe a trapping of defectors in cooperator clusters. As a consequence, cooperators tend to

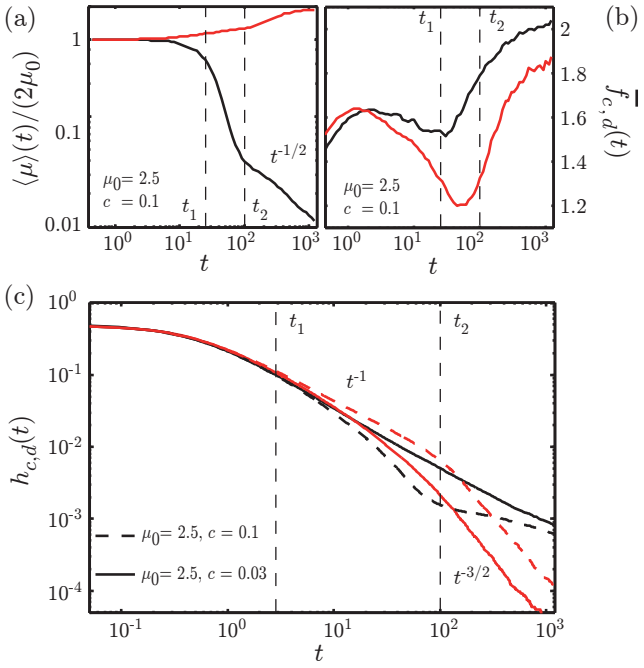

Figure 3. (Color online) (a) To understand the survival of cooperators in Regime III, we computed the average normalized mobility $\langle\mu\rangle/(2\mu_0)$ of cooperators (black) and defectors (red, gray) as a function of time. At a characteristic time $t_1 \approx 25$ the mean mobility of cooperators decreases rapidly. At a second time $t_2 \approx 100$ this decrease follows a power law, $\langle\mu\rangle \propto t^{-1/2}$, while the average mobility of defectors increases. (b) The average fitness $\overline{f}_{c,d}$ of cooperators and defectors indicates the potential of the subpopulations to grow. As a result of the decrease of their average mobility cooperators may form tight clusters and they predominantly play with other cooperators. As a result, their fitness increases. In response, the average mobility of defectors increases, such they can invade clusters of cooperators ($c = 0.1$, $\mu_0 = 2.5$, $b = 1$). (c) The rate of the loss of genetic diversity in the two subpopulations, $h_{c,t}(t)$, gives information about the underlying evolutionary dynamics. If $h_{c,t}(t) \propto t^{-1}$ evolution is neutral, which is the case for cooperators if the cost is low and for defectors if the cost is high. A faster decay indicates that a population is subject to evolutionary forces, such as cooperators for high costs and defectors for low costs.

form piles in the 'vertical' direction. Statistical evidence is given in the Supplemental Material. The reason for this 'honeypot effect' is that once cooperators form tight clusters, their fitness is, in average, higher than the average fitness of defectors. The latter can only gain payoff when playing with cooperators. When fast defectors enter clusters of cooperators and die they are with a high probability replaced by cooperators with a small mobility, who then stay in the cluster.

In conclusion, we showed that heterogeneous motility significantly enhances cooperation in the spatial prisoner's dilemma. The asymptotic composition of the population qualitatively depends on the average initial motil-

ity and the cost for cooperation. In particular, we identified three regimes which differ by the probability for the survival of cooperation and the average motility of cooperators and defectors at large times. Importantly, cooperation is significantly enhanced for a broad range of parameters. Our findings contribute to the understanding of the persistence of cooperation in biological systems.

This research was supported by the German Excellence Initiative via the program 'Nanosystems Initiative Munich' and the German Research Foundation via the SFB 1032 "Nanoagents for Spatiotemporal Control of Molecular and Cellular Reactions". We thank David Jahn for fruitful discussions.

* frey@lmu.de

[1] A. Buckling, F. Harrison, M. Vos, M. A. Brockhurst, A. Gardner, S. A. West, and A. Griffin, FEMS Microbiol. Ecol. **62**, 135 (2007).
[2] J. Hofbauer and K. Sigmund, Cambridge UP (1998).
[3] C. Hauert, F. Michor, M. A. Nowak, and M. Doebeli, J. Theor. Biol. **239**, 195 (2006).
[4] M. A. Nowak, Science **314**, 1560 (2006).
[5] J. Cremer, T. Reichenbach, and E. Frey, New J. Phys. **11**, 093029 (2009).
[6] A. J. Bladon, T. Galla, and A. J. McKane, Phys. Rev. E **81**, 66122 (2010).
[7] M. A. Nowak, J. Theor. Biol. **299**, 1 (2012).
[8] M. A. Nowak and R. M. May, Nature **359**, 826 (1992).
[9] G. Szabó and C. Tőke, Phys. Rev. E **58**, 69 (1998).
[10] G. Szabó and C. Hauert, Phys. Rev. Lett. **89**, 118101 (2002).
[11] G. Szabó, J. Vukov, and A. Szolnoki, Phys. Rev. E **72**, 047107 (2005).
[12] A. Gelimson, J. Cremer, and E. Frey, Phys. Rev. E **87**, 042711 (2013).
[13] D. Dubnau and R. Losick, Mol. Microbiol. **61**, 564 (2006).
[14] D. B. Kearns and R. Losick, Genes Dev. **19**, 3083 (2005).
[15] H. Hinrichsen, Adv. Phys. **49**, 815 (2000).

Range expansion of heterogeneous populations

Matthias Reiter, Steffen Rulands, and Erwin Frey*
Arnold Sommerfeld Center and Center of NanoScience, Department of Physics, Ludwig-Maximilians-Universität München, Theresienstr. 37, D-80333 München, Germany
(Dated: July 21, 2013)

We study range expansion of populations exhibiting phenotypic heterogeneity in motility and growth rates. We observe the formation of homogeneous sectors and we show that at different temporal regimes in the range expansion process different combinations of motility and reproduction are favored by the evolutionary dynamics. We determine the asymptotic composition of the population and reveal that this composition is intriguingly influenced by fluctuations.

PACS numbers: 87.17.Pq, 87.18.Tt, 02.50.Ey, 05.45.-a

Waves propagating into an unstable state are an ubiquitous phenomenon in nature. They describe, for example, the spreading of advantageous genes [1] or infectous diseases [2]. Recently, they have attracted considerable attention as a model for the range expansion of bacterial populations [3–5]. A key observation were gene segregation phenomena in populations subject to neutral random mutations [3–6]. This genetic drift appears to affect the diversity of the population [4]. Recent advances in microbiology have made it possible to investigate the phenotypic status of a population on the level of individual bacteria. It has been found that even clonal populations may be heterogeneous in their phenotypic properties [7]. As an example, many bacterial species are endowed with flagella which may be utilized to sense the cell's environment. Most importantly, flagella are, however, used for locomotion. For *Bacillus subtilis* it has been found that in mid exponential growth phase clonal populations consist of both, swarming cells that are propelled via flagella, and non-motile cells, which after division do not separate from each other, thereby forming long chains of cells [8]. Cells in the motile state do not divide. This bet hedging strategy allows the population to exploit its current location and at the same time disperse to new, possibly more favorable niches. As a result, colonies of *Bacillus subtilis* are heterogeneous with respect to the cells' motilities. The underlying mechanism behind this behavior is a bistable switch: in motile cells the alternative sigma factor σ^D is in the ON state, while for non-motile cells σ^D is in the OFF state. The switching between these states is purely stochastic. The statistical weight of the state, and thereby the fractions of the colony in each of these states, can be biased by the regulatory protein swrA and swrB [7, 8].

Motivated by these findings we here study a generic model for the expansion of heterogeneous populations. In particular, our model comprises particles which are endowed with distinct mobilities. These particles may reproduce upon consumption of limited resources. As in *B. subtilis*, motility and reproduction are complimentary skills. We observe the formation of homogeneous sectors and we show that at stages of the range expansion process different combinations of motility and reproduction are favored by the evolutionary dynamics. We determine the asymptotic composition of the population and reveal that this composition is intriguingly influenced by stochasticity.

Specifically, we study a spatially extended population, where each individual A is endowed with a distinct genotype, which encodes rates to migrate and reproduce. In particular, an individual i may reproduce with a rate μ_i upon consumption of resources B, in chemical notation $A_iB \xrightarrow{\mu_i} A_iA_i$. Upon reproduction, an individual's genotype is inherited to its offspring. In addition, individuals perform random walks with a rate ϵ_i. Motivated by the behavior of bacterial populations we assume that migration and reproduction are complementary skills. In particular, we set the characteristic time for individuals to react or migrate equal for all individuals, $1/(\epsilon_i+\mu_i) = 1$. This choice fixes the time scale in our model. We here consider a stochastic lattice gas model in one and two dimensions, where site can be occupied by an arbitrary number of individuals. While reproduction happens locally, i.e. the descendant is placed on the same lattice site, migration is implemented as a hopping process on neighboring sites.

The total number of particles A and B is conserved by the reaction. Therefore, with Ω being the mean number of particles per site, we may define a concentration density $a_\epsilon(\mathbf{r},t)$ and a concentration $b(\mathbf{r},t)$ by $N_A^\epsilon(\mathbf{r},t) \equiv \Omega a_\epsilon(\mathbf{r},t)$ and $N_B(\mathbf{r},t) \equiv \Omega b(\mathbf{r},t)$. Here, N_A^ϵ and N_B are the local number of particles of types A with mobility ϵ, or B, respectively. $\mathbf{r}$ denotes the position on a d-dimensional lattice. We assume that the mean field particle number Ω is large, and, in particular, much larger than the number of genotypes G. We also suppose that initially the population is genetically diverse, i.e. we consider the situation $\Omega \gg G \gg 1$. The spatio-temporal dynamics is then described by two cou-

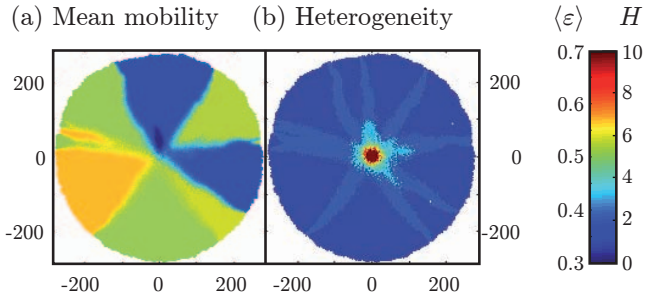

Figure 1. (Color online) (a) Typical configuration of a stochastic simulation for a circularly expanding population ($t = 490$). Color (gray scale) denotes the local average mobility $\langle\epsilon\rangle$, such that blue (dark gray) signifies a low mobility, yellow (light gray) a medium mobility and red (medium gray) a high mobility. We observe the formation of homogeneous sectors. (b) The same situation, but plotted is the local genetic heterogeneity, such that blue sites are homogeneous and red sites are heterogeneous. We find that genetic diversity is rapidly lost during the expansion process. The population remains diverse at the origin and at sector boundaries. Simulations were run on a hexagonal lattice with $L^2 = 500^2$, $\Omega = 100$, and $t = 490$.

pled integro difference-differential equations

$$\partial_t a_\epsilon(\mathbf{r},t) = \frac{\epsilon}{2d\delta^2}\Delta a_\epsilon(\mathbf{r},t) + (1-\epsilon)a_\epsilon(\mathbf{r},t)b(\mathbf{r},t) \quad \text{(1a)}$$

$$\partial_t b(\mathbf{r},t) = -b(\mathbf{r},t)\int_0^1 (1-\epsilon)a_\epsilon(\mathbf{r},t)\,\mathrm{d}\epsilon\,, \quad \text{(1b)}$$

where d is the spatial dimension, δ is the lattice constant and Δ is the lattice Laplacian. These equations comprise a stationary, spatially homogeneous state a^- given by $a(\mathbf{r},t) \equiv \int_0^1 a_\epsilon(\mathbf{r},t)\,\mathrm{d}\epsilon = 0$ and $b(\mathbf{r},t) = 1$ for all $\mathbf{r}$. A linear stability analysis reveals that the state a^- is locally unstable: small perturbations grow exponentially. This growth is limited by the availability of resources $b(\mathbf{r},t)$. In particular, it saturates when the total concentration reaches a level a^+ corresponding to concentrations $a(\mathbf{r},t) = 1$, $b(\mathbf{r},t) = 0$. Equations (1) therefore also comprise stable fixed points describing situations, where the system is locally fully occupied by individuals A. From the classical theory of front propagation we conclude that small perturbations in the homogeneous state a^- grow exponentially and asymptotically ensue solutions corresponding to traveling wave fronts in the total concentrations $a(\mathbf{r},t)$. Such front solutions are a unifying property of equations belonging to the FKPP class [9]. Our stochastic simulations indeed show propagating waves solutions. The spatio-temporal dynamics is, however, much more complex than in the case of homogeneous range expansion.

We performed extensive simulations of the stochastic lattice gas model and Eqs. (1). For our stochastic simulations, we implemented Gillespie's algorithm with sequential updating on square and hexagonal lattices. For the numerical solution of Eqs. (1) an ordinary Euler finite difference scheme was used. Initially, a small area in the origin is populated by individuals of type A while the rest of the system is occupied by resources B. The mobilities in the initial population are randomly drawn from a uniform distribution on $]0,1[$.

Figure 1(a) shows a typical configuration of the stochastic model in two spatial dimensions. We observe the expansion of a circular front out of the center. After a short time homogeneous sectors form. Our simulations show that for intermediate times genetic diversity is lost in the front region. However, a variety of genotypes manage to survive "surfing" on the tip of the front. For large times, genetic diversity is only maintained in the homeland and the front is dominated by multiple homogeneous sectors. As opposed to this behavior, in one spatial dimension, the selection process is irreversible since the two directions of propagation are strictly separated. While gene surfers manage to survive on intermediate time scales, each spatial direction is dominated by one genotype for large times.

The loss of genetic diversity in colonization processes has been observed in a variety of biological contexts, such as the human expansion out of Africa or bacterial invasion processes [3, 10–12]. While the overall number of distinct genotypes is constant, the relative fractions of different genotypes in the population changes during the expansion process. The rate at which genetic diversity is lost during expansion gives information about the underlying dynamic processes. Specifically relevant is the genetic diversity in the front region, as these individuals constitute the gene pool for the further expansion process [4]. We define the front as those points, where the concentration b of resources exceeds a value of $1/2$. In polar coordinates, this yields a parametrization $r(\varphi)$ of the front, giving its distance from the origin as a function of the angle φ. We computed the temporal evolution of the average number $H_f(t)$ of distinct genotypes in a region $r(\varphi) \pm \Delta$, where Δ is proportional to the typical length scale of the front, $\Delta \propto \sqrt{\langle\epsilon\rangle/[2d\delta^2(1-\langle\epsilon\rangle)]}$. Figure 2(a) shows $H_f(t)$ for the two-dimensional system. We identify two temporal regimes, which are characterized by different kinds of selection pressure acting on the individuals. After a short transient, for $10 \lesssim t \lesssim 100$, the decrease of diversity in the front region follows a power law, $H_f(t) \propto t^{-\alpha}$ with $\alpha \approx 1.4$. Hence, genetic diversity is lost faster then one would expect for neutral evolution. In this case, the theory of neutral coalescence processes predicts an exponent -1 [13]. We conjecture that in this regime the coalescence process is biased, meaning that some genotypes in the front region have a higher probability to go extinct than others. For even larger times, the genetic diversity in the front corresponds to the number of homogeneous sectors and genotypes in the front region are lost by the annihilation of sector boundaries. As a result, H_f decreases at a lower rate.

This behavior leaves two questions: First, what is the asymptotic composition of the population? Second, which dynamic processes characterize these temporal regimes?

To investigate which genotypes are selected by the expansion process we calculated the genetic composition of the population at large times, i.e. the probability that an individual has mobility ϵ and a reproduction rate $\mu = 1 - \epsilon$, [Fig. 1(c)]. We find that successful genotypes migrate and reproduce with approximately equal probability. "Specialists", who either reproduce or migrate at a high rate do not successfully colonize. The average mobility is, however, slightly shifted towards a higher reproduction rate, $\langle\epsilon\rangle \approx 0.46$ for $d = 1$ and $\langle\epsilon\rangle \approx 0.44$ for $d = 2$. While these values are characteristic for the behavior at large times, we will show that they do not necessarily represent the asymptotic composition of the population.

We now scrutinize the evolutionary dynamics of the expanding population and determine the asymptotic composition of the population. We then demonstrate the intriguing influence of intrinsic noise. To understand the role of evolutionary forces in the population we computed the temporal evolution of the mean mobility $\langle\epsilon\rangle$ in the population, both from stochastic simulations and from the numerical solution of Eqs. (1), cf. Supplementary Material. Figure 2(c) shows that the mean mobility decreases at small times and then increases again. At large times $\langle\epsilon\rangle$ takes a stationary value depending on the lattice spacing δ and the mean particle number Ω, cf. Fig. 3(a) and (b).

For small times $t \lesssim 15$, $\langle\epsilon\rangle$ decreases rapidly. Hence, there is a selective advantage for individuals with a high reproduction rate. To understand this, note that for small times the population dynamics is governed by a competition for resources [14]. In order to dominate the front, a potentially successful genotype must initially be capable of efficiently outgrowing its competitors by consumption of the majority of resources at the tip of the front. This necessity gives precedence to higher reproduction rates in this first regime, where H_f remains large and concentrations remain relatively small. Consequently genotypes with faster growth rate are advantageous and $\langle\epsilon\rangle$ decreases and reaches a minimum. This effect occurs independently of the spatial dimension and even in the deterministic limit, as direct numerical simulations of Eqs. (1) using an ordinary Euler finite difference scheme reveal. The minimum is always existent, even though its position and depth depend on the initial configuration.

In an intermediary regime $15 \lesssim t \lesssim 100$ macroscopic differences in the concentrations have formed and a propagating front in the overall concentration a has been established. To gain access to resources, it is essential to balance reproduction with diffusion. This is reflected in an increasing average mobility in the population, cf.

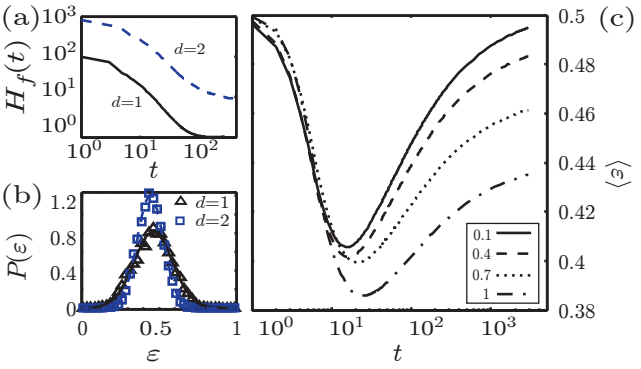

Figure 2. (a) Decrease of genetic diversity $H_f(t)$ in the front region for one and two spatial dimensions. After a short transient genetic diversity decreases rapidly. For $d = 1$ it reaches an asymptotic value, $H_f(t) = 1$. For $d = 2$ the decrease of H_f slows down for large times, which can be attributed to the formation of homogeneous sectors. (b) Probability to find a certain mobility at a large time $t = 220$. We find that the populations is dominated by individuals with an approximately equal probability to migrate or reproduce. The bias towards a lower mobility is a stochastic effect as is discussed in the text. The histograms were averaged over 10^3 sample runs with $\Omega = 100$. (c) To investigate which genotypes are selected by the evolutionary dynamics at specific times we numerically solved Eqs. (1) for various values of δ and computed the average mobility $\langle\epsilon\rangle$ in the population. We find that for small times, $t \lesssim 15$, $\langle\epsilon\rangle$ decreases. For larger times, it increases again until it approaches a stationary value. This value decreases with increasing values of the lattice spacing δ.

Fig. 2(c). In the following, we will argue that this behavior can be understood by considering the spreading velocities of uncoupled Fisher waves. Equations (1) show that different genotypes are coupled only indirectly via the availability of resources b. The velocity of a front is determined by its leading edge, where $b \approx 1$ [9]. Following the theory of front propagation [9, 15], we assume that traveling wave solutions $a_\epsilon(r,t) = a_\epsilon(r - vt) = a_\epsilon(z)$ decay continuously and exponentially at the leading edge of the front, $a_\epsilon(z) \sim \exp(-\gamma z)$ for $z \to \infty$. We also assume that at the leading edge $b \approx 1 - a$. Substituting the exponential ansatz into Eqs. (1) we may employ a saddle point approximation to the integrals and the equations for different values of ϵ uncouple. Keeping only the highest order exponential terms, we obtain a dispersion relation $v(\gamma) = \gamma^{-1}\{\epsilon/d\,[\cosh(\delta\gamma) - 1] + 1 - \epsilon\}$. The theory of front propagation into unstable states predicts that for sufficiently steep initial conditions the front solution with minimal velocity $v(\gamma_0)$ is selected [9, 16]. For a radially expanding front in two spatial dimensions, $v(\gamma_0)$ is approached asymptotically for $r \to \infty$ [17]. We find that a homogeneous subpopulation with mobility

$$\epsilon^* = \left[\sqrt{2/(d\delta^2) + 1}\,\operatorname{arccosh}\left(1 + d\delta^2\right)\right]^{-1} \qquad (2)$$

has the highest invasion speed. For $\delta \to 0$, ϵ^* converges to 1/2. For the stochastic lattice gas model $\delta = 1$ was used and hence $\epsilon^* \approx 0.438$ for $d = 1$ and $\epsilon^* \approx 0.401$ for $d = 2$. As the growth rate of a subpopulation is proportional to its invasion speed, the fastest propagating subpopulation will take an increasingly large fraction of the colony. The mean mobility therefore increases in the intermediary regime. Figure 3(a) shows ϵ^* for $d = 1$ and $d = 2$ and various values of δ. We find that the optimal mobility decreases with an increasing lattice spacing.

For large times, $t \gtrsim 100$, the deterministic behavior differs qualitatively in one and two spatial dimensions. For $d = 1$, the selection process is irreversible, as the spatial directions are strictly separated and the front fixates, as apparent from Fig. 2(a). As opposed to this, for $d = 2$, homogeneous sectors have formed and the loss of genetic diversity in the front region is governed by the merging of neighboring sector boundaries. The movement of the sector boundaries is influenced by deterministic and stochastic forces. We will first investigate the former and then ask which of both forces dominates boundary movement.

To study the deterministic movement of sector boundaries we consider two adjacent sectors of a circular front. The trajectory of the boundary is described by its angle $\varphi(r)$ and without loss of generality we assume that initially $\varphi(r_0) = 0$ and $r_0 = 1$. The sectors propagate at constant velocities v_1 and $v_2 > v_1$. Neglecting fluctuations the angle φ satisfies the differential equation [18]

$$r\varphi'(r) = -\sqrt{v_2^2/v_1^2 - 1}\,, \tag{3}$$

which is solved by $\varphi(r) = -\sqrt{v_2^2/v_1^2 - 1}\ln(r)$. Hence, the sector boundary moves logarithmically into the direction of the slower domain. For a front consisting of multiple sectors we conjecture that the population is ultimately dominated by the genotype with the fastest velocity. This genotype is given by Eq. (2). Specifically, we obtain $\langle\epsilon\rangle \to 1/2$ for $\Omega \to \infty$ and $\delta \to 0$ and we infer that asymptotically $H_f = 1$. This argument is supported by Fig. 3(a), which compares the mean genotype $\langle\epsilon\rangle$ to the genotype ϵ^* with the fastest homogeneous front velocity at large times for various values of δ. These two quantities only differ by a constant, which can be attributed to the fact that ϵ^* is an asymptotic quantity while $\langle\epsilon\rangle$ was measured at a finite simulation time.

Each biological system consists of a finite number of individuals and is therefore subject to stochastic fluctuations. The stochastic motion of domain boundaries is strongly influenced by the roughness of the front [19]. We measured the roughness $w(t) = \sqrt{\langle[r(x,t) - \langle r(x,t)\rangle_x]^2\rangle_x}$ in stochastic simulations of the sector boundaries of a planar, homogeneous front [20]. The roughness increases according to a power law, $w(t) \propto t^\beta$. For large times we obtain $\beta \approx 0.34$ which confirms

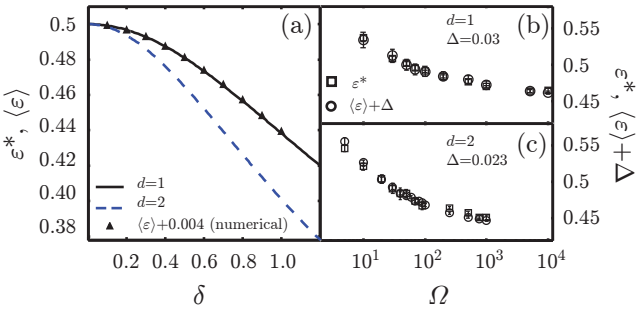

Figure 3. (a) The solid (dashed) line illustrates the analytical result for the genotype ϵ^* with the optimal front velocity in one (two) spatial dimensions, [Eq. (2)]. Triangles indicate the average genotype $\langle\epsilon\rangle$ obtained from the numerical solution of Eqs. (1), evaluated at a large time $t = 3000$ for $d = 1$. We added a constant value to $\langle\epsilon\rangle$ to account for the finite simulation time. We find an excellent agreement of the ϵ^* and $\langle\epsilon\rangle$ and conjecture that the asymptotic genotype is determined by the velocity of the corresponding homogeneous fronts. (b) and (c) To investigate the dependence of the asymptotic composition of the population on the strength of reaction noise, we computed $\langle\epsilon\rangle$ and ϵ^* via stochastic simulations. We find that both values decrease with Ω and they only differ by a value independent of δ. Hence, also for finite populations the asymptotic genotype is determined by the velocity of homogeneous fronts ($\delta = 1$). However, in $d = 1$ the shift Δ saturates at a finite value as the initial decrease of $\langle\epsilon\rangle$ is not fully reversible.

that the homogeneous sectors belong to the KPZ universality class [19, 21]. As a result, the stochastic movement of domain boundaries is super-diffusive, i.e. its rooted mean square displacement increases according to t^α. For a sector boundary in a planar front we measured $\alpha \approx 0.63$. Hence, the mean fluctuation driven displacement of the sector boundary scales with r^α, while the displacement due to different front velocities scales with $r \ln r$. As $r^\alpha/(r \ln r) \to 0$ for $r \to \infty$ we find that for large times these tangential fluctuations of domain boundaries become negligible in comparison to their deterministic drift given by Eq. (3).

Our stochastic model comprises two sources of noise. First, fluctuations due to reactions between particles are proportional to $\Omega^{-1/2}$. Second, a finite lattice constant δ represents an imperfect spatial continuum limit, resulting in fluctuations from the Brownian motion of individuals which scale proportional to $\delta^{1/2}$. Surprisingly, we find that both types of noise have contrasting influence on the genotype with the maximal velocity of a homogeneous front and the genotype ultimately dominating the population.

The effect of reaction noise on propagating fronts has been subject to extensive studies [15, 22–26]. To study the effect of reaction noise on the evolutionary dynamics we performed stochastic simulations for different values of the system size Ω. We find that noise stemming from

the stochastic nature of reproduction significantly influences the dynamics at large times. In particular, the asymptotic value of $\langle\epsilon\rangle$ and the genotype ϵ^* with the highest velocity of homogeneous fronts both descrease with Ω. In fact, $\langle\epsilon\rangle$ and ϵ^* differ only by a small constant, which can be attributed to the fact that $\langle\epsilon\rangle$ was measured at a finite time. This observation underscores our argument that $\langle\epsilon\rangle$ is mainly determined by ϵ^*.

In conclusion, we studied the range expansion of heterogeneous populations in one and two spatial dimensions. For the latter case we observed a radial spreading process and the formation of homogeneous sectors. Different genotypes are favored at different stages of the spreading process, which ultimately leads to a loss of genetic diversity in the front region. We determined the asymptotic composition of the population and showed that this composition is significantly influenced by stochastic fluctuations.

This research was supported by the German Excellence Initiative via the program 'Nanosystems Initiative Munich' and the German Research Foundation via contract FR 850/9-1. We thank Madeleine Leisner and David Jahn for fruitful discussions.

* frey@lmu.de

[1] R. A. Fisher, Ann. Eugen. **7**, 355 (1937).
[2] D. Mollison, J. Roy. Stat. Soc. B , 283 (1977).
[3] O. Hallatschek, P. Hersen, S. Ramanathan, and D. R. Nelson, Proc. Natl. Acad. Sci. USA **104**, 19926 (2007).
[4] O. Hallatschek and D. R. Nelson, Theor. Popul. Biol. **73**, 158 (2008).
[5] K. Korolev, M. Avlund, O. Hallatschek, and D. R. Nelson, Rev. Mod. Phys. **82**, 1691 (2010).
[6] O. Hallatschek and D. R. Nelson, Evolution **64**, 193 (2010).
[7] D. Dubnau and R. Losick, Mol. Microbiol. **61**, 564 (2006).
[8] D. B. Kearns and R. Losick, Genes Dev. **19**, 3083 (2005).
[9] W. van Saarloos, Phys. Rep. **386**, 29 (2003).
[10] S. Ramachandran, O. Deshpande, C. C. Roseman, N. A. Rosenberg, M. W. Feldman, and L. L. Cavalli-Sforza, Proc. Natl. Acad. Sci. USA **102**, 15942 (2005).
[11] G. Neve, A. Pavlicko, and M. Konvicka, Eur. J. Entomol. **106**, 11 (2009).
[12] B. M. Henn, L. Cavalli-Sforza, and M. W. Feldman, Proc. Natl. Acad. Sci. USA **109**, 17758 (2012).
[13] H. Hinrichsen, Adv. Phys. **49**, 815 (2000).
[14] .
[15] E. Brunet and B. Derrida, Phys. Rev. E **56**, 2597 (1997).
[16] M. Bramson, *Convergence of solutions of the Kolmogorov equation to travelling waves* (American Mathematical Society, 1983).
[17] J. D. Murray, Interdiscipl. Appl. Math. **17** (2002).
[18] K. S. Korolev, M. J. Müller, N. Karahan, A. W. Murray, O. Hallatschek, and D. R. Nelson, Phys. Biol. **9**, 026008 (2012).
[19] A. Ali and S. Grosskinsky, Adv. Complex Syst. **13**, 349 (2010).
[20] We considered a planar front to circumvent distortion of the results due to different velocitie sof homogeneous sectors in the heterogeneous model and lattice artifacts in radial range expansion.
[21] A.-L. Barabási and H. E. Stanley, *Fractal concepts in surface growth* (Cambridge university press, 1995).
[22] D. Panja, Phys. Rep. **393**, 87 (2004).
[23] E. Brunet, B. Derrida, A. Mueller, and S. Munier, Phys. Rev. E **73**, 056126 (2006).
[24] O. Hallatschek and K. Korolev, Phys. Rev. Lett. **103**, 108103 (2009).
[25] O. Hallatschek, PLoS Comput. Biol. **7**, e1002005 (2011).
[26] O. Hallatschek, Proc. Natl. Acad. Sci. USA **108**, 1783 (2011).

Supplementary Material

We here provide additional material and calculations supporting the arguments provided in the main text.

OPTIMAL VELOCITY FOR $\Omega \to \infty$

In this section we provide the mathematical steps to obtain the mobility ϵ^* for which a homogeneous front attains the highest velocity. In the thermodynamic limit $\Omega \to \infty$ our model is described by the equations

$$\partial_t a_\epsilon(\vec{r},t) = \frac{\epsilon}{2d\delta^2}\Delta a_\epsilon(\vec{r},t) + (1-\epsilon)a_\epsilon(\vec{r},t)b(\vec{r},t) \tag{1a}$$

$$\partial_t b(\vec{r},t) = -b(\vec{r},t)\int_0^1 (1-\epsilon)a_\epsilon(\vec{r},t)\,\mathrm{d}\epsilon\,, \tag{1b}$$

where $d \in \{1,2\}$ denotes the spatial dimension and Δ is the discrete laplacian for a lattice spacing δ, i.e.

$$\Delta a_\epsilon(x,t) = a_\epsilon(x-\delta,t) + a_\epsilon(x+\delta,t) - 2a_\epsilon(x,t), \qquad d=1 \tag{2a}$$

$$\Delta a_\epsilon(r,t) = a_\epsilon(r-\delta,t) + a_\epsilon(r+\delta,t) - 2a_\epsilon(r,t) + \frac{\delta}{r}\left[a_\epsilon(r-\delta,t) - a_\epsilon(r+\delta,t)\right], \qquad d=2. \tag{2b}$$

For $d=2$ we consider a rotationally symmetric population $a_\epsilon(\vec{r},t) = a_\epsilon(r,t)$, with $r = |\vec{r}|$. According to the theory of fronts propagating into unstable states the front's velocity is determined by the leading edge of the fronts, where concentrations are low. We make the traveling wave ansatz $a_\epsilon(r,t) = a_\epsilon(z)$, with $z = r - vt$. It is natural to assume an exponentially decaying front profile in this region, $a_\epsilon(z) \sim \exp(-\gamma z)$. At the leading edge of the front $b \approx 1 - \int_0^1 a_\epsilon(\vec{r},t)\,\mathrm{d}\epsilon$. Employing a saddle point approximation we obtain $b \approx 1 - a^*_\epsilon(z)$, where ϵ^* denotes the genotype with the least steep decay of the front.

Using this approximation in Eq. (1) yields

$$\partial_t a_\epsilon(\vec{r},t) \approx \frac{\epsilon}{2d\delta^2}\Delta a_\epsilon(\vec{r},t) + (1-\epsilon)a_\epsilon(\vec{r},t)\left(1 - a_{\epsilon^*}(\vec{r},t)\right). \tag{3}$$

Neglecting second order terms in the concentrations we obtain the linear dynamics in the region corresponding to the tip of the front,

$$\partial_t a_\epsilon(\vec{r},t) \approx \frac{\epsilon}{2d\delta^2}\Delta a_\epsilon(\vec{r},t) + (1-\epsilon)a_\epsilon(\vec{r},t). \tag{4}$$

The essential point here is that in the tip of the front the dynamics for the different genotypes uncouple. With the exponential profile $a_\epsilon(z) \sim \exp(-\gamma z) = \exp(\gamma(vt-r))$ we obtain:

$$\gamma v\,\mathrm{e}^{\gamma(\mathrm{r}-\mathrm{vt})} \approx \left[\frac{\epsilon}{2d\delta^2}\left(\mathrm{e}^{-\gamma\delta} + \mathrm{e}^{\gamma\delta} - 2\right) + (1-\epsilon)\right]\mathrm{e}^{\gamma(\mathrm{r}-\mathrm{vt})}, \qquad d=1 \tag{5a}$$

$$\gamma v\,\mathrm{e}^{\gamma(\mathrm{r}-\mathrm{vt})} \approx \left[\frac{\epsilon}{2d\delta^2}\left(\mathrm{e}^{-\gamma\delta} + \mathrm{e}^{\gamma\delta} - 2\right) + \frac{\delta}{r}\left(\mathrm{e}^{-\gamma\delta} + \mathrm{e}^{\gamma\delta}\right) + (1-\epsilon)\right]\mathrm{e}^{\gamma(\mathrm{r}-\mathrm{vt})}, \qquad d=2. \tag{5b}$$

In the limit of large radius the terms proportional to r^{-1} vanish in the laplacian for $d=2$ and therefore both equations become identical and independent of r after canceling the first order exponential terms. Solving for v one obtains the dispersion relation

$$v(\gamma,\epsilon) = \gamma^{-1}\left\{\frac{\epsilon}{d}\left[\cosh(\delta\gamma) - 1\right] + 1 - \epsilon\right\}. \tag{6}$$

For fixed ϵ the selected front solution has minimal velocity [1, 2] and therefore obeys $\frac{\partial}{\partial_\gamma} v(\gamma,\epsilon) = 0$. This condition relates ϵ and γ in the form

$$\epsilon(\gamma) = \frac{\delta}{\delta\gamma + \left[1 + d\delta^2 - \cosh(\delta\gamma)\right]\sinh^{-1}(\delta\gamma)}. \tag{7}$$

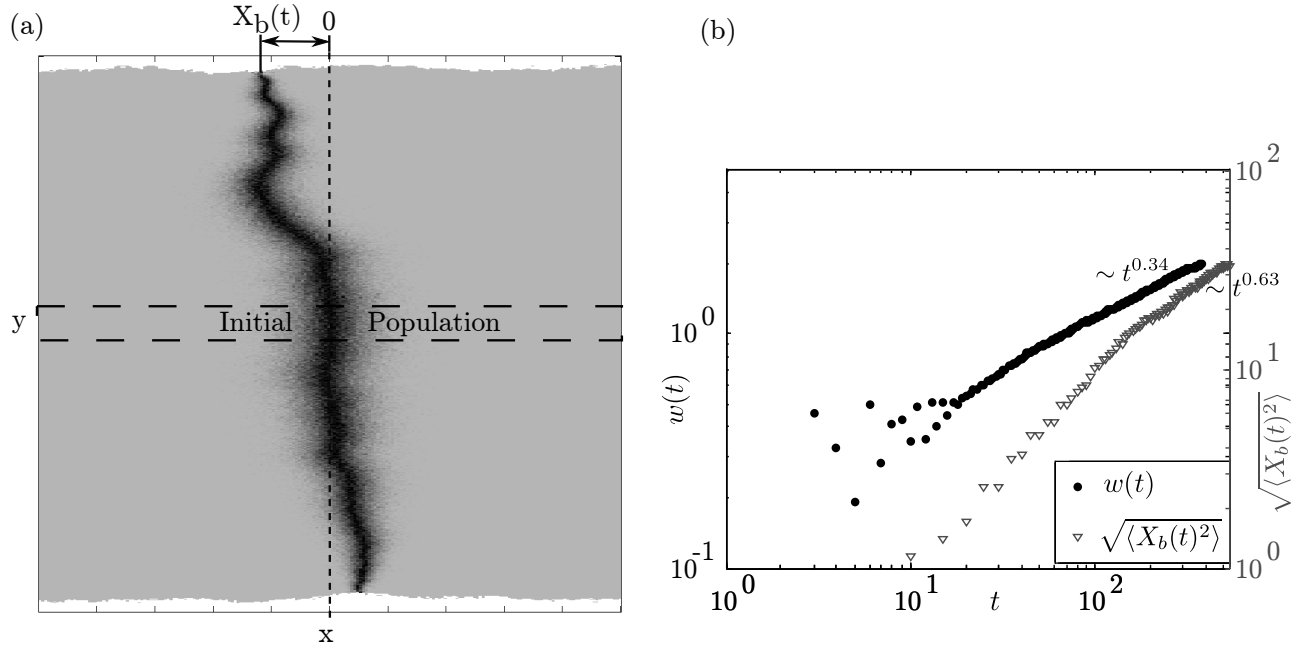

FIG. 1. (a) Configuration of a stochastic planar front propagating in positive and negative y direction at $t = 580$. The size of the initial population is indicated by the dashed rectangle. The population initially consists of two equally sized sectors of evolutionary neutral genotypes with mobility $\epsilon = 1/2$. Colors represent the absolute deviation of the concentration of a_B from $1/2$, i.e. $|a_B - 1/2|$. The definition of the lateral boundary position $X_b(t)$ is indicated in the figure. Paramters of the simulation were $\delta = 1$, $\Omega = 100$. (b) Rooted mean square displacement of the boundary position X_b averaged over 100 simulations. Moreover the growth of the roughness $w(t)$ in a planar, homogeneous front, averaged over 500 simulations, is given. For large times both graphs follow a power law. We find $\sqrt{\langle x_b^2(t)\rangle} \sim t^\alpha$, with $\alpha \approx 0.63$ and $w(t) \sim t^\beta$, with $\beta \approx 0.34$.

The mobility which maximizes the selected front velocity is therefore given by $\epsilon^* = \epsilon(\gamma^*)$, with γ^* defined by $\frac{\mathrm{d}}{\mathrm{d}\gamma} v(\gamma, \epsilon(\gamma))\Big|_{\gamma^*} = 0$. Performing these steps gives the result

$$\epsilon^* = \left[\sqrt{\frac{2}{(d\delta^2)} + 1}\,\operatorname{arccosh}\left(1 + d\delta^2\right)\right]^{-1}, \tag{8}$$

$$v^* = v(\gamma^*, \epsilon^*) = \delta \log^{-1}\left[1 + d\delta^2 + \delta\sqrt{d\,(2 + d\delta^2)}\right]. \tag{9}$$

Due to the mentioned approximations this result is valid in for $d = 1$ and in two spatial dimensions for $r \to \infty$.

FRONT ROUGHNESS AND STOCHASTIC MOVEMENT OF SECTOR BOUNDARIES

As explained in the main text, the stochastic properties of the lateral movement of sector boundaries determine its influence on the asymptotic configuration and the decrease of heterogeneity. We measured the statistics of the lateral position $X_b(t)$ of a sector boundary separating two neutral genotypes, i.e. with identical mobility and reproduction rate. The measurement was done in a linearly expanding front in 2 spatial dimensions, as shown in Fig. 1(a). Due to neutrality of the two populations $\langle X_b(t)\rangle = 0$ in an ensemble average $\langle\cdot\rangle$. For the rooted mean square displacement of the boundary position we obtain the curve in Fig. 1(b). For large times the best fit yields $\sqrt{\langle x_b^2(t)\rangle} \sim t^\alpha$, with $\alpha \approx 0.63$. Since $\alpha > 0.5$ our result indicates that the meandering tangential to the front is superdiffusive. This coincides with the observations in [3], even though the measured growth exponent is slightly different. According to [3], this superdiffusive behaviour may be attributed to the roughness of the front.

The roughness is defined as $w(t) = \sqrt{\langle [r(\varphi,t) - \langle r(\varphi,t)\rangle_\varphi]^2\rangle_\varphi}$ for a radially expanding front parametrized by the polar angle φ and $w(t) = \sqrt{\langle [y(x,t) - \langle y(x,t)\rangle_x]^2\rangle_x}$ for a planar front parametrized by the x-coordinate as shown in

Fig. 1(a), respectively. Following Ref. [4] the roughness is expected to grow according to a power law, $w(t) \sim t^{\beta}$. We measured the growth law as shown in Fig. 1(b) for a planar, homogeneous front. Measurement in a planar, homogenenous front ensures that the result is neither distorted by lattice artifacts nor by large scale structures from multiple sectors propagating at distinct velocities. From a fit for $t \geq 100$ we obtain $\beta \approx 0.34$, confirming that homogeneous fronts of Fisher type belong to the KPZ universality class with respect to the statistical properties of the front. The KPZ class predicts $\beta = 1/3$ [4]

[1] M. Bramson, *Convergence of solutions of the Kolmogorov equation to travelling waves* (American Mathematical Society, Providence, 1983).
[2] W. van Saarloos, Phys. Rep. **386**, 29 (2003).
[3] A. Ali and S. Grosskinsky, Adv. Complex Syst. **13**, 349 (2010).
[4] A.-L. Barabási and H. E. Stanley, *Fractal concepts in surface growth* (Cambridge university press, Cambridge, 1995).

Part II

Stability of localized wave fronts in bistable Systems

4 Stability of localized wave fronts in bistable Systems

Bistable systems are ubiquitous in nature. For example, genetic switches are bistable systems that store the activation state of a gene [1, 140]. On the other hand, in population dynamics, a minimum population size is often needed to establish a stable population. In this case one says that the population is subject to a strong Allee effect [141]. The spatial versions of such systems admit traveling wave solutions, describing for example the outbreak of viruses or the colonization of territory [142–144]. If bistable systems are subject to external spatial gradients, traveling waves may localize in restricted spatial domains [145–147]. An important example arises in early embryogenesis of *Drosophila melanogaster* where maternal morphogen gradients provide positional information for gene regulation [3, 5, 6, 12]. The morphogen Bicoid is present as a monotonically decreasing concentration in the embryo and controls the step-like activation of the gene Hunchback, which also enhances its own activation, thereby effectively producing a bistable system. The exact position of the Hunchback front is pivotal to the embryo's fate [12]. Hence, the front's stability to extrinsic perturbations or internal noise is paramount. Wave localization and the stability of the front also play an important role in other contexts. In ecology, birth rates may have spatial dependence, for example due to spatial variance in temperature or resource availability [148, 149]. The localized boundaries between species are subject to large fluctuations due to the low number of individuals in the boundary region. This may eventually lead to the extinction of one of the species due to demographic stochasticity [150]. Last, in bio-technological applications, this mechanism might be used to create localized fronts of proteins [151].

Motivated by these processes, we investigate a broad class of bistable diffusion-reaction models with reaction terms comprising self-activation, external activation, and degradation. While self-activation and degradation are assumed to be spatially uniform, the external activation is taken to be position-dependent. We consider two qualitatively different types of external gradients and determine the parameter range for which wave localization is possible. Moreover, we ask how stable these localized fronts are with respect to extrinsic and intrinsic noise, and we determine optimality conditions minimizing the front's susceptibility to such perturbations.

In this chapter, we will first give an introduction to bistable systems and their spatially extended versions. In Section 4.3 we introduce a paradigmatic class of bistable models and show that under certain circumstances it admits the localization of trigger waves. We then investigate the robustness of this mechanism and the susceptibility of the localized wave to extrinsic and intrinsic perturbations (Section 4.4).

4.1 Bistability in nature

Bistability is one of the most fundamental concepts in nature. A system is said to be bistable if it can rest in either of two stable states. Small perturbations to such states result in an exponentially fast relaxation process back into these states [152].

One of the most fundamental examples of bistability is a toggle switch. In nature, switches arise in gene regulatory networks, where they store the activation state of a gene [1, 140]. As a prominent example, the mode of growth of bacteriophage λ in an *E.coli* host is determined by a bistable regulatory system. [1]. In the prophage state a repressor protein is synthesized, which activates its own synthesis and turns off the synthesis of the Cro protein. In a second state, the lytic state, the bacteriphage produces the Cro protein which deactivates the repressor protein. In this state, viral DNA replicates in the *E.coli* bacterium and, by producing bacteriophage particles, eventually kills it. In ecology, bistability may arise if the rate of reproduction is small below a certain population size, increases above this threshold value and saturates for large populations. Then, a critical populations size must be exceeded in order to establish a stable population. This behavior is often referred to as the *strong Allee effect* [141, 142, 144, 145, 153].

Biological systems are often highly complex, involving a multitude of different interacting species and time scales. However, two key requirements have been identified as a requirement for a system to exhibit bistability [76, 80, 154]: first, particles should amplify the production of particles of the same type, which is known as positive feedback. Second, the system needs to display nonlinear kinetics. In gene regulatory networks, such nonlinearities can arise as the result of multimerization, cooperative binding to target sequences on the DNA, or phosphorylation of certain amino acid residues [80] and it manifests itself as a sharp increase in transcription rates when a certain threshold concentration is reached.

Mathematically, bistable systems are studied in the framework of the theory of dynamic systems and their temporal evolution is described by nonlinear differential equations for the concentrations,

$$\dot{\mathbf{u}} = \mathbf{f}(\mathbf{u})\,. \tag{4.1}$$

Here, $\mathbf{f}(\mathbf{u})$ is a nonlinear function determining concentration dependent reaction rates. Equations 4.1 describe a multistable system, if the potential $\mathbf{V}(\mathbf{u}) \equiv \int \mathbf{f}(\mathbf{u})\mathrm{d}\mathbf{a}$ has local minima separated by potential wells.

4.2 Spatially extended bistable systems admit traveling waves solutions

In many biological applications, individuals or particles are endowed with mobility. As it has been shown in the first part of this thesis, the spatial arrangement of

particles is paramount for many biological systems. The simplest form of mobility is Brownian motion, which leads to diffusion on a macroscopic scale. The connection between mobility and diffusion is a prominent application of the fluctuation-dissipation theorem and it is best known in the form of the Einstein-Smoluchowski relation,

$$D = k_B T \mu, \tag{4.2}$$

linking the diffusion constant D and the mobility μ.

4.2.1 The Turing instability

The combined effects of nonlinear reactions and diffusion have gathered much interest in the context of pattern forming systems. Such systems have successfully been employed to understand a broad variety of developmental processes, cf. Fig. 4.1. In his visionary work, Alan Turing investigated the stability of the simplest possible reaction-diffusion system which is capable of forming a pattern from a uniform state [100].

1. First, at least two interacting species are needed for the formation of spatial patterns.

2. While diffusion is naively thought of as a process smoothing out differences in the concentration of reacting species, Turing showed that it can actually lead to the destabilization of uniform states and thereby to the occurrence of patterns.

3. This diffusion-induced instability can cause the formation of structures of a particular wavelength. The significance of this result is that it provides a mechanism for producing a variety of regular patterns, ranging from the segmentation patterns in the fruit fly to the periodic arrangement of tentacles around the mouth of the Hydra organism, or zebra stripes [35].

4. Last, pattern formation requires the separation of the length scales corresponding to the mobile species. In other words, the respective diffusion constants must differ substantially.

Turing's model comprises two species, an activator A and an inhibitor B. The activator and the inhibitor are, due to diffusion, linked to length scales l_A and l_B. Turing assumes that the activator diffuses much more slowly than the inhibitor, $l_A \ll l_B$. Furthermore, the activator A is auto-catalytic and also enhances the production of the inhibitor B. On the other hand, the inhibitor represses the activation of A. These reaction locally yield a linear stable state. How does the system react to a small spatial perturbation? Due to the different length scales associated with the activator and the inhibitor, the latter will spread out of the region of the perturbation, yielding to a relatively higher concentration of the activator as compared to

the inhibitor. As a result, the repressive effect of the inhibitor on the production of the activator is decreased, resulting in a growing concentration of the activator. At some concentration the concentration of the activator saturates as a result of nonlinearities in the reactions. As opposed to this, in the outer region there is a relative surplus of inhibitors, i.e. the concentration of activators is decreased as compared to the inhibitor. In conclusion, short-range activation in combination with long range inhibition yields the growing of instabilities to stable spatial patterns. The locally stable state looses its stability due to diffusive transport.

4.2.2 Bistable excitable media

While in Turing's simple model the locally stable state looses its stability due to diffusive transport, we are here interested in how pattern formation is possible if the stable state is globally stable to small perturbations. Such systems are commonly called *excitable media* and they arise in a variety of fundamental problems in biology, chemistry, physiology and medicine [35]. As we will see, excitable media may admit the propagation of waves. These waves are paramount for some of the most fundamental processes in living organisms [35]: Excitable electrical waves are used by some single cell organisms such as *Paramecium* to control the mechanical rotation of their cilia, allowing them to adjust their swimming motions. Such excitable electrical waves also prevent multiple sperm cells from merging with an egg. When a first sperm has entered the egg an excitable wave triggers a rapid change in the egg's membrane preventing other sperms from entering. In the nervous system of multi-cellular organisms excitable electrical waves enable the reliable transport of information over large distances. The Hodgkin-Huxley model of action potentials is the most widely used model for transmission of information between neurons. FitzHugh and Nagumo introduced a reduced version of the Hodgkin-Huxley model which has become a paradigmatic model for excitable media [35],

$$\partial_t u = f(u,v) + D\Delta u\,, \tag{4.3}$$

$$\partial_t v = g(u,v)\,, \tag{4.4}$$

with reaction rates $f(u,v) = \eta^{-1}(3u - u^3 - v)$ and $g(u,v) = u - a - bv$. Finally, on an even larger scale, invasion processes of species subject to a strong Allee effect can be understood in terms of excitable dynamics [142, 144, 145, 153].

For large particle numbers, the dynamics of spatially extended system of reacting and diffusing particles is aptly described by partial differential equations of the form

$$\partial_t \mathbf{u}(\mathbf{x},t) = \mathbf{f}(\mathbf{u}(\mathbf{x},t)) + \underline{\underline{D}}\Delta\mathbf{u}(\mathbf{x},t)\,. \tag{4.5}$$

Here, the first term on the right hand side accounts for concentration changes due to reactions. The second term is the diffusion term, punishing spatial fluctuations in the field u. The diagonal matrix $\underline{\underline{D}}$ contains the diffusion constants of the respective

species. Such reaction-diffusion systems have recently gathered much interest as prototype models for pattern forming systems. There, the combined effect of nonlinear reactions and diffusion allows for the stable establishment of spatial patterns. The most prominent example certainly is Turing's model [100].

What can we infer about the solutions of Eq. (4.5) if the reaction term is bistable? For the sake of simplicity we now consider a single species in one spatial dimension. In dimensionless form we may write the correponding reaction diffusion equation as $\partial_t u(x,t) = f(u(x,t)) + D\Delta u(x,t)$. If the potential $V(u) = \int f(u)\mathrm{d}u$ has two local maxima at concentrations u^- and u^+ seperated by a minima, i.e. the reaction term is bistable, solutions are stationary profiles moving with a constant velocity c,

$$u(x,t) = \phi(\xi),\ \xi = x - ct\,, \tag{4.6}$$

with $\phi(\xi \pm \infty) = u^{\pm}$. The shape $\phi(\xi)$ of the front profile can be obtained by solving the stationary differential equation, $\partial_{xx}\phi + \partial_\phi V(\phi) = 0$. Such solutions are called *traveling wave solutions* and they allow us to formulate Eq. (4.5) in terms of an ordinary differential equation, namely

$$\phi'' + c\phi' + \partial_\phi V(\phi) = 0\,. \tag{4.7}$$

Here, the prime denotes derivatives with respect to ξ. Equation (4.7) can be interpreted in terms of an analogous mechanical problem: it may be interpreted as a force balance equation for a particle (sliding ball) with mass 1, friction c and potential $V(\phi)$. The boundary conditions are determined by the asymptotic values $u^{\pm}$ of the front profile, i.e. the ball starts at one maximum and ends at the other maximum. To determine the front's velocity we have to solve the Eigenvalue problem defined by Eq. (4.7). In the language of the sliding ball analogy, this problem can be formulated as follows: for which friction c does the ball, when starting at the maximum u^+ at high concentrations, stop exactly at the maximum u^- at low concentrations? If the friction is positive, solutions are traveling waves propagating in the positive x direction. On the other hand, if the friction is negative, the front propagates into the negative x direction.

To derive and expression for the front's velocity we multiply Eq. (4.7) with ϕ' and integrate over ξ. We obtain

$$\int_{-\infty}^{\infty} f(\phi)\frac{\mathrm{d}\phi}{\mathrm{d}\xi}\mathrm{d}\xi + \int_{-\infty}^{\infty} \phi''\phi'\mathrm{d}\xi + c\int_{-\infty}^{\infty}(\phi')^2\mathrm{d}\xi = 0\,. \tag{4.8}$$

From the asymptotic values of the front solution, $\phi(\pm\infty) = u^{\pm}$ we find that the first term on the left hand side equals $-\int_{u^-}^{u^+} f(\phi)\mathrm{d}\phi \equiv -\Delta V$. The second integral on the left hand side vanishes, as one may see by employing the substitution law. We obtain an expression for the front's velocity,

$$c = \frac{\Delta V}{\int_{-\infty}^{\infty}(\phi')^2\mathrm{d}\xi}\,. \tag{4.9}$$

(a)  (b) 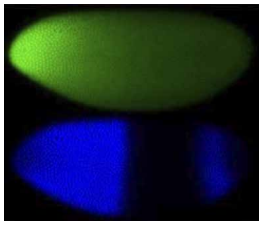 (c) 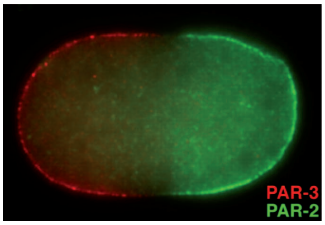

Figure 4.1: Examples for spatial patterns in nature. (a) The stripe like patterns in the angelfish *Pomacanthus semicirculatus* have been proposed as a biological manifestation of the Turing mechanism [155]. The picture has been taken from [16]. (b) An embryo of *Drosophila melanogaster* in mid-nuclear cleavage cycle 11A. The concentrations of Bicoid (green) and Hunchback (blue) have been made visible by immunostaining. The picture shows that from a smooth gradient of the maternal morphogen Bicoid a sharp boundary in the concentration of Hunchback is created. The picture has been taken from Ref. [12]. (c) Polarization in the *C. elegans* cygote. The proteins PAR-2 (green) and PAR-3 (red) localize at separate anterior and posterior domains. Anterior is to the left. The picture has been taken from Ref. [156].

Therefore, two factors determine the speed of the propagating wave front: the difference in potential between the stable states gives the direction of propagation and the absolute value of the velocity. If ΔV is positive, the front propagates into the positive x-direction and vice versa for negative values of ΔV. The denominator can be thought of as a measure for the maximum steepness of the front. We infer that steep fronts move slower than shallow fronts.

4.3 Localization of wave fronts

We will now show that if bistable systems are subject to external spatial gradients, traveling waves may localize in restricted spatial domains [145–147].

4.3.1 Morphogenesis in *Drosophila melanogaster*

During the development of an embryo cells differentiate into a variety of distinct cell types, such as nerve cells, phosphoreceptor cells of the retina in the eye, or muscle cells. How form and patterns emerge from a homogeneous cluster of cells has already fascinated Aristotle in the fourth century B.C.. He described the multiple forms of morphogenesis in birds, plants and cephalopods, already noting that an animal's egg contained the "potential" for its later differentiation. In 1969, Lewis Wolpert was the first to propose that asymmetric concentrations of a chemical signal (morphogens) provide positional information for the developmental system [157]. The positional

signal serves as an input to the gene regulatory system allowing the cell or nucleus to differentiate accordingly.

An important example arises in the early embryogenesis of *Drosophila melanogaster* where maternal morphogen gradients provide positional information for downstream gene regulatory processes [3, 5, 6, 12]. The morphogen Bicoid is translated from RNA which is located at the anterior end of the egg. The combined effect of this source, degradation and diffusion leads to an exponentially decreasing concentration of Bicoid. This gradient defines an anterior-posterior axis, thereby providing positional information to processes determining cell differentiation.

The first gene activated by Bicoid is called Hunchback, which is expressed at the anterior end of the embryo. Importantly, it exhibits a sharp on-off boundary changing from its largest to its lowest concentration in only one tenth of the egg's length along the anterior-posterior axis [Fig. 4.1(b)]. Experimental studies have shown that the production of Hunchback is governed by cooperative self-activation and cooperative activation by Bicoid [9, 10, 12, 14]. As Hunchback again serves as a positional signal for downstream developmental processes, such as the formation of the gap genes giant, krüppel and knirps, the exact position of the Hunchback front is pivotal to the embryo's fate [12]. Hence, the boundary's stability to extrinsic perturbations or internal noise is paramount.

Spatially inhomogeneous activation is also relevant in other contexts. In ecology, birth rates may have spatial dependence, *e.g.* due to spatial variance in temperature or resource availability [148, 149]. In cell biology, bistability and spatially inhomogenous activation has been proposed as a mechanism responsible for the polarization of cells [146, 147, 158].

4.3.2 A paradigmatic class of bistable models

Motivated by these processes, we investigate a broad class of bistable diffusion-reaction models with reaction terms comprising self-activation, external activation, and degradation. While self-activation and degradation are assumed to be spatially uniform, the external activation is taken to be position-dependent.

In the tradition of theoretical science it is not our goal to give a quantitative description of a specific biological system. Indeed, the details of gene regulatory networks in embryogenesis are not fully understood, even today. A quantitative analysis of a model comprising many parameters is therefore not always the best strategy. One might argue that the amount of insight one gains from a theoretical description decreases with the complexity of the model and it vanishes at a point, where one ends in a purely statistical fitting of experimental data. Although this approach has its raison d'être and it is increasingly becoming popular, we here follow the philosophy of Turing who opened his seminal paper on morphogenesis with the following words [100]:

> *"In this section a mathematical model of the growing embryo will be described. This model will be a simplification and an idealization, and consequently a falsification. It is to be hoped that the features retained for discussion are those of greatest importance in the present state of knowledge."*

In this spirit, we here study the simplest model allowing for the stable establishment of a sharp boundary. In the context of embryogenesis it can be thought of as a coarse grained biochemical network, which despite being simple comprises essential characteristics of the more complex networks found in biology. Specifically, we consider a one-dimensional system where diffusing particles are subject to three types of reactions: First, there are gain processes with a concentration-dependent rate that accounts for self-activation in gene regulatory systems or reproduction in population dynamics. Typically, these rates are small for low concentrations, then rise and finally saturate at high concentrations. In populations dynamics, this behavior is referred to as the strong Allee effect [141, 144]. In gene regulation, it can be due to cooperative transcription factor binding to a gene promoter. A common choice for the overall reaction rate is $k_r R^n_{a_0}(a)$ with the Hill function $R^n_{a_0}(a) \equiv a^n/(a_0^n + a^n)$, k_r the maximum intrinsic production rate, and a the particle concentration. The Hill coefficient n measures the degree of cooperative binding in the promoter region, or, in ecology, the strength of an Allee effect. Second, we account for loss processes, where particles vanish with a certain rate λ. Third, in addition to self-activation, there may also be external sources for particle production. Here, we are interested in systems where this source is position-dependent and characterized by the overall rate $k_M M(x)$. The prefactor k_M denotes the maximum rate of external activation, and $M(x)$ is a monotonically decreasing positive density profile with normalization $M(0) = 1$. In the simplest case, where the profile results from a source-degradation dynamics [7, 159], it is exponential $M(x) = e^{-x/\xi}$ with the decay length ξ, cf. Fig. 4.2 (a). Prominent examples are the concentration profile of Bicoid in *Drosophila* [7] and temperature or nutrient gradients in population dynamics [153]. Since the production of Hunchback by Bicoid is mediated by cooperative binding, the profile $M(x)$ entering the overall production rate is commonly described by $M(x) \sim R^m_{I_0}(e^{-x/\xi})$ [10]. The exponentially decaying signal induced by maternal source-degradation dynamics serves as an input to the gene regulation system. The latter is described by a Hill coefficient m typically in the range from 1 to 5, and an activation threshold I_0. The model is summarized in Fig. 4.2(a).

In the limit of a large system size, fluctuations are of minor importance and the spatio-temporal dynamics is then aptly described by a reaction-diffusion equation, which in dimensionless form reads

$$\partial_t u = f(u, x) + \partial_{xx} u \,. \tag{4.10}$$

Here $f(u, x) \equiv r R^n_{u_0}(u) + M(x) - u$ comprises self-activation, external activation and degradation. Concentration u, time t, and space x are measured in units of k_M/λ,

$1/\lambda$ and $\sqrt{D/\lambda}$, respectively. The ratio $r \equiv k_r/k_M$ denotes the relative amplitude of self-activation and external activation mediated through $M(x)$.

4.3.3 Sliding ball analogy for inhomogeneous systems

Traveling wave solutions of Eq. (4.5) may be localized due to the combined effect of spatially varying external sources and bistability [145–147]. The basic mechanism can be best understood in terms of the well-known sliding ball analogy [35], which here is complicated by the fact that the reaction term is space-dependent. Since in most biological situations a steep profile in u is induced by a smooth external profile $M(x)$, we may assume a separation of length scales $\xi \gg \sqrt{D/\lambda}$ and ξ much smaller than the system size. Then one can make a generalized traveling wave ansatz $U = U(x - q(t), y)$, where x is a fast varying variable describing changes in the concentration profile, $y = x/\xi$ is a slowly varying variable describing changes in the external profile $M(x)$, and $q(t)$ denotes the front position. Substituting the generalized traveling wave ansatz into Eq. 4.10 we obtain to leading order in the inverse length of the external gradient,

$$-\dot{q}\partial_x U = \partial_{xx} U + \partial_U V(U, y) + \mathcal{O}(\xi^{-1})\,. \tag{4.11}$$

This differential equation may be interpreted as a force balance for a particle (sliding ball) with mass 1, friction $\dot{q}$ and potential $V(u, y) = \int^u f(\tilde{u}, y)\mathrm{d}\tilde{u}$. Importantly, the potential parametrically depends on y, see Fig. 4.2(b). For parameter regimes where V has two maxima at $u^+(x)$ and $u^-(x)$, and a local minimum at $u^s(x)$, the velocity $\dot{q}$ must be chosen such that the sliding ball starting from the upper branch u^+ ends up at the lower branch u^-. The front speed is proportional to the difference between the two maxima of $V(u, y)$ and becomes zero if the Maxwell condition $\Delta V(y) \equiv \int_{u^-}^{u^+} f(u, y)\mathrm{d}u = 0$ is satisfied. More quantitatively, in analogy to the homogeneous case [13, 35, 160], one finds

$$\dot{q} \approx \frac{\Delta V(q)}{\int_{-\infty}^{\infty} [\partial_x U(x - q, y)]^2 \mathrm{d}x} \equiv c(q)\,, \tag{4.12}$$

where $U(x-q, y)$ is the traveling wave solution. The denominator roughly equals the maximum steepness of the front profile, and implies that steep fronts move slower [35]. One may also arrive at this equation employing a variational ansatz called Whitham principle [13, 160].

In our class of models, a single branch of stable solutions at high concentrations typically undergoes a fold bifurcation for growing x, where the system is bistable on a confined spatial interval, see Fig. 4.2 (d). For large x, a single branch at low concentrations remains. Within the bistable regime, the velocity $c(q)$ may change sign and thereby lead to a localization of the traveling wave front.

4.3.4 Derivation of the localization position

Where does a propagating front in an inhomogeneous, strictly monotonic medium localize? Equation (4.10) admits traveling waves solutions if the potential $V(u,x) = \int^u \mathrm{d}\tilde{u}\, f(\tilde{u},x)$ exists locally. In our case we obtain

$$V(u,x) = -u\left[\frac{u}{2} - M(x) - r + F\left(\frac{u^n}{u_0^n}\right)\right], \tag{4.13}$$

where $F(z) \equiv {}_2F_1(1,1/n,1+1/n,-z)$ and ${}_2F_1$ is the Gauss hypergeometric function. The wave localizes if the difference in the maximum values of the potential is zero, $\Delta V(q_0) \equiv \int_{u_-}^{u^+} \mathrm{d}u\, f(u,q_0) = 0$. Using the linearized stable states $u^+(x) \approx M(x) + r$ and $u^-(x) \approx M(x)$ gives an expression for the difference between the two maximum values of the potential,

$$\begin{aligned}\Delta V(q) &= V(u^+(q)) - V(u^-(q)) &\text{(4.14a)}\\ &= \frac{1}{2}r\left[r + 2M(q)F\left(\frac{M(q)^n}{u_0^n}\right) - 2\Big(M(q)+r\Big)F\left(\frac{(M(q)+r)^n}{u_0^n}\right)\right]. &\text{(4.14b)}\end{aligned}$$

As ΔV is to a good approximation linear in $M(x)$ we linearize around $M(x) = 0$,

$$\Delta V(x) \approx \frac{1}{2}r\left\{r + M(x)\left[2 - \frac{2}{1+\left(\frac{r}{u_0}\right)^n}\right] - 2rF\left(\frac{r^n}{u_0^n}\right)\right\}. \tag{4.15}$$

The localization position q_0 is then determined by $\Delta V(q_0) = 0$. Solving this equation for the concentration of the external source at which the front localizes, $M(q_0)$, we find

$$M_0 \equiv M(q_0) \approx \frac{1}{2}r\left[1 + \left(\frac{r}{u_0}\right)^n\right]\left(\frac{u_0}{r}\right)^n\left[2F\left(\frac{r^n}{u_0^n}\right) - 1\right]. \tag{4.16}$$

To obtain an intuitive understanding of the expression for the front position M_0 we investigate the dependence of M_0 on the parameters r and u_0. To this end, we first take the derivative with respect to r,

$$\partial_r M_0 = \frac{1}{2}\left(\frac{u_0}{r}\right)^n\left[1 + n - \left(\frac{r}{u_0}\right)^n - 2nF\left(\frac{r^n}{u_0^n}\right)\right]. \tag{4.17}$$

In bistable systems the relative amplitude of self-activation r is typically greater than the activation threshold u_0. Noting that $F(z) \sim 1/z$ for $z \to \infty$ we get $\partial_r M_0 \approx 1/2$, proving that M_0 is linear in r. On the other hand, taking the derivative with respect to u_0 we get

$$\begin{aligned}\partial_{u_0} M_0 &= \frac{1}{2}\left(\frac{u_0}{r}\right)^{n-1}\left\{2\left[1 + n + \left(\frac{r}{u_0}\right)^n\right]F\left(\frac{r^n}{u_0^n}\right) - 2 - n\right\}\\ &\approx \frac{1}{2}\left(\frac{u_0}{r}\right)^{n-1}\cdot 2\left(\frac{r}{u_0}\right)^n\cdot\left(\frac{u_0}{r}\right) &\text{(4.18)}\\ &= 1\,,\end{aligned}$$

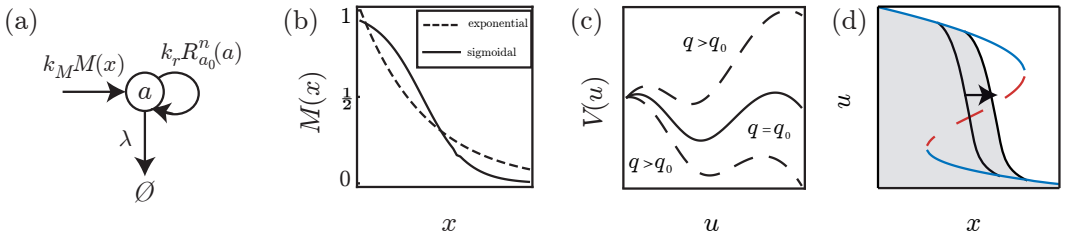

Figure 4.2: (a) Our paradigmatic model comprises self-activation with a rate $k_r R^n_{a_0}(a)$ depending nonlinearly on the concentration a, degradation with a rate λ and activation by an external positional signal $M(x)$. (b) Two types of gradients: exponential decay (dashed line) and a sigmoidal profile ensuing from regulating an exponentially decaying input (solid line). (c) The potential for different values of the front position q. The sliding ball analogy states that the front localizes where the two maximum values of the potential are equal. (d) Sketch of the bifurcation diagram and traveling wave solution of Eq. (4.5). Blue lines denote stable solutions while the dashed (red) line corresponds to the unstable branch. Wave fronts (black lines and shaded area) penetrating the bistable region slow down and eventually come to rest at a stable fixed point of the front dynamics.

which proves that M_0 is also linear in u_0. Note that although the arguments above strictly hold in the limit $n \to \infty$ we numerically found that they are valid even for relatively small values of n. In conclusion, we showed that M_0 can be approximated by a linear function of the form $g(n) \cdot (u_0 - r/2)$, where the pre factor $g(n)$ only depends on n. By taking the limit $n \to \infty$ first, and then doing the above calculations we find that $g(n) \to 1$ for $n \to \infty$.

4.4 Stability of localized wave fronts

The development of many biological systems comprising localized fronts essentially depends on their stability to perturbations. As an example, the fate of the *Drosophila* embryo crucially depends on the exact location of the Hunchback boundary. Failure in the establishment of a sharp Hunchback boundary results in a deformed embryo, hence the name Hunchback. In the following, we ask how much different kinds of perturbations affect the position of the localized front and which design principles we can infer for gene regulatory networks creating the boundary. In particular, we first study the conditions under which wave localization is possible and robust. We then consider two kinds of perturbations: extrinsic perturbations refer to perturbations to the front or the driving signal stemming from sources outside the model. Intrinsic perturbations are fluctuation arising due to a finite particle number and the random nature of reactions and diffusion. We will show that stability is enhanced upon regulating a positional signal and, surprisingly, also for a low degree of binding cooperativity. We further show a contrasting impact of self-activation to the stability

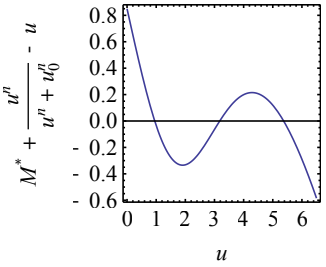

Figure 4.3: Illustration of the condition for bistability. There exists a bistable region in the bifurcation diagram, if for some value M^* of $M(x)$ the reaction term of Eq. (4.5) has three real valued roots.

of these two sources of destabilization.

4.4.1 Robustness of the mechanism

Under which conditions is wave localization possible and robust? In *Drosophila*, the parameters r, u_0 and n are of special importance as they are main determinants of the gene regulation network [12]. Wave localization is possible if there exists a bistable region in the bifurcation diagram. We treat $M(x)$ as a parameter and investigate if $M(x)$ takes values such that the reaction term $f(u,x)$ has three real roots. Such a value for $M(x)$ exists, if the maximum value of the derivative of $f(u,x)$ is greater than zero, $\max_u \partial_u f(u,x) > 0$. For an illustration, see Fig. 4.6 (a). The reaction term is steepest at the steepest point of the Hill function, which is given by

$$u^* = \left(\frac{n-1}{n+1}\right)^{1/n} u_0\,. \tag{4.19}$$

From $\partial_u f(u,x)|_{u=u^*} \geq 0$ we obtain a first condition for the parameters, which allow the localizetion of wave fronts,

$$\frac{u_0}{r} \leq \frac{n^2-1}{4n}\left(\frac{n+1}{n-1}\right)^{1/n}. \tag{4.20}$$

Further conditions can be obtained by the constraints on $M(x)$ given by the definition of the model, namely $0 < M(x) \leq 1$. The range of parameters is bounded below by the condition $M_0 > 0$. Inverting Eq. (4.16) we obtain $u_0/r \geq \left[-F^{-1}\left(1/2\right)\right]^{-1/n}$, where $F^{-1}(1/2)$ denotes the inverse of F evaluated at the point $1/2$. From above the range of parameters is approximately bounded by $u_0/r \leq 1/2 + 1/r$.

4.4.2 Stability with respect to extrinsic perturbations

We are now interested in how the front reacts to extrinsic perturbations. By determining the parameters optimizing the front's stability to such perturbations we identify possible design principles in the construction of gene regulatory networks.

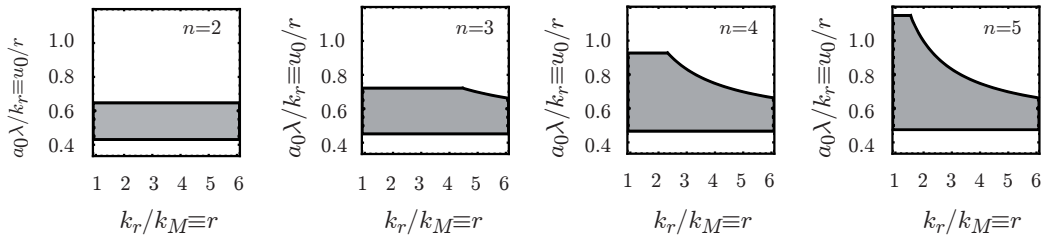

Figure 4.4: Phase diagrams for wave localization in models with different Hill coefficient n. The shaded areas denote possible parameter values allowing the localization of wave fronts. The parameter range and thereby the robustness of the mechanisms increases with the Hill coefficient n.

Perturbations in the front positions

To be stable against extrinsic perturbations the front should both relax back quickly into its equilibrium position and be insensitive to perturbations in the driving signal $M(x)$. Since a high relaxation rate implies that a front can follow changes in the signal quickly, the two stability criteria seem to be somewhat at odds. However, as shown below, they are in full accordance with the latter being less restrictive.

The relaxation rate of the front back into its equilibrium position q_0 can be assessed within the framework of a linear stability analysis [152]. Mathematically, the relaxation rate is obtained by expanding Eq. (4.12) at q_0: $c(q) = -\sigma(q-q_0) + \mathcal{O}(q-q_0)^2$, where $\sigma \equiv -\partial_q c(q)\big|_{q=q_0}$. The quantity σ measures the stability of the fixed point q_0, such that large values of σ correspond to a stably localized front. Taking the derivative of Eq. 4.12 with respect to the position q we find

$$\sigma = -\frac{\partial_{M(q)}\Delta V(M(q)) \cdot \partial_q M(q)}{\int_{-\infty}^{\infty}[\partial_x U(x-q)]^2 \mathrm{d}x}\bigg|_{q=q_0} \tag{4.21}$$

revealing that extrinsic stability is determined by three factors: In the numerator, the first factor describes how sensitively the potential difference of the stable states depends on the external source. The second factor, $\mu \equiv |\partial M(q)/\partial q|_{q_0}$, gives the steepness of the external profile at the localization position. While, therefore, a steeper source profile enhances front stability, the steepness of the front profile, given by the denominator, has the opposite effect. The reason simply is that according to Eq. (4.12), steeper fronts move slower and therefore also relax back more slowly.

In the following we derive analytical results for two important cases of spatial inhomogeneities by making use of the approximate expressions for the stable states, $u^+(x)$ and $u^-(x)$. As an ansatz for the stationary solution of Eq. (4.5) we assume a

connection of the stable states as shown in Fig. 4.2(d),

$$U(x-q) = M(x) + r \begin{cases} 1 - \frac{1}{2}e^{x-q} & (x < q) \\ \frac{1}{2}e^{-(x-q)} & (x \geq q) \end{cases} , \tag{4.22}$$

which is a good approximation for n is not too small. Indeed, using $M(q_0) \approx u_0 - r/2$ we find that $u^n/(u_0^n + u^n)$ evaluates to 1 for $q < q_0$ and 0 for $q > q_0$. Hence, $f(U,x) + \partial_{xx}U = \partial_{xx}M(x) \sim \xi^{-2} \approx 0$. This confirms that U is an approximate stationary solution of Eq. (4.10).

For exponentially decaying external profiles we assume that $M(x)$ is constant for negative values of x. As a result negative values of x do not contribute to the integrals. For large ξ we obtain for the stability to external perturbations

$$\sigma_e \approx \frac{-8rM_0\left[M_0^n - (r+M_0)^n\right]u_0^n}{(4 + r^2\xi + 16rM_0)\left(M_0^n + u_0^n\right)\left[(r+M_0)^n + u_0^n\right]} . \tag{4.23}$$

For sigmoidal gradients, after expanding the integrand in to first order in the inverse length ξ^{-1} of the morphogen, we obtain

$$\sigma_s \approx \frac{-4m\left(\tilde{k} - M_0\right)M_0\left[M_0^n - (r+M_0)^n\right]u_0^n}{\left[(\tilde{k}-1)m + \tilde{k}r\xi\right]\left(M_0^n + u_0^n\right)\left[(r+M_0)^n + u_0^n\right]} . \tag{4.24}$$

For both types of gradients we find that $\sigma > 0$ such that q_0 is a stable fixed point. For large ξ, the extrinsic stability decreases linearly with ξ^{-1} ($\sigma_e \sim \xi^{-1}$, $\sigma_s \sim m\xi^{-1}$), and ξ^{-1} is a measure for the steepness of the external source.

Figure 4.5 shows the results of the numerical evaluation of σ for both types of external sources. For both types of gradients we find that the localized wave front is most stable if r is small, *i.e* if self-activation is weak or birth rates are low compared to the strength of the external source [Figs. 4.5 (a) and (b)]. This can mainly be attributed to a decreased front steepness: reducing self-activation relative to external activation decreases the distance between the fixed points $u^{\pm}$ and thereby the steepness of the wave front. The front's stability is further optimized if it is localized at the steepest position of the external signal. For signals with a sigmoidal profile, this corresponds to $M_0 \approx 1/2$, and with $M_0 \approx u_0 - r/2$ in dimensionless form, it implies a relation between the degradation rate and the activation rates: $a_0\lambda = (k_r + k_M)/2$. Similarly, for an exponential profile with $M_0 = 1$ one finds $a_0\lambda = k_r/2 + k_M$. We can then give the following, biologically more meaningful form: For exponential gradients the degradation rate at the threshold should equal the maximum external production rate plus half of the maximum internal production rate. For sigmoidal gradients the degradation rate at the threshold should equal the average of the maximum internal and external production rates.

How does cooperative binding influence stability? Since cooperativity in the kinetics of the external source implies a steeper sigmoidal profile, large values for the Hill

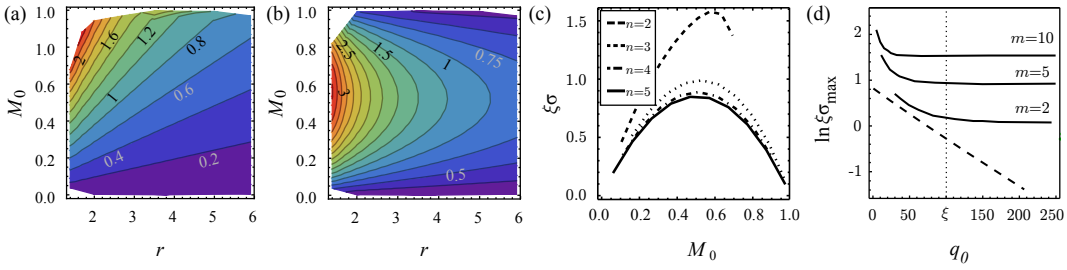

Figure 4.5: Stability $\xi\sigma$, normalized to the steepness of the external profile, for (a) exponential and (b) sigmoidal [$m = 5$] external profiles; the Hill coefficient for self-activation is $n = 5$. Stability increases from blue to red: values of $\xi\sigma$ on lines of equal stability are indicated in the graph. While in both cases stability is optimized for weak self-activation r, they differ in the spatial position of the localized front as measured by the value of M_0. (c) For sigmoidal profiles, small Hill coefficients n for self-activation are optimal for front stability. Parameters for plots (a-c) were $\xi = 100$, and $k = 0.2$. (d) To study if regulation of an exponential signal is biologically beneficial we determined the optimal stabilities which can be achieved for a front localized at a specific position. For each q_0 there are parameters r, k and M_0 such that the linear stability σ is maximal. Parameters were $n = 5$, $2 \leq r \leq 6$, $0.1 \leq k \leq 1$. The plot shows the corresponding optimal values for σ for exponential (dashed line) and sigmoidal external profiles (solid line, m indicated in the graph). Sigmoidal gradients are generally more stable and in addition allow stable localization of fronts in a significant distance from the gradients source at $x = 0$.

coefficient m increase the front's stability; see also the explicit expression for σ above. Conversely, we find that stability is optimized for small values of n, *i.e* a low degree of cooperativity in the self-activation reaction [Fig. 4.5 (c)] [1]. This somewhat counterintuitive result can be attributed to a less steep front profile for small n. Experimental data for Hunchback indeed indicate that the Hill coefficient n for self-activation is rather low [9, 12]. Figure 4.5 (d) shows that stability for sigmoidal external gradients is, all other things being equal, generally higher than for exponential gradients. This implies that regulating an external positional signal is advantageous to the front's stability, since in this case the non-linear amplification of the signal makes it possible to create a steep signal even far away from the origin.

Sensitivity with respect to changes in the positional signal

The localized front might be subject to perturbations in the positional signal $M(x)$. In the context of embryogenesis one can argue that the front should be insensible to

1 This statement applies for exponential as well as sigmoidal external profiles

these changes. In the following we investigate the properties of this kind of stability. We show that the optimal parameters for the extrinsic stability also optimize the front's insensitivity with respect to perturbations in the positional signal.

Intuitively two points become immediately clear: Firstly, perturbations in the driving signal that are outside the front region do not affect the front position. They merely result in a change in the shape of the front profile. Hence, the front position q_0 can only be shifted due to changes in the concentration of the external signal at position q_0. In other words, $q_0[M(x)] \equiv \int_0^1 M^{-1}(m)\delta(m-M_0)dm \equiv q_0(M_0)$. Secondly, the front position depends strongly on changes in $M(x)$ if $M(x)$ is shallow at the localization position. On the other hand, if the driving signal is steep at the front position, perturbations will only have a small effect on the front position. Hence, the influence of perturbations in the external signal on the front position is described by $\mathrm{d}q_0(M)/\mathrm{d}M|_{M_0}$. This can also be seen by evaluating the variation of q_0 with respect to $M(x)$.

Stability of the front with respect to changes in $M(x)$ implies that the front averages out perturbations in the external signal. We therefore investigate the inverse of the magnitude of change in the front position in response to a change in the driving signal, $\left|[\mathrm{d}q(M)/\mathrm{d}M]^{-1}\right|_{M_0}$. This expression is equal to $|\mathrm{d}M(q)/\mathrm{d}q|_{q_0}$, the insensitivity to perturbations in the external signal is given by the steepness of the external signal at the localization position. As demonstrated by Eq. (4.21) extrinsic stability also depends on the signal's steepness. We therefore expect that properties of Eq.(4.21), which are independent of the front profile, translate into properties for the tracking of the positional signal. This is indeed the case. As shown in Fig. 4.7(a) and (b) insensitivity is optimal for $M_0 = 1$ and $M_0 = 1/2$ for exponential gradients and sigmoidal gradients, respectively. In both cases, insensitivity is indifferent to changes in the parameters r or n.

Summarizing, if the gene regulatory network is optimized to cope with extrinsic perturbations, this also implies optimality in the insensitivity to changes in the external signal.

4.4.3 Stability with respect to intrinsic noise

In each biological system intrinsic noise naturally arises due to the finite number of particles and the stochastic nature of interactions. As a result, the front fluctuates around its equilibrium position. One can therefore formally assign a diffusion constant D_f to the fluctuating front. Comparing the front's diffusion constant with the particles' diffusion constant gives a measure for the stability to intrinsic noise. Several ways exist to calculate D_f.

To describe the stochastic dynamics we consider a lattice with lattice spacing h. The vector $\mathbf{s} = \{s_1, \ldots, s_i, \ldots, s_L\}$ gives the number of particles on the lattice sites

enumerated by i. We introduce a multivariate probability distribution function $P(\mathbf{s},t)$ such that $P(\mathbf{s},t)\mathrm{d}\mathbf{s}\mathrm{d}t$ gives the probability that the system is in state $\mathbf{s}$ at time t. The time evolution is given by a set of *Master equations*,

$$\begin{aligned}\partial_t P(\mathbf{s},t) &= \sum_i \Big\{ \Big[k_M M_i(s_i-1) + k_r R^n_{k_0}(s_i-1)\Big] P(\{s_1,\ldots,s_i-1,\ldots,s_L\},t) \\ &\quad +\lambda(s_i+1)P(\{s_1,\ldots,s_i+1,\ldots,s_L\},t) \\ &\quad -\Big[s_i(\lambda+k_M M_i)+R^n_{k_0}(s_i)\Big]P(\mathbf{s},t)\Big\} \qquad (4.25)\\ &+ \frac{D}{h^2}\sum_i \Big\{ (s_{i-1}+1)P(\{s_1,\ldots,s_{i-1}+1,s_i-1,\ldots,s_L\},t) \\ &\quad +(s_{i+1}+1)P(\{s_1,\ldots,s_i-1,s_{i+1}+1,t,\ldots,s_L\}) - 2s_iP(\mathbf{s},t)\Big\}.\end{aligned}$$

Here, the first sum gives probability currents flowing inward and outward of each state due to the local interactions. The second sum accounts for changes of particle numbers due to diffusion. If the typical number of particles N is large we may employ a truncated expansion in N and arrive at the *Fokker-Planck equation*, given the time evolution of the the probability for the concentrations $\mathbf{a} = \mathbf{s}/N$ as the combined effect of drift and diffusion terms. We obtain

$$\begin{aligned}\partial_t P(\mathbf{a},t) = &-\sum_i \partial a_i \Big\{ \Big[k_M M_i + k_r R^n_{a_0}(a_i) - \lambda a_i\Big]P(\mathbf{a},t) \\ &-\frac{1}{2K}\partial_{a_i}\Big[k_M M_i + k_r R^n_{a_0}(a_i) + \lambda a_i\Big]P(\mathbf{a},t)\Big\} \qquad (4.26)\\ &+\frac{D}{h^2}\sum_i\Big(\partial_{a_i}-\partial_{a_{i+1}}\Big)\left[(a_i-a_{i+1})P(\mathbf{a},t) + \frac{a_i-a_{i+1}}{2K}(\partial_{a_i}-\partial_{a_{i+1}})P(\mathbf{a},t)\right],\end{aligned}$$

where h is the lattice constant and the large parameter K is the typical local population size. The Fokker-Planck equation is equivalent to a *Langevin equation* [161],

$$\begin{aligned}\partial_t a =& k_r R^n_{a_0}(a) + k_M M(x) - \lambda a + D\partial_{xx}a \qquad (4.27)\\ &+\sqrt{\frac{h}{K}}\left\{\sqrt{\lambda a + k_r R^n_{a_0}(a) + k_M M(x)}\,\eta(x,t) + \partial_x\left[\sqrt{2a}\chi(x,t)\right]\right\}. \qquad (4.28)\end{aligned}$$

η and χ are independent Gaussian noises with zero mean and correlations

$$\langle\eta(x,t)\eta(x',t')\rangle = \langle\chi(x,t)\chi(x',t')\rangle = \delta(x-x')\delta(t-t'), \qquad (4.29)$$

and h is the lattice spacing as measured in units of the the typical length scale associated with the diffusion of particles A. In Equation (4.28), the first four terms on the right hand side give the deterministic evolution due to reactions and diffusion. These terms correspond the dimensional form of Eq. (4.10). The term proportional

to $\eta(x,t)$ describes multiplicative noise stemming from the local reactions. The last term has the form of a flux and it accounts for noise stemming from the random walks of particles. The magnitude of these two sources of noise is comparable. We rescale t, x and a by $1/\lambda$, $\sqrt{D/\lambda}$ and k_M/λ, respectively, and obtain

$$\partial_t u = f(u,x) + \partial_{xx} u + N^{-1/2} R(x,t,u)\,. \tag{4.30}$$

$R(x,t,u)$ summarizes the noise terms,

$$R(x,t,u) \equiv \sqrt{r R^n_{u_0}(u) + M(x) + u}\,\eta(x,t) + \partial_x \left[\sqrt{2u}\chi(x,t,u)\right]\,. \tag{4.31}$$

The prefactor $N^{-1/2}$ with $N = K\sqrt{D/\lambda}/h$ gives the magnitude of noise. The intuitive meaning of N can be understood by noting that $\sqrt{D/\lambda}$ is the length scale associated with diffusion. In other words, $\sqrt{D/\lambda}$ is the length in which the front changes from its maximum value to its minimum value. Therefore, $\sqrt{D/\lambda}/h$ is the number of lattice sites in the front region.

As N is large, the magnitude of intrinsic noise is small compared to changes in the concentration due to the deterministic reaction and diffusion terms. In analogy to the steps in Refs. [150, 162, 163] we proceed by solving Eq. (4.30) perturbatively around a generalized traveling wave solution $U_0(x-q(t)-X(t),y)$ of the deterministic reaction-diffusion equation (4.10), where $X(t)$ denotes the noise driven displacement of the front and $y = x/\xi$ describes the dependence on the slowly varying spatial variable. We make the ansatz

$$U(x-q(t)-X(t),y,t) = U_0(x-q(t)-X(t),y) + U_1(x-q(t)-X(t),y,t)\,, \tag{4.32}$$

assuming that the contribution explicitly depending on t is small compared to the stationary profile, $|U_1| \ll U_0$. We substitute (4.32) into Eq. 4.30 and linearize around U_0. We obtain [2]

$$\partial_t U_1 = \hat{\mathcal{L}} U_1 + \dot{X}\partial_x U_0 + N^{-1/2} R(x,t,U_0) + \mathcal{O}(\xi^{-1})\,, \tag{4.33}$$

with the differential operator $\hat{\mathcal{L}}$ given by

$$\hat{\mathcal{L}} = \partial_{xx} + q(t)\partial_x + \partial_U f(U_0,y)\,. \tag{4.34}$$

We are interested in the probability distribution for the stochastic displacement X. To this end, we calculate $\dot{X}$, which is determined by the solvability of Eq. (4.33). We expand U_1 in eigenmodes of the hermitian operator $\hat{\mathcal{L}}$,

$$U_1(\xi,y,t) = \sum_l b_l(t)\varphi(\xi,y)\,,\ \text{with } \xi = x - q(t)\,, \tag{4.35}$$

2 We made use of the fact that U_0 solves Eq. (4.10) and that $U' = \partial_x U + \mathcal{O}(\xi^{-1})$, where the prime denotes derivatives with respect to the first argument.

and fix the definition of X by setting $b_0(t) = 0$. In analogy to the deterministic case we now multiply Eq. (4.33) by $e^{\dot{q}(t)[x-q(t)]}$ and integrate over x. One obtains [3]

$$\dot{X} = \frac{\int_{-\infty}^{\infty} \mathrm{d}x \partial_x U_0 e^{\dot{q}(t)[x-q(t)]} R(x,t,U_0)}{N^{1/2} \int_{-\infty}^{\infty} \mathrm{d}x \left(\partial_x U_0\right)^2 e^{\dot{q}(t)[x-q(t)]}} \,. \tag{4.36}$$

To asses how much intrinsic noise affects the front's position we calculate the growth rate of the mean square displacement. If the mean square displacement grows linearly with time, we can formally assign a diffusion constant D_f to the front in the co-moving frame. From $\dot{X}$ the front's diffusion constant can be obtained by

$$D_f = \lim_{t\to\infty} \frac{\int_0^t \mathrm{d}t_1 \int_0^t \mathrm{d}t_2 \langle \dot{X}(t_1)\dot{X}(t_2)\rangle}{2t} \,. \tag{4.37}$$

The evaluation of the integral is in full analogy to the calculations presented in Ref. [150]. The result is

$$\begin{aligned}\frac{D_f}{D} =& \frac{\int_{-\infty}^{\infty} \mathrm{d}x \left\{ \frac{1}{2} \left[(\partial_x U_0) e^{\dot{q}(t)[x-q(t)]} \right]^2 \left[R^n_{u_0}(U_0) + M(x) + U_0 \right] \right\}}{N \left[\int_{-\infty}^{\infty} \mathrm{d}x \left(\partial_x U_0\right)^2 \right]^2 e^{\dot{q}(t)[x-q(t)]}} \\ &+ \frac{\int_{-\infty}^{\infty} \mathrm{d}x + U_0 \partial_x \left[(\partial_x U_0) e^{\dot{q}(t)[x-q(t)]} \right]^2}{N \left[\int_{-\infty}^{\infty} \mathrm{d}x \left(\partial_x U_0\right)^2 \right]^2 e^{\dot{q}(t)[x-q(t)]}} \,.\end{aligned} \tag{4.38}$$

The diffusivity D_f of the front is a measure for the front's susceptibility to intrinsic noise. We therefore compare D_f to the diffusion constant of the particles, D. The inverse, D/D_f, gives a measure of how much the front ins displaced by intrinsic noise. We are here interested in fronts which are localized, $q(t) = q_0$ and $\dot{q}(t) = 0$. In this case, the expression for the front's stability to intrinsic noise reduces to

$$\frac{D}{D_f} = N \frac{\left[\int_{-\infty}^{\infty} \mathrm{d}x \left(\partial_x U_0\right)^2 \right]^2}{\int_{-\infty}^{\infty} \mathrm{d}x \left[\frac{1}{2} (\partial_x U_0)^2 \left(R^n_{u_0}(U_0) + M(x) + U_0 \right) + U_0 (\partial_{xx} U_0)^2 \right]} \Bigg|_{q=q_0} \,. \tag{4.39}$$

where U is a stationary solution of Eq. (4.5) and we omitted the explicit dependence on x in the notation for the stationary solution U. Generally, the front's diffusion constant is smaller than the particle's diffusion constant by a factor N, which corresponds to the typical number of particles in the front region. The integral in the numerator gives the maximum steepness of the front. Hence, as opposed to extrinsic stability, intrinsic stability is optimal for steep fronts. Shallow fronts are prone to stochastic switching, as the entropy barrier between the stable states is reduced in the front region. The terms in the denominator account for the reaction and diffusion noise.

---

3 As $\hat{\mathcal{L}}$ is hermitian the different eigenmodes are proportional if weighted with $e^{\dot{q}(t)[x-q(t)]}$, i.e. $\int_{-\infty}^{\infty} \mathrm{d}x \varphi_l \varphi_k e^{\dot{q}(t)[x-q(t)]} = \delta_{kl}$.

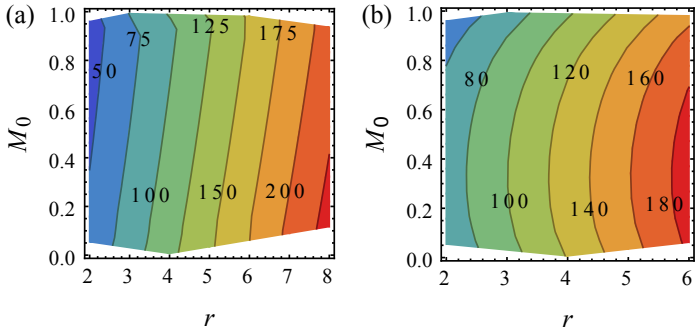

Figure 4.6: (a) Stability to intrinsic noise for an exponential gradient. Color denotes intrinsic stability, such that red means high stability and blue means low stability. In contrast to extrinsic stability, intrinsic stability is maximized for strong self activation. (b) Qualitatively the same holds for sigmoidal gradients ($n = 5$, $m = 5$). Parameters for all plots were $\xi = 10$, $k = 0.2$.

In the following, we provide explicit analytical results supporting these statements. The only problematic integral involved in Eq. (4.39) is $\int_{-\infty}^{\infty} \mathrm{d}x\,(U')^2 R_{u_0}^n(U)$. If n is sufficiently large we see that $R_{u_0}^n(U)$ is small for $U > u_0$. Further, we note that $U(q_0, q_0) = M(q_0) + r/2$. By using the approximate expression for the localization position, $M(q_0) \approx u_0 - r/2$, we find that $U(q_0, q_0) \approx u_0$. Hence, we can rewrite the integral as

$$\int_{-\infty}^{\infty} \mathrm{d}x\,(U')^2 R_{u_0}^n(U)\Big|_{q=q_0} \approx \int_{-\infty}^{q_0} \mathrm{d}x\,(U')^2\,. \tag{4.40}$$

For exponentially decreasing external sources the analytical result can be brought to a short form by only keeping the dominant terms in ξ,

$$\frac{D}{D_f} \approx \frac{3Nr^2\left(4 + r^2\xi + 16rM_0\right)}{2\left\{8 + 12r + 5r^3\xi + 6rM_0\left[r(7+\xi) + 6M_0\right]\right\}}\,. \tag{4.41}$$

For sigmoidal profiles, we expand $M(x)$ to first order in the inverse lengthscale of the external gradient ξ^{-1}, $M(x) \approx 1 - k^m m x/[\xi(1+k^m)]$. We can now perform the integrals in (4.39) analytically and obtain

$$\frac{D}{D_f} \approx \frac{3N(8(\tilde{k}-1)m + \tilde{k}r\xi)^2}{2\tilde{k}\xi^2\left[\tilde{k}\,(6+5r) - 6(\tilde{k}-1)\ln\left(\frac{\tilde{k}-M_0}{(\tilde{k}-1)M_0}\right)\right]}. \tag{4.42}$$

In both cases we find a linear increase in stability to intrinsic noise with the relative amplitude of self-activation, r. Figure 4.6 (b) and (c) show the results of the numerical evaluation of Eq. (4.39). It confirms the linear increase of stability with r. In contrast to extrinsic stability, we here find that the front is most robust against fluctuations for strong self-activation r. The reason for this is that, as r determines the amount of reactions necessary to locally switch between the stable states, the rate of stochastic switching decreases for large r.

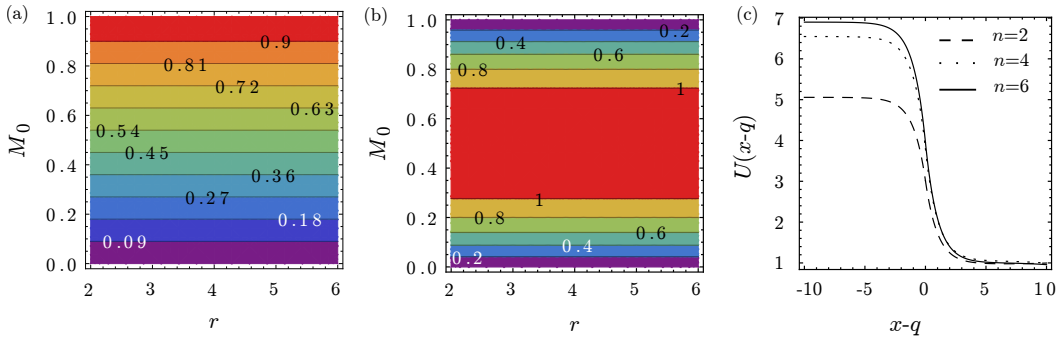

Figure 4.7: (a) Insensitivity $\xi \left|[\mathrm{d}q(M)/\mathrm{d}M]^{-1}\right|_{M_0}$ to perturbations in the driving signal normalized to the steepness of the external source. Color is chosen, such that red denotes a high insensitivity and blue a low insensitivity. The numbers denote the values on the lines of equal insensitivity. For exponential sources the optimal value for M_0 is 1, in correspondence to the results for the relaxation rate. Insensitivity is indifferent to the specific choice of r ($n = 5$, $\xi = 10$). (b) For sigmoidal gradients the optimal value of M_0 is $1/2$ ($n = 5$, $\xi = 10$, $m = 5$, $k = 0.5$). (c) Stationary solutions for different values of n for sigmoidal gradients ($r = 6$, $u_0 = 3.5$, $m = 5$, $k = 0.2$, $\xi = 10$). The steepness of the front increases with the degree of cooperative binding.

4.4.4 Sharpness of the front

In many applications the front serves as a signal for further downstream processes, *e.g.* to determine stripe-like patterning of the *Drosophila* embryo [4, 164]. In those instances it is also important that a front is not only stable against perturbations, but also sharply distinguishes between active and inactive regions. This requires a steep front. Starting from the stationary solution, Eq. (4.22), we find that the steepness of the front is given in dimensional form by

$$k_M M'(q_0) - \frac{k_r}{2k_M}\sqrt{\frac{\lambda}{D}}\,. \tag{4.43}$$

Hence, three factors determine the steepness of the front. Firstly, the steepness of the front is increased, when the amplitude of internal activation compared to external activation is strong. Secondly, a high degradation rate and a small diffusion constant result in steep fronts. Last, the steepness of the external source at the front position is important. The dependence of the front's steepness on the binding cooperativity is not captured by the stationary solution, as it is the result of a large n expansion. Here, nonlinear corrections to the linear approximation of the stable states have the effect, that for small n the front becomes shallower, as demonstrated in Fig. 4.7 (c).

The front's steepness effects extrinsic and intrinsic stability in different ways. Generally, steep fronts move slower, as demonstrated by Eq. 4.12. The reason for this is,

that as, opposed to shallow fronts, for steep fronts the total rate of reactions moving the front forward is lower. As a result, steep front also relax back to their equilibrium position more slowly and are therefore less stable to extrinsic perturbations.

On the other hand, steep fronts are less susceptible to intrinsic fluctuations, as demonstrated by Eq. (4.39). Intuitively this becomes clear if one notes that for stochastic switching to happen, an entropy barrier between the stable states has to be overcome. Hence, the rate of stochastic switching increases, if this barrier is low. This is the case for shallow fronts. where due to diffusion or properties of the bifurcation diagram the entropy barrier is decreased on a larger portion of the front.

In summary, a steep front is generally obtained if self-activation is strong compared to external activation and, to a lesser degree, if binding cooperativity is strong. Sharp fronts, however, are susceptible to extrinsic fluctuations and one has to sacrifice front stability for the precision of the transmitted signal.

4.5 Papers and Manuscripts

4.5.1 Stability of localized wave fronts in bistable systems

In our article "Stability of localizaed wave front in bistable systems" by Steffen Rulands, Ben Klünder, and Erwin Frey, *Phys. Rev. Lett.* **110**, 038102 (2013) we investigate how stable domain borders can be established by the combined effect of bistability and spatially inhomogeneous activation. In particular, we study a broad class of bistable models subject to self-activation, degradation and spatially inhomogeneous activating agents. We determine the conditions under which wave-front localization is possible and analyze the stability thereof with respect to extrinsic perturbations to front or the driving signal on the one hand, and intrinsic noise on the other hand. It is found that extrinsic stability is enhanced upon regulating a positional signal and, surprisingly, also for a low degree of binding cooperativity. Importantly, we find that the design of the underlying gene regulatory network cannot be simultaneously be optimized for both, intrinsic and extrinsic perturbations.

4.5.2 Conlusion and Outlook

In a paradigmatic model we studied how stable domain borders can be established by bistability and a gradient providing positional information. We identified conditions optimizing the stability and robustness of localized wave fronts for different types of perturbations. We calculated the phase diagram of parameter values allowing the localization of wave fronts. Increasing cooperativity in self-activation enhances the robustness of the localization mechanism. Our calculations also reveal that there is a trade-off between the stability of the wave front to extrinsic perturbations and

intrinsic noise stemming from the random nature of the reactions and diffusion. While weak self-activation or low birth rates enhance the stability with respect to extrinsic perturbations to the front or the driving signal, stochastic defocussing is minimized for strong self-activation. The latter also increases the spatial precision of the signal transmitted by the front to downstream processes.

From conflict between the optimal parameters for extrinsic and intrinsic stability we conclude that the design of the underlying gene regulatory network cannot be optimized to suppress intrinsic and extrinsic perturbations at the same time. This affects, for example, the design of gene circuits in developmental systems. If a large number of molecules is involved in the system, intrinsic noise becomes irrelevant and the parameters of the genetic network may be optimized for robustness against external perturbations. This is achieved by weak self-activation and strong cooperativity in external activation. Conversely, if particle numbers are low, robustness against intrinsic noise requires strong and cooperative self-activation. To also safeguard against external perturbation then requires additional mechanisms beyond those included in our simplified model. Beyond these results we showed that the stability of fronts localized far away from the morphogen's source can be enhanced by a cooperative preprocessing step of the positional signal.

These general results were obtained for a generic class of bistable models. We therefore expect our results to apply to be important guiding principles in the context of biological pattern forming systems, such as cell polarization or the segmentation of embryos. Further work may extend these results to match specific biological systems. What are, for example, the minimal ingredients that are necessary to quantitatively describe the formation of the Hunchback kink in the embryogenesis of *Drosophila melanogaster*? Employing analytical results could also make it possible to implement evolutionary optimization algorithms to infer the parameters of the gene regulatory network.

Stability of Localized Wave Fronts in Bistable Systems

Steffen Rulands, Ben Klünder, and Erwin Frey*

Arnold Sommerfeld Center for Theoretical Physics and Center for NanoScience, Department of Physics, Ludwig-Maximilians-Universität München, Theresienstraße 37, D-80333 München, Germany

(Received 28 June 2012; published 18 January 2013)

Localized wave fronts are a fundamental feature of biological systems from cell biology to ecology. Here, we study a broad class of bistable models subject to self-activation, degradation, and spatially inhomogeneous activating agents. We determine the conditions under which wave-front localization is possible and analyze the stability thereof with respect to extrinsic perturbations and internal noise. It is found that stability is enhanced upon regulating a positional signal and, surprisingly, also for a low degree of binding cooperativity. We further show a contrasting impact of self-activation to the stability of these two sources of destabilization.

DOI: 10.1103/PhysRevLett.110.038102 PACS numbers: 87.17.Pq, 02.50.Ey, 05.45.−a, 87.18.Tt

Bistable systems are ubiquitous in nature. For example, genetic switches are bistable systems that store the activation state of a gene [1,2]. In population dynamics, a minimum population size is often needed to establish a stable population [3]. The spatial versions of such systems admit traveling wave solutions, e.g., describing the outbreak of viruses or the colonization of territory [4–7]. If bistable systems are subject to external spatial gradients, traveling waves may localize in restricted spatial domains [8–10]. An important example arises in early embryogenesis of *Drosophila melanogaster* where maternal morphogen gradients provide positional information for gene regulation [11–14]. The morphogen Bicoid is present as a monotonically decreasing concentration in the embryo and controls the steplike activation of the gene hunchback, which also enhances its own activation, effectively producing a bistable system. The exact position of the hunchback front is pivotal to the embryo's fate [13]. Hence, the front's stability to extrinsic perturbations or internal noise is paramount. Wave localization and the stability of the front also play an important role in other contexts. In ecology, birth rates may have spatial dependence, e.g., due to spatial variance in temperature or resource availability [15,16]. The localized boundaries between species are subject to large fluctuations due to the low number of individuals in the boundary region. This may eventually lead to the extinction of one of the species due to demographic stochasticity [17]. Last, in biotechnological applications, this mechanism might be used to create localized fronts of proteins [18].

Motivated by these processes, we investigate a broad class of bistable diffusion-reaction models with reaction terms comprising self-activation, external activation, and degradation. While self-activation and degradation are assumed to be spatially uniform, the external activation is taken to be position-dependent. We consider two qualitatively different types of external gradients and determine the parameter range for which wave localization is possible. Moreover, we ask how stable these localized fronts are with respect to extrinsic and intrinsic noise, and we determine optimal conditions minimizing the front's susceptibility to such perturbations.

Specifically, we consider a one-dimensional system where diffusing particles are subject to three types of reactions: First, there are gain processes with a concentration-dependent rate that accounts for self-activation in gene regulatory systems or reproduction in population dynamics. Typically, these rates are small for low concentrations, then rise and finally saturate at high concentrations. In populations dynamics, this is referred to as the strong Allee effect [3,6]. In gene regulation, it can be due to cooperative transcription factor binding to a gene promoter. A common choice for the overall reaction rate is $k_r R^n_{a_0}(a)$ with the Hill function $R^n_{a_0}(a) \equiv a^n/(a_0^n + a^n)$, k_r the maximum intrinsic production rate, and a the particle concentration. The Hill coefficient n measures the degree of cooperative binding in the promoter region or, in ecology, the strength of an Allee effect. Second, we account for loss processes, where particles vanish with a certain rate λ. Third, in addition to self-activation, there may also be external sources for particle production. Here, we are interested in systems where this source is position-dependent and characterized by the overall rate $k_M M(x)$. The prefactor k_M denotes the maximum rate of external activation, and $M(x)$ is a monotonically decreasing positive density profile with normalization $M(0) = 1$. In the simplest case, where the profile results from a source-degradation dynamics [19,20], it is exponential $M(x) = e^{-x/\xi}$ with the decay length ξ, cf. Fig. 1(a). Prominent examples are the concentration profile of Bicoid in *Drosophila* [19] and temperature or nutrient gradients in population dynamics [21]. Since the production of hunchback by Bicoid is mediated by cooperative binding, the profile $M(x)$ entering the overall production rate is commonly described by $M(x) \sim R^m_{I_0}(e^{-x/\xi})$ [22]. The exponentially decaying signal induced by maternal source-degradation dynamics serves as an input to the

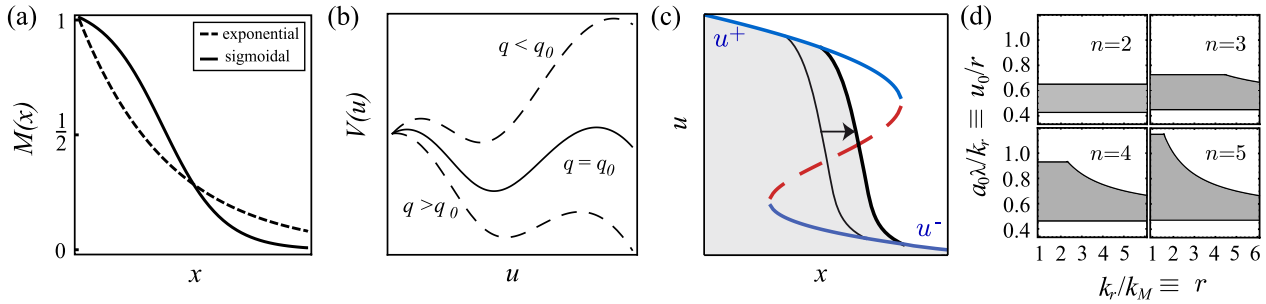

FIG. 1 (color online). (a) Two types of gradients: exponential decay (dashed line) and a sigmoidal profile ensuing from regulating an exponentially decaying input (solid line). (b) The potential for different values of the front position q. The sliding ball analogy states that the front localizes where the two maximum values of the potential are equal. (c) Sketch of the bifurcation diagram and traveling wave solution of Eq. (1). Blue (dark gray) lines denote stable solutions whereas the dashed (red) line corresponds to the unstable branch. Wave fronts (black lines and shaded area) penetrating the bistable region slow down and eventually come to rest at a stable fixed point of the front dynamics. (d) Phase diagrams of possible parameter values allowing wave localization. The parameter range of wave localization increases with the Hill coefficient n.

gene regulation system. The latter is described by a Hill coefficient m typically in the range from 1 to 5 and with an activation threshold I_0.

In the limit of a large system size, fluctuations are of minor importance and the spatiotemporal dynamics is then aptly described by a reaction-diffusion equation, which in dimensionless form reads

$$\partial_t u = f(u, x) + \partial_{xx} u. \tag{1}$$

Here, $f(u, x) \equiv r R^n_{u_0}(u) + M(x) - u$ comprises self-activation, external activation, and degradation. Concentration u, time t, and space x are measured in units of k_M/λ, $1/\lambda$, and $\sqrt{D/\lambda}$, respectively. The ratio $r \equiv k_r/k_M$ denotes the relative amplitude of self-activation and external activation mediated through $M(x)$.

Traveling wave solutions of Eq. (1) may be localized due to the combined effect of spatially varying external sources and bistability [8–10]. The basic mechanisms can be best understood in terms of the well-known sliding ball analogy [23], which here is complicated by the fact that the reaction term is space-dependent. Since in most biological situations a steep profile in u is induced by a smooth external profile $M(x)$, we may assume a separation of length scales $\xi \gg \sqrt{D/\lambda}$ and ξ much smaller than the system size. Then one can make a generalized traveling wave ansatz $U = U(x - q(t), y)$, where x is a fast-varying variable describing changes in the concentration profile, $y = x/\xi$ is a slowly varying variable describing changes in the external profile $M(x)$, and $q(t)$ denotes the front position. To leading order, this gives

$$-\dot{q}\partial_x U = \partial_{xx} U + \partial_U V(U, y) + \mathcal{O}(\xi^{-1}), \tag{2}$$

which may be interpreted as a force balance for a particle (sliding ball) with mass 1, friction $\dot{q}$, and potential $V(u, y) = \int^u f(\tilde{u}, y) d\tilde{u}$. Importantly, the potential parametrically depends on y; see Fig. 1(b). For parameter regimes where V has two maxima at $u^+(x)$ and $u^-(x)$ and a local minimum at $u^s(x)$, the velocity $\dot{q}$ must be chosen such that the sliding ball starting from the upper branch u^+ ends up at the lower branch u^-. The front speed is proportional to the difference between the two maxima of $V(u, y)$ and becomes zero if the condition $\Delta V(y) \equiv \int_{u^-}^{u^+} f(u, y) du = 0$ is satisfied. More quantitatively, following standard steps [23–25], one finds [26]

$$\dot{q} \approx \frac{\Delta V(q)}{\int_{-\infty}^{\infty} [\partial_x U(x - q, y)]^2 dx} \equiv c(q), \tag{3}$$

where U is the traveling wave solution. The denominator roughly equals the maximum steepness of the front profile and implies that steep fronts move slower [23].

In our class of models, a single branch of stable solutions at high concentrations typically undergoes a fold bifurcation for growing x, where the system is bistable on a confined spatial interval; see Fig. 1(c). For large x values, a single branch at low concentrations remains. Within the bistable regime, the velocity $c(q)$ may change sign and thereby lead to a localization of the traveling wave front.

We first determine the localization position q_0 of the front from $\Delta V(q_0) = 0$. Approximations for $u^{\pm}(x)$ can be obtained by expanding f as Taylor or Laurant series: $u^-(x) = M(x) + \mathcal{O}(u^n)$ and $u^+(x) = M(x) + r + \mathcal{O}(u^{-n})$. For a given external profile $M(x)$, the potential reads $V(u, x) = -u[u/2 - M(x) - r + rF(u^n/u_0^n)]$, where $F(z) \equiv {}_2F_1(1, 1/n, 1 + 1/n, -z)$ and ${}_2F_1$ signifies the hypergeometric function. Keeping the dominant terms of $M(x)$ in ΔV we then obtain an expression for $M_0 \equiv M(q_0)$ determining the localization position q_0,

$$M_0 \approx \frac{1}{2} r \left[1 + \left(\frac{r}{u_0}\right)^n\right]\left(\frac{u_0}{r}\right)^n \left[2F\left(\frac{r^n}{u_0^n}\right) - 1\right].$$

This is well approximated by a linear function of the form $g(n)(u_0 - r/2)$ and converges to $u_0 - \frac{1}{2} r$ for $n \to \infty$. For

exponentially decaying gradients, the equilibrium front position is then given by $q_0 = \xi \ln M_0$. For sigmoidal gradients, $M(x) \equiv \tilde{k} R_k^m(e^{-x/\xi})$ with dimensionless threshold k and normalization factor $\tilde{k} \equiv k^m + 1$, the front localizes at $q_0 = \xi/m \ln\{(\tilde{k} - M_0)/[(\tilde{k} - 1)M_0]\}$.

Under which conditions is wave localization possible and robust? In *Drosophila*, the parameters r, u_0, and n are of special importance as they are main determinants of the gene regulation network [13]. The wave localizes if there is a bistable region in the bifurcation diagram, i.e., if for some x, the reaction term in Eq. (1) has three real roots. Such values of x exist if the maximum value of the derivative of $R_n^{u_0}(u) - u$ is greater than zero. We obtain an approximate expression for the phase boundaries

$$-[F^{-1}(1/2)]^{1/n} \lesssim \frac{u_0}{r} \lesssim \frac{n^2 - 1}{4n}\left(\frac{n+1}{n-1}\right)^{1/n} \quad (4)$$

and $\frac{u_0}{r} \lesssim \frac{1}{2} + \frac{1}{r}$. Figure 1(d) shows that the range of allowed parameters grows with n. For large n values, the phase boundaries are well approximated by $\frac{1}{2} \leq \frac{u_0}{r} \leq \frac{1}{2} + \frac{1}{r}$. This translates to $a_0\lambda \approx k_r$; i.e., for front localization, the overall degradation rate at the threshold must be of the same order as the maximum production rate.

To be stable against extrinsic perturbations, the front should both relax back quickly into its equilibrium position and be insensitive to perturbations in the driving signal $M(x)$. Since a high relaxation rate implies that a front can follow changes in the signal quickly, the two stability criteria seem to be somewhat at odds. However, as shown below, they are in full accordance with the latter being less restrictive.

The relaxation rate of the front back into its equilibrium position q_0 can be assessed within the framework of a linear stability analysis. Mathematically, this is given by expanding Eq. (3) at q_0: $c(q) = -\sigma(q - q_0) + \mathcal{O}(q - q_0)^2$, where $\sigma \equiv -\partial_q c(q)|_{q=q_0}$. The quantity σ measures the stability of the fixed point q_0, such that large values of σ correspond to a stably localized front. We find

$$\sigma = -\frac{\partial_{M(q)}\Delta V(M(q))\partial_q M(q)}{\int_{-\infty}^{\infty}[\partial_x U(x-q)]^2 dx}\Bigg|_{q=q_0}, \quad (5)$$

revealing that extrinsic stability is determined by three factors: In the numerator, the first factor describes how sensitively the potential difference of the stable states depends on the external source. The second factor, $\mu \equiv |\partial M(q)/\partial q|_{q_0}$, gives the steepness of the external profile at the localization position. Whereas, therefore, a steeper source profile enhances front stability, the steepness of the front profile (denominator) has the opposite effect. The reason simply is that steeper fronts move slower and therefore also relax back more slowly; cf. Eq. (3).

Figure 2 shows the results of the numerical evaluation of σ for both types of external sources; analytical results are given in the Supplemental Material [27]. For both types of gradients we find that the localized wave front is most stable if r is small, i.e., if self-activation is weak or birth rates are low compared to the strength of the external source [Figs. 2(a) and 2(b)]. This can mainly be attributed to a decreased front steepness: reducing self-activation relative to external activation decreases the distance between the fixed points $u^{\pm}$ and thereby the steepness of the wave front. The front's stability is further optimized if it is localized at the steepest position of the external signal. For signals with a sigmoidal profile, this corresponds to $M_0 \approx 1/2$, and with $M_0 \approx u_0 - r/2$ in dimensionless form, it implies a relation between the degradation rate and the activation rates, $a_0\lambda = (k_r + k_M)/2$. Similarly, for

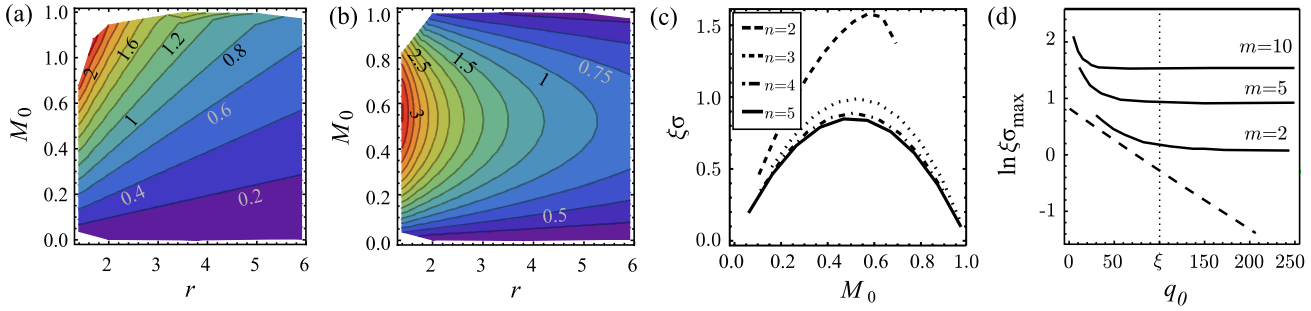

FIG. 2 (color online). Stability $\xi\sigma$, normalized to the steepness of the external profile, for (a) exponential and (b) sigmoidal [$m = 5$] external profiles; the Hill coefficient for self-activation is $n = 5$. Stability increases from blue to red (grayscale is from dark gray over light gray to medium gray): values of $\xi\sigma$ on lines of equal stability are indicated in the graph. While in both cases stability is optimized for weak self-activation r, they differ in the spatial position of the localized front as measured by the value of M_0. (c) For sigmoidal profiles, small Hill coefficients n for self-activation are optimal for front stability. Parameters for plots (a)–(c) were $\xi = 100$ and $k = 0.2$. (d) To study if regulation of an exponential signal is biologically beneficial, we determined the optimal stabilities that can be achieved for a front localized at a specific position. For each q_0, there are parameters r, k, and M_0 such that the linear stability σ is maximal. Parameters were $n = 5$, $2 \leq r \leq 6$, $0.1 \leq k \leq 1$. The plot shows the corresponding optimal values for σ for exponential (dashed line) and sigmoidal external profiles (solid line, m indicated in the graph). Sigmoidal gradients are generally more stable and in addition allow stable localization of fronts a significant distance from the gradients source at $x = 0$.

an exponential profile with $M_0 = 1$, one finds $a_0\lambda = k_r/2 + k_M$.

How does cooperative binding influence stability? Since cooperativity in the kinetics of the external source implies a steeper sigmoidal profile, large values for the Hill coefficient m increase the front's stability; see also the explicit expression for σ in the Supplemental Material [27]. Conversely, we find that stability is optimized for small values of n, i.e., a low degree of cooperativity in the self-activation reaction [Fig. 2(c)] [28]. This somewhat counterintuitive result can be attributed to a less steep front profile for small n; see the Supplemental Material [27]. Experimental data for the hunchback gene indeed indicate that the Hill coefficient n for self-activation is rather low [13,29]. Figure 2(d) shows that stability for sigmoidal external gradients is, all other things being equal, generally higher than that for exponential gradients. This implies that regulating an external positional signal is advantageous to the front's stability, since in this case the nonlinear amplification of the signal makes it possible to create a steep signal even far from the origin.

To ensure stable localization, the front must also be robust against perturbations in $M(x)$. Specifically, its position q_0 should only weakly depend on the local signal strength, $|\partial q_0(M)/\partial M|_{M_0} \ll 1$. This condition is equivalent to a steep source profile, $\mu = |\partial M(q)/\partial q|_{q_0} \gg 1$, and hence in full accordance with a large relaxation rate σ. It is, however, less restrictive since it is indifferent to changes in parameters that mainly affect the shape of the front, e.g., the rate of self-activation r and the Hill coefficient n; see Supplemental Material [27].

In many applications, the front serves as a signal for further downstream processes, e.g., to determine stripelike patterning of the *Drosophila* embryo [30,31]. In those instances, it is also important that a front is not only stable against perturbations but also sharply distinguishes between active and inactive regions. This requires a steep front that is generally obtained if self-activation is strong compared to external activation and, to a lesser degree, if binding cooperativity is strong; see the Supplemental Material [27]. Sharp fronts, however, are susceptible to extrinsic fluctuations, and one has to sacrifice front stability for the precision of the transmitted signal.

Intrinsic noise resulting from small copy number fluctuations also affects the stability of the localized wave front. In this case, stability can be measured in terms of the ratio D/D_f between the individual particle's and the front's diffusion constants. The latter can be calculated following the steps outlined in Ref. [17],

$$\frac{D}{D_f} = \frac{N[\int_{-\infty}^{\infty} dx (U')^2]^2}{\int_{-\infty}^{\infty} dx [\frac{1}{2}(U')^2 h(U) + U(U'')^2]}\Bigg|_{q=q_0}, \quad (6)$$

where $h(U) \equiv R^n_{u_0}(U) + M(x) + U$, and U denotes the stationary solution. Generally, the front's diffusion constant is smaller than the particle's diffusion constant by a factor N, which corresponds to the typical number of particles in the front region. The integral in the numerator gives the maximum steepness of the front. Hence, as opposed to extrinsic stability, intrinsic stability is optimal for steep fronts. Shallow fronts are prone to stochastic switching, as the entropy barrier between the stable states is reduced in the front region. The terms in the denominator account for the reaction and diffusion noise. In contrast to extrinsic stability, we here find that the front is most robust against fluctuations for strong self-activation r. The reason for this is that, as r determines the amount of reactions necessary to locally switch between the stable states, the rate of stochastic switching decreases for large r values. Explicit analytical results can be found in the Supplemental Material [27].

In conclusion, we identified conditions optimizing the stability and robustness of localized wave fronts for different types of perturbations. We find that increasing cooperativity in self-activation broadens the parameter regime where wave localization becomes possible and thereby increases the robustness of the localization mechanism. Interestingly, there is a trade-off between the stability of the wave front to extrinsic and intrinsic perturbations. While weak self-activation or low birth rates enhance the stability with respect to extrinsic perturbations, stochastic defocusing is minimized for strong self-activation. The latter also increases the spatial precision of the signal transmitted by the front to downstream processes. Moreover, we showed that processing input from external sources with a cooperative gene activation mechanism generally enhances the front's stability even far from the source. Surprisingly, while cooperativity in external activation increases the front's stability with respect to extrinsic perturbations, the opposite holds true for self-activation.

The conflict between intrinsic and extrinsic stability affects, for example, the design of gene circuits in developmental systems. Our results suggest different design principles depending on the particle number. If the number of involved particles is large, intrinsic noise is irrelevant. Then the parameters of the genetic network may be optimized for robustness against external perturbations, which is achieved by weak self-activation and strong cooperativity in external activation. Conversely, if particle numbers are low, robustness against intrinsic noise requires strong and cooperative self-activation. To also safeguard against external perturbation then requires additional mechanisms beyond those included in our simplified model. We expect these general results to be important guiding principles in the context of biological pattern-forming systems, such as cell polarization or the segmentation of embryos.

This research was supported by the German Excellence Initiative via the program "Nanosystems Initiative Munich" and the German Research Foundation via the SFB 1032 "Nanoagents for Spatiotemporal Control of Molecular and Cellular Reactions."

*frey@lmu.de

[1] B. Alberts, A. Johnson, J. Lewis, M. Raff, K. Roberts, and P. Walter, *Molecular Biology of the Cell* (Garland Science, New York, 2002), 4th ed.

[2] A. Altland, A. Fischer, J. Krug, and I. G. Szendro, Phys. Rev. Lett. **106**, 088101 (2011).

[3] P. A. Stephens, W. J. Sutherland, and R. P. Freckleton, Oikos **87**, 185 (1999).

[4] M. A. Lewis and P. Kareiva, Theor. Popul. Biol. **43**, 141 (1993).

[5] O. Diekmann and J. A. P. Heesterbeek, *Mathematical Epidemiology of Infectious Diseases: Model Building, Analysis, and Interpretation*, Wiley Series in Mathematical and Computational Biology (John Wiley, Hoboken, NJ, 2000).

[6] C. M. Taylor and A. Hastings, Ecol. Lett. **8**, 895 (2005).

[7] J. Das, M. Kardar, and A. K. Chakraborty, J. Chem. Phys. **130**, 245102 (2009).

[8] T. H. Keitt, M. A. Lewis, and R. D. Holt, Am. Nat. **157**, 203 (2001).

[9] Y. Mori, A. Jilkine, and L. Edelstein-Keshet, Biophys. J. **94**, 3684 (2008).

[10] Y. Mori, A. Jilkine, and L. Edelstein-Keshet, SIAM J. Appl. Math. **71**, 1401 (2011).

[11] W. Driever and C. Nüsslein-Volhard, Cell **54**, 95 (1988).

[12] W. Driever and C. Nüsslein-Volhard, Cell **54**, 83 (1988).

[13] F. J. P. Lopes, F. M. C. Vieira, D. M. Holloway, P. M. Bisch, and A. V. Spirov, PLoS Comput. Biol. **4**, e1000184 (2008).

[14] F. Tostevin, P. R. ten Wolde, and M. Howard, PLoS Comput. Biol. **3**, e78 (2007).

[15] R. Putman and S. D. Wratten, *Principles Of Ecology* (University of California, Berkeley, 1984).

[16] T. Czárán, *Spatiotemporal Models of Population and Community Dynamics* (Springer, New York, 1998), p. 284.

[17] B. Meerson, P. V. Sasorov, and Y. Kaplan, Phys. Rev. E **84**, 011147 (2011).

[18] M. Loose, E. Fischer-Friedrich, C. Herold, K. Kruse, and P. Schwille, Nat. Struct. Mol. Biol. **18**, 577 (2011).

[19] O. Grimm, M. Coppey, and E. Wieschaus, Development (Cambridge, U.K.) **137**, 2253 (2010).

[20] O. Wartlick, P. Mumcu, A. Kicheva, T. Bittig, C. Seum, F. Jülicher, and M. González-Gaitán, Science **331**, 1154 (2011).

[21] P. C. Tobin, S. L. Whitmire, D. M. Johnson, O. N. Bjørnstad, and A. M. Liebhold, Ecol. Lett. **10**, 36 (2007).

[22] D. S. Burz, R. Rivera-Pomar, H. Jäckle, and S. D. Hanes, EMBO J. **17**, 5998 (1998).

[23] M. Cross and H. Greenside, *Pattern Formation and Dynamics in Nonequilibrium Systems* (Cambridge University, New York, 2009).

[24] A. K. Abramyan and S. A. Vakulenko, Teor. Mat. Fiz. **155**, 678 (2008).

[25] S. Vakulenko, Manu, J. Reinitz, and O. Radulescu, Phys. Rev. Lett. **103**, 168102 (2009).

[26] One may also arrive at this equation employing a variational ansatz (Whitham principle) [24,25].

[27] See Supplemental Material at http://link.aps.org/supplemental/10.1103/PhysRevLett.110.038102 for more detailed calculations supporting the results presented in the text.

[28] This statement applies for exponential as well as sigmoidal external profiles.

[29] J. Treisman and C. Desplan, Nature (London) **341**, 335 (1989).

[30] T. Gregor, D. W. Tank, E. F. Wieschaus, and W. Bialek, Cell **130**, 153 (2007).

[31] S. Surkova, D. Kosman, K. Kozlov, Manu, E. Myasnikova, A. A. Samsonova, A. Spirov, C. E. Vanario-Alonso, M. Samsonova, and J. Reinitz, Dev. Biol. **313**, 844 (2008).

Supplementary Material

We here provide more detailed calculations yielding the results presented in the main text.

DERIVATION OF THE LOCALIZATION POSITION

We consider the reaction-diffusion equation

$$\partial_t u = f(u,x) + \partial_{xx} u\,, \tag{1}$$

with $f(u,x) \equiv rR^n_{u_0}(u) + M(x) - u$. Equation (1) admits traveling waves solutions if the potential $V(u,x) = \int^u \mathrm{d}\tilde{u}\, f(\tilde{u},x)$ exists locally. In our case we obtain

$$V(u,x) = -u\left[\frac{u}{2} - M(x) - r + F\left(\frac{u^n}{u_0^n}\right)\right], \tag{2}$$

where $F(z) \equiv {}_2F_1(1,1/n,1+1/n,-z)$ and ${}_2F_1$ is the Gauss hypergeometric function. The wave localizes if the difference in the maximum values of the potential is zero, $\Delta V(q_0) \equiv \int_{u_-}^{u^+} \mathrm{d}u\, f(u,q_0) = 0$. Using the linearized stable states $u^+(x) \approx M(x) + r$ and $u^-(x) \approx M(x)$ gives an expression for the difference between the two maximum values of the potential,

$$\Delta V(q) = V(u^+(q)) - V(u^-(q)) = \frac{1}{2}r\left[r + 2M(q)F\left(\frac{M(q)^n}{u_0^n}\right) - 2\big(M(q)+r\big)F\left(\frac{(M(q)+r)^n}{u_0^n}\right)\right]. \tag{3}$$

As ΔV is to a good approximation linear in $M(x)$ we linearize around $M(x) = 0$,

$$\Delta V(x) \approx \frac{1}{2}r\left\{r + M(x)\left[2 - \frac{2}{1+\left(\frac{r}{u_0}\right)^n}\right] - 2rF\left(\frac{r^n}{u_0^n}\right)\right\}. \tag{4}$$

The localization position q_0 is then determined by $\Delta V(q_0) = 0$. Solving this for the concentration of the external source at which the front localizes, $M(q_0)$, we find

$$M_0 \equiv M(q_0) \approx \frac{1}{2}r\left[1 + \left(\frac{r}{u_0}\right)^n\right]\left(\frac{u_0}{r}\right)^n\left[2F\left(\frac{r^n}{u_0^n}\right) - 1\right]. \tag{5}$$

To get an insight into the behavior of the front position we study the dependence of M_0 on the parameters r and u_0. To this end, we first take the derivative with respect to r,

$$\partial_r M_0 = \frac{1}{2}\left(\frac{u_0}{r}\right)^n\left[1 + n - \left(\frac{r}{u_0}\right)^n - 2nF\left(\frac{r^n}{u_0^n}\right)\right]. \tag{6}$$

For bistability the relative amplitude of self-activation r is typically greater than the activation threshold u_0. Noting that $F(z) \sim 1/z$ for $z \to \infty$ we get $\partial_r M_0 \approx 1/2$, proving that M_0 is linear in r. On the other hand, taking the derivative with respect to u_0 we get

$$\begin{aligned}\partial_{u_0} M_0 &= \frac{1}{2}\left(\frac{u_0}{r}\right)^{n-1}\left\{2\left[1 + n + \left(\frac{r}{u_0}\right)^n\right]F\left(\frac{r^n}{u_0^n}\right) - 2 - n\right\} \\ &\approx \frac{1}{2}\left(\frac{u_0}{r}\right)^{n-1}\cdot 2\left(\frac{r}{u_0}\right)^n\cdot\left(\frac{u_0}{r}\right) \\ &= 1\,,\end{aligned} \tag{7}$$

proving that M_0 is also linear in u_0. Note that although the arguments above strictly hold in the limit $n \to \infty$ we numerically found that they are valid even for small values of n. In conclusion, we showed that M_0 can be approximated by a linear function of the form $g(n)\cdot(u_0 - r/2)$, where the pre factor $g(n)$ only depends on n. By taking the limit $n \to \infty$ first, and then doing the above calculations we find that $g(n) \to 1$ for $n \to \infty$.

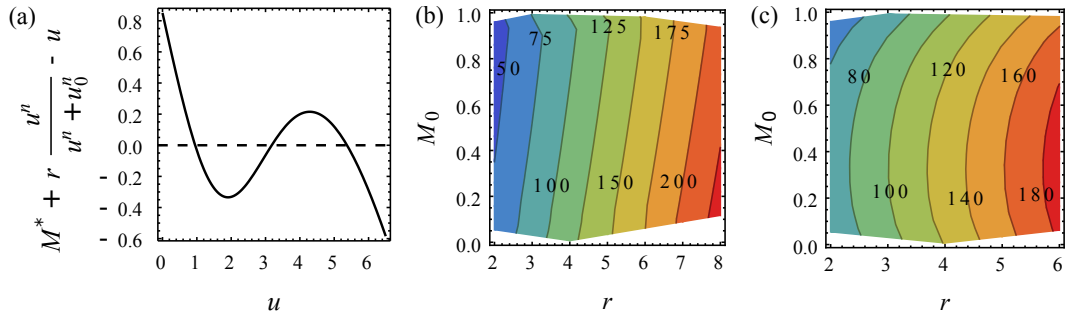

Figure 1. (Color online) (a) Illustration of the condition for bistability. There exists a bistable region in the bifurcation diagram, if for some value M^* of $M(x)$ the reaction term of Eq. (1) has three real roots. Such an M^* exists if the maximum value of the derivative of $f(u,x)$ with respect to u is greater than zero. (b) Intrinsic stability for exponential gradient. Color denotes intrinsic stability, such that red means high stability and blue means low stability. In contrast to extrinsic stability, intrinsic stability is maximized for strong self activation. (c) Qualitatively the same holds for sigmoidal gradients ($n = 5$, $m = 5$). Parameters for all plots were $\xi = 10$, $k = 0.2$.

DERIVATION OF THE PHASE DIAGRAM

Wave localization is possible if there exists a bistable region in the bifurcation diagram. We treat $M(x)$ as a parameter and investigate if $M(x)$ takes values such that the reaction term $f(u,x)$ has three real roots. Such a value for $M(x)$ exists, if the maximum value of the derivative of $f(u,x)$ is greater than zero, $\max_u \partial_u f(u,x) > 0$. For an illustration, see Fig. 1 (a). The reaction term is steepest at the steepest point of the Hill function, which is given by

$$u^* = \left(\frac{n-1}{n+1}\right)^{1/n} u_0\,. \tag{8}$$

From $\partial_u f(u,x)|_{u=u^*} \geq 0$ we obtain a first condition for the parameters, which allow the localizetion of wave fronts,

$$\frac{u_0}{r} \leq \frac{n^2-1}{4n}\left(\frac{n+1}{n-1}\right)^{1/n}. \tag{9}$$

Further conditions can be obtained by the constrains on $M(x)$ given by the definition of the model, namely $0 < M(x) \leq 1$. The range of parameters is bounded below by the condition $M_0 > 0$. Inverting Eq. (5) we obtain $u_0/r \geq \left[-F^{-1}(1/2)\right]^{-1/n}$, where $F^{-1}(1/2)$ denotes the inverse of F evaluated at the point $1/2$. From above the range of parameters is approximately bounded by $u_0/r \leq 1/2 + 1/r$.

STABILITY TO EXTRINSIC PERTURBATIONS

In the following we present analytical results for two important cases of spatial inhomogeneities by making use of the approximate expressions for the stable states, $u^+(x)$ and $u^-(x)$. As an ansatz for the stationary solution of Eq. (1) we assume a connection of the stable states as shown in Fig. 1 (b),

$$U(x-q) = M(x) + r\begin{cases} 1-\frac{1}{2}e^{x-q} & (x<q) \\ \frac{1}{2}e^{-(x-q)} & (x\geq q)\end{cases}, \tag{10}$$

which is a good approximation for n is not too small. For exponential external profiles we assume that $M(x)$ is constant for negative values of x. As a result negative values of x do not contribute to the integrals. For large ξ we obtain for the stability to external perturbations

$$\sigma_e \approx \frac{-8rM_0\left[M_0^n - (r+M_0)^n\right]u_0^n}{\left(4+r^2\xi+16rM_0\right)\left(M_0^n+u_0^n\right)\left[(r+M_0)^n+u_0^n\right]}.$$

For sigmoidal gradients, after expanding the integrand in to first order in ξ^{-1}, we obtain

$$\sigma_s \approx \frac{-4m\big(\tilde{k}-M_0\big)M_0\left[M_0^n - (r+M_0)^n\right]u_0^n}{\Big[(\tilde{k}-1)m+\tilde{k}r\xi\Big]\left(M_0^n+u_0^n\right)\left[(r+M_0)^n+u_0^n\right]}.$$

In both cases, $\sigma > 0$ such that q_0 is a stable fixed point. For large ξ, the extrinsic stability decreases linearly with ξ^{-1} ($\sigma_e \sim \xi^{-1}$, $\sigma_s\ m\xi^{-1}$), and ξ^{-1} is a measure for the steepness of the external source.

SENSITIVITY WITH RESPECT TO CHANGES IN THE POSITIONAL SIGNAL

The localized front might be subject to perturbations in the positional signal $M(x)$. In the context of embryogenesis one can argue that the front should be insensible to these changes. In the following we investigate the properties of this kind of stability. We show that the optimal parameters for the extrinsic stability also optimize the front's insensitivity with respect to perturbations in the positional signal.

Intuitively two points become immediately clear:

- Firstly, perturbations in the driving signal that are outside the front region do not affect the front position. They merely result in a change in the shape of the front profile. Hence, the front position q_0 can only be shifted due to changes in the concentration of the external signal at position q_0. In other words, $q_0[M(x)] \equiv \int_0^1 M^{-1}(m)\delta(m - M_0)dm \equiv q_0(M_0)$.
- Secondly, the front position depends strongly on changes in M(x) if M(x) is shallow at the localization position. On the other hand, if the driving signal is steep at the front position, perturbations will only have a small effect on the front position.

Hence, the influence of perturbations in the external signal on the front position is described by $\left.\frac{\mathrm{d}q_0(M)}{\mathrm{d}M}\right|_{M_0}$. This can also be seen by evaluating the variation of q_0 with respect to $M(x)$.

Stability of the front with respect to changes in $M(x)$ implies that the front averages out perturbations in the external signal. We therefore investigate the inverse of the magnitude of change in the front position in response to a change in the driving signal, $\left.\left|\left(\frac{\mathrm{d}q(M)}{\mathrm{d}M}\right)^{-1}\right|\right|_{M_0}$. This expression is equal to $\left.\left|\frac{\mathrm{d}M(q)}{\mathrm{d}q}\right|\right|_{q_0}$, the insensitivity to perturbations in the external signal is given by the steepness of the external signal at the localization position. As demonstrated by Eq. (5) extrinsic stability as defined in the manuscript also depends on the signal's steepness. We therefore expect that properties of Eq. (5), which are independent of the front profile, translate into properties for the tracking of the positional signal. This is indeed the case. As shown in Fig. 2 (a) and (b) insensitivity is optimal for $M_0 = 1$ and $M_0 = 1/2$ for exponential gradients and sigmoidal gradients, respectively. In both cases, insensitivity is indifferent to changes in the parameters r or n.

In conclusion, optimality in sigma implies optimality in the insensitivity to changes in the external signal.

STABILITY WITH RESPECT TO INTRINSIC NOISE

As each biological system intrinsic noise naturally arises due to the finite number of particles and the stochastic nature of interactions. As a result, the front fluctuates around its equilibrium position. One can therefore formally assign a diffusion constant D_f to the fluctuating front. Comparing the front's diffusion constant with the particles' diffusion constant gives a measure for the stability to intrinsic noise. Several ways exist to calculate D_f. Following the steps in Ref. [17] we may employ a generalized traveling wave ansatz and obtain an expression for the front's stability with respect to intrinsic noise,

$$\frac{D}{D_f} = N \left.\frac{\left[\int_{-\infty}^{\infty} \mathrm{d}x\,(U')^2\right]^2}{\int_{-\infty}^{\infty} \mathrm{d}x\left[\frac{1}{2}(U')^2\left(R^n_{u_0}(U) + M(x) + U\right) + U(U'')^2\right]}\right|_{q=q_0}. \tag{11}$$

where U is a stationary solution of Eq. (1) and we omitted the explicit dependence on x in the notation for the stationary solution U. Using $M(q_0) \approx u_0 - r/2$ we find that $u^n/(u_0^n + u^n)$ evaluates to 1 for $q < q_0$ and 0 for $q > q_0$. Hence, $f(U, x) + \partial_{xx}U = \partial_{xx}M(x) \sim \xi^{-2} \approx 0$. This confirms that U is an approximate stationary solution of Eq. (1).

The only problematic integral involved in Eq. (11) is $\int_{-\infty}^{\infty} \mathrm{d}x\,(U')^2 R^n_{u_0}(U)$. If n is sufficiently large we see that $R^n_{u_0}(U)$ is small for $U > u_0$. Further, we note that $U(q_0, q_0) = M(q_0) + r/2$. By using the approximate expression for the localization position, $M(q_0) \approx u_0 - r/2$, we find that $U(q_0, q_0) \approx u_0$. Hence, we can rewrite the integral as

$$\left.\int_{-\infty}^{\infty} \mathrm{d}x\,(U')^2 R^n_{u_0}(U)\right|_{q=q_0} \approx \int_{-\infty}^{q_0} \mathrm{d}x\,(U')^2\,. \tag{12}$$

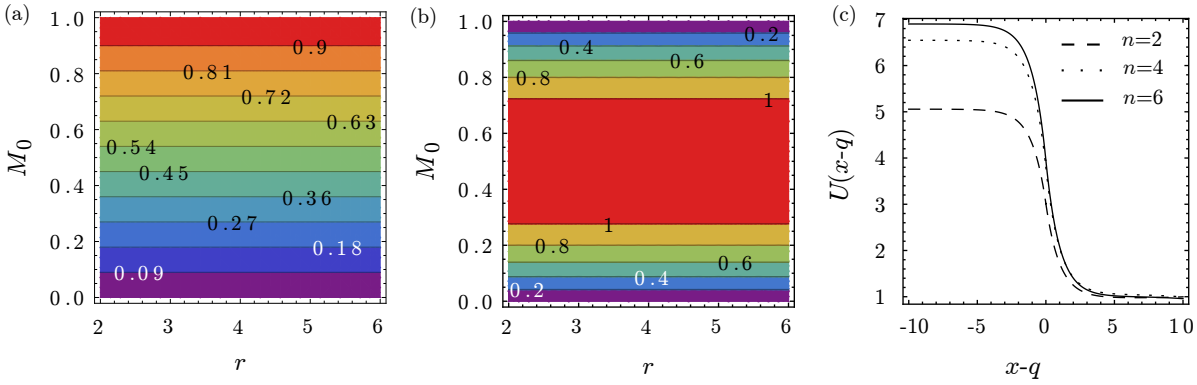

Figure 2. (a) Insensitivity $\xi \left|\left(\, \mathrm{d}q(M)/\,\mathrm{d}M\,\right)^{-1}\right|_{M_0}$ normalized to the steepness of the external source. Color is chosen, such that red denotes a high insensitivity and blue a low insensitivity. The numbers denote the values on the lines of equal insensitivity. For exponential sources the optimal value for M_0 is 1, in correspondence to the results for the relaxation rate. Insensitivity is indifferent to the specific choice of r ($n = 5$, $\xi = 10$). (b) For sigmoidal gradients the optimal value of M_0 is 1/2 ($n = 5$, $\xi = 10$, $m = 5$, $k = 0.5$). (c) Stationary solutions for different values of n for sigmoidal gradients ($r = 6$, $u_0 = 3.5$, $m = 5$, $k = 0.2$, $\xi = 10$). The steepness of the front increases with the degree of cooperative binding.

For exponentially decreasing external sources the analytical result can be brought to a short form by only keeping the dominant terms in ξ,

$$\frac{D}{D_f} \approx \frac{3Nr^2\left(4 + r^2\xi + 16rM_0\right)}{2\left\{8 + 12r + 5r^3\xi + 6rM_0\left[r(7+\xi) + 6M_0\right]\right\}}.$$

For sigmoidal profiles, we expand $M(x)$ to first order in ξ^{-1}, $M(x) \approx 1 - \frac{k^m m x}{\xi(1+k^m)}$. We can now perform the integrals in (11) analytically and obtain

$$\frac{D}{D_f} \approx \frac{3N(8(\tilde{k}-1)m + \tilde{k}r\xi)^2}{2\tilde{k}\xi^2\left[\tilde{k}\,(6+5r) - 6(\tilde{k}-1)\ln\left(\frac{\tilde{k}-M_0}{(\tilde{k}-1)M_0}\right)\right]}.$$

In both cases we find a linear increase in stability to intrinsic noise with the relative amplitude of self-activation, r. Figure 1 (b) and (c) show the results of the numerical evaluation of Eq. (11). It confirms the linear increase of stability with r.

STEEPNESS OF THE FRONT

In some applications, for example in Drosophila embryogenesis, the steepness of the front itself is an important quantity. Starting from the stationary solution, Eq. (10), we find that the steepness of the front is given in dimensional form by

$$k_M M'(q_0) - \frac{k_r}{2k_M}\sqrt{\frac{\lambda}{D}}.$$

Hence, three factors determine the steepness of the front. Firstly, the steepness of the front is increased, when the amplitude of internal activation compared to external estivation is strong. Secondly, a high degradation rate and a small diffusion constant result in steep fronts. Last, the steepness of the external source at the front position is important. The dependence of the front's steepness on the binding coperativity is not captured by the stationary solution, as it is the result of a large n expansion. Here, nonlinear corrections to the linear approximation of the stable states have the effect, that for small n the front becomes shallower, as demonstrated in Fig. 2 (c).

The front's steepness effects extrinsic and intrinsic stability in different ways. Generally, steep fronts move slower, as demonstrated by Eq. (3) in the main text. The reason for this is, that as, opposed to shallow fronts, for steep fronts the total rate of reactions moving the front forward is lower. As a result, steep front also relax back to their equilibrium position more slowly and are therefore less stable to extrinsic perturbations.

On the other hand, steep fronts are less susceptible to intrinsic fluctuations, as demonstrated by Eq. (11). Intuitively this becomes clear if one notes that for stochastic switching to happen, an entropy barrier between the stable states has to be overcome. Hence, the rate of stochastic switching increases, if this barrier is low. This is the case for shallow fronts. where due to diffusion or properties of the bifurcation diagram the entropy barrier is decreased on a larger portion of the front.

Bibliography

[1] B. Alberts, A. Johnson, J. Lewis, M. Raff, K. Roberts, and P. Walter, *Molecular Biology of the Cell*, Garland Science, New York, 4 edition, 2002.

[2] J. Gerhart and M. Kirschner, *Cells, Embryos and Evolution*, Wiley, Hoboken, 1997.

[3] F. Tostevin, P. R. ten Wolde, and M. Howard, Fundamental limits to position determination by concentration gradients., PloS Comput. Biol. **3**, e78 (2007).

[4] T. Gregor, D. W. Tank, E. F. Wieschaus, and W. Bialek, Probing the limits to positional information., Cell **130**, 153 (2007).

[5] W. Driever and C. Nüsslein-Volhard, The bicoid protein determines position in the Drosophila embryo in a concentration-dependent manner, Cell **54**, 95 (1988).

[6] W. Driever and C. Nüsslein-Volhard, A gradient of bicoid protein in Drosophila embryos, Cell **54**, 83 (1988).

[7] O. Grimm, M. Coppey, and E. Wieschaus, Modelling the Bicoid gradient, Development **137**, 2253 (2010).

[8] A. Goldbeter, D. Gonze, and O. Pourquié, Sharp developmental thresholds defined through bistability by antagonistic gradients of retinoic acid and FGF signaling., Dev. Dynam. **236**, 1495 (2007).

[9] J. Treisman and C. Desplan, The products of the Drosophila gap genes hunchback and Krüppel bind to the hunchback promoters., Nature **341**, 335 (1989).

[10] D. S. Burz, R. Rivera-Pomar, H. Jäckle, and S. D. Hanes, Cooperative DNA-binding by Bicoid provides a mechanism for threshold-dependent gene activation in the Drosophila embryo., EMBO J, **17**, 5998 (1998).

[11] J. Reinitz, S. Hou, and D. Sharp, Transcriptional Control in Drosophila.

[12] F. J. P. Lopes, F. M. C. Vieira, D. M. Holloway, P. M. Bisch, and A. V. Spirov, Spatial Bistability Generates hunchback Expression Sharpness in the Drosophila Embryo, PloS Comput. Biol. **4**, e1000184 (2008).

[13] S. Vakulenko, Manu, J. Reinitz, and O. Radulescu, Size Regulation in the Segmentation of Drosophila: Interacting Interfaces between Localized Domains of Gene Expression Ensure Robust Spatial Patterning, Phys. Rev. Lett. **103**, 168102 (2009).

[14] M. W. Perry, J. P. Bothma, R. D. Luu, and M. Levine, Precision of Hunchback Expression in the Drosophila Embryo., Curr. Biol. **22**, 2247 (2012).

[15] S. Rulands, B. Klünder, and E. Frey, Stability of Localized Wave Fronts in Bistable Systems, Phys. Rev. Lett. **110**, 038102 (2013).

[16] Wikipedia.

[17] Y. Sasai, Cytosystems dynamics in self-organization of tissue architecture., Nature **493**, 318 (2013).

[18] T. M. Scanlon, K. K. Caylor, S. A. Levin, and I. Rodriguez-Iturbe, Positive feedbacks promote power-law clustering of Kalahari vegetation., Nature **449**, 209 (2007).

[19] V. Torsvik, J. Goksø yr, and F. L. Daae, High diversity in DNA of soil bacteria., Appl. Environ. Microbiol. **56**, 782 (1990).

[20] G. E. Hutchinson, The Paradox of the Plankton, Am. Nat. **95**, 137 (1961).

[21] S. Levin, Dispersion and Population Interactions, Am. Nat. **108**, 207 (1974).

[22] R. Durrett and S. Levin, The Importance of Being Discrete (and Spatial), Theor. Pop. Biol. **46**, 363 (1994).

[23] B. Sinervo and C. M. Lively, The rock-scissors-paper game and the evolution of alternative male strategies, Nature **380**, 240 (1996).

[24] R. Durrett and S. Levin, Allelopathy in Spatially Distributed Populations, J. Theor. Biol. **185**, 165 (1997).

[25] R. Durrett and S. Levin, Spatial Aspects of Interspecific Competition, Theor. Pop. Biol. **53**, 30 (1998).

[26] B. Kerr, M. A. Riley, M. W. Feldman, and B. J. Bohannan, Local dispersal promotes biodiversity in a real-life game of rock-paper-scissors., Nature **418**, 171 (2002).

[27] B. Kerr, The Ecological and Evolutionary Dynamics of Model Bacteriocin Communities, in *Bacteriocins*, edited by M. A. Riley and M. A. Chavan, pages 111–134, Springer, New York, 2007.

[28] T. Reichenbach, M. Mobilia, and E. Frey, Mobility promotes and jeopardizes biodiversity in rock-paper-scissors games., Nature **448**, 1046 (2007).

[29] T. Reichenbach, M. Mobilia, and E. Frey, Noise and Correlations in a Spatial Population Model with Cyclic Competition, Phys. Rev. Lett. **99**, 238105 (2007).

[30] T. Reichenbach, M. Mobilia, and E. Frey, Self-organization of mobile populations in cyclic competition, J. Theor. Biol **254**, 368 (2008).

[31] J. Knebel, T. Krüger, M. F. Weber, and E. Frey, Coexistence and Survival in Conservative Lotka-Volterra Networks, Phys. Rev. Lett. **110**, 0168106 (2013).

[32] L. Boltzmann, *Theoretical physics and philosophical problems: selected writings*, volume 1974, KLUWER ACADEMIC, 1974.

[33] C. Gardiner, *Handbook of Stochastic Methods*, Springer-Verlag, 2004.

[34] N. G. van Kampen, *Stochastic Processes in Physics and Chemistry*, Elsevier, Amsterdam, third edit edition, 2007.

[35] M. Cross and H. Greenside, *Pattern formation and dynamics in nonequilibrium systems*, Cambridge University Press, New York, 2009.

[36] H. Hinrichsen, Non-equilibrium critical phenomena and phase transitions into absorbing states, Adv. Phys. **49**, 815 (2000).

[37] M. Smoluchowski, Drei Vorträge über Diffusion, Brownsche Molekularbewegung und Koagulation von Kolloidteilchen, Physik. Zeit. **17**, 557 (1916).

[38] M. V. Smoluchowski, Versuch einer mathematischen Theorie der Koagulationskinetic kolloider Lösungen, Z. Phys. Chem. **92** (1917).

[39] J. F. C. Kingman, The coalescent, Stochastic Processes Appl. **13**, 235 (1982).

[40] J. F. C. Kingman, Origins of the Coalescent 1974-1982, Genetics (2000).

[41] E. Brunet, B. Derrida, and D. Simon, Universal tree structures in directed polymers and models of evolving populations, arXiv **cond-mat.d** (2008).

[42] S. Tavare, D. J. Balding, R. C. Griffiths, and P. Donnelly, Inferring Coalescence Times From DNA Sequence Data, Genetics (1997).

[43] J. Wakeley, Coalescent Theory, Book (2009).

[44] R. A. Fisher, The Wave of Advance of Advantageous Genes, Annals of Eugenics **7** (1937).

[45] W. van Saarlos, Front propagation into unstable states, Phys. Rep. **386**, 29 (2003).

[46] K. I. Tainaka, Vortices and strings in a model ecosystem, Phys. Rev. E **50**, 3401 (1994).

[47] K. I. Tainaka, Stationary pattern of vortices or strings in biological systems: Lattice version of the Lotka-Volterra model, Phys. Rev. Lett. **63**, 2688 (1989).

[48] M. Mobilia, Oscillatory dynamics in rock-paper-scissors games with mutations., J. Theor. Biol. **264**, 1 (2010).

[49] X. Ni, W.-X. Wang, Y.-C. Lai, and C. Grebogi, Cyclic competition of mobile species on continuous space: Pattern formation and coexistence, Phys. Rev. E **82**, 066211 (2010).

[50] A. Traulsen, J. C. Claussen, and C. Hauert, Stochastic differential equations for evolutionary dynamics with demographic noise and mutations, Phys. Rev. E **85**, 041901 (2012).

[51] M. Berr, T. Reichenbach, M. Schottenloher, and E. Frey, Zero-One Survival Behavior of Cyclically Competing Species, Phys. Rev. Lett. **102**, 048102 (2009).

[52] B. Andrae, J. Cremer, T. Reichenbach, and E. Frey, Entropy Production of Cyclic Population Dynamics, Phys. Rev. Lett. **104**, 218102 (2010).

[53] T. Reichenbach and E. Frey, Bacterial Games, in *Principles of Evolution: From the Planck Epoch to Complex Multicellular Life*, Springer, New York, 2011.

[54] A. Roman, D. Konrad, and M. Pleimling, Cyclic competition of four species: domains and interfaces, J. Stat. Mech. **2012**, P07014 (2012).

[55] J. C. Claussen and A. Traulsen, Cyclic Dominance and Biodiversity in Well-Mixed Populations, Phys. Rev. Lett. **100**, 058104 (2008).

[56] Q. He, M. Mobilia, and U. C. Täuber, Spatial rock-paper-scissors models with inhomogeneous reaction rates, Phys. Rev. E **82**, 051909 (2010).

[57] Q. He, U. C. Täuber, and R. K. P. Zia, On the relationship between cyclic and hierarchical three-species predator-prey systems and the two-species Lotka-Volterra model, Eur. Phys. J. B **85**, 141 (2012).

[58] A. Dobrinevski and E. Frey, Extinction in neutrally stable stochastic Lotka-Volterra models, Phys. Rev. E **85**, 051903 (2012).

[59] L. Frachebourg, P. L. Krapivsky, and E. Ben-Naim, Spatial organization in cyclic Lotka-Volterra systems, Phys. Rev. E **54**, 6186 (1996).

[60] S. Venkat and M. Pleimling, Mobility and asymmetry effects in one-dimensional rock-paper-scissors games, Phys. Rev. E **81**, 21917 (2010).

[61] T. Reichenbach, M. Mobilia, and E. Frey, Coexistence versus extinction in the stochastic cyclic Lotka-Volterra model, Phys. Rev. E **74**, 051907 (2006).

[62] A. P. O. Müller and J. A. C. Gallas, How community size affects survival chances in cyclic competition games that microorganisms play, Phys. Rev. E **82**, 052901 (2010).

[63] Q. He, M. Mobilia, and U. C. Täuber, Coexistence in the two-dimensional May-Leonard model with random rates, Eur. Phys. J. B **82**, 97 (2011).

[64] L.-L. Jiang, T. Zhou, M. Perc, and B.-H. Wang, Effects of competition on pattern formation in the rock-paper-scissors game, Phys. Rev. E **84**, 021912 (2011).

[65] P. P. Avelino, D. Bazeia, L. Losano, J. Menezes, and B. F. Oliveira, Junctions and spiral patterns in generalized rock-paper-scissors models, Phys. Rev. E **86**, 036112 (2012).

[66] T. Reichenbach and E. Frey, Instability of Spatial Patterns and Its Ambiguous Impact on Species Diversity, Phys. Rev. Lett. **101**, 058102 (2008).

[67] D. Lamouroux, S. Eule, T. Geisel, and J. Nagler, Discriminating the effects of spatial extent and population size in cyclic competition among species, Phys. Rev. E **86**, 021911 (2012).

[68] Q. He, M. Mobilia, and U. C. Täuber, Coexistence in the two-dimensional May-Leonard model with random rates, Eur. Phys. J. B **82**, 97 (2011).

[69] S. Rulands, T. Reichenbach, and E. Frey, Threefold way to extinction in populations of cyclically competing species, J. Stat. Mech. **2011**, L01003 (2011).

[70] M. Peltomaki and M. Alava, Three- and four-state rock-paper-scissors games with diffusion, Phys. Rev. E **78**, 31906 (2008).

[71] R. M. May and W. J. Leonard, Nonlinear Aspects of Competition Between Three Species, SIAM J. Appl. Math. **29**, 243 (1975).

[72] T. Reichenbach and E. Frey, Instability of spatial patterns and its ambiguous impact on species diversity, Phys. Rev. Lett. (2008).

[73] S. Rulands, A. Zielinski, and E. Frey, Global attractors and extinction dynamics of cyclically competing species, Phys. Rev. E **87**, 052710 (2013).

[74] P. J. Brockert, S. A. Lachke, T. Srikantha, C. Pujol, R. Galask, and D. R. Soll, Phenotypic Switching and Mating Type Switching of Candida glabrata at Sites of Colonization, Infect Immun. **71**, 7109 (2003).

[75] N. Q. Balaban, J. Merrin, R. Chait, L. Kowalik, and S. Leibler, Bacterial persistence as a phenotypic switch., Science (New York, N.Y.) **305**, 1622 (2004).

[76] W. K. Smits, O. P. Kuipers, and J.-W. Veening, Phenotypic variation in bacteria: the role of feedback regulation., Nature reviews. Microbiology **4**, 259 (2006).

[77] A. M. Porman, K. Alby, M. P. Hirakawa, and R. J. Bennett, Discovery of a phenotypic switch regulating sexual mating in the opportunistic fungal pathogen Candida tropicalis., Proc. Nat. Acad. Sci. USA **108**, 21158 (2011).

[78] D. W. Whitman and A. A. Agrawal, What is Phenotypic Plasticity and Why is it important?, in *Phenotypic Plasticity of Insects: Mechanisms and Consequences*, edited by D. Whitman and T. Ananthakrishnan, pages 1–63, Science Publishers, 2009.

[79] S. A. Lachke, S. Joly, K. Daniels, and D. R. Soll, Phenotypic switching and filamentation in Candida glabrata., Microbiol. **148**, 2661 (2002).

[80] J.-W. Veening, W. K. Smits, and O. P. Kuipers, Bistability, epigenetics, and bet-hedging in bacteria., Ann. Rev. Microbiol. **62**, 193 (2008).

[81] O. Gefen and N. Q. Balaban, The importance of being persistent: heterogeneity of bacterial populations under antibiotic stress., FEMS Microbiol. Rev. **33**, 704 (2009).

[82] I. Tirosh, N. Barkai, and K. J. Verstrepen, Promoter architecture and the evolvability of gene expression., Journal of biology **8**, 95 (2009).

[83] D. R. Soll, High-frequency switching in Candida albicans., Clin. Microbiol. Rev. **5**, 183 (1992).

[84] D. Dubnau and R. Losick, Bistability in bacteria., Mol. Microbiol. **61**, 564 (2006).

[85] J. Stricker, S. Cookson, M. R. Bennett, W. H. Mather, L. S. Tsimring, and J. Hasty, A fast, robust and tunable synthetic gene oscillator, Nature **456**, 516 (2008).

[86] M. Leisner, K. Stingl, E. Frey, and B. Maier, Stochastic switching to competence., Curr. Opin. Microbiol. **11**, 553 (2008).

[87] J. Chen and Y.-M. Deng, Influenza virus antigenic variation, host antibody production and new approach to control epidemics., Virol. J. **6**, 30 (2009).

[88] M. W. van der Woude and A. J. Bäumler, Phase and antigenic variation in bacteria., Clin. Microbiol. Rev. **17**, 581 (2004).

[89] A. J. Wolfe and K. L. Visick, Get the message out: cyclic-Di-GMP regulates multiple levels of flagellum-based motility., J. Bacteriol. **190**, 463 (2008).

[90] B. Ramírez-Zavala, O. Reuss, Y.-N. Park, K. Ohlsen, and J. Morschhäuser, Environmental induction of white-opaque switching in Candida albicans., PLoS Pathog. **4**, e1000089 (2008).

[91] M. Leisner, K. Stingl, J. O. Rädler, and B. Maier, Basal expression rate of comK sets a 'switching-window' into the K-state of Bacillus subtilis., Mol. Microbiol. **63**, 1806 (2007).

[92] M. A. Schumacher, K. M. Piro, W. Xu, S. Hansen, K. Lewis, and R. G. Brennan, Molecular mechanisms of HipA-mediated multidrug tolerance and its neutralization by HipB., Science (New York, N.Y.) **323**, 396 (2009).

[93] M. Leisner, J.-T. Kuhr, J. O. Rädler, E. Frey, and B. Maier, Kinetics of genetic switching into the state of bacterial competence., Biophys. J. **96**, 1178 (2009).

[94] D. B. Kearns and R. Losick, Cell population heterogeneity during growth of Bacillus subtilis., Genes Dev. **19**, 3083 (2005).

[95] P. B. Rainey, H. J. E. Beaumont, G. C. Ferguson, J. Gallie, C. Kost, E. Libby, and X.-X. Zhang, The evolutionary emergence of stochastic phenotype switching in bacteria., Microb. Cell Fact. **10 Suppl 1**, S14 (2011).

[96] M. G. Miller and A. D. Johnson, White-Opaque Switching in Candida albicans Is Controlled by Mating-Type Locus Homeodomain Proteins and Allows Efficient Mating, Cell **110**, 293 (2002).

[97] H. S. Moyed and K. P. Bertrand, hipA, a newly recognized gene of Escherichia coli K-12 that affects frequency of persistence after inhibition of murein synthesis., J. Bacteriol. **155**, 768 (1983).

[98] A. M. Walczak and G. Tkačik, Information transmission in genetic regulatory networks: a review, page 31 (2011).

[99] A. Buckling, F. Harrison, M. Vos, M. A. Brockhurst, A. Gardner, S. A. West, and A. Griffin, Siderophore-mediated cooperation and virulence in Pseudomonas aeruginosa., FEMS Microbiol. Ecol. **62**, 135 (2007).

[100] A. M. Turing, The Chemical Basis of Morphogenesis, Philos. T. Roy. Soc. B **237**, 37 (1952).

[101] G. Hardin, The Competitive Exclusion Principle, Science **131**, 1292 (1960).

[102] B. Sinervo, Lizardland.

[103] Y. Itoh, The Boltzmann equation on some algebraic structure concerning struggle for existence, Proc. Jpn. Acad. **47**, 854 (1971).

[104] M. Frean and E. R. Abraham, Rock-scissors-paper and the survival of the weakest, Proc. R. Soc. **268**, 1323 (2001).

[105] J. Cremer, *Evolutionary Dynamics of Finite Populations*, Diploma thesis, Ludwigs-Maximilians Universität, 2008.

[106] K. I. Tainaka, Lattice Model for the Lotka-Volterra System, J. Phys. Soc. Jpn. **57**, 2588 (1988).

[107] L. Frachebourg, P. L. Krapivsky, and E. Ben-Naim, Segregation in a one-dimensional model of interacting species, Phys. Rev. Lett. **77**, 2125 (1996).

[108] T. L. Czárán, R. F. Hoekstra, and L. Pagie, Chemical warfare between microbes promotes biodiversity., Proc. Nat. Acad. Sci. USA **99**, 786 (2002).

[109] A. A. Winkler, T. Reichenbach, and E. Frey, Coexistence in a one-dimensional cyclic dominance process, Phys. Rev. E **81**, 60901 (2010).

[110] E. Frey, Evolutionary game theory: Theoretical concepts and applications to microbial communities, Physica A **389**, 4265 (2010).

[111] B. Szczesny, M. Mobilia, and A. M. Rucklidge, When does cyclic dominance lead to stable spiral waves?, Europhys. Lett. **102**, 28012 (2013).

[112] U. Dobramysl and U. C. Täuber, Spatial Variability Enhances Species Fitness in Stochastic Predator-Prey Interactions, Phys. Rev. Lett. **101**, 258102 (2008).

[113] A. J. Lotka, Undamped oscillations derived from the law of mass action, J. Am. Chem. Soc. **42**, 1595 (1920).

[114] V. Volterra, Variazioni e fluttuazioni del numero d'individui in specie animali conviventi, Mem. Accad. Lincei **2**, 31 (1926).

[115] R. P. Boland, T. Galla, and A. J. McKane, Limit cycles, complex Floquet multipliers, and intrinsic noise, Phys. Rev. E **79**, 51131 (2009).

[116] M. Parker and A. Kamenev, Extinction in the Lotka-Volterra model, Phys. Rev. E **80**, 21129 (2009).

[117] P. Szabó, T. Czárán, and G. Szabó, Competing associations in bacterial warfare with two toxins., J. Theor. Biol. **248**, 736 (2007).

[118] G. Szabó, A. Szolnoki, and I. Borsos, Self-organizing patterns maintained by competing associations in a six-species predator-prey model, Phys. Rev. E **77**, 041919 (2008).

[119] N. Mitarai, J. Mathiesen, and K. Sneppen, Emergence of diversity in a model ecosystem, Phys. Rev. E **86**, 011929 (2012).

[120] J. Mathiesen, N. Mitarai, K. Sneppen, and A. Trusina, Ecosystems with Mutually Exclusive Interactions Self-Organize to a State of High Diversity, Phys. Rev. Lett. **107**, 188101 (2011).

[121] R. Abta, M. Schiffer, and N. M. Shnerb, Amplitude-dependent frequency, desynchronization, and stabilization in noisy metapopulation dynamics, Phys. Rev. Lett. **98**, 98104 (2007).

[122] R. Abta and N. M. Shnerb, Angular velocity variations and stability of spatially explicit prey-predator systems, Phys. Rev. E **75**, 51914 (2007).

[123] C. Lugo and A. McKane, Quasicycles in a spatial predator-prey model, Phys. Rev. E **78**, 051911 (2008).

[124] T. Butler and N. Goldenfeld, Robust ecological pattern formation induced by demographic noise, Phys. Rev. E **80**, 030902 (2009).

[125] J. C. C. A. Traulsen and C. Hauert, Coevolutionary Dynamics: From Finite to Infinite Populations, Phys. Rev. Lett. **95**, 238701 (2005).

[126] M. B. Elowitz, A. J. Levine, E. D. Siggia, and P. S. Swain, Stochastic gene expression in a single cell., Science **297**, 1183 (2002).

[127] W. J. Blake, M. KAErn, C. R. Cantor, and J. J. Collins, Noise in eukaryotic gene expression., Nature **422**, 633 (2003).

[128] R. E. Michod, M. F. Wojciechowski, and M. A. Hoelzer, DNA Repair and the Evolution of Transformation in the Bacterium Bacillus subtilis, Genetics **118**, 31 (1988).

[129] R. M. May, *Stability and Complexity in Model Ecosystems*, Princeton University Press, Princeton, 2001.

[130] D. Mollison, Spatial contact models for ecological and epidemic spread, J. Roy. Stat. Soc. B , 283 (1977).

[131] O. Hallatschek, P. Hersen, S. Ramanathan, and D. R. Nelson, Genetic drift at expanding frontiers promotes gene segregation, Proc. Natl. Acad. Sci. USA **104**, 19926 (2007).

[132] O. Hallatschek and D. R. Nelson, Gene surfing in expanding populations, Theoretical Population Biology **73**, 158 (2008).

[133] K. S. Korolev, M. Avlund, O. Hallatschek, and D. R. Nelson, Genetic demixing and evolution in linear stepping stone models, Rev. Mod. Phys. **82**, 1691 (2010).

[134] D. Panja, Effects of fluctuations on propagating fronts, Phys. Rep. **393**, 87 (2004).

[135] J. Hofbauer and K. Sigmund, Evolutionary Games and Population Dynamics, Cambridge UP (1998).

[136] G. Szabó and C. Hauert, Phase Transitions and Volunteering in Spatial Public Goods Games, Phys. Rev. Lett. **89**, 118101 (2002).

[137] G. Szabó, J. Vukov, and A. Szolnoki, Phase diagrams for an evolutionary prisoner's dilemma game on two-dimensional lattices, Phys. Rev. E **72**, 047107 (2005).

[138] G. Szabó and C. Töke, Evolutionary prisoner's dilemma game on a square lattice, Phys. Rev. E **58**, 69 (1998).

[139] A. Gelimson, J. Cremer, and E. Frey, Mobility, fitness collection, and the breakdown of cooperation, Phys. Rev. E **87**, 042711 (2013).

[140] A. Altland, A. Fischer, J. Krug, and I. G. Szendro, Rare Events in Population Genetics: Stochastic Tunneling in a Two-Locus Model with Recombination, Phys. Rev. Lett. **106**, 88101 (2011).

[141] P. A. Stephens, W. J. Sutherland, and R. P. Freckleton, What Is the Allee Effect?, Oikos **87**, 185 (1999).

[142] M. A. Lewis and P. Kareiva, Allee Dynamics and the Spread of Invading Organisms, Theor. Popul. Biol. **43**, 141 (1993).

[143] O. Diekmann and J. A. P. Heesterbeek, *Mathematical epidemiology of infectious diseases: model building, analysis, and interpretation*, Wiley series in mathematical and computational biology, John Wiley, Hoboken, 2000.

[144] C. M. Taylor and A. Hastings, Allee effects in biological invasions, Ecol. Lett. **8**, 895 (2005).

[145] T. H. Keitt, M. A. Lewis, and R. D. Holt, Allee effects, invasion pinning, and species' borders., Am. Nat. **157**, 203 (2001).

[146] Y. Mori, A. Jilkine, and L. Edelstein-Keshet, Wave-pinning and cell polarity from a bistable reaction-diffusion system, Biophys. J. **94**, 3684 (2008).

[147] Y. Mori, A. Jilkine, and L. Edelstein-Keshet, Asymptotic and bifurcation analysis of wave-pinning in a reaction-diffusion model for cell polarization, SIAM J. Appl. Math. **71**, 1401 (2011).

[148] R. Putman and S. D. Wratten, *Principles Of Ecology*, University of California Press, Berkeley, 1984.

[149] T. Czárán, *Spatiotemporal Models of Population and Community Dynamics*, Springer, New York, 1998.

[150] B. Meerson, P. Sasorov, and Y. Kaplan, Velocity fluctuations of population fronts propagating into metastable states, Phys. Rev. E **84**, 011147 (2011).

[151] M. Loose, E. Fischer-Friedrich, C. Herold, K. Kruse, and P. Schwille, Min protein patterns emerge from rapid rebinding and membrane interaction of MinE., Nat. Struct. Mol. Biol. **18**, 577 (2011).

[152] S. Wiggins, *Introduction to Applied Nonlinear Dynamical Systems and Chaos*, Springer, Berlin, 1990.

[153] P. C. Tobin, S. L. Whitmire, D. M. Johnson, O. N. Bjø rnstad, and A. M. Liebhold, Invasion speed is affected by geographical variation in the strength of Allee effects., Ecol. Lett. **10**, 36 (2007).

[154] J. E. Ferrell, Self-perpetuating states in signal transduction: positive feedback, double-negative feedback and bistability., Curr. Opin. Cell Biol. **14**, 140 (2002).

[155] S. Kondo and R. Asai, A reaction-diffusion wave on the skin of the marine angelfish Pomacanthus, Nature **376**, 765 (1995).

[156] J. Nance and J. A. Zallen, Elaborating polarity: PAR proteins and the cytoskeleton., Development **138**, 799 (2011).

[157] L. Wolpert, Positional information and the spatial pattern of cellular differentiation, J. Theor. Biol. **25**, 1 (1969).

[158] W. M. Bement, A. L. Miller, and G. von Dassow, Rho GTPase activity zones and transient contractile arrays., BioEssays **28**, 983 (2006).

[159] O. Wartlick, P. Mumcu, A. Kicheva, T. Bittig, C. Seum, F. Jülicher, and M. González-Gaitán, Dynamics of Dpp signaling and proliferation control, Science **331**, 1154 (2011).

[160] A. K. Abramyan and S. A. Vakulenko, Nonlinear Ritz method and the motion of defects, Teoret. Mat. Fiz. **155**, 202 (2008).

[161] C. Gardiner, *Stochastic Methods: A Handbook for the Natural and Social Sciences.*, Springer, New York, 4th edition, 2009.

[162] A. Mikhailov, L. Schimansky-Geier, and W. Ebeling, Stochastic motion of the propagating front in bistable media, Phys. Lett. A **96**, 453 (1983).

[163] A. Rocco, J. Casademunt, U. Ebert, and W. van Saarloos, Diffusion coefficient of propagating fronts with multiplicative noise, Phys. Rev. E **65**, 012102 (2001).

[164] S. Surkova, D. Kosman, K. Kozlov, Manu, E. Myasnikova, A. A. Samsonova, A. Spirov, C. E. Vanario-Alonso, M. Samsonova, and J. Reinitz, Characterization of the Drosophila segment determination morphome., Dev. Biol. **313**, 844 (2008).

Danksagung

Zuerst möchte ich mich bei meinem Doktorvater, Prof. Erwin Frey, bedanken. Von den spannenden Diskussionen und seiner Art über Physik zu denken habe ich viel gelernt. Die freie und kollegiale Atmosphäre am Lehrstuhl ist ein fruchtbarer Nährboden für neue Ideen. Besonders dankbar bin ich für die Möglichkeit, mit talentierten Studenten zusammen an Projekten arbeiten zu dürfen.

Des weiteren bedanke ich mit bei meinen Master- und Bachelorstudenten, die nicht unerheblich zu dieser Arbeit beigetragen haben. David Jahn ist zwar manchmal etwas zerstreut, überraschte mich aber durch seine kreative Art immer wieder mit neuen Ergebnissen und Denkanstößen. Alejandro Zielinski, der Projektmanager, hat mit großer Akribie ein sehr technisches Thema bearbeitet. Was er sagt, ist immer über jeden Zweifel erhaben. Matthias Reiter schrieb eine Bachelorarbeit, die es mit so mancher Masterarbeit aufnehmen konnte. Vor allem verfasste er anschließend mit großem Engagement eine Publikation. Jörg Martin war ebenso exzellent, nur haben wir ihn leider an die Mathematik verloren. Bei Moritz Zehl bedanke ich mich, weil er in seiner Bachelorarbeit mit großer Motivation ein sehr hartnäckiges Modell untersuchte. Frank Schlosser arbeitet noch kein halbes Jahr an seiner Masterarbeit, hat aber schon erste, interessante Ergebnisse vorzuweisen. Schließlich Raphaela Geßele, die ein analytisches Thema berarbeiten möchte. Ich bin gespannt, wann sie mit der Numerik anfängt.

Ich bedanke mich auch bei der Evodyn Gruppe. Allen voran Johannes Knebel für die Diskussionen, das Korrekturlesen meiner Manuskripte und die Mitbetreuung zweier Masterstudenten. Madeleine Leisner hat einen Vortrag über phänotypische Heterogenität gehalten, der mir sehr viel Arbeit ersparte. Bei Markus F. Weber bedanke ich mich für fruchtbare Diskussionen. Fabian Drube war mir über die Jahre ein treuer Büronachbar und Begleiter auf Seminaren. Vielen Dank auch allen Korrekturlesern, namentlich Fabian Drube, Ulrike Harder und Frederik Beaujean.

Ganz besonders bedanke ich mich bei meinen Eltern, denen ich jahrelang auf der Tasche lag. Sie haben mich über all die Jahre unterstützt und gefördert. Ich bedanke mich auch bei meinen Schwiegereltern in spe, die meine Freundin und meine Tochter zu sich genommen haben und mir so ermöglichten, diese Dissertation rechtzeitig fertigzustellen. Ganz besonderer Dank gilt Ulrike Harder, für die Geduld und dafür, dass sie mir in dieser anstrengenden Zeit den Rücken freihält. Zuletzt grüße ich mein Töchterchen Faina, die uns in Ihrem erst kurzen Leben schon viele schöne Momente bereitet hat.

Ich versichere, die Arbeit selbstständig angefertigt und dazu nur die im Literaturverzeichnis angegebenen Quellen benutzt zu haben.

München, den 25. Juli 2013